IBn
INSTITUTE OF BIOPHYSICS AND NANOSYSTEMS RESEARCH

ANNUAL REPORT 2005

10 YEARS SAXS BEAMLINE

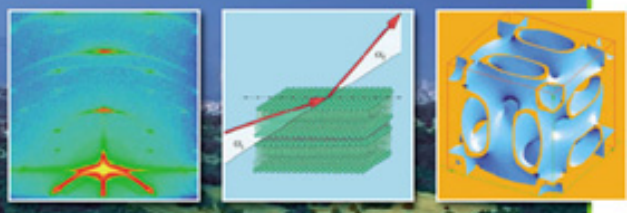

AUSTRIAN SAXS BEAMLINE AT elettra

Austrian Small Angle X-ray Scattering (SAXS) Beamline at ELETTRA

Annual Report 2005

Compiled by the SAXS-Group:

- for IBN: B. Sartori, M. Rappolt & H. Amenitsch
- for ELETTRA: S. Bernstorff

Table of Contents

Preface

10 years Austrian SAXS beamline at ELETTRA: In May 1996, five months after the start of construction, the first experiments were performed together with the group of Zehetbauer, Vienna, on a metallurgical problem, and September of the same year, the first official user series was received, starting with work on muscle fibres by the group of Cecchi, Florence. It was one of the first beamlines to be commissioned for user operation at Elettra. It had started as a joint project of Sincrotrone Trieste and the Austrian Academy of Sciences, and under this status the station has become a place for exciting and highly successful experiments, not only for a large number of scientists from Austria and Italy, but also for an impressively growing, international user community. Today it is one of the most versatile and useful stations of this kind, worldwide, and an acknowledged part of the European scientific infrastructure. This is also documented by the participation in the EU-project SAXIER (http://www.saxier.org/), starting this year, which is aimed at developing cutting-edge methodology and instrumentation related to SAXS. Thus, the station will continue to be among the top-places in this important analytical area.

Many important scientific developments have seen the light during this first decade, which coincides with the explosive upsurge of nanoscience and technology. In SAXS, specifically, the technical realization of an impressive range of new experimental approaches, from *in-situ* monitoring of self-assembly at solid interfaces, to the analysis of processes in complex biomaterials and tissues, to nanoparticle formation in the gas phase, and to the investigation of single microparticles held by 'optical tweezers' could be witnessed. SAXS has grown from a specialized technique of colloiod and polymer science to a general microscopy tool, by which any nanoscale object and process can be investigated.

This development has been followed - and in some parts even triggered - by the constant improvement of the SAXS station over the years. The conditions provided at Elettra are excellent, and this is mainly due to the very smooth and professional interaction between the management at Sincrotrone Trieste and our station management. In the end it is always the people that count, and I want to thank particularly the two persons responsible for the day-to-day operation and station development, Sigrid Bernstorff and Heinz Amenitsch, who have been the strong anchors from the very start, in times of constant change. Together with their team of scientists and technicians, and with the stimulating input by the users they have made the station to what is today: a highly valuable source for science and innovation.

May the stream of change persist.

Peter Laggner
Director
Institute of Biophysics and Nanosystems Research
Austrian Academy of Sciences

This year we are especially pleased to welcome the publication of the Annual Report of the SAXS Beamline of the Austrian Academy of Sciences because we are celebrating two anniversaries, namely the 10th year of user operation of the SAXS beamline at Elettra and the 20th anniversary of the foundation of Sincrotrone Trieste S.C.p.A., the managing company of the Elettra Laboratory. Elettra was one of the first two medium-energy third-generation synchrotron radiation sources in the world. Many people in our organization have been here since the beginning and recall the heady feeling of seeing a world-class laboratory emerge from green fields. Today, there are 22 beamlines in operation and four under construction, most of them built and operated together with our Partners. We are hosting over 100 staff and some important central facilities and laboratories of such Partners, and welcoming approximately 1,000 users a year to perform experiments.

The financial crisis of 2003 and 2004 is fortunately behind us. Our laboratory is again at a beginning - this time the start of an important transition period. A new 5-year plan has been developed and the structure of our organization has been reconfigured to offer our scientists, technicians, managers, and administrators a flexible and responsive environment for growth and facilitate interaction with our Partners and external Users. We have evaluated critically the mission, vision and core values of our organization, defined our strategic objectives and developed a project-oriented operational structure to better pursue such objectives.

Major investments are being directed at the Elettra synchrotron source, that is being upgraded with a new full-energy injector and top-up operation scheduled for 2008, and at FERMI, one of the first free electron lasers (FEL) of its kind in the world, that is being built through extensive international collaborations and will provide femtosecond pulses of unparalleled brilliance at nanometer wavelengths. These facilities and resources are to support an expanded and strengthened network of researchers worldwide and, in particular, among new EU-member states. The knowledge developed from these initiatives will be transferred to the community through education and strategic partnerships with the private sector.

To successfully implement such an ambitious 5-year plan we will need the support of our most successful Partners such as the Austrian Academy of Sciences. The SAXS beamline has remained an essential facility for the users' community in the life sciences, materials chemistry and materials physics, yielding over fifty high-quality research contributions in 2005 alone. We take this opportunity to thank the management and staff of the SAXS beamline at Elettra for their enthusiasm and dedication and look forward to increased involvement of the Austrian Academy of Sciences in the exploitation of an upgraded Elettra and of the new FEL source FERMI.

Alfonso Franciosi
Director, ELETTRA Laboratory
Chief Executive Officer, Sincrotrone Trieste S.C.p.A.

The SAXS-Group

HEAD OF PROJECT: Peter Laggner[1)]

e-mail: Peter.Laggner@oeaw.ac.at

SENIOR SCIENTIST: Heinz Amenitsch [1), 3)]

e-mail: Heinz.Amenitsch@elettra.trieste.it

Sigrid Bernstorff [2)]

e-mail: Sigrid.Bernstorff@elettra.trieste.it

Michael Rappolt [1), 3)]

e-mail: Michael.Rappolt@elettra.trieste.it

POST DOCS: Benedetta Marmiroli [1, 3)]

e-mail: Benedetta.Marmiroli@elettra.trieste.it

Shyjumon.Ibrahimkutty [1, 3)]

e-mail: Shyju.Ibrahimkutty@elettra.trieste.it

PHD-STUDENT: Fabian Schmid [1), 3)]

e-mail: Fabian.Schmid@elettra.trieste.it

CHEMICAL ASSISTANT: Barbara Sartori [1, 3)]

e-mail: Barbara.Sartori@elettra.trieste.it

TECHNICIAN: Christian Morello[2)]

e-mail: Christian.Morello@elettra.trieste.it

1) Institute for Biophysics and Nanosystems Research, Austrian Academy of Sciences, Schmiedlstraße 6, 8042 Graz, Austria.
Tel 0043-316-4120 302
Fax 0043-316-4120 390

2) Sincrotrone Trieste, Strada Statale 14, km 163.5, 34012 Basovizza (TS), Italy.
Tel 0039-040-375 81
Fax 0039-040-938 0902

3) Institute for Biophysics and Nanosystems Research, Austrian Academy of Sciences c/o Sincrotrone Trieste

The SAXS-Beamline in General

Small Angle X-ray Scattering has become a well known standard method to study the structure of various objects in the spatial range from 1 to 1000 Å, and therefore instruments capable to perform such experiments are installed at most of the synchrotron research centers. The high-flux SAXS beamline at ELETTRA is mainly intended for time-resolved studies on fast structural transitions in the sub-millisecond time region in solutions and partly ordered systems with a SAXS-resolution of 10 to 1400 Å in real-space.
The photon source is the 57-pole wiggler whose beam is shared and used simultaneously with a Macromolecular Crystallography beamline. The wiggler delivers a very intense radiation between 4 and 25 keV of which the SAXS-Beamline accepts 3 discrete energies, namely 5.4, 8 and 16 keV. The beamline optics consists of a flat double crystal monochromator and a double focusing toroidal mirror.
A versatile SAXS experimental station has been set-up, and an additional wide-angle X-ray scattering (WAXS) detector monitors simultaneously diffraction patterns in the range from 1 to 9 Å. The sample station is mounted move-able onto an optical table for optimising the sample detector distance with respect to SAXS resolution and sample size.
Besides the foreseen sample surrounding the users have the possibility to install their own specialised sample equipment. In the design phase, besides technical boundary conditions, user friendliness and reliability have been considered as important criteria.
The optimisation of the beamline with respect to high-flux and consequently high flux density, allows to perform the following experiments:

- Low Contrast Solution Scattering
- Grazing Incidence Surface Diffraction
- Micro-Spot Scanning
- X-ray Fluorescence Analysis
- Time-Resolved Studies ≥ 11 μs
- Simultaneously Performed Small- and Wide-Angle Measurements (SWAXS) on:
    - Gels
    - Liquid Crystals
    - (Bio) Polymers
    - Amorphous Materials
    - Muscles

Furthermore, using 5.4 and 16 keV energies, the beamline is widely applicable also to very thin, e.g. single muscle fibers, and optically thick (high Z) specimen, as often used in e.g., material science and solid state physics.

THE INSERTION DEVICE

The wiggler for the SAXS beamline consists of three 1.5 m long segments, each having 19 poles. The device can work with a minimum gap of 20 mm, which corresponds to K=20 at 2 GeV. The main parameters of the wiggler are:

- Critical Energy 4.1 keV
- Radiation Power 8.6 kW
- Flux 3.5×10^{14} ph/s/mrad/0.1%BW (at 400 mA)

The wiggler radiation cone has a horizontal width of 9 mrad. From this the SAXS-beamline accepts vertically 0.3 mrad, and horizontally +/-0.5 mrad at a 1.25 mrad off-axis position. The resulting source size for 8 keV photons is 3.9 x 0.26 mm^2 (horiz. x vert.).

THE OPTICS

The optics common with the diffraction beamline consists of:

- C-Filter and Beryllium window assembly to reduce the power load on the first optical elements by a factor of 2 and to separate the beamline vacuum from the storage ring.
- Beam defining slit chamber which allows to define the SAXS beam on three sides before the monochromator in order to reduce the straylight in the downstream beamline sections.

The SAXS beamline optics consists of:

- A double-crystal monochromator consisting of four individual chambers, in which three interchangeable asymmetric Si(111) crystal pairs are used to select one of three fixed energies. Each of the crystal pairs is optimised for the corresponding energy to accomplish a grazing angle of 2°. The energy resolution $\Delta E/E$ of the monochromator is in the range of 0.7 - 2.5 10^{-3}.
- A baffle chamber after the monochromator is used as an adjustable straylight fenditure.
- A segmented toroidal mirror focuses the light in horizontal and vertical direction with a 1/2.5 magnification onto the SAXS-detector.
- An aperture slit reduces the straylight after the monochromator and the toroidal mirror.
- A guard slit defines the illuminated region around the focal spot. The spot size on the detector is 1.6 mm horizontally and 0.6 mm vertically. The calculated flux at the sample is in the order of 10^{13} ph/s at 400 mA. For a maximum sample size of 5.4 x 1.8 mm^2 correspondingly a flux density of 10^{12} ph/s/mm^2 has been calculated.

SAMPLE STAGE

The multipurpose sample stage allows to perform fast time-resolved relaxation studies based on temperature- or pressure-jumps as well as stopped flow experiments. Shear jump relaxation experiments are planned. Specifically, T-jumps can be induced by an infra-red light pulse (2 ms) from an Erbium-Glass laser, raising the temperature about 20 °C in an aqueous sample volume of 10 µl. A hydrostatic pressure cell with a maximal accessible angular range of 30° for simultaneous SAXS and WAXS measurements is available. P-jumps are realised by switching fast valves between a low and a high pressure reservoir, increasing or decreasing the hydrostatic pressure in the range from 1 bar to 2.5 kbar within a few ms. A Differential Scanning Calorimeter (DSC) allows for DSC-scans simultaneously to SWAXS measurements. In an overview, the following sample manipulations are possible (further details, see page 32-38):

- Temperature Manipulations: Ramps, Jumps and Gradient Scans
- Pressure Manipulation: Scan and Jumps
- Stopped Flow Experiments
- SWAXS Measurements Applying Mechanical Stress
- Calorimetric measurements

Scientific applications	Low Contrast Solution Scattering, Grazing Incidence Surface Diffraction, Micro-Spot Scanning, X-ray Fluorescence Analysis, Time-Resolved Studies ≥ 11 μs and Simultaneously Performed Small- and Wide-Angle Measurements (SWAXS) on: Gels Liquid Crystals (Bio) Polymers Amorphous Materials Muscles
Source characteristics	Wiggler (NdFeB Hybrid): Period: 140 mm No. full poles: 57 Gap: 20 mm B_{max}: 1.607 T Critical Energy ε_c: 4.27 keV Power (9 mrad): 8.6 kW Effective source size FWHM: 3.9 x 0.26 mm^2(HxV)
Optics	Optical elements: Double crystal monochromator: Si (111) asym. cut, water cooled. / Mirror: two–segment,toroidal, Pt coated. Distance from source: 18.4 m / 26.5 m Acceptance: 1 mrad/0.3 mrad (HxV) Energy (3 selectable): 5.4, 8, 16 keV (0.77, 1.54, 2.3 Å) Energy resolution $\Delta E/E$: 0.7-2.5 x 10^{-3} Focal spot size FWHM: 1.2 x 0.6 mm^2 (HxV) Spot at Sample FWHM: 5.4 x 1.8 mm^2(HxV) Flux at sample: 5 x 10^{12} ph s^{-1}(2 GeV, 200 mA, 8 keV)
Experimental apparatus	Resolution in real space: 10-1400 Å (small-angle), 1- 9 Å (wide-angle) Sample stage: temperature manipulations: ramps, jumps and gradient scans, pressure manipulation: scan and jumps, stop flow experiments, SWAXS measurements applying mechanical stress, SWAXS measurements applying magnetic fields. In-line calorimetric measurements simultaneously with SWAXS. Detectors: 1D gas-filled detectors for simultaneous small- and wide-angle (Gabriel type), 2D CCD-detector for small-angle.
Experiment control	Beamline control: Program-units written in LabView for Windows 1 D detector control: PC-card and software from Hecus X-ray Systems GmbH, Graz. 2 D detector control: Software from Photonic Science, Oxford.

CURRENT STATUS

The beamline has been built by the Institute for Biophysics and Nanosystems Research (IBN), Austrian Academy of Science in collaboration with staff members from Sincrotrone Trieste, and is in user operation since September 1996. The set-up of the beamline started at the beginning of January 1995 with the installation of the support structure. Until the end of 1995, the 8 keV single energy system had been realised. The upgrade to the full three energy system was finished in spring 1998. Time resolved experiments require fast X-ray detectors and data acquisition hard- and software. Depending on the desired resolution in time and in reciprocal space, on isotropic or anisotropic scattering of the sample, one-dimensional position sensitive (delay-line type) or two-dimensional CCD detectors are employed.

In August 2002 our new chemistry and X-ray laboratory went into operation. The chemistry unit serves mainly for sample preparation and analysis for both, in house research and external user groups, whereas the X-ray laboratory allows on-site testing of samples before moving on to the SR beamline (see page 31).

In conclusion, due to wide versatility of the beamline and the highly flexible sample stage, there are nearly no limits for the realisation of an experiment, and you are welcome by our team to propose any interesting and highlighting investigation for the benefit of material and life sciences.

Application for Beamtime at ELETTRA

1. Beamtime Policy at SAXS beamline

According to the agreement from March 2001 regarding the co-operation between the Austrian Academy of Sciences and Sincrotrone Trieste, at the Austrian SAXS-beamline the available beamtime of about 5000 hours/year is distributed as follows:

- 35% for Austrian Users, type: "CRG" (Collaborating Research Group)
- 35% for Users of Sincrotrone Trieste (General Users (GU))
- 30% is reserved for beamline maintenance and in-house research

In both user beamtime contingents also any industrial, proprietary and confidential research can be performed according to the "General User Policy" of Sincrotrone Trieste.

To apply for CRG and GU user beamtime proposals must be submitted according to the rules of Sincrotrone Trieste. The international review committee at ELETTRA will rank the proposals according to their scientific merit assessment. Based on this decision beamtime will be allocated according to the specific quotes for the beamtimes (CRG/GU) either for the following semester ("normal application") or for the next two years ("long term application"). However, at the moment no more than a maximum of 10% of the beamtime will be assigned to "long term" projects.

2. How to apply for beamtime

There are two deadlines each year for proposals, namely August 31st and February 28th. Accepted proposals will receive beamtime either in the then following first or second half year period, respectively. The Application Form must be completed on-line according to the following instructions.

ELETTRA USERS OFFICE
Strada Statale 14 - km 163.5
34012 Basovizza (Trieste), ITALY
Tel: +39 040 375 8628 - fax: + 39 040 375 8565
e-mail: useroffice@elettra.trieste.it

INSTRUCTIONS GIVEN BY THE USERS OFFICE
(see also http://www.elettra.trieste.it/UserOffice/)

1. Read carefully the General Guidelines.

2. Connect to the Virtual Unified Office: https://vuo.elettra.trieste.it/pls/vuo/guest.startup using your favorite browser with JavaScript enabled.

3. Select the Virtual Unified Office link.

4. When prompted, insert your ID and password. If you are a new user fill in the registration form with your data and choose your institution with the search button; in case your institution does not appear in the list, please contact useroffice@elettra.trieste.it giving all the details about it. When registered, you will receive an acknowledgment with your ID and password. You can change your password, if you wish. In case you forget your password, please don't register again but contact useroffice@elettra.trieste.it. At any moment you can select the help button and view more detailed instructions. By inserting your ID and password you will be able to continue.

5. Select the proposals button in the User functions group.

6. Select add and fill in on-line the proposal form. Please, type your proposal in English. Repeat this procedure for each proposal you intend to submit.

7. In case of continuation proposal: a) attach the experimental report of previous measurements; b) give your previous proposal number.

8. When finished, submit the proposal electronically, selecting the save button.

9. Print the proposal form together with each related safety form.

10. Sign the safety form(s).

11. Mail all signed safety form(s) as printed copy to the Users Office.

NOTE:

For technical questions related to proposals submission or other practical issues contact useroffice@elettra.trieste.it

For scientific questions related to the possibility of performing a given experiment contact bernstorff@elettra.trieste.it or amenitsch@elettra.trieste.it

List of Institutes Participating in Experiments

Austria

Austrian Academy of Science, Institute for Biophysics and Nanosystmes Research, Graz

AMENITSCH Heinz
DANNER Sabine
HODZIC Aden
JOCHAM Philipp
KRIECHBAUM Manfred
LAGGNER Peter
PABST Georg
RAPPOLT Michael
SARTORI Barbara
SCHMID Fabian

Material Center Leoben, Erich Schmid Institute of Material Science and Department of Material Physics, University of Leoben

GINDL Wolfgang
KECKES Josef
MAIER Günther A.

Polymer Competence Center Leoben and Institute of Materials Science and Testing of Plastics, University of Leoben

LANG Reinhold W.
WALLNER Gernot M.

University of Natural Resources and Applied Life Sciences, Institute of Physics and Materials Science, Vienna

LOIDL Dieter

University of Technology, Institute of Applied Synthetic Chemistry, Vienna

BINDER Wolfgang H.
FARNIK Dominique
KLUGER Christian
PETRARU Laura

University of Technology, Institute of Materials Chemistry, Vienna

BRANDHUBER Doris

University of Technology, Institute of Materials Science & Technology

FRITSCHER Christina
KOCH Thomas
LICHTENEGGER Helga C.
SEIDLER Sabine

University of Technology, Institute of Structural Analysis, Computational Biomechanics, Graz

SOMMER Gerhard

University of Vienna, Institute of Materials Physics

KERBER Michael
PETERLIK Herwig)
PUCHEGGER Stephan
RENNHOFER Harald
SCHAFLER Erhard
ZEHETBAUER Michael

Canada

National Research Council of Canada, Steacie Institute for Molecular Sciences, Chalk River Laboratories, Chalk River, Ontario

KATSARAS John

Croatia

Institute of Physics, Zagreb

SALAMON Kresimir

"Ruder Boskovic" Institute, Zagreb

BULJAN Maya
DESNICA-FRANKOVIC Ida-Dunja
DESNICA Uros
DUBCEK Pavo
GAJOVIC A.
GRACIN, Davor
JURAIC' Krunoslav
KOVACEVIC Ivana
KRUNO Jurajic
PAVLOVIC Mladen
PIVAC Branko
RADIC Nikola
SANTIC Branko
TURKOVIC Aleksandra

University of Split, Faculty of Chemical Technology, Split

LUCIC-LAVCEVIC Magdi

University of Zagreb, Faculty of Sciences, Zagreb

TONEJC Antun
DJERDJ I.

Czech Republic

Academy of Sciences of the Czech Republic, Institute of Macro- molecular Chemistry, Prague

BALDRIAN Josef

University of Pardubice, Department of Physics, Pardubice, and Academy of Sciences of the Czech Republic, Institute of Macro-molecular Chemistry, Prague

STEINHART Milos

Finland

Åbo Akademi University, Dept. of Physical Chemistry, Turku

LINDÉN Mika
TEIXEIRA Cilaine Veronica

France

Centre de Recherche sur la Matière Divisée, Orléans

ERRE René
SINTUREL Christophe
VAYER Marylène

C.N.R.S., Université de Paris Sud, Chatenay-Malabry

FAIVRE Vincent
GLIGOEM Hela

Technologie SERVIER, Orléans

PÉAN JM.
WÜTHRICH P.

Technologie SERVIER, Orléans, and Université de Paris Sud, Physico-Chimie des Systemes Polyphases, Chatenay

CHEMIN Caroline

Université de Paris Sud, Physico-Chimie des Systemes Polyphases, Chatenay

BOURGAUX Claudie
KALNIN Daniel
KELLER Gerhard
OLLIVON Michel
COUVREUR P.

Université Blaise Pascal, Laboratoire des Matériaux Inorganiques, Aubière Cedex

TAVIOT-GUÉHO Christine
LÉONE Philippe

Université Pierre et Marie Curie, Chimie de la Matière Condensée, Paris

BABONNEAU Florence
BACCILE Niki
BOISSIÉRE Cédric
GROSSO David
KUEMMEL Monika
SANCHEZ Clement
YOLANDA GESTRO Martin

Germany

Max Planck Institute of Colloids and Interfaces, Dep. of Biomaterials, Potsdam

FRATZL Peter

University of Bremen, Institute of Applied and Physical Chemistry

BÄUMER M.
GEHL Bernhard

University of Bremen, Institute of Solid State Physics

CLAUSEN Torben
FALTA Jens
FLEGE Jan-Ingo
SCHMIDT Thomas

Justus Liebig University, Institute of Inorganic and Analytical Chemistry, Giessen

FRÖBA Michael
MAXIMILIAN Cornelius
MORELL Juergen
TIEMANN Michael

University of Hamburg, Institute of Physical Chemistry

ALEKSANDROVIC Vesna
WELLER Horst

University of Ulm, Institute of Inorganic Chemistry I

HÜSING Nicola Karola
GEIST Steffi

Greece

National Hellenic Research Found - Dept. of Chemistry

MAVROMOUSTAKOS Thomas
ZOUMPOULAKIS Panagiotis

Hungary

Eötvös University, Department of General Physics, Budapest

BALOGH Levente
NYILAS Krystian
UNGÁR Tamas

India

Indian Institute of Science, Solid State and Structural Chemistry Unit, Bangalore

SANTRA Pralay K.
SARMA Dipankar Das
VISWANATHA Ranjani

Inter University Consortium for DAE Facilities, Univ. Campus, Khandwa Road, Indore

GUPTA Ajay
KUMAR Dileep

Ireland

University College Cork (UCC), Dept. of Chemistry, Cork City

COPLEY Mark P.
HOLMES Justin D.
MORRIS M.A.
O'CALLAGHAN J. M.
PETKOV N.
SPALDING T.R.

Italy

Associazione CIVEN, Nano Fabrication Facility, Venice

FALCARO Paolo
SCHIAVUTA P.

CNR, Istituto Processi Chimico-Fisici, Messina

TRIOLO Alessandro

Istituto Motori C.N.R., Aerosol and Nanostructures Lab, Napoli

DI STASIO Stefano
FORTE P.

Sincrotrone Trieste, Trieste

BERNSTORFF Sigrid
MENK Ralf
MORELLO Christian

Università di Firenze, Dip. Scienze Fisiologiche, Firenze
BAGNI Maria Angela
CECCHI Giovanni
COLOMBINI Barbara

Genoa University di Genoa, Department D.I.B.E Genova
CARRARA Sandro
Di PASQUALE Marina
Di ZITTI Ermanno
PARODI Maria Teresa
RICCI Davide

Università di Palermo, Dipartimento di Chimica Fisica, Palermo
LO CELSO Fabrizio

Università Politecnica delle Marche, Dipartimento di Scienze Applicate ai Sistemi Complessi, sez. Scienze Matematiche Fisiche e Naturali, Ancona
MARIANI Paolo
PACCAMICCIO Lydia
ORTORE Maria Grazia
RENGHINI Chiara
RUSTICHELLI Franco
SINIBALDI Raffaele
SPINOZZI Francesco

Università Politecnica delle Marche, Dipartimento di Fisica e Ingegneria dei Materiali e del Territorio, Ancona
FRANCESCANGELI Oriano

Università Politecnica delle Marche, Dipartimento di Scienze e Tecnologie Chimiche, Ancona
BRUNI P.
PISANI Michela

Università di Roma "La Sapienza", Dip. di Chimica
CAMINITI Ruggero
CARACCIOLO Giulio
LUCIANI Paola
POZZI Daniela

Università di Sassari, Dipartimento di Architettura e Pianificazione, Laboratorio di Scienza dei Materiali e Nanotecnologie, Alghero/ Sasseri
INNOCENZI Plinio
KIDCHOB Tongjit
MALFATTI Luca
COSTACURTA Stefano

Slovenia

Josef Stefan Institute, Ljubljana

KUNSTELJ Klemen

Sweden

Royal Institute of Technology, Department of Solid Mechanics, Stockholm, Sweden

HOLZAPFEL Gerd A.

The Netherlands

ECN-Solar Energy, Petten

DEVILEE C.
MUFFLER H.J.
SOPPE W.J.

United Kingdom

Cranfield University, Dept. Materials & Medical Sciences, Shrivenham

ZIOUPOS P.

University Laboratory of Physiology, Oxford

ASHLEY Christopher Charles
GRIFFITHS Peter John

USA

University of California, Department of Chemistry and Biochemistry, Los Angeles

TOLBERT Sarah

List of Performed Experiments

2005 (first half year)

Proposal	Proposer	Institution	Country	Title	Research Area
2004874	SCHAFLER Erhard	Univ. of Vienna Inst. of Materials Physics	Austria	Use of In-situ Synchrotron X-Ray Profile Analysis for Clarification of Enhanced Ductility of Bulk Nanocrystalline Cu Achieved by Severe Plastic Deformation	Materials Science
2004871	SCHMID Fabian	Inst. of Biophysics and Nanosystems Research (IBN), Austrian Academy of Sciences (AAS), Graz	Austria	Layer and Age Specific Tensile Testing of Human Carotid Arteries	Life Sciences
2004829	SARMA Dipankar Das	Indian Inst. of Science, Bangalore	India	Study of growth and ordering in CdSe nanocrystals in the sub-second time-scale	Chemistry
2004826	LINDEN Mika	Dep. of Physical Chemistry, Åbo Akademi Univ., Turku	Finland	Influence of linker structure on the formation of hybrid surfactant templated mesostructured organosilica with a crystalline wall structure	Chemistry
2004825	DUBCEK Pavo	Rudjer Boskovic Institute, Zagreb	Croatia	Magnetron sputtered Ge quantum dots on diverse surfaces	Materials Science
2004756	KECKES Jozef	A.A.S., Leoben	Austria	In-situ WAXS combined with tensile tests on bacterial cellulose-based biomimetic composites	Life Sciences
2004729	DI STASIO Stefano	Istituto Motori C.N.R., Aerosol and Nano-structures Lab, Napoli	Italy	In-situ TR-SWAXS experiments of zinc nanoparticles undergoing an oxidation process	Chemistry
2004728	MARIANI Paolo	Dip. di Scienze Applicate ai Sistemi Complessi, Ancona	Italy	Temperature and concentration effects on structure and molecular conformation of DMPG vescicle aqueous dispersions	Life Sciences
2004700	BABONNEAU Florence	Chimie de la Matière Condensée, Université Pierre et Marie Curie, Paris	France	In situ Small Angle X-ray Scattering and X-ray Diffraction Study of the Formation of Surfactant templated Silicas with 3D-periodic Structures	Chemistry
2004699	FRANCESCANGELI Oriano	Dipartimento di Fisica e Ingegneria dei Materiali e del Territorio, Ancona	Italy	Surface Functionalized Lipid-DNA-Metal Complexes for Gene Delivery: X-ray Diffraction Study of PEGylated Lamellar Complexes	Chemistry

2004623	LINDEN Mika	Dep. of Physical Chemistry, Åbo Akademi Univ., Turku	Finland	Mechanism of formation of the novel mesophase Fd3m in inorganic-surfactant systems.	Chemistry
2004582	MARIANI Paolo	Dip. di Scienze Applicate ai Sistemi Complessi, Ancona	Italy	SAXS and GISAXS studies of proteins immobilised in atmospheric plasma polymerised thin coatings	Life Sciences
2004571	FALTA Jens	Institute of Solid State Physics, University of Bremen	Germany	Ordering of 2-dimensional colloidal self-assembling nanoparticle films	Materials Science
2004527	BINDER Wolfgang	Inst. of Applied Synthetic Chemistry, Division of Macromolecular Chemistry, Vienna Univesity of Technology	Austria	Continuation of : Investiagtions on Phase Segregated, Supramolecular Block Copolymers: Dynamics of Nanostructure Formation by SAXS	Chemistry
2004519	LAGGNER Peter	IBN, AAS, Graz	Austria	Solid-supported lipid mesophases	Life Sciences
2003095	MARIANI Paolo	Dip. di Scienze Applicate ai Sistemi Complessi, Ancona	Italy	LONG TERM: Phase behaviour, molecular conformation and compressibility of lipid systems	Life Sciences
2003093	LAGGNER Peter	IBN, AAS, Graz	Austria	LONG TERM: Solid-supported lipid mesophases	Life Sciences
2003021	GROSSO David	Chimie de la Matière Condensée, UMR UPMC-CNRS 7574, Paris	France	LONG TERM: Self-assembly mechanismens during aerosol generation of mesostructured macro-spheres	Chemistry
In-house	AMENITSCH Heinz OLLIVON Michel	IBN, AAS, Graz + Physico-Chimie des Systèmes Polyphasés, UMR 8612, Univ. Paris-Sud, Chatenay	France	Triglyceride crystallisation under shear: Study of the crystalline structures and phase transitions by coupling of Differential Scanning Calorimetry and High Resolution Small Angle X-ray Scattering	Life Sciences
In-house	BERNSTORFF Sigrid PIVAC Branko	Sincrotrone Trieste + Rudjer Boskovic Institute, Zagreb	Croatia	GISAXS study of nanostructures formed in SiO/SiO2 superstructures	Materials Science
In-house	BERNSTORFF Sigrid GRACIN Davor	Sincrotrone Trieste + Rudjer Boskovic Institute, Zagreb	Croatia	SAXS on amorphous silicon-carbide alloys	Materials Science
In-house	AMENITSCH Heinz TAVIOT-GUEHO Christine	IBN, AAS, Graz + Blaise Pascal Uni, LASMEA	France	In situ characterization of the structure of LDH-DNA nanohybrids by SAXS - A new gene delivery system	Life Sciences
In-house	BERNSTORFF Sigrid CARRARA Sandro	Sincrotrone Trieste + DI.B.E., Genoa Univ., Genova	Italy	Diameter measurements by Small Angle X-ray Scattering for size-selected thiol encapsulated gold nanoparticles	Life Sciences

In-house	AMENITSCH Heinz CARACCIOLO Giulio	IBN, AAS, Graz + Univ. Roma La Sapienza, Dip. di Chimica	Italy	Solid-supported oriented lipid/DNA complexes	Life Sciences
In-house	AMENITSCH Heinz CARACCIOLO Giulio	IBN, AAS, Graz + Dep. of Chemistry, Univ. di Roma "La Sapienza"	Italy	Interactions of Phospholipid Vesicles with Cationic Gemini Surfactants	Life Sciences
In-house	AMENITSCH Heinz TRIOLO Alessandro	IBN, AAS, Graz + Istituto per i Processi Chimico-Fisici - CNR, Messina	Italy	Phase diagram of polyolefin-resin mixtures	Chemistry
In-house	BERNSTORFF Sigrid TURKOVIC Aleksandra	Sincrotrone Trieste + Rudjer Boskovic Institute, Zagreb	Croatia	Determination of grain sizes and porosity in nanophase vanadium oxide and V/Ce oxides via GISAXS, GIWAXD and GIXR techniques for better theoretical model	Materials Science

2005 (second half year)

Proposal	Proposer	Institution	Country	Title	Research Area
2005408	SCHMID Fabian	IBN, AAS, Graz	Austria	Layer and Age Specific Tensile Testing of Human Carotid Arteries	Life Sciences
2005387	PETERLIK Herwig	University di Vienna, Institute of Materialphysics	Austria	Time resolved SAXS investigation of human bone during tensile loading and subsequent stress relaxation	Life Sciences
2005357	SCHAFLER Erhard	University di Vienna, Institute of Materialphysics	Austria	Enhanced background scattering caused by deformation induced vacancies: In-Situ Synchrotron WAXS, Part I: Face Centered Cubic Metals (fcc)	Materials Science
2005324	FRITSCHER Christina	Vienna Univ. of Technology, Institute of Materials Science and Technology	Austria	Inorganic-organic nanocomposites from gels prepared with new polymerizable surfactants	Chemistry
2005322	GUPTA Ajay	UGC-DAE Consortium for Scientific Research, Indore	India	Depth resolved in-plane diffraction studies of melting of Langmuir-Blodgett films using x-ray standing waves	Materials Science
2005290	KRIECHBAUM Manfred	IBN, AAS, Graz	Austria	Effects of sterols (cholesterol and plant sterol) on the structure and phase behavior of lipid membranes	Life Sciences
2005287	BALDRIAN Josef	Institute of Macromolecular Chemistry, Academy of Sciences	Czech Republic	Disorder-order-crystallization phenomena in block-copolymer blends (BCP)	Chemistry

2005239	RAPPOLT Michael	IBN, AAS, Graz	Austria	Transition between lamellar, cubic and hexagonal lipid phases studied by highly temperature resolved (<10 mK) SAXS/WAXS scattering	Life Sciences
2005236	AMENITSCH Heinz	IBN, AAS, Graz	Austria	Evaporation induced self assembly of phospholipids into non lamellar phases on solid supports	Life Sciences
2005219	TURKOVIC Aleksandra	Rudjer Boskovic Institute, Zagreb	Croatia	Morphology and crystallization kinetics of solid polymer electrolyte (PEO)8ZnCl2 via combined Time-resolved synchrotrone SAXS-WAXD techniques	Materials Science
2005160	GRIFFITHS Peter John	University Laboratory of Physiology, Oxford	United Kingdom	Dynamic spacing changes in the myofilaments in response to sudden loading.	Life Sciences
2005132	SINTUREL Christophe	Université di Orléans - Centre de Recherche sur la Matiére Divisée	France	Self Organisation of Block Copolymers in Reactive Polymer Blends	Materials Science
2005129	DESNICA Uros	Rudjer Boskovic Institute, Zagreb	Croatia	Germanium Quantum Dots in multylayers produced by magnetron sputtering	Materials Science
2005077	SARMA Dipankar Das	Indian Institute of Science, Bangalore	India	In-situ study of one-dimensional growth and dynamics in TiO_2 nanorods	Chemistry
2005070	HOLMES Justin	University College Cork (UCC) - Dept. of Chemistry	Ireland	The formation of CO_2-in-Water (C/W) microemulsions using hydrocarbon triblock copolymer surfactants	Chemistry
2005056	INNOCENZI Plinio	Lab. of Materials Science and Nanotechnology, Univ. of Sassari and Nanoworld Institute, Alghero	Italy	Self-assembling "mono-crystal like" and defect free mesostructures	Chemistry
2005051	FALTA Jens	Institute for Solid Physics, Univ. Bremen	Germany	In-situ characterization of self-assembled nanoparticle films under harsh conditions	Materials Science
2005036	HODZIC Aden	IBN, AAS, Graz	Austria	In situ study of antihypertensive drug effects on lipid model membranes	Life Sciences
2005031	OLLIVON Michel	Physico-Chimie des Systemes Polyphases, Univ, Paris-Sud, Chatenay	France	Insertion of cytotoxic anticancer agent in sphingomyelin-cholesterol liposomes: Study of liquid crystalline structures by coupling of Differential Scanning Calorimetry and High Resolution SAXS	Life Sciences
2005028	PABST Georg	IBN, AAS, Graz	Austria	Finite-Size Effects in Thin Lipid Films	Life Sciences
In-house	BERNSTORFF Sigrid RADIC Nikola	Sincrotrone Trieste + Rudjer Boskovic Institute, Zagreb	Croatia	Dynamics of Ge quantum dots growth	Materials Science

In-house	BERNSTORFF Sigrid PIVAC Branko	Sincrotrone Trieste + Rudjer Boskovic Institute, Zagreb	Croatia	GISAXS study of Si nanoobjects formed in SiO2/SiO superstructures	Materials Science
In-house	BERNSTORFF Sigrid GRACIN Davor	Sincrotrone Trieste + Rudjer Boskovic Institute, Zagreb	Croatia	SAXS on amorphous silicon-carbide alloys	Materials Science
In-house	BERNSTORFF Sigrid MARIANI Paolo	Sincrotrone Trieste + Universita' Politecnica delle Marche, Ancona	Italy	SAXS and GISAXS studies of proteins immobilised in atmospheric plasma polymerised thin coatings	Life Sciences
In-house	AMENITSCH Heinz CARACCIOLO Giulio	IBN, AAS, Graz + Dep. of Chemistry, Univ. di Roma "La Sapienza"	Italy	Multi-componen cationic lipid/DNA complexes: a new strategy for gene delivery	Life Sciences

User Statistics

1. Number of submitted proposals and assigned shifts from 1995 until December 2006

The Austrian SAXS-beamline at ELETTRA opened to users in September 1996. Since then many experiments have been performed related to the fields of life science, materials science, physics, biophysics, chemistry, medical science, technology and instrumentation.

From September 96 on users gained access to the SAXS-beamline on the basis of the proposals received for the periods shown in Fig. 1. The assignment of beamtime at this beamline is done separately for the group of "General Users" (GU) and the "Collaborating Research Group" (CRG), i.e., the Austrian users. Beamtime was assigned to the proposals of each group in the order of the rating received by the Scientific Committee, and up to the maximum number of shifts available to each group according to the contract between "The Austrian Academy of Sciences" and the "Sincrotrone Trieste". Until December 1997 up to 30 % of the beamtime was given to CRG, up to 55 % to GU, and 15% was reserved for maintenance purposes. From January 98 to June 2001 the quota for beamtime was up to 35 % for CRG, up to 50 % for GU, and again 15% reserved for maintenance purposes. From July 2001 on the two contingents for user proposals from CRG and GU receive up to 35% of the beamtime each. The remaining 30 % of beamtime are used for inhouse research projects as well as for maintenance purposes.

Fig. 1 gives an overview of the numbers of received proposals, the numbers of requested and assigned shifts, as well as the percentage between assigned and requested shifts. Included in Fig.1 are also the same data for the period End 1995 - August 1996, during which some beamtime had been given already to users in order to perform first pilot- and test-experiments together with the beamline staff. These first experiments during the commissioning phase were not yet based on proposals, since the goal was mostly to evaluate and improve the performance of the beamline and the equipment of its experimental station. As can be seen in Fig.1, the request for beamtime at the SAXS-beamline increased continuously and strongly until the first half year of 1999 (also during the period Sept.-Dec. 1997, if one takes into account that this period was only 4 instead 6 month long, and that for this reason less proposals were submitted). Then, probably due to the high rejection rates, the number of submitted proposals decreased somewhat during 2001, which resulted in a better ratio of accepted / rejected proposals. This oscillating behaviour of beamtime request can also be seen for the period 2002 - 2006, where after higher numbers of submitted proposals slightly reduced request periods follow.

In 2005, in total 84 proposals (18 from CRG, and 66 from GU) were submitted. From these 20 proposals (4 from CRG and 16 from GU) were submitted by "new" usergroups, i.e. groups which so far had never beamtime at the SAXS beamline. From these 3 proposols (2 CRG and 1 GU) were officially accepted.

Figure 1 (Next page). The statistical information about the beamtime periods since end of 1995 are given for the groups "CRG", and "GU" separately, as well as for both together ("Total"). Shown are, for all beamtime periods (from top to bottom):

- Number of received proposals, ● Number of requested shifts,
- Number of assigned shifts, and ● Relation between assigned and requested shifts

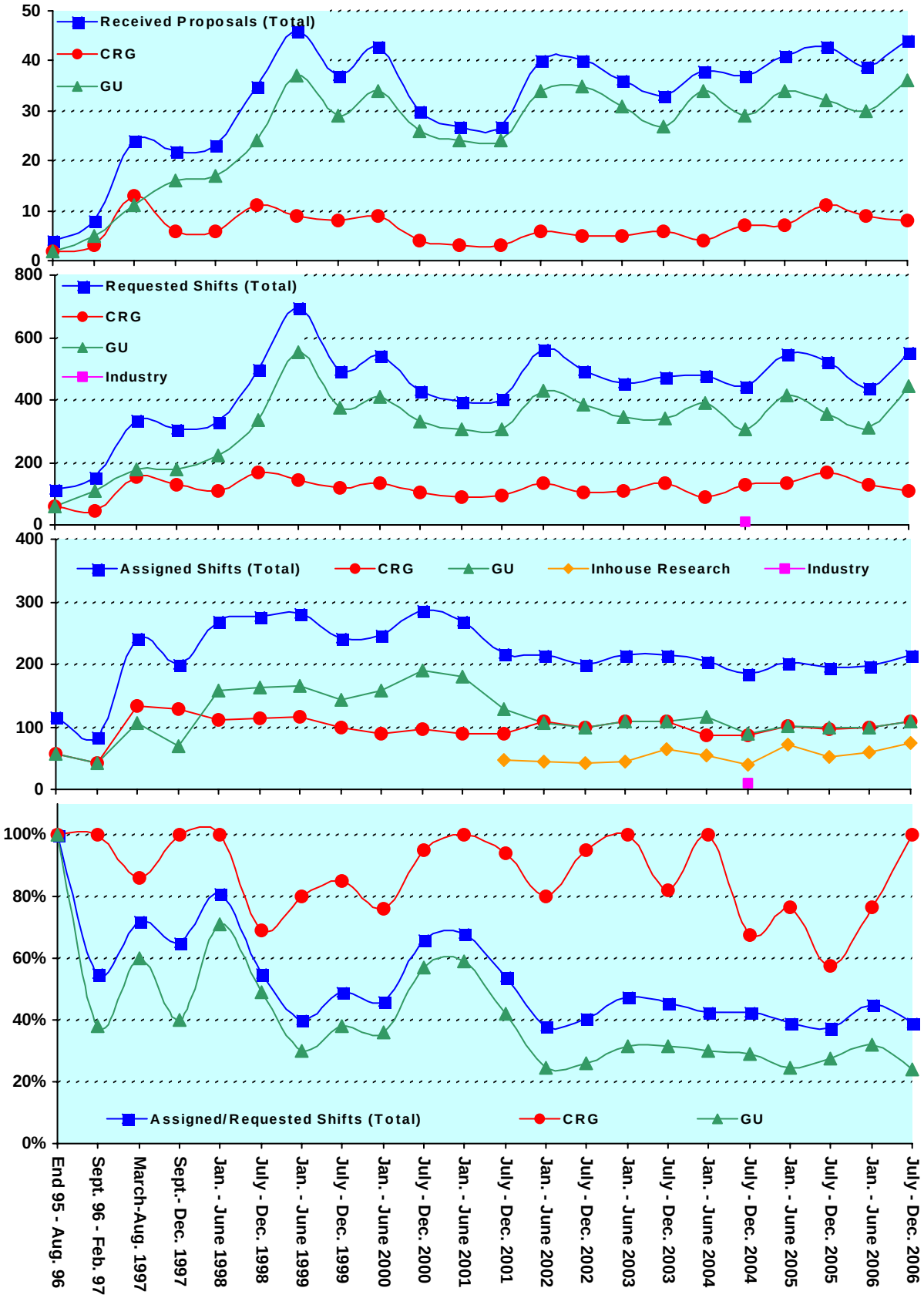
Received Proposals (Total)
CRG
GU
Requested Shifts (Total)
CRG
GU
Industry
Assigned Shifts (Total)
CRG
GU
Inhouse Research
Industry
Assigned/Requested Shifts (Total)
CRG
GU
End 95 - Aug. 96
Sept. 96 - Feb. 97
March-Aug. 1997
Sept.- Dec. 1997
Jan. - June 1998
July - Dec. 1998
Jan. - June 1999
July - Dec. 1999
Jan. - June 2000
July - Dec. 2000
Jan. - June 2001
July - Dec. 2001
Jan. - June 2002
July - Dec. 2002
Jan. - June 2003
July - Dec. 2003
Jan. - June 2004
July - Dec. 2004
Jan. - June 2005
July - Dec. 2005
Jan. - June 2006
July - Dec. 2006

2. Provenience of users

During 2005, 152 users from 53 institutes in 17 countries have performed experiments at the SAXS beamline. In Fig. 2 are shown both the provenience of these users, and of their respective institutes. Each user or institute was counted only once, even though many users performed experiments in both beamtime periods of 2005.

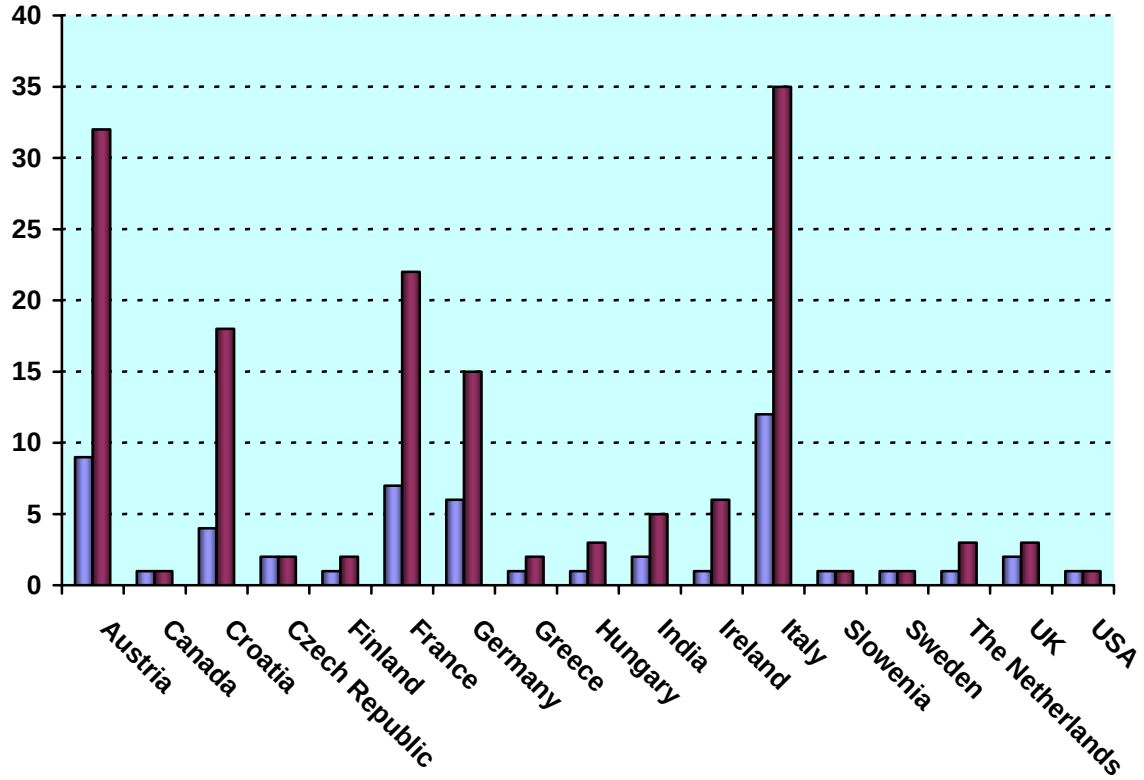

Figure 2. Provenience of users (dark grey) and of their corresponding institutes (light grey).

3. Documentation of experimental results

As could be expected, with the start of user-operation at the SAXS-beamline the number of contributions to conferences started to increase strongly. With a delay of one year - the average time needed for paper publications - also the number of publications increased accordingly, as can be seen in Fig. 3.

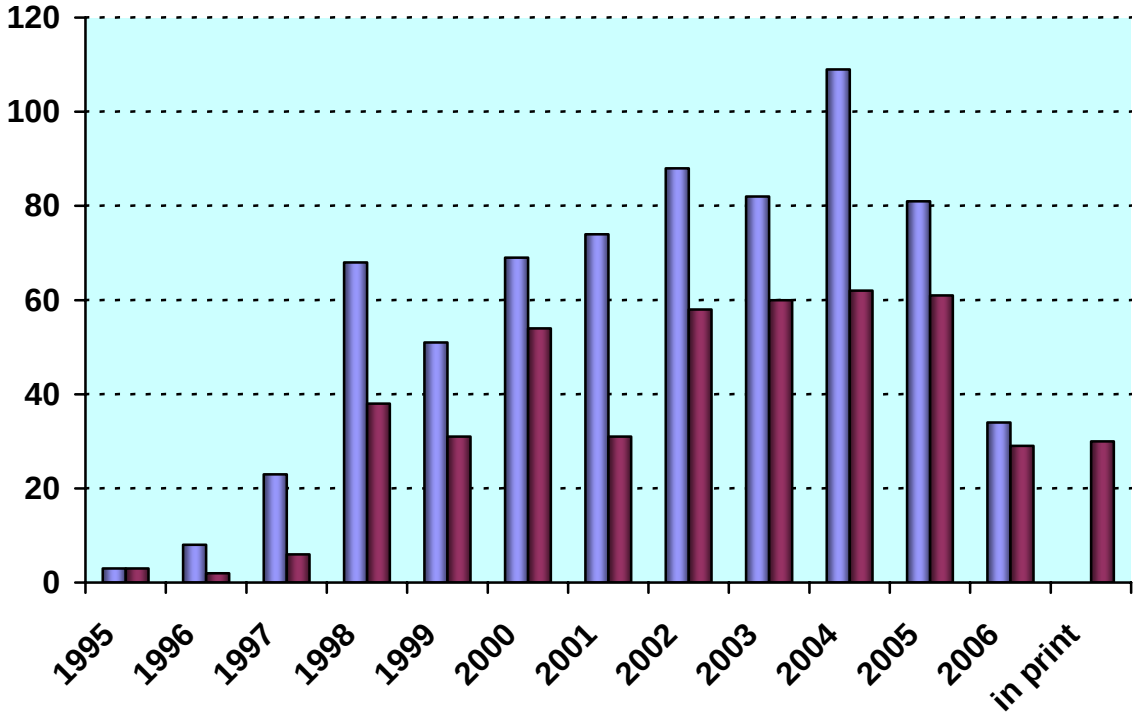

Figure 3. Number of conference contributions (light grey) and of refereed paper publications (dark grey) for the years 1995-2005. Also contributions, which have been published until September 2006 as well as those in print at that time are included.

In addition, from 1995 until September 2006, the following documentations based on instrumentation of the SAXS-beamline, or on data taken with it, have been produced.

Unrefereed publications:

Technical Reports on Instrumentation:	5
Contributions to Elettra Newsletters:	15
Contributions to Elettra Highlights:	22
Habil Thesis:	2
PhD Thesis:	52
Master Thesis :	27

Experimental Possibilities at the SAXS-beamline

1. Latest Developments

1. Flow through cell

In the year 2005 a new flow through cell has been developed and tested successfully. The flow through cell (see Figure 1) works in a simple manner: Special quartz capillaries (Glas Technik & Konstruktion, Schönwalde/Berlin) of 1.5 mm diameter and wide openings of about 3 mm at each end, can be inserted into the standard Anton Paar sample holder, which allows various temperature treatments (T-range 25-300 or –30-70 °C, respectively). Thin tubes are connected directly to the capillary ends and a constanst flow is achieved by a peristaltic pump.

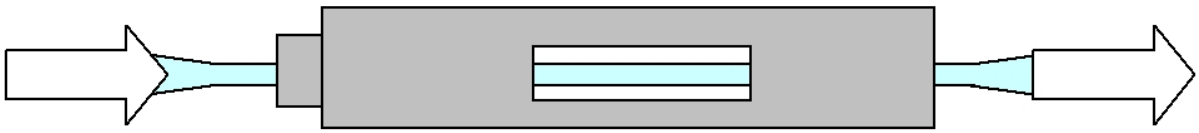

Figure 1. New flow through cell (for details see text).

2. Monochromator feedback/control system

Due to the decaying ring current the heat load on the first monochromator is constantly changing, too. Thus a fine pitch correction of the second monochromator is necessary to guarantee maximum flux on the sample. So far the monochromator fine pitch was regulated manually, but now a new feedback/control systems allows remote operation of the second monochromator crystal. Three different functions can be executed within a new LabView programme. First, at the beginning of the measurement session (i.e. after injection) the optimum position of the 2nd monochromator can be found by a fine pitch scan. Second, the fine pitch can be set to an explicit value, and third, a special feed back mode allows to control the monochromator crystal fine pitch automatically.

2. Accessible SAXS and WAXS ranges

Simultaneous SAXS- and WAXS-measurements can be performed using a linear sensitive gas detector (Gabriel type, windows size 8 x 100 mm, active length 86.1 mm with a resolution of 0.135 mm/channel) for the WAXS-range, and either a second linear Gabriel type detector (windows size 10 x 150 mm, active length 134 mm with a resolution of 0.159 mm/channel), or the 2D CCD-system for the SAXS-range. A specially designed vacuum chamber (SWAXS-nose, see Annual Report of 1996/97, p. 32) allows to use both scattering areas below (for SAXS) and above (for WAXS) the direct beam, respectively.

Depending on the photon energy maximum SAXS resolutions of 2000 Å (5.4 keV), 1400 Å (8 keV) or 630 Å (16 keV) are available. The available possible WAXS-ranges are summarised in Table 1. The overall length of the SWAXS-nose in the horizontal direction, measured from the sample position, is 512 mm and the fixed sample to WAXS-detector distance is 324 mm. At the shortest SAXS camera-length an overlap in the d-spacings covered by the SAXS- and WAXS-detectors, respectively, is possible: then, the common regime lies around 9 Å.

Table 1. Possible d-spacing ranges in the WAXS-regime at the SAXS-beamline at ELETTRA. Since the WAXS-detector can be mounted at four different fixed positions on the SWAXS-nose (range 1-4), with the three possible energy choices (5.4, 8 and 16 keV) this results in 12 different d-spacing regimes. In italic the most common choice (8 keV, range 1) is highlighted. This range is suited for experiments, e.g., on lipid-systems and (bio)polymers.

Range	2θ [deg]	d-spacing (Å)		
		8 keV	5.4 keV	16 keV
1	9.4	*9.40*	14.03	4.27
	27.6	*3.23*	4.82	1.47
2	27.4	3.25	4.86	1.48
	45.6	1.99	2.97	0.90
3	45.4	2.00	2.98	0.91
	63.6	1.46	2.18	0.66
4	63.4	1.47	2.19	0.67
	81.6	1.18	1.76	0.54

3. Calibration of the s-axis and flat field correction

At the SAXS beamline various standards are used for the angular (s-scale) calibration of the different detectors:

- Rat tail tendon for the SAXS detector - high resolution (rtt*.dat)
- Silver behenate for the SAXS detector – medium and low resolution (agbeh*.dat)
- Para-bromo benzoic acid for the WAXS detector – WAXS range 1 and 2 (pbromo*.dat)
- Combination of Cu, Al foils and Si powder for the WAXS detector – WAXS range 2 and higher

In Fig. 2 a typical diffraction pattern of rat tail tendon is shown, depicting the diffraction orders (from the first to the 14th order) measured with a "high" resolution set-up (2.3 m) and the delay-line gas detector. The d-spacing is assumed to be 650 Å, but this value can vary depending on humidity up to 3%. Thus, the rat tail tendon is often used only to determine the position of the direct beam (zero order), while the absolute calibration is performed using the diffraction pattern of Silver behenate powder. Fig. 3 depicts a diffraction pattern of Silver behenate measured with "medium" resolution set-up (1.0 m) from the first to the 4th order (repeat spacing 58.4 Å) [1].

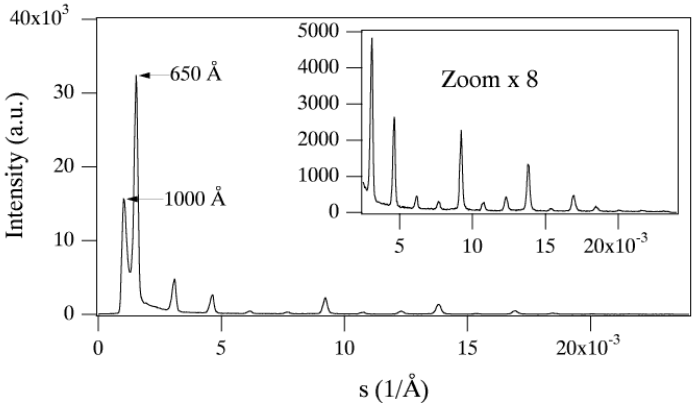

Figure 2. SAXS diffraction pattern of the collagen structure of rat tail tendon fibre at a distance of 2.3 m.

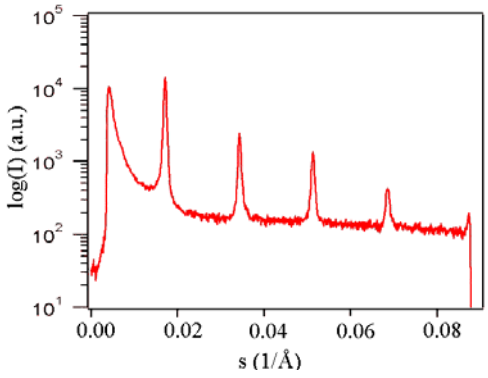

Figure 3. SAXS diffraction pattern of Ag behenate powder at a distance of 1.0 m

In Fig. 4 a typical WAXS pattern of p-bromo benzoic acid is shown. The diffraction peaks are indexed according to the values given in Table 2, taken from [2].

Table 2. d-spacings and relative intensities of p-bromo benzoic acid according to [2].

d-spacing/Å	rel. intensity	d-spacing/Å	rel. intensity
14.72	18000	4.25	490
7.36	1200	3.96	2380
6.02	330	3.84	10300
5.67	980	3.74	26530
5.21	6550	3.68	1740
4.72	26000	3.47	760

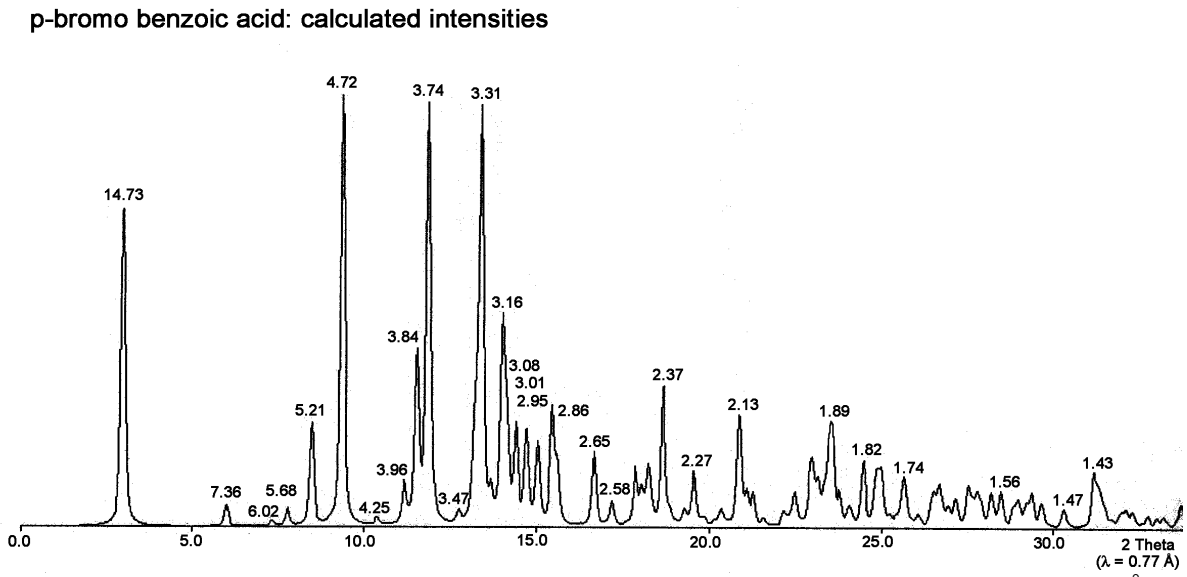

Figure 4. Calculated diffraction pattern of p-bromo benzoic acid. d-spacings are given in Å.

The s-scale for both, the SAXS and the WAXS range, can be obtained by linear regression, i.e., the linear relation between the kown s-values of the calibrant versus the measured peak positions has to be found.

A further correction is regarding the flat field response (efficiency) of the detectors. For this correction, the fluorescence light of various foils are used to illuminate the detectors rather homogeneously:

At 8 keV: iron foil (100 μm thick), fluorescence energy: 6.4 keV K_{α}, 7.1 keV K_{β}(effic*.dat)
At 16 keV: copper foil (> 100 μm thick), fluorescence energy: 8.028 keV $K_{\alpha 2}$, 8.048 keV $K_{\alpha 1}$, 8.905 keV K_{β} (effic*.dat)

The measured scattering pattern are corrected for the detector efficiency simply by dividing them by the fluorescence pattern. Note: The average of the detector efficiency data should be set to unity and a small threshold should be applied to avoid any division by zero.

[1] T.N. Blanton et. al., Powder Diffraction 10, (1995), 91
[2] K. Ohura, S. Kashino, M. Haisa, J. Bull. Chem. Soc. Jpn. 45, (1972), 2651

4. Elettra Virtual Collaboratory

During 2005, a new possibility for data file sharing between ELETTRA and external laboratories went into operation. The Elettra Virtual Collaboratory (EVC) is a collaborative virtual environment (i.e., a computer system that supports human to human and human to machine communication and collaboration) for X-ray experiments at the Elettra Synchrotron Light Laboratory, Trieste, Italy. The EVC allows a distributed team of researchers to share experimental data, exchange ideas, discuss problems, from data collection to results publication.

Connecting to https://evc.elettra.trieste.it/ with a web browser it is possible to enter the EVC environment. A new user can easily register from any PC workstation at ELETTRA filling in a dedicated form in the EVC web page. An already registered user then can login, open a new project folder, add new members, who will share all the information and files of the project, and operate on all projects he takes part in. However, we note these actions can only be carried out from an ELETTRA intranet workstation.

From home a registered user can download the experimental data via web browser, work on them and perform a data backup in his own PC workstation: thus a researcher can partecipate in an experimental session even if not physically present at ELETTRA. In the near future, it will also be possible to perform the data reduction online, through the web browser.

A system for data backup on DVD is also available on the EVC workstation at the SAXS beamline. For more informations, please have a look at the EVC web page, https://evc.elettra.trieste.it/

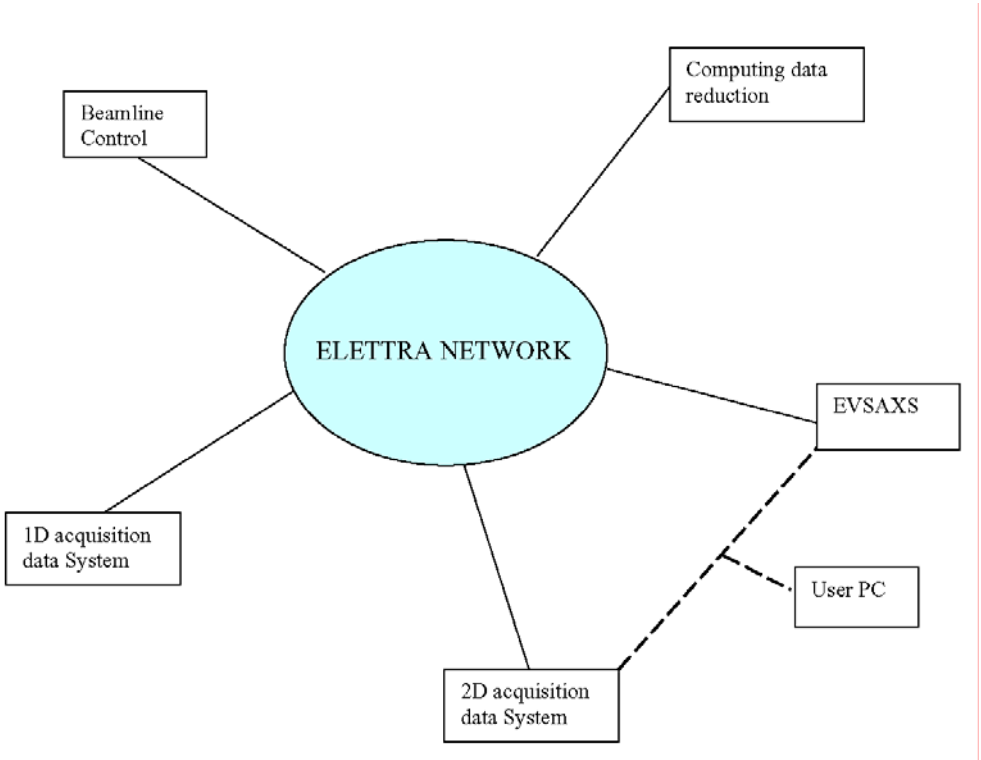

Figure 5. Overview of the local network of the SAXS beamline at ELETTRA

5. Site laboratories

In August 2002 our new chemistry and X-ray laboratory went into operation. The 70 m^2 big laboratory is divided in two parts, in which the bigger share of 43 m^2 is occupied by the chemistry lab. This unit serves mainly for sample preparation and analysis for both, in house research and external SAXS user groups. In the X-ray laboratory the set-up of a SWAX camera for simultaneous small and wide angle scattering has been completed (Hecus X-ray Systems, Graz, Austria: www.hecus.at), which allows on-site testing of samples before moving on to the SR beamline. The chemistry lab is meanwhile equipped with:

- micro centrifuge (max. 13200 rpm; model 5415D from Eppendorf , Hamburg, Germany)
- chemical fume hood (model GS8000 from Optolab, Concondordia, Italy)
- vacuum drying oven (min. pressure 1 mbar; max. T: 200 °C; Binder WTB, Tuttlingen. Germany)
- balance (min.-max.: 0.001 - 220 g; model 770 from Kern & Sohn, Balingen, Germany)
- magnetic stirrer with heating plate and a vortexer for microtubes (model MR 3001 and REAX; both from Heidolph, Schwabach, Germany)
- two water baths (the model Unistat CC is freely programmable in range from -30 to 100 °C from Huber, Offenburg, Germany; the model M3 from Lauda can only heat; Lauda-Könighofen, Germany)
- ultrasonic bath (VWR International, Milano, Italy)

Further, two working benches (one with a water sink), two fridges and a separate freezer (- 20 °C), standard glassware, syringes and needles of different sizes, µ-pipettes (10 - 50 - 200 - 1000), as well as some standard solutions (e.g., chloroform, ethanol, methanol) and de-ionized water are available.

Figure 6.
Typical lab activity: Barbara Sartori loads the centrifuge (September 2003).

6. Available sample manipulations stages

1. General

Usually the sample is mounted onto the sample alignment stage which allows the user to place the sample into the beam with a precision of 5 µm (resolution: 1 µm). In Fig. 7 the ranges for vertical and horizontal alignment as well as the maximum dimensions of the sample holders are given. The maximum weight on the sample stage is limited to 10 kg. In case the envelope dimensions of a sophisticated sample station provided by the users are slightly larger than those given in Fig. 7, the user can ask the beamline responsible for a check up of his space requirements. If it does not fit at all to these specifications, user equipment can also be mounted directly onto the optical table, which allows much larger spatial dimensions.

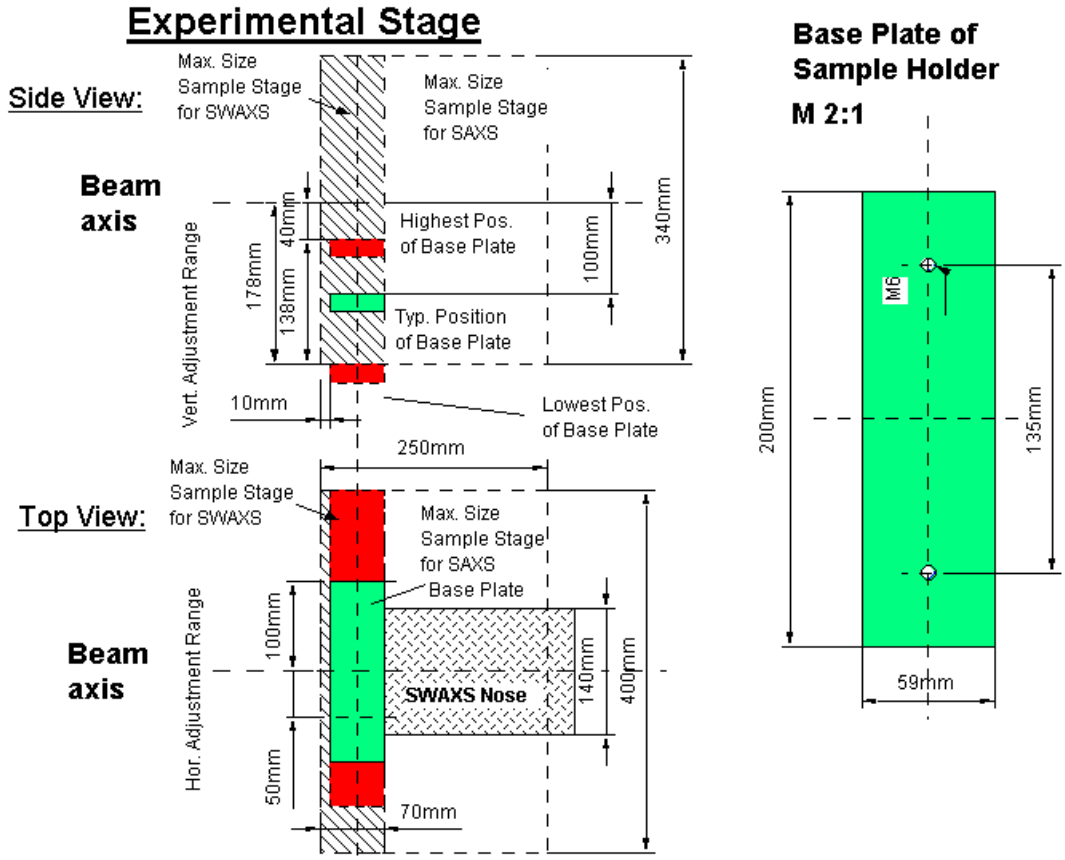

Figure 7. Maximum dimensions and alignment range of the sample holder to be mounted via a base-plate onto the standard alignment stage (left), and dimensions of the base-plate (right).

2. Sample holders

As standard equipment for liquid samples Paar capillaries (diameter: 1 and 2 mm) are used thermostated with the KHR (electrical heating) or KPR (Peltier heating/cooling) sample holders (Anton Paar, Graz, Austria). For use in these sample holders flow through capillaries and Gel holders are standard equipment. Temperature scans can be performed with KHR (25-300 °C) or KPR (-30-70 °C). Typically the precision and the stability of this systems is 0.1 °C. Additionally thermostats for temperature control or cooling proposes can be used at the

beamline (-40 - 200 °C). Helium and Nitrogen gas bottles are available at the beamline, for other gases please contact the beamline responsible.
Multiple-sample holders can be mounted onto the standard sample manipulator. At present holders are available for measuring in automatic mode up to 30 solid samples at ambient temperature or up to 4 liquid or gel samples in the temperature range 0 – 95 °C.

3. Online exhaust system

At the experimental station is available a custom-built fume cover and chemical exhaust system for toxic gases. Thus it is possible to e.g. study in-situ chemical reactions, during which toxic gases might develop.

4. Stopped Flow Apparatus

A commercial stopped flow apparatus (manufactured by Bio-Logic, Paris, France), especially designed for Synchrotron Radiation SAXS investigations of conformation changes of proteins, nucleic acids and macromolecules, is available. The instrument consists of a 4 syringe cell with 3 mixer modules manufactured by Bio-Logic. Each syringe is driven independently from the others by an individual stepping-motor, which allows a high versatility of the mixing sequence (flow-rate, flow duration, sequential mixing). For example, injection sequences using one or up to 4 syringes, unequal filling of syringes, variable mixing ratio, reaction intermediate ageing in three- or four-syringe mode etc.. The solution flow can be entirely software-controlled via stepping motors, and can stop in a fraction of a millisecond.

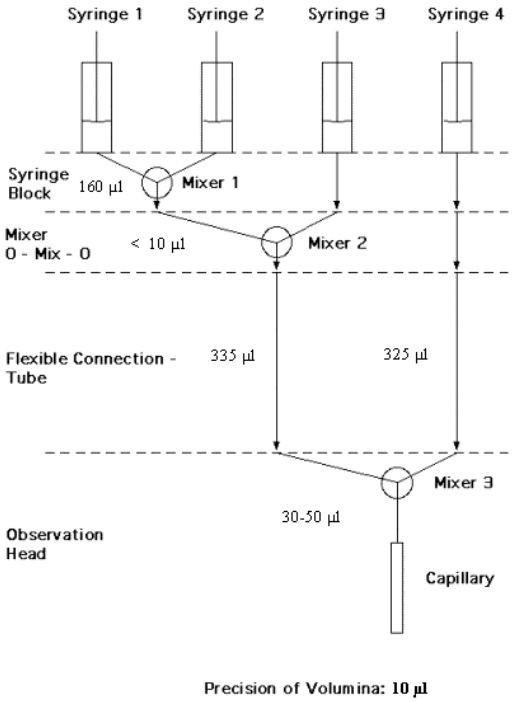

The software allows the set-up of the shot volumes of each of the 4 syringes in a certain time interval. Up to 20 mixing protocols can be programmed. Additionally macros for the repeated execution of individual frames can be defined. Furthermore, the input and output trigger accessible for user operation can be programmed. In the usual operation modus the start of rapid mixing sequence is triggered from our X-ray data-acquisition system (input trigger).

After the liquids have been rapidly mixed, they are filled within few ms into a 1 mm quartz capillary - situated in the X-ray beam- , which is thermostated with a water bath. Depending on the diffraction power of the sample time resolutions of up to 10 ms can be obtained.

Figure 8. Sketch of the stop flow system.

The main parameter of the system are:

- Thermostated quartz capillary (1 mm)
- Temperature stability 0.1 °C
- Total sample used per mixing cycle (shot volume): 100 µl
- Maximum 2θ angle of 45°
- Total Volume 8 ml
- Dead volume 550 µl
- Speed: 0.045 – 6 ml/s
- Duration of flow 1 ms to 9999 ms/Phase
- Dead time: 1 ms
- Reservoir volume: 10 ml each

Further information can be found at the webpage: http://www.bio-logic.fr/

5. Grazing Incidence Small Angle X-ray Scattering

Grazing incidence studies on solid samples, thin film samples or Langmuir-Blodget-films can be performed using a specially designed sample holder, which can be rotated around 2 axes transversal to the beam. Furthermore the sample can be aligned by translating it in both directions transversal to the beam. The precisions are 0.001 deg for the rotations and 5 µm for the translations. Usually the system is set to reflect the beam in the vertical direction. According to the required protocol and the actual assembly of the rotation stages ω, θ, 2θ and φ scans can be performed.

6. Temperature Gradient Cell

A temperature gradient cell for X-ray scattering investigations on the thermal behaviour of soft matter manybody-systems, such as in gels, dispersions and solutions, has been developed. Depending on the adjustment of the temperature gradient in the sample, on the focus size of the X-ray beam and on the translational scanning precision an averaged thermal resolution of a few thousands of a degree can be achieved.

7. IR-Laser T-Jump System for Time-Resolved X-ray Scattering on Aqueous Solutions and Dispersions

The Erbium-Glass Laser available at the SAXS-beamline (Dr. Rapp Optoelektronik, Hamburg, Germany) delivers a maximum of 4 J per 2ms pulse with a wavelength of 1.54 µm onto the sample. The laser-beam is guided by one prism onto the sample, which is filled in a glass capillary (1 or 2 mm in diameter) and Peltier or electronically thermostated in a metal sample holder (A. Paar, Graz, Austria). With a laser spotsize of maximal 7 mm in diameter a sample-volume of maximal 5.5 µl or 22 µl, respectively, is exposed to the laser-radiation. In a water-solutions/dispersions with an absorption coefficient of A = 6.5 cm^{-1} T-jumps up to 20 °C are possible.

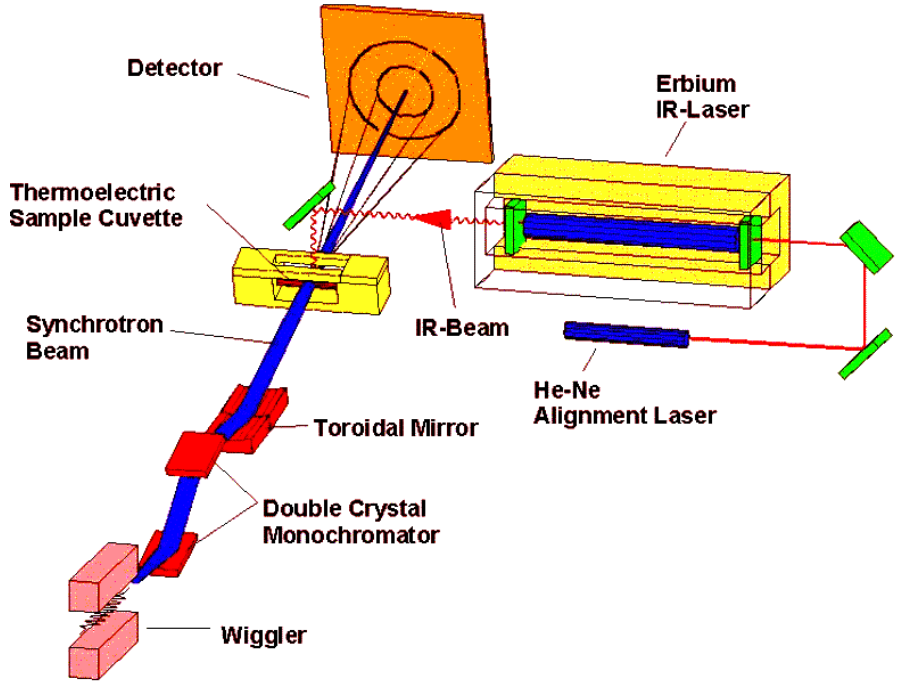

Figure 9. Sketch of the T-jump set-up.

8. High Pressure Cell System

SWAXS measurements of samples under pressure can be performed from 1 to 2500 bar, from 0 to 80 °C in the scattering angle region up to 30 degrees, both in the static or time-resolved mode, e.g. p-jump or p-scan, with a time-resolution down to the ms range. Precise pressure scans of any speed within a broad range (e.g. ca. 1.0 bar/s - 50 bar/s in the case of water as pressurising medium, and a typical sample volume) can be performed. Alternatively, dynamic processes can be studied in pressure-jump relaxation experiments with jump amplitudes up to 2.5 kbar/10ms in both directions (pressurising and depressurising jumps).
In most applications diamond windows of 0.75 mm thickness (each) are used. The transmission of one pair (entrance and exit window) is 0.1 at 8 keV, i.e. lower than 0.3, the value for the originally used 1.5 mm thick Be-windows. However the loss in intensity is more than compensated for by the considerably lower background scattering of diamond thus leading to higher q-resolution in the experiments.
The sample thickness can be 0.6-4.0 mm, with a volume of approximately 0.5-3 mm^3 completely irradiated by pin-hole collimated (< 1.0 mm diameter) X-rays.
The pressure cell system is flexible and can be built according to the needs of the particular experiment. Normally, a liquid (water, ethanol or octanol) is used as pressurising medium.

But in principle, also gaseous media can be employed as well. N_2 has been successfully tested, and measurements in supercritical CO_2 became frequent.
Beside bulk measurements on samples in transmission set-up, also grazing incidence experiments using silicon wafer with highly aligned samples on its surface inserted in the high-pressure cell have been carried out successfully.

9. Oxford Cryostream Cooler

The Cryostream cooler creates a cold environment only a few millimeters from the nozzle position. The temperature and the flow of the nitrogen gas stream is controlled and regulated by a Programmable Temperatur Controller based on an 'in stream' heater and a thermo-sensor before it passes out over the sample.

The system has been especially developed for X-ray crystallography to perform diffraction experiments on e.g. shock frozen bio-crystals. However, the programmable temperature controller allows further implication for SAXS-experiments, e.g., rapid temperature drops in solvents. The design of the Cryostream Cooler facilitates:

- Nitrogen stream temperatures from -190 to 100 °C
- Stability of 0.1 °C,
- Refill without any disturbance of the temperature at the sample
- Temperature ramps can easily be carried out remotely controlled with scan rates up 6 °C/min
- Individual temperature protocols can be cycled
- T-jumps in both directions can be performed by rapid transfer of the sample in a pre-cooled or -heated capillary using an fast syringe driver reaching a minimum temperature of -80 °C. Here, typical scan rates are about 15 °C/sec with a total process time in the order of 10 sec.

Further information can be found at the webpage: http://www.oxfordcryosystems.co.uk/

10. In-line Differential Scanning Calorimeter (DSC)

The in-line micro-calorimeter built by the group of Michel Ollivon (CNRS, Paris, France) allows to take simultaneously time-resolved synchrotron X-ray Diffraction as a function of the Temperature (XRDT) and high sensitivity DSC from the same same sample.
The microcalorimetry and XRDT scans can be performed at any heating rate comprised between 0.1 and 10 °C/min with a 0.01 °C temperature resolution in the range -30/+130 °C. However, maximum cooling rates are T dependent and 10°C/min rates cannot be sustained below 30°C since cooling efficiency is a temperature dependent process. Microcalorimetry scans can be recorded independently, and also simultaniously, of X-ray patterns. The microcalorimeter head can also be used as a temperature controlled sample-holder for X-ray measurements while not recording a microcalorimetry signal. Isothermal microcalorimetry is also possible when a time dependent thermal event such as meta-stable state relaxation or self-evolving reaction, is expected. The sample capillaries have a diameter of 1.5 mm and are filled over a length of 10 mm.

11. The 2D CCD-camera system

The CCD has a 115 mm diameter input phosphor screen made of a gadolinium oxysulphide polycrystalline layer. The screen is coupled by means of a fiber optic to the image intensifier. The image intensifier is coupled again with an additional taper to the CCD itself. The achieved spatial resolution of a pixel is 79 μm for the whole set-up.
The number of pixels is 1024 x 1024 and they can be pinned down to 2 x 2 and 4 x 4. The dynamic range of the CCD is 12 bit. The dark current of the CCD is in the order of 100 ADU (off-set) and the readout noise (read out speed: 10 MHz) is in the order of 6 ADU. (The CCD is cooled by multistage Peltier element for reducing the dark noise.) The intensifier gain is adjustable between 200 and 20000 photons full dynamic range. Typical readout times and exposure times are 150 ms and 100 ms, respectively. The readout times can be reduced down to 100 ms by using the pinning mode of the CCD. Between the frames additional wait times can be programmed e.g. for reducing the radiation damage in the sample or to extend the time for measuring long time processes.
For the external control a TTL trigger signal is provided (active low, when the CCD is accumulating an image), which is used to control the electromagnetic fast shutter of the beamline on one hand. On the other hand this signal can be used also to trigger processes as requested by the user.
The CCD is controlled by Image Pro+, which also includes non too sophisticated data treatment capabilities. The program is featuring a comprehensive set of functions, including:

- flat fielding/background corrections
- enhanced filters and FFT
- calibration utilities (spatial and intensity)
- segmentation and thresholding
- arithmetic logic operations
- various measurements, like surface, intensity, counts, profiles
- advanced macro management

The data are stored in 12 bit – TIFF format. At the present state up to 300 full images (1024 x 1024) can be recorded by the system, but a strict conservation of the timing sequence is maintained only for the first 15 - 17 frames until the RAM memory is full. Afterwards the images are stored in the virtual memory on the hard disk. At present a software development for the CCD readout system is under way to improve the stability of the readout cycles.
For the treatment of the 2D-data the programe FIT2D of Dr. Andy Hammersley is used. It allows to perform both interactive and 'batch' data processing. Furthermore FIT2D supports spatial, flat field and background corrections and elevated data-treatment like circular integration, segment integration and similar can be performed (see also the webpage: http://www.esrf.fr/computing /expg/subgroups/data_analysis/FIT2D/index.html).

12. Tension cell

Together with the external user group Schulze-Bauer/Holzapfel the research team constructed a general-purpose tension cell. This particular cell was designed for *in-situ* tensile testing with the particular feature that the sample could be completely immersed in a solvent (e.g. physiological solution), which is of particular interest for the blood vessel or collagen fiber testing. The sample container can be attached to a thermal bath to control the temperature in the range from 5 to 95 ºC. A screw with an appropriate opening for the passage of the X-ray beam can adjust the optical thickness of the sample container continuously and optimize the set-up for different sample geometries.
The fully remote controlled system allows to control not only the fiber extension from 0 to 50 mm, but also it records simultaneously the force signal in the range from 0 to 25 N and as an option the optically determined Video extensometer signal to measure the transversal contraction of the sample.

User Contributions

1. Materials Science

DIAMETER MEASUREMENTS OF SIZE-SELECTED THIOL ENCAPSULATED GOLD NANOPARTICLES BY SMALL ANGLE X-RAY SCATTERING

S. Carrara[1], S. Bernstorff[2], M. Di Pasquale[1], M.T. Parodi[1], D. Ricci[1] and E. Di Zitti[1]

1.) DI.B.E., Genoa University, Via Opera Pia 11a, 16145 Genova, Italia
2.) Sincrotrone Trieste, Strada Statale 14, km 163.5, 34012 Basovizza/Trieste, Italy

Nanoparticles with sizes below 10 nm may give rise to clear single electron phenomena at room temperature [1]. Nanoparticles from arachidic precursors show room temperature single electron conductivity [2] due to Coulomb blockade [3]. In addition to Coulomb blockade, semiconductor nanoparticles exhibit interesting optical properties. Charging of particles affects their absorption [4] and emission spectra [5], that are shifted according to the particle size. Gold nanoparticles stabilized by thiol encapsulation have been synthesized obtaining highly crystalline metallic clusters with diameters ranging from 10 nm down to 1 nm [6]. By using these nanoparticles, it has been possible to produce a single electron junction using a 1D piezo-mover [7], but the method is not exploitable for manufacturing electronic devices. On the other hand, other techniques are now available to fabricate nanoelectronics devices. By using sculpting or printing techniques, it is possible to make nanocontacts [8], namely electrode pairs separated by nanometric gaps. For example, experiments employing high resolution lithography at a Synchrotron radiation source and aiming at the fabrication of nanocontacts are still running at the beam-line Lilit in Elettra [9,10]. However, in order to obtain a device working at room temperature, the particle capacitance needs to be of the order of 10^{-18} F, thus requiring a diameter below 5 nm. Moreover, a little variation of nanoparticle size results in a huge change in the device functioning. Therefore, it became crucial to know accurately the nanoparticle size distribution. Using vapour phase selection and gel chromatography, the possibility to obtain size-selected gold nanoparticles [11, 12] was shown, and the particle size distribution was painstakingly established using Transmission Electron Microscopy (TEM). TEM acquires local images in a nm^2 area. On the other hand, Small Angle X-ray Scattering (SAXS) is a well established technique for the estimation of the gyration radius of scattering centres [13,14] and it averages on a mm^2 area. Therefore, accurate SAXS experiments have been performed in order to determine with high precision the size of the particles previously fabricated by chemical synthesis. This more accurate knowledge is required in order to have the possibility to tune the working conditions of the device on the basis of the particle properties. In fact, it often happens that the application of published chemical procedures for the fabrication of gold nanoparticles does not return mono-dispersed samples (see figure 1A). The same could happen with commercially available gold nanoparticle solutions (figure 1B). In fact, also TEM investigation, although a local measurement, may present images with nanoparticles with different radii (figure 2A). Further size-selection procedures, described elsewhere [11,12], return samples with nanoparticles mono-disperse in radius, as shown in figure 2B. In fact, SAXS spectra acquired on such samples do not show multiple linear behaviours in logarithmic plots (Figure 3A). The histogram calculated on a collection of TEM images confirms the mono-dispersion of the particle radii around a well defined value, and shows a further positive effect of the size selection, i.e. the shift of the peak towards smaller radii (Figure 3B). These results demonstrate the necessity to perform size-selection on the as produced gold nanoparticles in order to obtain mono-disperse samples necessary for the tuning of the nanostructured devices. Moreover, the aim of this

research combined with the other already running at Elettra Synchrotron [9] is to develop a precise procedure to fabricate nanostructures based on size-selected nanoparticles and nanocontacts fabricated by high resolution lithography in order to obtain nanoelectronic or nano-photonic devices useful for single electron computing. Both topics are strategically positioned in the state of the art research in nano-electronics, field within which a strong effort is made to obtain single electron transistors to build logical circuits [15] or biosensors with improved performance [16].

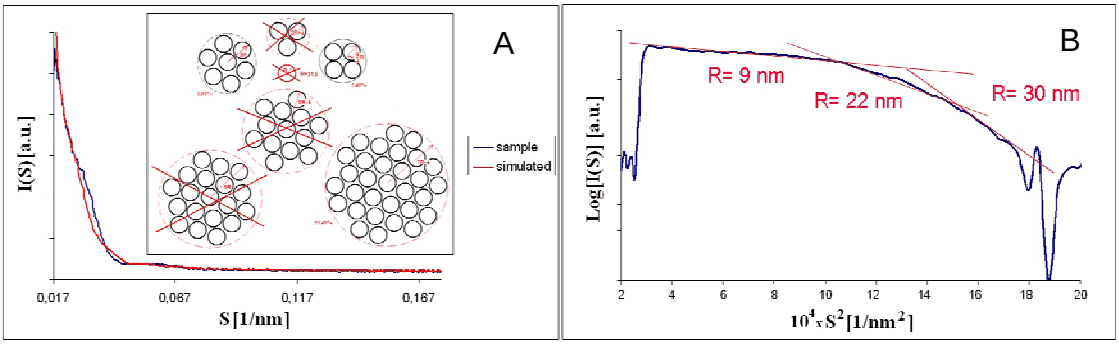

Figure 1. SAXS spectra acquired on a sample constituted by gold nanoparticles in ethanol. In this case the gold nanoparticles were partially aggregated (A) or they are different in radii (B).

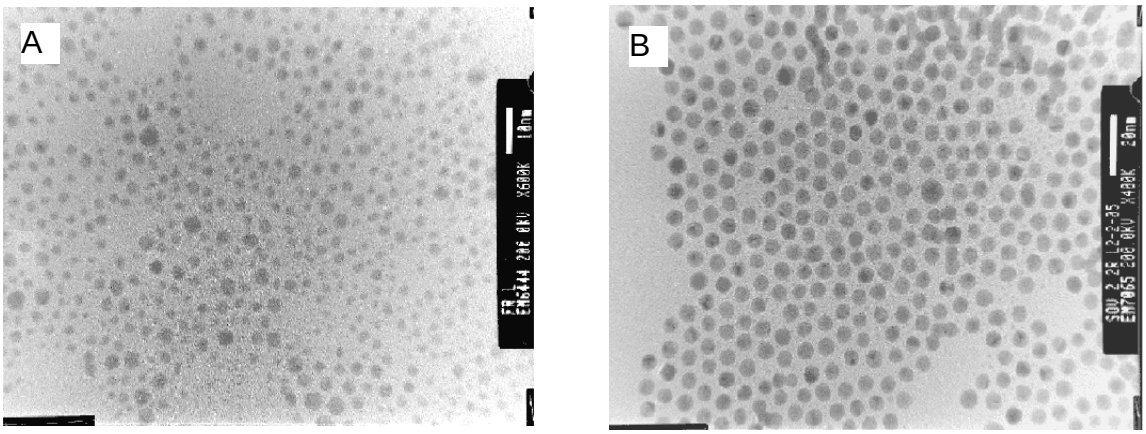

Figure 2. TEM images acquired on gold nanoparticle thin films formed by solution casting directly on TEM grids. In the first case (A) the sample is constituted by particles having different radii. In the second (B) the sample is constituted by mono-disperse particles.

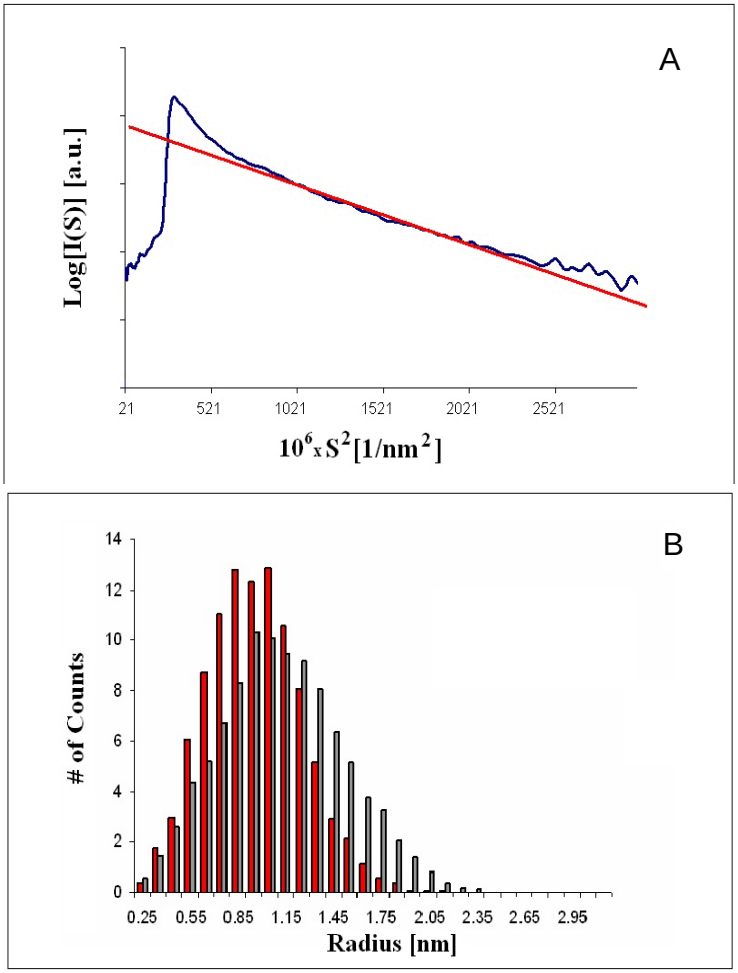

Figure 3. SAXS spectrum acquired on a sample constituted by mono-dispersed gold nanoparticles in ethanol (A). The histogram calculated on a TEM image (B) shows the mono-dispersion of the particle radii around a well defined value (green bars), and the further effect of the distribution shift towards smaller radii due to the size selection (red bars).

References:

[1] Carrara S., Erokhin V., Facci P., Nicolini C. In "Nanoparticle in Solid and Solutions", NATO ASI Series Vol. 18, Fendler J. & Dékány I. (Eds), Kluwer, Dordrecht (NL), pp. 497-503, 1996.
[2] Erokhin V., Facci P., Carrara S., Nicolini C. J.Phys.D: Appl. Phys. 28, 1-5, 1995.
[3] Erokhin V, Carrara S., Bernstorff S., Amenitsch H., Nicolini C. Nanotechnology, 9, 158-161, 1998.
[4] Peter, L.M., D.J. Riley, R.I. Wielgosz, P.A. Snow, R.V. Penty, I.H. White, and E.A. Meulenkamp. Thin Solid Films,. 276, 123-129, 1996.
[5] Hickey, S.G., D.J. Riley, and E.J. Tull. J. Phys. Chem. B, 104, 7623-7626, 2000.
[6] Brust, M.et al.. J. Chem. Soc., Chem. Commun., 801-804, 1994
[7] Facci P., Erokhin V., Carrara S., Nicolini C. Proc. Nat. Acad. Sci. (USA), 93, 10556-10559, 1996
[8] Carrara S, Riley J., Stura E., Bavastrello V., Nicolini C. Sensors and Actuators B:Chemical, B105, 542-548, 2005
[9] S.Carrara: "Nanocontacts Fabrication for addressing single-molecules", Project running at the LILIT beamline at ELETTRA Synchrotron, project code 2003758.
[10] S. Carrara, D.Ricci, E.Di Zitti, E. Di Fabrizio M. Altissimo, M. Tormen. Materials Letters, 2006, in press.
[11] F. Sbrana, M.T. Parodi, D. Ricci, E. Di Zitti, C.Natale, S Thea. Materials Science and Engineering B, 96, 193-198, 2002
[12] F. Sbrana, M.T. Parodi, D. Ricci, E. Di Zitti. Materials Science and Engineering C, 22, 187-191, 2002
[13] Feigin L A and Svergun D I "Structures Analysis by Small-angle X-ray and Neutron Scattering", New York, 1987, Plenum Press
[14] S.Carrara: "Structural characterization of supramulecular heterostructures" Chapter in Manoj Kumar Ram (Ed) "Supramolecular engineering of conducting material", Research Signpost, Kerala, 2005.
[15] F.Nakajima, Y.Miyoshi, J.Motoshisa, T.Fukui. Appl. Phys. Lett. 83, 2680-2682, 2003
[16] V.V. Shumyantseva et al.. Biosensors & Bioelectronics, 21, 217-222, 2005

GERMANIUM QUANTUM DOTS IN MULTYLAYERS PRODUCED BY MAGNETRON SPUTTERING

U.V. Desnica[1], P. Dubcek[1], K. Salamon[2], I.D. Desnica-Frankovic[1], M. Buljan[1]and S. Bernstorff[3]

1.) R. Boskovic Institute, Bijenicka 54, 10000 Zagreb, Croatia
2.) Institute of Physics, 10000 Zagreb, Croatia
3.) Sincrotrone Trieste, SS 14 km163,5, 34012 Basovizza, Italy

When the size of a crystal reduces to the nanometer range (nanocrystals or quantum dots, QDs) the quantum confinement effects start to dominate, resulting in changed basic properties of the material. Semiconductor materials in the form of QDs display significant dependence of electronic, optical and other properties on the size of nanoparticles [1-3]. The particularly strong dependence of the band-gap of nano-Ge on the size of Ge-QDs [4] enables tunability of the nano-Ge band-gap over the considerable part of visible light wavelength-range.This opens a large number of potential applications in semiconductor and other industries.
This Report presents results obtained by Grazing Incidence Small Angle X-ray Scattering (GISAXS) technique in studying the synthesis and properties of Ge nanoparticles in SiO2 after co-deposition of Ge and SiO2 with magnetron sputtering followed by thermal treatment.

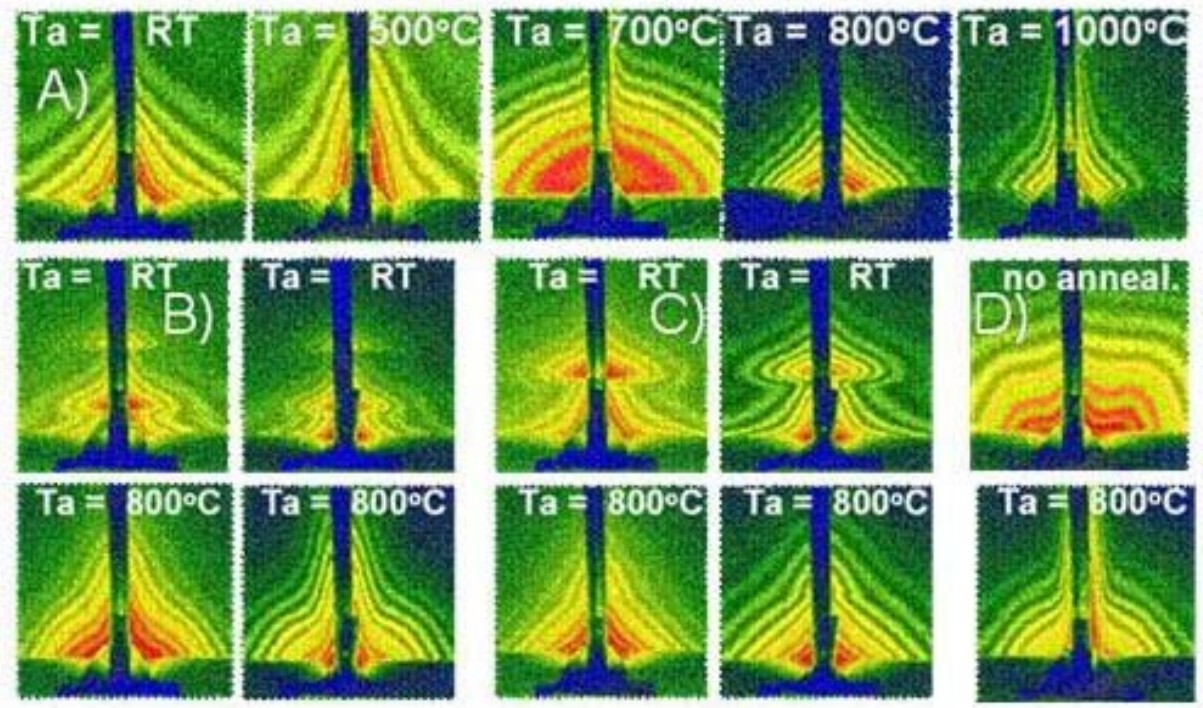

Figure 1. 2 D GISAXS patterns of Ge+SiO2 (40%:60% mol fraction) magnetron sputtering co-deposited layers: **A)** First row: thick (Ge+SiO2) films, **B)**: (Ge+SiO2)/SiO2 multi-layers (8+8 nm thick) deposited on SiO2 substrate (B left) or Si substrate (B, right).each bi-layer comprises of: 8 nm (Ge+SiO2) and 8 nm SiO2. **C**): Same as B), but the thickness of Ge+SiO2 was 4 nm. **D)**: uniform (Ge+SiO2) films deposited on SiO2 substrate, but deposited at 700^{o} C.

GISAXS, the most important finding (Figure 1):
Uniform films (part A of Fig. 1.): Spherical nanocrystals (QDs) of cca 3 nm Guinier radius are formed after annealing to 700 ^{o}C. The average size of QDs almost doubles after annealing at 800 ^{o}C, and further more after Ta = 1000 ^{o}C.

Multi-layered films (B and C): the as-deposited 2D GISAXS patterns clearly show the bi-layered structure of the film: The shape of the pattern is dominated by the thickness of the Ge-containing layer, but particles are not formed jet. Annealing causes both the forming of spherical QDs and the gradual disordering/mixing of the layers.
In both uniform and layered films the size of Ge QDs were found to be strongly dependent on the annealing temperature. The best Ta for the formation of the spherical Ge-QDs is in the Ta = 700 - 800 ^{o}C range. For a given Ta the average size of QDs is related to the thickness of the Ge-SiO2 co-sputtered layer. The deposition on either SiO2 or Si substrate yielded very similar patterns as well as similar changes with annealing.
The **deposition on the heated substrate** (Td=700 ^{o}C) (D) resulted in the formation of non-spherical, faceted nanoparticles in the uniform films. In layered films, however, besides formation of QDs, the intermixing of (Ge+SiO2) and SiO2 layers occurs to considerable degree already in as-deposited samples.

Summary of results on same samples with other methods (not shown here, please see ExpRep2005129 experimental report in Elettra Reports):
Rutherford-Back-Scattering (RBS) most important findings: For samples deposited at RT (Td=RT)**,** uniform thickness**:** all sputtered Ge atoms are successfully deposited. Outdifussion og Ge strats after Ta = 800 ^{o}C, (10 %) and is very significant after Ta =1000 ^{o}C (about 30%). For Td= 700 ^{o}C, the deposition rate is dramatically lower, resulting in thinner film with less Ge content.
Raman, most important findings: Already in as-deposited samples Ge-atoms cluster into amorphous Ge (a-Ge) nanoparticles. After annealing at Ta = 700 ^{o}C or above, a-Ge crystallizes into Ge QDs. Findings are very similar to those obtained from samples where SiO2 substrate was implanted with high-dose of Ge atoms.
This work was a successful continuation of previous work in SAXS line in Elettra on semiconductor nanoparticles, which only in y. 2003-5 results in 7 CC papers (Refs. [5]- [11]; several other manuscripts are in the process of refereeing). In these papers we have also demonstrate that we have developed an analytical methodology to obtain unique characterization (size, shape, interparticle distance, size distribution…) of such QDs from the GISAXS spectra taken either with the two-dimensional (2D) CCD detector, or 1D gas detector.

References:

[1] W. Scorupa, L. Rebohle, T. Gebel. Appl. Phys. A 76 (2003) 1049
[2] A. Meldrum, R.F. Haglund, Jr., L.A. Boatner, C.W. White. Advanced Materials 13 (2001) 1431
[3] J.D. Budai, C.W. White, S.P. Wiothrow, M.F. Chisholm, J. Zhu, R.A. Zuhr. Nature 390 (1997) 384
[4] C. Boested, T.van Buuren, T.M. Willey, N. Franco, L.J. Terminello,C.Heske, T.Moeller. Apl. Phys. Lett., 84 (2004) 4056-58
[5] M. Buljan, K. Salamon, P. Dubcek, S. Bernstorff, I.D. Desnica-Frankovic, O. Milat and U.V. Desnica. Vacuum, 71 (2003) 65-70
[6] P. Dubcek, U.V. Desnica, I.D. Desnica-Frankovic, S. Bernstorff, A. Nucl. Instr. Methods Phys. Res. B, 200 (2003) 138
[7] I.D. Desnica-Frankovic, U.V. Desnica, P. Dubcek, M. Buljan, S. Bernstorff, H. Karl, I. Großhans, and B. Stritzker J. Appl. Cryst., 36 (2003) 439-442
[8] U.V. Desnica, P. Dubcek, I.D. Desnica-Frankovic, M. Buljan, K. Salamon, O. Milat, S. Bernstorff, and C.W. White. Nucl. Instr. Methods Phys. Res. B, 200 (2003) 191-195 (2003)
[9] U.V. Desnica, P. Dubcek, I.D. Desnica-Frankovic, M. Buljan, S. Bernstorff and S.W. White. J. Appl. Cryst. 36, 443-446 (2003)
[10] U.V. Desnica, M. Buljan, I.D. Desnica-Frankovic, P. Dubcek, S. Bernstorff, M. Ivanda, H. Zorc. Nucl. Instr. Methods Phys. Res. B 216 (2004) 407-413
[11] U.V. Desnica, P. Dubcek, K. Salamon, I.D. Desnica-Frankovic, M. Buljan, S. Bernstorff, U. Serincan, R. Turan. Nucl. Instr. Methods Phys. Res. B, 238 (2005) 272-275

THERMAL ANNEALING OF COLLOIDAL NANOPARTICLE ARRAYS

J. I. Flege[1], B. Gehl[2], Th. Schmidt[1], V. Aleksandrovic[3], T. Clausen[1], S. Bernstorff[4], H. Weller[3], M. Bäumer[2] and J. Falta[1]

1.) Institute of Solid State Physics, University of Bremen, Otto-Hahn-Allee 1, 28359 Bremen, Germany
2.) Institute of Applied and Physical Chemistry, University of Bremen, Leobener Strasse, 28359 Bremen, Germany
3.) Institute of Physical Chemistry, University of Hamburg, Grindelallee 117, 20146 Hamburg, Germany
4.) Sincrotrone Trieste, Strada Statale 14, km 163.5, 34012 Basovizza/Trieste, Italy

The preparation of ultra-thin colloidal nanoparticle films has attracted considerable interest from science and industry due to their giant potential for future applications, e. g., in storage media, heterogeneous catalysis, and bio-medicine. Although quite some success has been reached regarding the nanoparticle synthesis for a wide range of possible materials [1], the nanoparticles are surrounded by a protective ligand shell. While these organic ligands may be of advantage in the preparation of ordered nanoparticle arrays, they inhibit, e.g., their powerful catalytic capabilities. Hence, it is obvious that following the film preparation the passivating ligands have to be removed reliably and non-destructively, i.e. without significant modification of the structural properties of the nanoparticle film. These issues were addressed by applying grazing-incidence small-angle x-ray scattering (GISAXS) and scanning electron microscopy (SEM).

$CoPt_3$ nanoparticles of well-defined size and shape were obtained by hot metal-organic synthesis as described previously [2]. Sequentially, the nanoparticles were spin-coated onto the SiO_2 substrate wafer at room temperature, which results in the formation of hexagonally ordered patches of nanoparticles. As the simplest approach to stripping the ligand shell, the $CoPt_3$ nanoparticle films employed here were thermally heated under ambient conditions to temperatures varied step-wise up to 700°C. For each sample, SEM and GISAXS data were recorded prior and after the annealing step. For efficient sample characterization, two-dimensional (2D) GISAXS patterns were recorded using a CCD camera (Photonic Science, 1024×1024 pixels) and blanking out the intense specularly reflected beam by virtue of an aluminum attenuator of appropriate thickness.

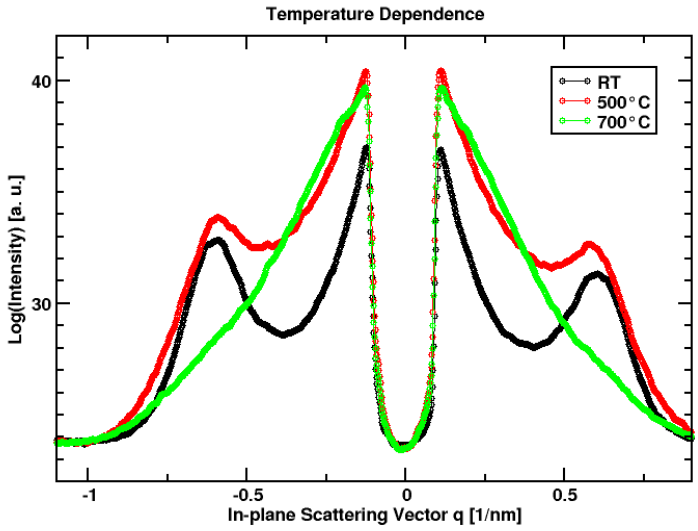

Figure 1. One-dimensional in-plane x-ray scattering data of spin-coated $CoPt_3$ nanoparticle films on SiO_2 after annealing.

Figure 1 shows one-dimensional GISAXS profiles recorded for samples heated to 500°C and 700°C for one hour, respectively, along with the reference scattering signal obtained for the as-prepared nanoparticle film (marked as "room temperature"). These curves have been extracted from the 2D scattering pattern by taking horizontal in-plane cuts through the vertical scattering rods at the maximum intensity of the scattering signal, i.e. at the vertical scattering component which corresponds to the Yoneda peak. It is clearly evident that the strong scattering features at $q_{par} = \pm 0.6$ nm^{-1} are considerably less pronounced after annealing at 500°C, and that they are gone completely at 700°C. However, annealing to temperatures between room temperature and 400°C did not induce any significant changes in the GISAXS pattern.

In Figure 2, the corresponding SEM images for heating up to 500°C (a) and 700°C (b) are displayed. At 500°C, a significant fraction of the film has already re-organized into a more condensed phase that exhibits slightly contracted inter-particle distances (see left side of Figure 2(a)) which suggests an at least partially removed ligand shell. However, the remaining nanoparticle layer still seems quite undisturbed (right side of Figure 2(a)). Annealing to 700°C, however, induces frequent merging of the nanoparticles, which results in a significantly changed film morphology, and hence a complete loss of the scattering contrast. This may be attributed to an extended oxidation and melting process of the nanoparticles which leads to the formation of large Co-Pt islands. This interpretation is underlined by the observed increase in the diffuse scattering intensity in the proximity of the specular scattering rod (Figure 1).

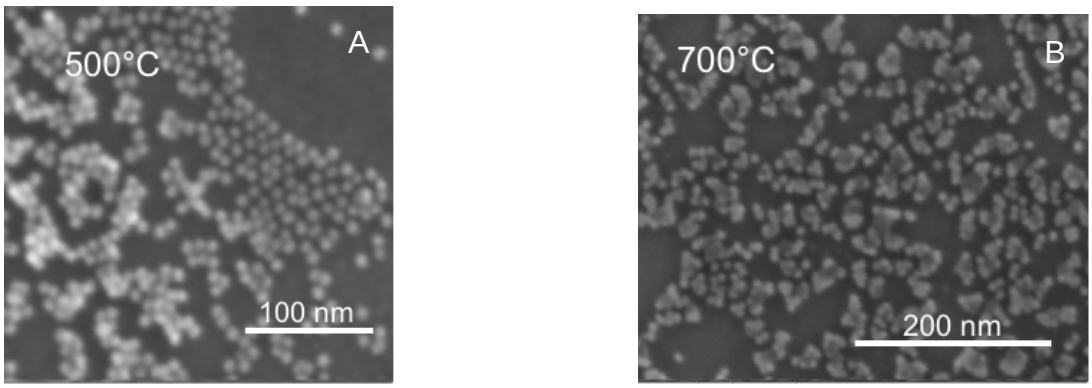

Figure 2. Scanning electron microscopy images taken of $CoPt_3$ nanoparticle assemblies after thermal annealing to 500°C (a) and 700°C (b).

In conclusion, our combined GISAXS and SEM experiments indicate annealing temperatures below 500°C for ligand removal to avoid structural changes of the nanoparticle film. Nevertheless, the effectiveness of this approach will have to be confirmed by other methods, e.g. in-situ x-ray photoelectron spectroscopy, to prove the successful removal of the ligand shell.

References:

[1] G. Schmid (Ed.); Nanoparticles; (2004)

[2] E. V. Shevchenko, D. V. Talapin, H. Schnablegger, A. Kornowski, Study of Nucleation and Growth in the Organometallic Synthesis of Magnetic Alloy Nanocrystals: The Role of Nucleation Rate in Size Control of CoPt3 Nanocrystals, J. Am. Chem. Soc. 125, 9090-9101 (2003)

THE STRUCTURAL ORDERING OF THIN SILICON FILMS AT THE AMORPHOUS TO NANO-CRYSTALLINE PHASE TRANSITION BY GISAXS AND RAMAN SPECTROSCOPY

D. Gracin[1], K. Juraic[1], A. Gajovic[1], P. Dubcek[1], C. Devilee[2], H.J. Muffler[2], W.J. Soppe[2] and S. Bernstorff[3]

1.) Rudjer Boskovic Institute, 10000 Zagreb, Bijenicka 54, Croatia
2.) ECN-Solar Energy, P.O. Box 1, 1755 ZG Petten, The Netherlands
3.) Sincrotrone Trieste, SS 14, km 163.5, Basovizza (TS), Italy

The structural ordering was studied on thin silicon films deposited by the PECVD method using microwave (MW) and standard 13,6 MHz (RF) gas discharge in silane gas diluted by hydrogen. The dilution was varied from low values that produce amorphous layers up to the high dilution that leads to a high degree of crystalline fraction. The average crystallinity and average crystal sizes in the samples were estimated by Raman spectroscopy. The ratio of the areas under corresponding TO phonon peaks in Raman, taken as a ratio between crystal and amorphous fraction, varied between 0 and 70%. The crystalline TO peak positions varied between 514 and 521 cm^{-1} which corresponds to a crystalline size between 3 and 9 nm. However, the line-width was broad suggesting also the existence of smaller and larger crystals.

The average density of samples was estimated upon measuring the optical properties and by using effective medium approximation theory (EMA) [1]. According to EMA, the fact that the values of the long wavelength refraction index were lower than the high density "voids free" samples (Fig.1), indicates that the samples are porous. The porosity was larger for samples with a higher degree of crystallinity, especially for MW PECVD deposited samples (Fig.1).

The more detailed analysis of nano-ordering of deposited films was done by GISAXS. The dominant contribution to the GISAXS signal for amorphous samples came from the surface roughness while for structures close to the amorphous to crystalline transition, the contribution of “particles” from the bulk of the material became clearly visible and with the appearance of the first nano-crystals, the signal originating from “particles” started to dominate. Since the samples are porous, the "particles" are most probably voids. Those voids, with sizes between 2 and 12 nm, in MWPECVD deposited samples showed pronounced anisotropy (Fig.2) while for the RFPECVD samples the GISAXS signals were more spherically symmetric (Fig.3). The rod-like voids and the fact that the voids are larger closer to the surface indicate columnar growth and non-homogeneous samples which is characteristic for too fast grown samples. For MWPECVD samples this appeared at higher temperatures (Fig.2) while for RFPECVD samples it was typical for a high RF power (Fig.3). A more detailed study of correlation between growth conditions and GISAXS nanostructure is expected in near future.

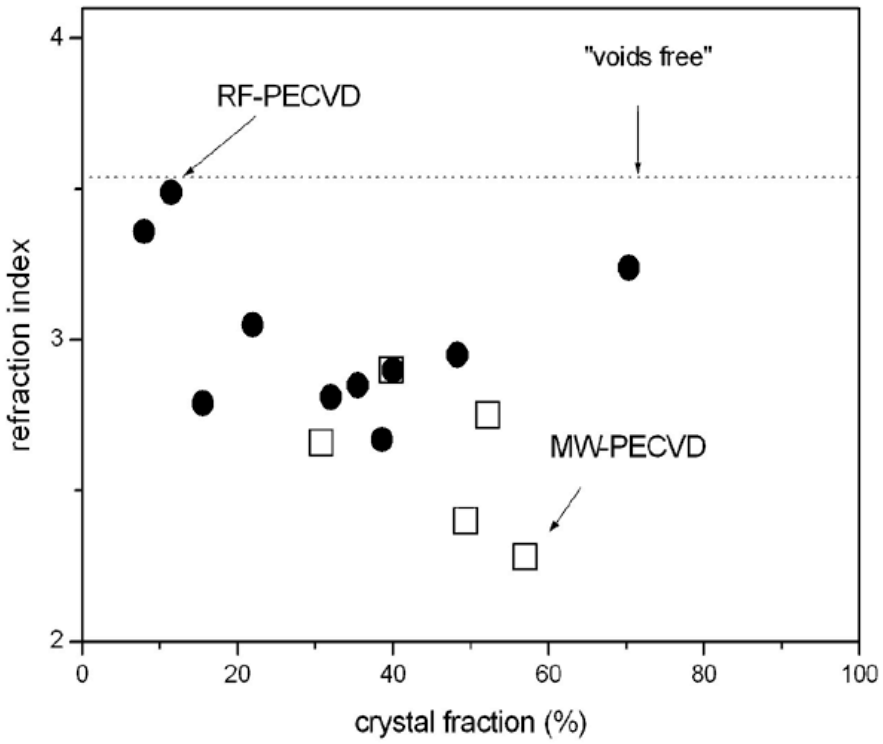

Figure 1. Long wavelength refraction index versus degree of crystallinity (crystal fraction) for a series of amorphous-nanocrystalline samples deposited by MW and RF PECVD methods.

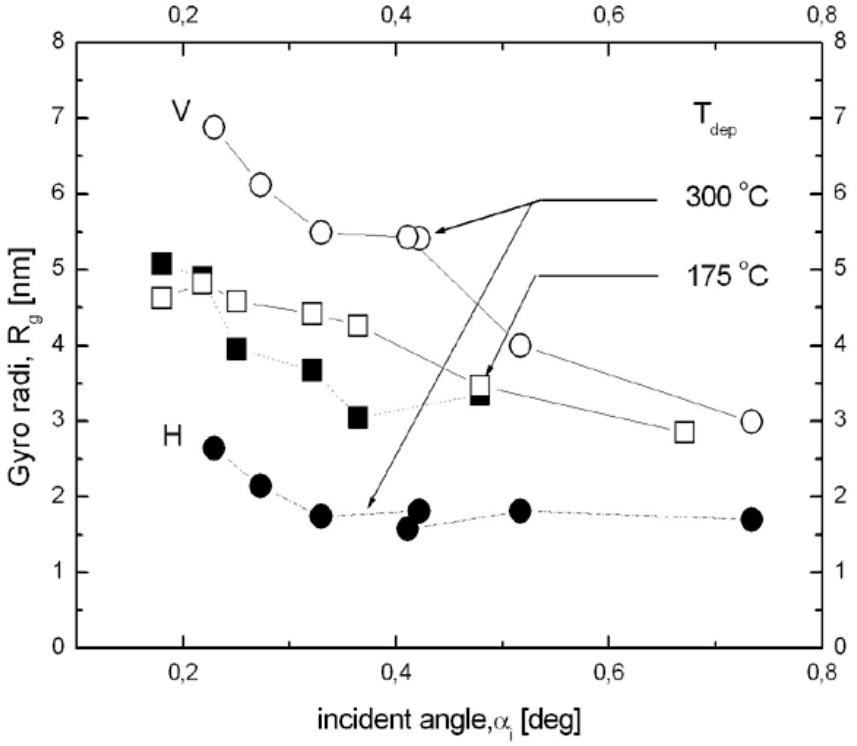

Figure 2. Gyro radius versus incident angle for samples deposited by MW PECVD at a dilution of 5% SiH_4 in the working gas and at two different substrate temperatures; the open symbols are for the direction perpendicular to the surface (V) while the filled symbols are for the direction parallel to surface (H).

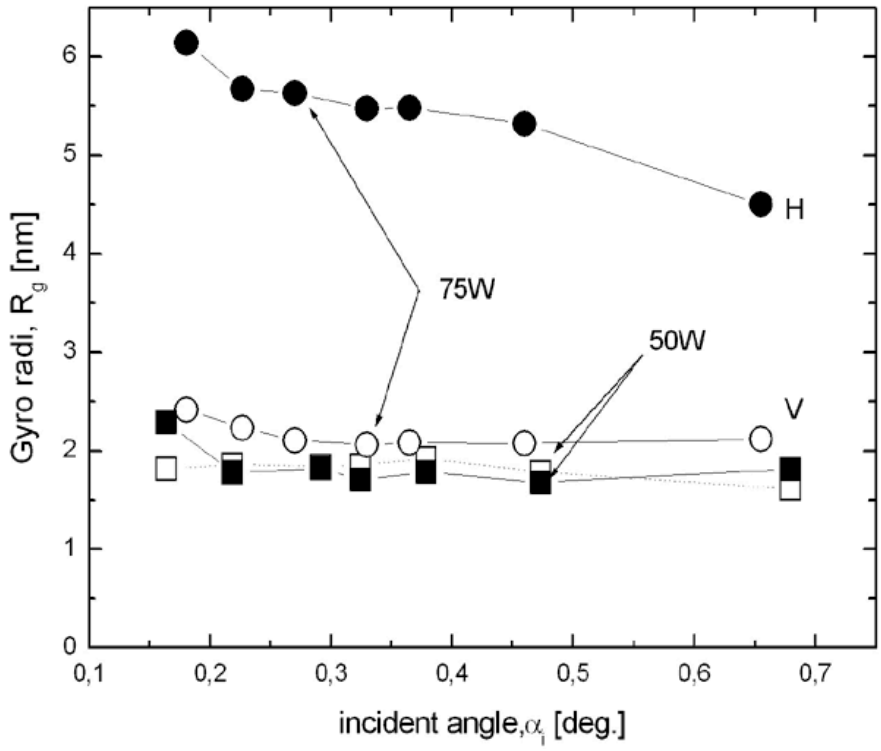

Figure 3. Gyro radius for samples deposited at 6% of SiH_4 in the working gas by RF PECVD at two different RF powers, 50W (rectangles) and 75W (circles); the open symbols are for the vertical direction (V) while the filled ones are for the direction parallel to the surface (H)

References:

[1] D. Gracin, K.. Juraic and I. Bogdanovic Radovic, Vacuum. **80** 146-150 (2005)

DEPTH RESOLVED IN-PLANE DIFFRACTION STUDIES OF MELTING OF LANGMUIR-BLODGETT FILMS USING X-RAY STANDING WAVES

A. Gupta[1], P. Rajput[1], D. Kumar[1], S. Bernstorff[2] and H. Amenitsch[3]

1.) UGC-DAE Consortium for Scientific Research, Khandwa Road, Indore, India
2.) Sincrotrone Trieste, SS 14, Km 163.5, I-34012 Basovizza, Trieste, Italy
3.) Institute for Biophysics and Nanosystems Research, Austrian Academy of Sciences, A-8010 Graz, Austria

The objective of the proposal is to study melting of cadmium arachidate (CdA) Langmuir-Blodgett (LB) multilayers using depth resolved in-plane diffraction under x-ray standing wave condition. The structure of multilayer is Si substrate/ Ni (70 nm) / CdA (13 monolayers). X-ray standing waves are generated through total external reflection from a Ni underlayer (at an angle of incidence below the critical angle of Ni). In-plane diffraction measurement done under such condition would provide selective information from the region of antinodes. By varying the angle of incidence the position of an antinode can be moved along the z-direction, thus providing information about the in-plane structure as a function of depth. It may be noted that, while x-ray standing waves have been used in literature for doing depth resolved fluorescence and EAXS studies [1,2], the technique has not yet been used for depth resolved in-plane diffraction measurements.

X-rays of 8 keV were used for simultaneous measurement of reflectivity (using a 1D detector) and in-plane diffraction (using a CCD camera) at SAXS beam line of Elettra synchrotron. Figure 1 gives the x-ray reflectivity of the above multilayer as well as the CdA (13 monolayers) film on glass substrate. The LB film on glass exhibits well-defined Bragg peaks due to multilayer periodicity. In case of multilayer with Ni underlayer, the Bragg peaks got obscured due to strong reflection from Ni layer. Temperature dependent in-plane diffraction measurements were done at two different angles of incident roughly corresponding to the situation in which either the first antinodes (Angle A) or successive node (Angle B) coincides with the surface of the multilayer. In the first case the information is obtained preferentially from the surface region while in the second case it is obtained from the center of the layer. Figure 2 gives the temperature dependent diffraction pattern corresponding to the angle A. Two strong peaks are observed at q_x = 1.56 Å^{-1} and 1.68 Å^{-1} corresponding to $(01+1\bar{1})$ and (10) reflections respectively [3]. This suggests that inconformity with earlier works [3], the in-plane structure is distorted hexagonal lattice.

One may note that with increasing temperature both the peaks shift to lower angles due to thermal expansion. However the peak corresponding to (10) reflection shifts at a faster rate. The distortion of the lattice from regular hexagonal one can be quantified in terms of parameter $\Delta\gamma = 60°-\gamma$, where $\gamma = \cos^{-1}\frac{q_2}{2q_1}$, q_1 and q_2 being the positions of the $(01+1\bar{1})$ and (10) reflections respectively. Figure 3 gives the parameter $\Delta\gamma$ as a function of temperature at the two angles. In both the cases, initially $\Delta\gamma$ does not change much with temperature. However around 360 K it suddenly drops down, showing rather abrupt decrease in the distortion. Figure 4 gives the width of diffraction peaks at the two angles. While the width of the peak corresponding to $(01+1\bar{1})$ reflection remains almost constant with temperature, that of (10) reflection exhibits substantial variation with temperature. The line width will have two possible contributions: i) because of finite domain size, and ii) due to a distribution in the angle γ. Since a change in domain size should effect the width of both peaks, the fact that the width of first peak is almost independent of temperature suggest that the contribution of the

variation in domain size to the width is negligible. Therefore, the variation in the width of the second peak is mainly due to distribution in the angle γ. From figure 4 one may note that in the surface region (corresponding to angle A) the distribution in γ increase rather rapidly with temperature as compare to that in the center of the multilayer (corresponding to angle B).
In conclusion, present studies shows that in-plane diffraction under standing wave condition can be used to get depth resolved information about structural transformation occurring in CdA LB multilayer as a function of temperature. The melting behaviour in the surface region and in the bulk is qualitatively very similar. However surface region exhibits significantly more disorder as compare to the bulk as evidence by larger increase in the width of (10) reflection as a function of temperature.

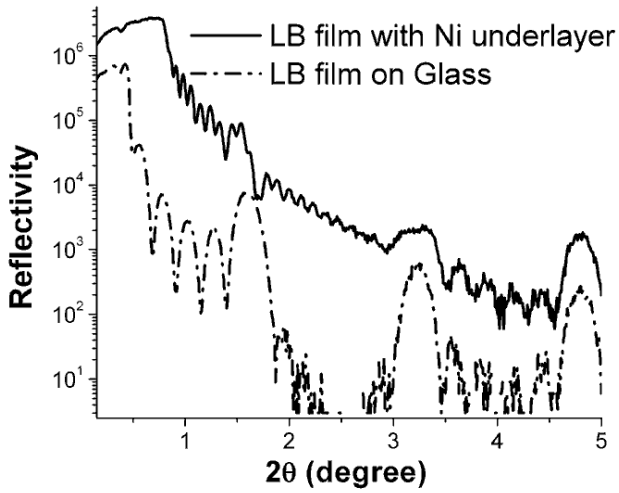

Figure 1. X-ray reflectivity of CdA (13 monolayers) on Glass and with Ni underlayer.

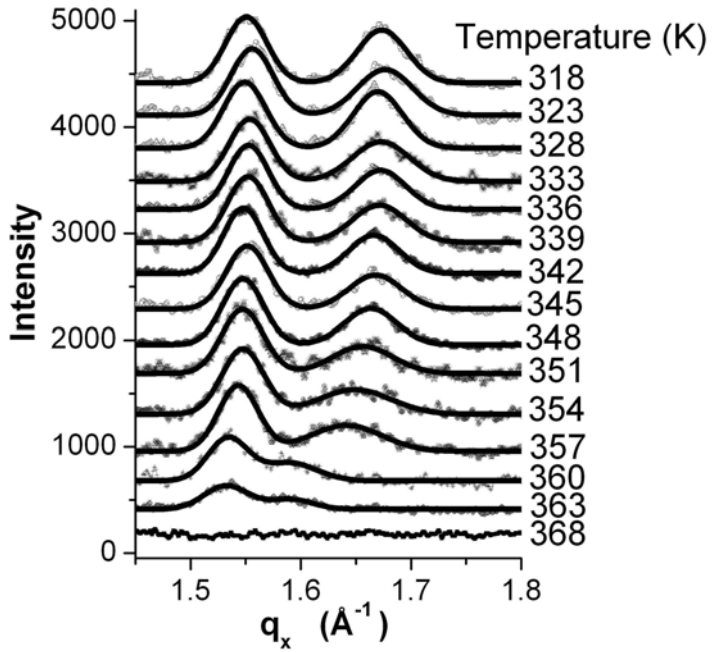

Figure 2. The diffraction pattern of CdA multilayer with Ni underlayer at angle B, as a function of temperature.

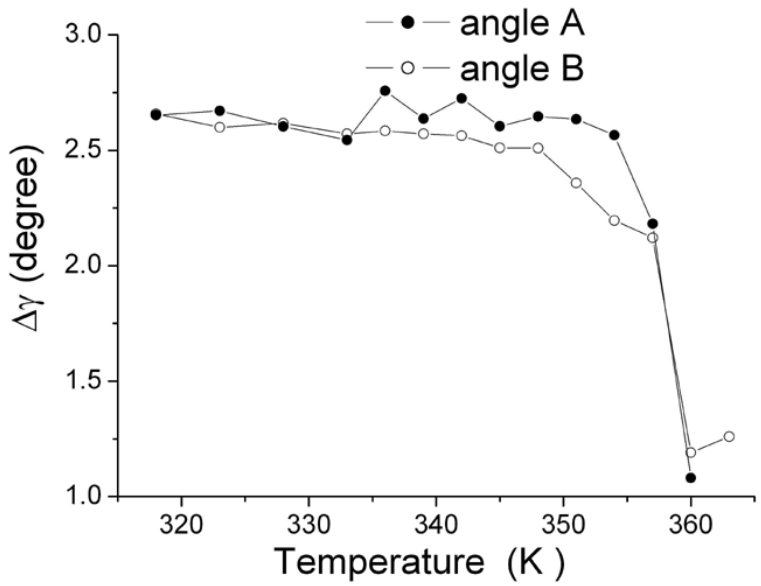

Figure 3. Parameter Δγ as a function of temperature at the two angles.

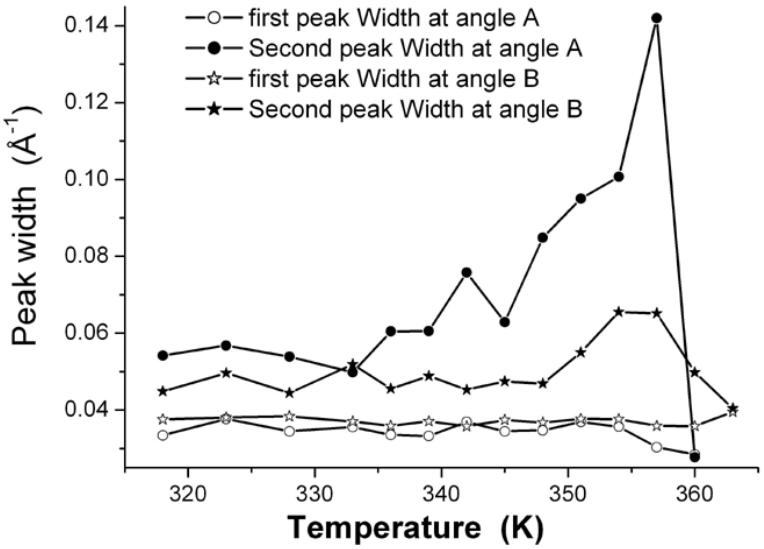

Figure 4. The width of diffraction peaks at the two angles.

References:

[1] M.J. Bedzyk, G. M. Bommarito, J. S. Schildkraut; X-ray Standing Waves at Reflecting Mirror Surface; Phys. Rev. Letters **62**, 1376 (1989)

[2] Ajay Gupta, C. Meneghini, A. Saraiya, G. Principi, D. K. Avasthi; Depth selective XANES study of swift heavy ion irradiation effects in metal/Si systems; Nucl. Instr. Meth. Phys. Res. B **212**, 458 (2003)

[3] M.K. Mukhopadhyay, M.K. Sanyal, A. Datta, M. Mukherjee, Th. Geue, J. Grenzer, U. Pietsch; Transition from two-dimensional to three-dimensional melting in Langmuir-Blodgett films; Phys. Rev. B **70**, 245408 (2004)

FRACTURE OF PVDF – A COMBINED SYNCHROTRON AND LABORATORY *IN-SITU* X-RAY SCATTERING STUDY

G.A. Maier[1], G.M. Wallner[2], R.W. Lang[2], J. Keckes[1], H. Amenitsch[3,4], S. Bernstorff[3] and P. Fratzl[5]

1.) Material Center Leoben, Erich Schmid Institute of Material Science and Department of Material Physics, University of Leoben, Leoben, Austria
2.) Polymer Competence Center Leoben and Institute of Materials Science and Testing of Plastics, University of Leoben, Leoben, Austria
3.) Sincrotrone Trieste, Trieste, Italy
4.) Institute of Biophysics and Nanosystems Research, Austrian Academy of Sciences, Graz
5.) Max Planck Institute of Colloids and Interfaces, Dep. of Biomaterials, 14424 Potsdam, Germany

Experiment

Semi-crystalline polymers show a complex fracture mechanism, which is controlled by the micro mechanisms associated with formation and breakdown of a plastic deformation region at notches, cracks or other stress raising defects. Recently, *in-situ* small and wide angle X-ray scattering approaches with time resolutions in the seconds range, have demonstrated to make investigations of materials during external loading possible, and the structural information at the supramolecular level accessible. Such *in-situ* measurements were used in the present investigation to study the structural details during formation and breakdown of plastic zones ahead of cracks in films of poly(vinylidene fluoride) (PVDF) at two different time-scales.

Results

Figure 1 shows a typical force extension along with photographic illustrating the various deformation states. The x-ray beam, marked as point in Figure 1 "sees" the different rising structural properties within the plastic deformation zone. Figure 2 shows examples of recorded SAXS pattern together with the load, invariant, and long period and β/α ratio drawn vs. extension. In the SAXS patterns the change of the structer of material due to mechanical forces can be seen clearly: Beginning with a ring rising from isotropic arrangement of lamellae, changing to a streak orthogonal to the drawing direction and a second scattering signal oriented parallel to the tensile direction after an elongation of 2mm. Continued extension changed the patterns to a sharp streak orthogonal to the strain axis. The invariant vs. extension curve shows the same characteristics as the force extension curve and could therefore be divided in four different regions: Deformation region (I) with no changes in the overall electron-density differences in the material, with a non-gradient linear behavior of the invariant-curve. In region II, just after the maximum load point, the invariant increased strongly. A change in the electron-density distribution had occurred, caused by formation of cavities and the reorientation from spherulitic to a shish kebab like lamellae structure. In region III, a plateau occurred in the invariant vs. extension curve, indicating that there were no ongoing changes in the electron density distribution. At the end of zone III and the beginning of zone IV, the invariant suddenly began to decrease in a linear way. At the same time, the α to β PVDF phase transition, revealed by the WAXS-pattern, occurred (f). In Figure 2(f) also the long period (L) and the thickness (d) of the lamellae were plotted against the extension. In the drawing direction, the lamellae were separated from each other by stretching the amorphous zone in-between the crystals. This is indicated by the fact that the long period increases strongly while lamellae thickness nearly stayed constant. No changes in morphological parameters occurred orthogonal to the drawing direction during the experiments.

Discussion

Using *in-situ* scattering techniques allowed for studding kinetics of the formation of the plastic zone. At the beginning of deformation mainly elastic deformation occurred, caused by the extension of the amorphous phase parallel to the applied force. Plastic zone formation, associated with cavity formation allowes for stress reduction in the amorphous phase and continued lamellae separation. Reorientation of the spherulitic material to a fibrous, shish-kebab like morphology followed at continued extension. Upon further deformation the fibrils were transformed to *β*-PVDF-fibrils, being thinned until final fracture occurred.

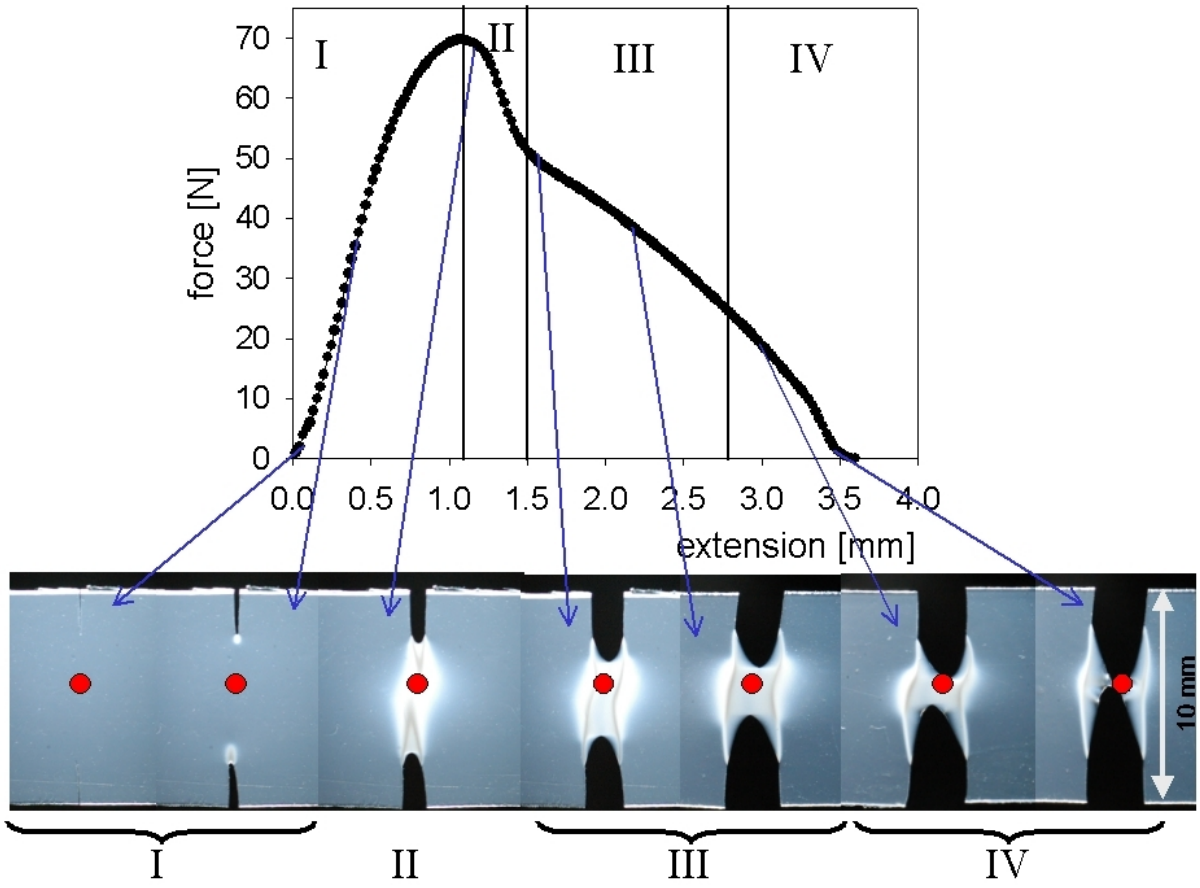

Figure 1. Typical load-extension curve of PVDF-DENT samples and the corresponding photographic pictures taken at different extension levels. Drawn points indicate the size and position of the X-ray beam on the sample.

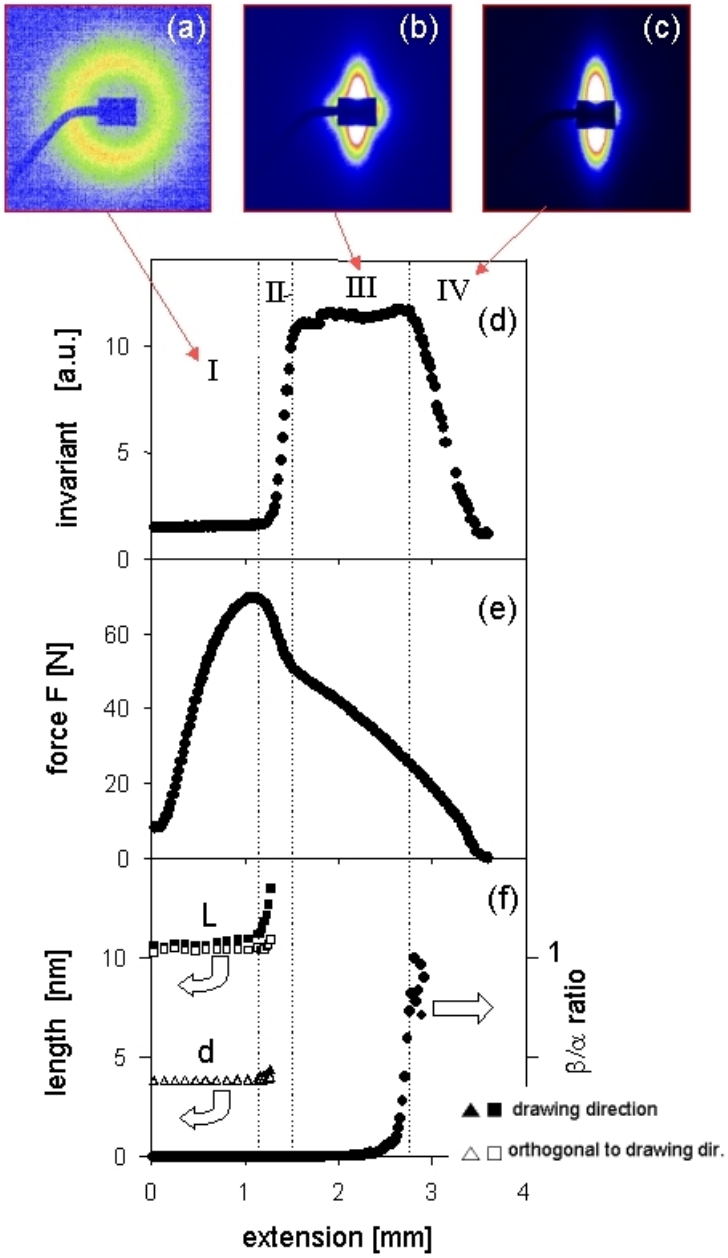

Figure 2. Synchrotron experiments: Selected scattering patterns (a,b,c), the invariant (d) and force (e), α/β ratio, long period (L) and lamellar thickness (d) (f) plotted against the extension.

References:

[1] Kepler R., Anderson R., *Advances in Physics* (1992) **41(1)** 1-57
[2] Maier G.A., Wallner G., Lang R., Fratzl P. *Macromolecules* (2005) **38,14,** 6099-6105
[3] Maier G.A., Wallner G., Lang R., Keckes J., Amenitsch H., Fratzl P., *J. Appl. Cryst.,* submitted.

GISAXS STUDY OF GOLD IMPLANTED GLASS

B. Pivac[1], P. Dubcek[1], I. Kovacevic[1]and S. Bernstorff[2]

1.) R. Boskovic Institute, P.O. Box 180, Zagreb, Croatia
2.) Sincrotrone Trieste, SS 14, km 163.5, Basovizza (TS), Italy

Silica based composites with embedded metallic nanometer sized clusters are often studied due to their optical, magnetic and catalytic properties exhibited when the clusters size becomes comparable to or less than the electronic mean free path. Recently, ion implantation has been explored to introduce foreign ions into pure silica to change its linear and nonlinear optical properties in layers near the surface [1]. To form nanoclusters after ion implantation the material must be treated either by thermal annealing, by laser annealing or by inert ion bombardment.

The glass substrates were cleaned according to a standard procedure before ion implantation [2]. Gold ions were implanted at room temperature at an energy of 1.1 MeV and at doses 1, 3 and $6x10^{16}$ ions/cm^2. The samples were annealed in a furnace at temperatures between 900 - 1100°C for an hour in the air.

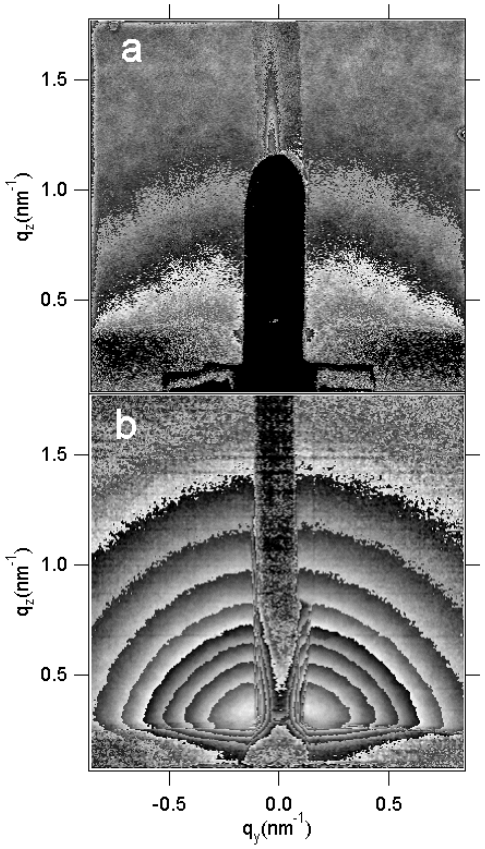

Figure 1: GISAXS on a) 1 x 10^{16} ions/cm^2 implanted sample b) the same sample annealed at 1100ºC

Figure 1 a) shows the GISAXS pattern obtained from the sample implanted up to 1 x 10^{16} ions/cm^2. Apart from the surface scattering features located mainly in the specular plain, under the central absorbing strip, a broad, ring like scattering can be seen, the center of the ring being at the direct beam position. This is the scattering pattern characteristic of isotropic scattering: the spherical scattering centers are placed randomly in the sample (within the range of penetration depth), their size being within a rather narrow range, and the central part of the intensity close to the direct beam is depleted due to particle to particle correlation defined by a rather short inter particle distance that is also restricted to a reduced range around the average

value. Since the maximum damage produced by implantation is at the projected range depth of 270 nm, it is expected that the particles form dominantly at this depth by heterogeneous nucleation mechanism. This brings anisotropy to the scattering since x-rays are scattered also from the surface of the film like structure in the substrate, with the shallowest particles distributed close to the surface of this particle containing layer.

Figure 1 b) shows the same sample scattering recorded after 1 hour annealing at the highest, 1100ºC temperature. The intensity is much stronger since a larger number of particles is formed and the particle size is increased. The scattering intensity maximum (ring) is shrunk close to the direct beam position as a consequence of the increment of the average inter particle distance. The ring like structure of the scattered intensity is preserved, since the relative size and inter particle distribution are not changed significantly, although the size and distances themselves are increased.

Apart from the annealing temperature, the implantation dose itself is another parameter which influences the formed particles size and especially the inter particle distance.

Fig. 2 shows the scattered intensity as a function of the scattering angle obtained along the vertical direction, close and parallel to the specular plane for 1 x 10^{16} (a), 3 x 10^{16} (b) and 6 x 10^{16} ions/cm^2 dose (c). The average particle size (R_G) and inter particle distance (D) obtained from the Guinier fit and maximum intensity position, respectively, are shown in the insert. The influence of the implantation dose and the annealing temperature is shown quite clearly here.

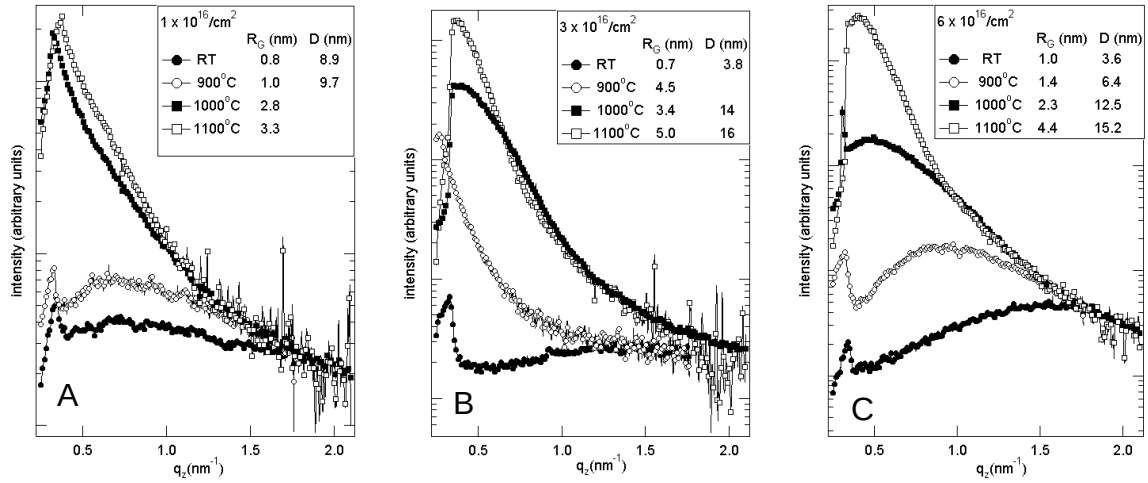

Figure 2. GISAXS intensity taken from 2D patterns as those in previous figures along q_y=0.2nm^{-1} for different annealing temperatures and implantation doses: a) 1 x 10^{16} ions/cm^2 b) 3 x 10^{16} ions/cm^2 c) 6 x 10^{16} ions/cm^2.

In the case of 6 x 10^{16} ions/cm^2 dose (Fig. 2 c) the scattering intensities have qualitatively the same shape. The scattering intensity is characterized by the inter particle interference maximum, whose position is used to estimate the dominating inter particle distance and at wider angles the intensity is decaying at a rate defined by the mean particle size (Guinier approximation). It is a good example of the particle size and spatial distribution control by means of annealing temperature.

When the dose is lower (3 x 10^{16} ions/cm^2, Fig.2.b) the interference maximum is partly missing. In the as implanted sample (the lowest curve) the particles are of similar size and evenly distributed throughout the sample, as controlled by the energy absorbed during the implantation itself and the gold concentration. Upon annealing at 900ºC (open circles), bigger particles start to grow (as can be seen from the enhancement of the intensity), but this is limited by the somewhat low gold concentration probably, and the result is uneven size of the

particles. This can be partly attributed to gold migration towards the substrate surface and bottom due to the intrinsic gold concentration gradient along this direction. With further annealing the particle growth becomes better controlled by temperature with the particle size distribution width getting narrower, and the intensity interference maximum reappears.
A similar explanation can be used in the case of the lowest dose (1 x 10^{16} ions/cm^2 Fig.2.a). Here the interference maximum can be seen for the as implanted and 900ºC annealed sample. The particle size is quite small (about 2nm in diameter) and they are distributed at great distances from each other (about 10nm), but retain similar sizes until the annealing temperature is elevated to 1000ºC. The diffusion range becomes big enough for substantially bigger particles to grow, but also the initial, small ones remain present in significant concentration, leading to the concave shape of the scattering intensity. Only at the highest annealing temperature (1100ºC), the size distribution is reduced partly, but its convex shape of intensity is still missing the interference maximum.

References

[1] D. Ila, Z. Wu, C.C. Smith, D.B. Poker, D.K. Hensley, C. Klatt, S. Kalbitzer, Nucl. Instr. and Meth. B **127/128**, 570 (1997).
[2] R. Mu, F. Jin, S.H. Morgan, D.O. Henderson and E. Silberman, J. Chem. Phys. **100**, 7749 (1994).

Si NANOSTRUCTURES FORMATION IN SiO/SiO_2 MULTILAYERS

B. Pivac[1], I. Kovačević[1], P. Dubček[1], N. Radić[1] and S. Bernstorff[2]

[1] R. Bošković Institute, P.O.Box 180, Zagreb, Croatia
[2] Sincrotrone Trieste, SS 14, km 163.5, Basovizza (TS), Italy

The actual research on Si nanosized structures embedded in a host matrix is focused on Si nanocrystals prepared by different methods (Si ion implantation in SiO_2, sputtering of Si rich oxides or reactive evaporation of Si rich oxides) and on Si/insulator multilayers. The last method, also known as superlattice approach, was first suggested by Z.H.Lu et al. [1]. The application of such Si/SiO_2 superlattice has also attracted great interest in photovoltaic engineering for its possibility to increase significantly the efficiency of solar cells at low cost [2]. Moreover, given the recent demonstration of stimulated emission in silicon nanocrystals, it represents a possible approach to produce a silicon laser operating at around 750 nm [3].
In spite of intensive research, the correlation between the structural and optoelectronic properties of Si nanocrystals prepared by a variety of methods is still an unresolved problem. For a better understanding, it is necessary to learn more about the structural properties of Si nanocrystals. That includes their size, morphology, spatial position, density and volume fraction.
Amorphous SiO/SiO_2 superlattices were prepared by high vacuum evaporation of alternating films of SiO and SiO_2, each 3 nm thick (forming a stack of 10 bilayers plus one SiO_2 capping layer) on clean Si (100) substrate held at room temperature. Rotation of the Si substrate during evaporation ensured homogeneity of the films over the whole substrate surface. After deposition, samples were annealed at 1100 °C for 1h in vacuum better than 10^{-6} Pa to induce Si nanocrystals formation in t6his SiO/SiO_2 superstructure.

A 1D cut obtained from the measured 2D SAXS pattern of an annealed sample is shown in Fig. 1 with full circles and is compared to the corresponding one from a not annealed sample: The layered structure of the film has been perturbed due to silicon nanocrystals formation, and the oscillatory nature of the GISAXS pattern has changed. The formed nanocrystals have also increased the surface roughness considerably, thus reducing the film to substrate surface correlation substantially and the oscillations corresponding to the overall film thickness are completely missing from GISAXS. There is a maximum of intensity though at q_z=0.65 nm^{-1} which nearly coincides with an intensity maximum from the not annealed sample. The scattering in the annealed sample is obviously dominated by the formed nanocrystals contribution. Here we note that the electron density difference is much bigger between Si and SiO_2 than the one between SiO and SiO_2. Making a fit of the intensity to the Guinier approximation we obtained a value of R_G=2.4nm, and using the position of the peak in intensity as a gauge for the interparticle distance, we found that they are about 11 nm apart.
All these values are obtained from the intensity distribution in the direction perpendicular to the film surface, and we can conclude that the size of the formed silicon nanocrystalline particles in this direction is abut 5nm (which roughly corresponds to the thickness of the bilayer), while the distance between two adjacent particles in vertical direction corresponds to double the bilayer thickness. This means that the particles tend to grow in vertical direction one above another in every other bilayer, i.e. the growth of a particle above one in the next bilayer below is unfavorable. This type of arrangement potentially enhances the ordering further, because half way between two vertically correlated particles from every other layer would be a preferred position for the midway between two adjacent particles in the layer between the former two, but we have not observed it.
From the intensity distribution in the direction parallel to the film surface we obtained the

particle size in this direction. Again a fit to the Guinier approximation was applied and the obtained value is R_G=4.2nm. The intensities from the horizontal and vertical cut are compared in Fig 2. In the direction parallel to the film surface, the maximum in SAXS is missing, indicating the absence of a preferred interparticle distance. Due to the continuity of the SiO layer, the size of the grown nanoparticles is controlled mostly by diffusion, and this seems to be less effective in restricting the growth to a specific size. Probably both the size distribution as well as the interparticle distance variation are large [4]. Thus no in-plain ordering is achieved in spite of the tendency of correlated growth in every other layer.

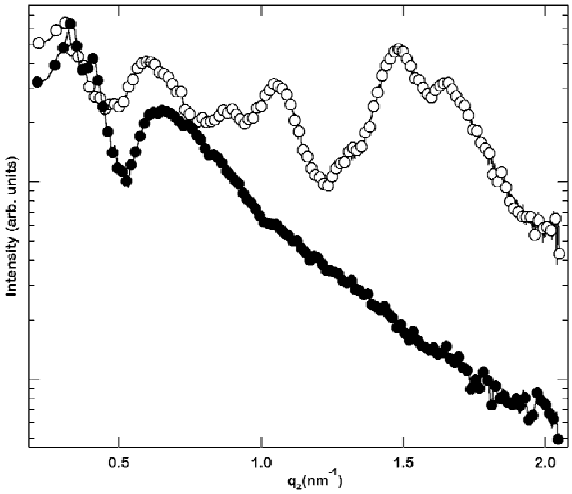

Figure 1. Vertical 1D cuts from a measured 2D GISAXS pattern of a not annealed sample (open circles) and an annealed sample (full circles)

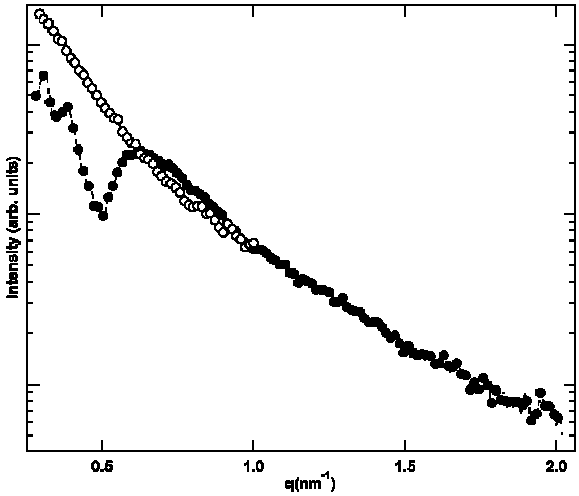

Figure 2. Comparison of the scattered intensities (1D cuts) in vertical (full circles) and horizontal (open circles) direction.

References

[1] Z.H.Lu, D.J.Lockwood and J.M.Baribeau, Nature **378**, 258 (1995).

[2] M.A. Green, Progress in Photovoltaics, **9,** 257 (2001).

[3] M. Cazzanelli, D. Navarro-Urrios, F. Riboli, N. Daldosso, L. Pavesi, J. Heitmann, L.X. Yi, R. Scholz, M. Zacharias, and U. Goesele, J. Appl. Phys. **96**, 3164 (2004).

[4] I. Kovacevic, P. Dubcek, S. Duguay, H. Zorc, N. Radic, B. Pivac, A. Slaoui and S. Bernstorff, Physica E, in print

STRUCTURAL STUDY OF NANOCRYSTALLINE NICKEL THIN FILMS

N. Radić[1], P. Dubček[1], S. Bernstorff[2], I. Djerdj[3] and A.M. Tonejc[3]

1.) Rudjer Bošković Institute, HR-10000, Zagreb, Croatia
2.) Sincrotrone Trieste, I-34012 Basovizza (TS), Italy
3.) Faculty of Sciences, Dept. Physics, HR-10000 Zagreb, Croatia

Nanocrystalline nickel (nc-Ni) is a very interesting material due to its enhanced mechanical, corrosion and catalytic [1] properties. Among the PVD methods of the nc-Ni production, magnetron sputtering has been relatively seldom employed for the preparation of nanocrystalline nickel. A rather limited range of preparation conditions has been examined in the case of sputter-deposited nanocrystalline nickel so far. Here we present the results of the Grazing Incidence Small Angle X-ray Scattering (GISAXS) study of nanocrystalline nickel films prepared by magnetron sputtering in a rather wide range of deposition conditions.

Nickel thin films were deposited by dc magnetron sputtering onto fused silica and single crystalline Si - in the same run. The deposition rate was about 7-8 nm/min at 240-300 W magnetron power, and the final film thickness was about 400 nm. In order to examine the effects upon the film structure, the argon pressure was varied in the range 0,33-1,33 Pa, and the substrate temperature was varied in the room temperature (RT) - 700 °C range.

Apart from the nanocrystals of different sizes which are present in the nc-Ni films, a considerable fraction of the films consists of a non-homogenous, disordered part mixed with the nanocrystals. Up to our knowledge, this is the first GISAXS analysis of nanocrystalline nickel.

The GISAXS patterns for three samples deposited at different substrate temperatures (room temperature, 150ºC and 300ºC) are shown in Fig. 1. Basically, the GISAXS patterns consist of two distinct parts whose relative intensity depends on the substrate temperature during deposition. At low temperatures (Fig.1a) isotropic scattering is dominating in the GISAXS pattern, while the scattered intensity is anisotropic and elongated along the specular plain (q_y=0) at high substrate temperature (Fig. 1c). The intermediate substrate temperature (Fig. 1b) results in both contributions present at similar intensity levels. In order to follow the changes/ evolution of the inhomogeneities with the substrate temperature, in Fig. 2 we show the intensities which we extracted from the patterns shown in Fig.1 along two different directions parallel to the specular plane, e.g. at q_y=0.75nm and q_y=0.20nm for a series of substrate temperatures. The chosen cuts were convenient to separate the two distinct contributions to the scattering, since there the isotropic/ anisotropic contributions to the scattering are dominant, respectively.

Apart from the Porod (q^{-4}) type scattering above about q_z=1.2nm^{-1} (coming from the contrast between disordered part and larger nanocrystals that are embedded in the film), there is a particle-like scattering at the smaller angles and Guinier approximation was used in order to obtain the typical sizes of the inhomogeneities as a function of temperature for both contributions to the GISAXS. The results are presented in insert of Fig.2. Contrary to the sizes of the nanocrystals, which grew rapidly from 6.7 nm at RT to even 152 nm at 700ºC,as determined by XRD, the isotropic inhomogenities sizes fall above 50ºC from 8 nm down to 4 nm at 150ºC, where this contribution to the scattering fades away. At this temperature, the vertical sizes of the anisotropic inhomogeneities begin to decrease and are down to 3 nm at the highest temperatures (400-700 ºC), while horizontally they increase up to 14 nm.

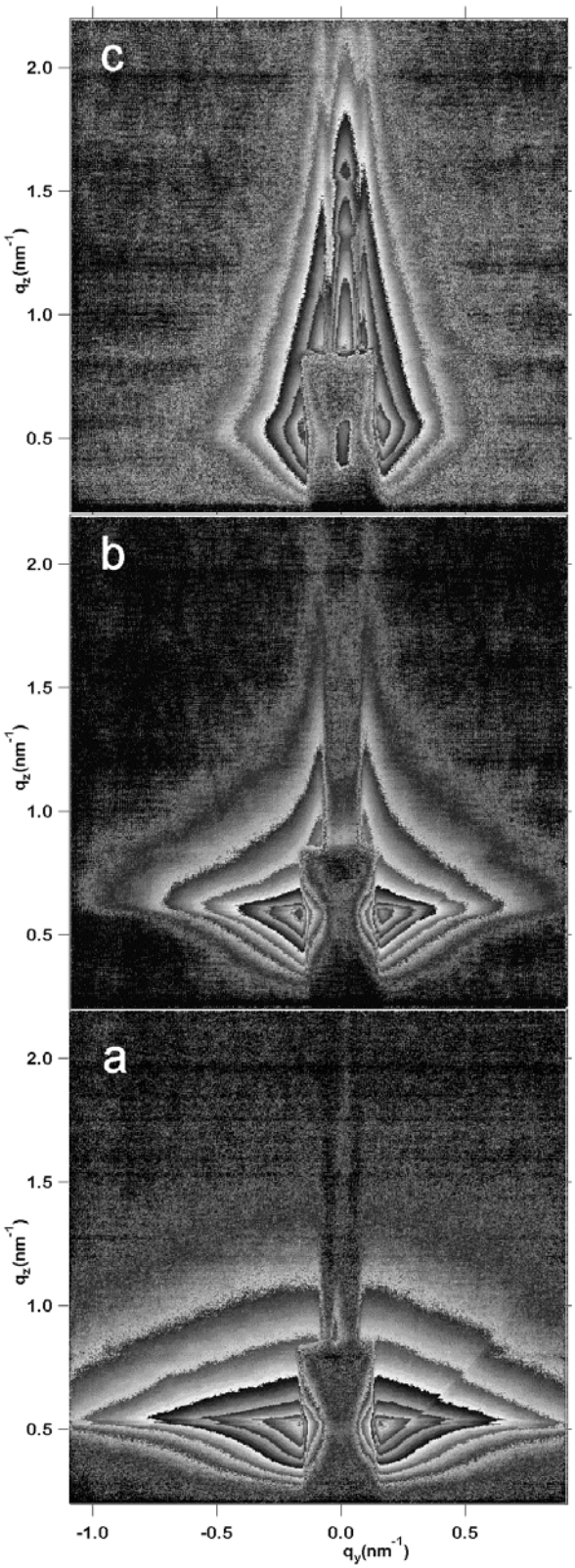

Figure 1 The GISAXS patterns for the nc-Ni samples deposited at different substrate temperatures.

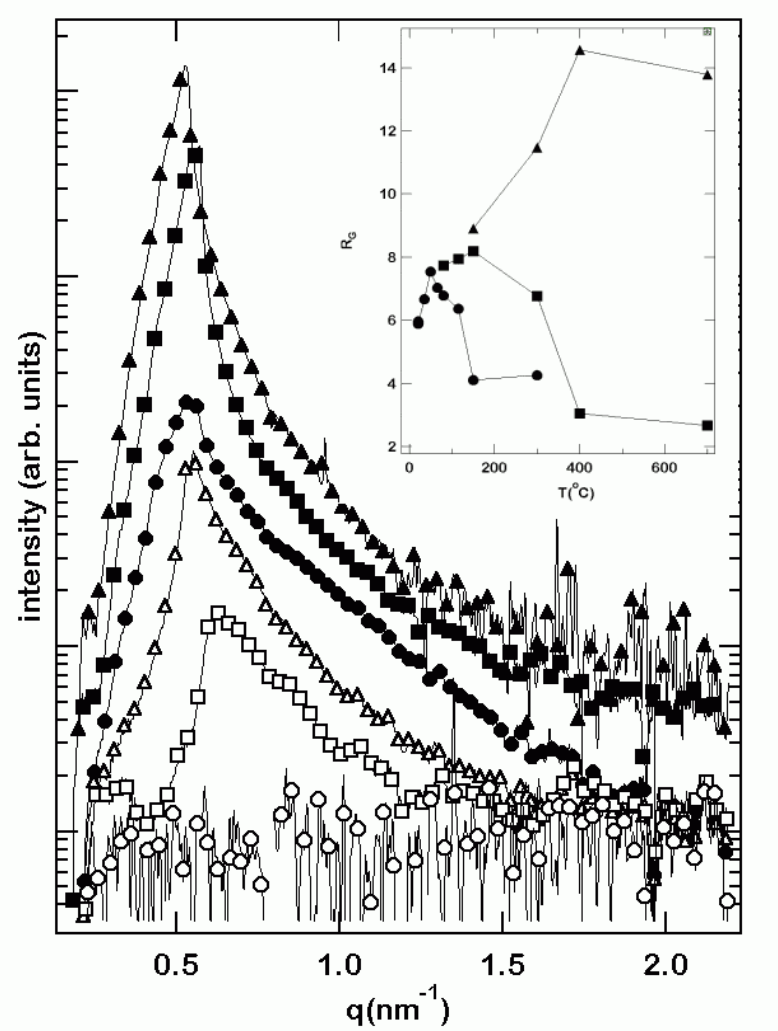

Figure 2 GISAXS intensities along q_y=0.20nm (full symbols) and q_y=0.75 nm (open symbols) vs scattering angle for nc-Ni samples deposited at different substrate temperatures. The spectra are offset verticaly for the sake of clarity. In insert, size of the inhomogeneities in nc-Ni thin filmsis shown: Rg was derived from GISAXS patterns for two kinds of inhomogeneities/"particles" - a) spherical (●), and b) platelet-like (■ and ▲).

Finally, it should be noted that the evolution/change of the ratio between the nanocrystalline and intercrystalline isotropic phases as observed by XRD and GISAXS, respectively, corresponds well to the variation of the electric resistance of the nc-Ni samples deposited at different temperatures, as well as with the IHER catalytic activity of the nanocrystalline nickel films [2].

References:

[1] M. Metikoš-Huković, Z. Grubač, N. Radić, A. Tonejc, Journal of Molecular Catalysis A: Chemical. 249 (2006); 172-180
[2] M. Metikoš-Huković, et al., to be published in Electrochemistry Communications

ENHANCED BACKGROUND SCATTERING CAUSED BY DEFORMATION INDUCED VACANCIES: IN−SITU SYNCHROTRON WAXS, PART I: FACE CENTERED CUBIC METALS

E. Schafler[1], M. Kerber[1], L. Balogh[2], K. Nyilas[2], T. Ungàr[2], S. Bernstorff[3] and M.J. Zehetbauer[1]

1.) Institute of Materials Physics, University of Vienna, A-1090 Wien, Austria
2.) Department of General Physics, Eötvös University Budapest, H-1518 Budapest, Hungary
3.) Sincrotrone Trieste, Basovizza, I-34012 Trieste, Italy

The generation of point defects by plastic deformation is well known since the measurement of different physical quantities, especially residual electrical resistivity, as a function of deformation, cf. [1-3]. By assuming certain mechanisms for point defect generation which all include some interaction of dislocations, several models predict different strain dependent evolution laws for vacancy generation which have never checked by experiment so far [3]. One lack of hitherto experiments was that the vacancies could not be kept stabile in density and/or in arrangement: They either annealed out or at least rearranged immediately after plastic deformation so that neither the density nor the arrangement of vacancies measured in the "dead" sample was representative for the deformation process. It has been the idea of the present investigation to check whether it is possible to measure vacancy concentrations in-situ during deformation in order to receive reliable data which can be compared with the models mentioned.

In situ X-ray line profile measurements were carried out at the SAXS beamline at ELETTRA in Trieste. Single- and polycrystalline copper specimens of high purity have been deformed in compression by a compact test machine mounted on a 5-axes goniometer for the compensation of the shape and orientation changes during the deformation process. The (400) peak profiles of the specimen were measured in reflection by a linear position-sensitive detector. A [001]-oriented Cu single crystal and a polycrystalline copper specimen of about 80 μm average grain size have been investigated *in-situ* with a very low strain rate $\dot{\varepsilon} \sim 5\text{x}10^{-5}\ \text{s}^{-1}$. The diffraction peaks were recorded in 30 to 60 seconds, in this time interval the true strain ε was smaller than 10^{-3}. From the diffraction peaks the dislocation densities were evaluated described in detail in [4] by fitting the Wilkens-type strain profile functions to the measured profiles as described in [5] (see. Fig.1a). Due to the low noise of the detector, the increase of the background to peak ratio R is attributed to diffuse scattering caused by deformation induced point defects, in particular by vacancies and/or vacancy clusters.

In the case of the undeformed specimens only a vanishing background intensity was observed, for the single- as well as the polycrystals. With increasing deformation the diffuse background intensity increased considerably. For the quantification of the diffuse background scattering, the ratio of the integrated background, A_{BG}, and the integrated peak intensity, A_{Peak}, has been introduced (see Fig. 1b) which is also a measure for the ratio between the densities of deformation induced vacancies and the dislocations [6]:

$$R = \frac{A_{BG}}{A_{peak}} \ . \qquad (1)$$

The resulting deformation dependent evolutions of this ratio, both for the single- (R_{S}) and the polycrystalline sample (R_{P}), are presented in Fig. 2a (please note the logarithmic scale). At small values of ε, the increase of R_{P} fairly exceeds that of R_{S}. R_{P} remains much larger than R_{S} throughout the entire deformation range.

After calibration with reliable residual resistivity measurements of deformation induced vacancy and dislocation densities in polycrystalline Cu [7], the following correlation between the average vacancy concentration, $C_{p,vac}$ and the dislocation density ρ_{14} (this means ρ in units $10^{14}\ \text{m}^{-2}$) has been derived:

$$C_{p,vac} \cong 5\text{x}10^{-4}\ \{1 - \exp[\ - 8\text{x}10^{-8}\ (\rho_{14})^5\ ]\} \qquad (2)$$

The average vacancy concentrations, in a representative poly- and single crystal specimen, calculated with this equation are plotted in Fig.2(b). The evaluated data from X-ray diffuse background scattering indicate that the vacancy concentrations generated in polycrystalline specimens are more than one

order of magnitude larger than those produced in single crystalline samples. Such a difference still is observed if one considers the number of generated vacancies normalized to the actual dislocation density. In [7] we also concluded that the vacancy concentration in the grain boundary regions are much larger than in the grain interior ones, and reach values similar to those of thermal vacancies close at the melting temperature. This result suggests marked similarities between the microstructure of the grain boundary regions and that usually observed at the melting temperature.

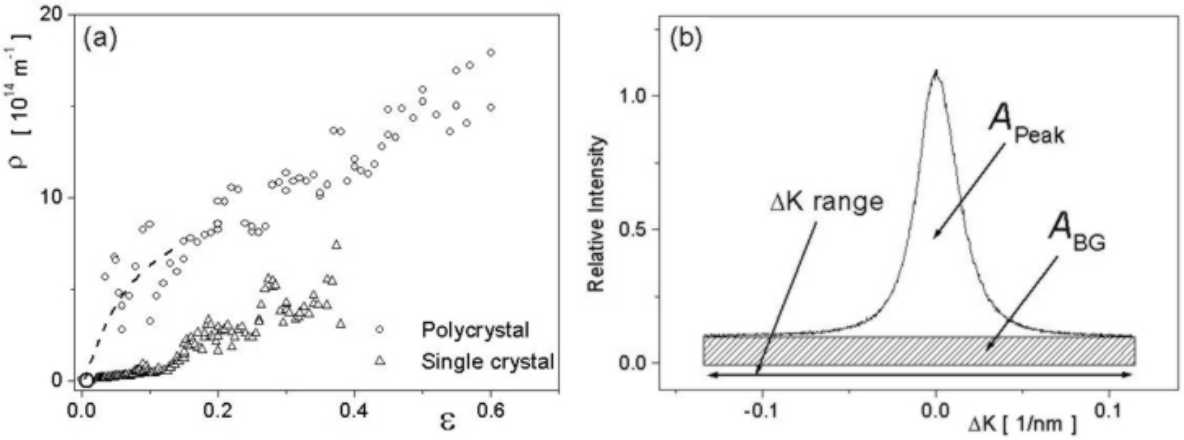

Figure1. (a) Typical peak profile of the (400) Bragg reflections. A_{Peak} and A_{BG} are the area under the peak and the area of the background in the ΔK range, respectively. (b) The dislocation density as a function of compression, ε, measured during the *in-situ* synchrotron experiments.

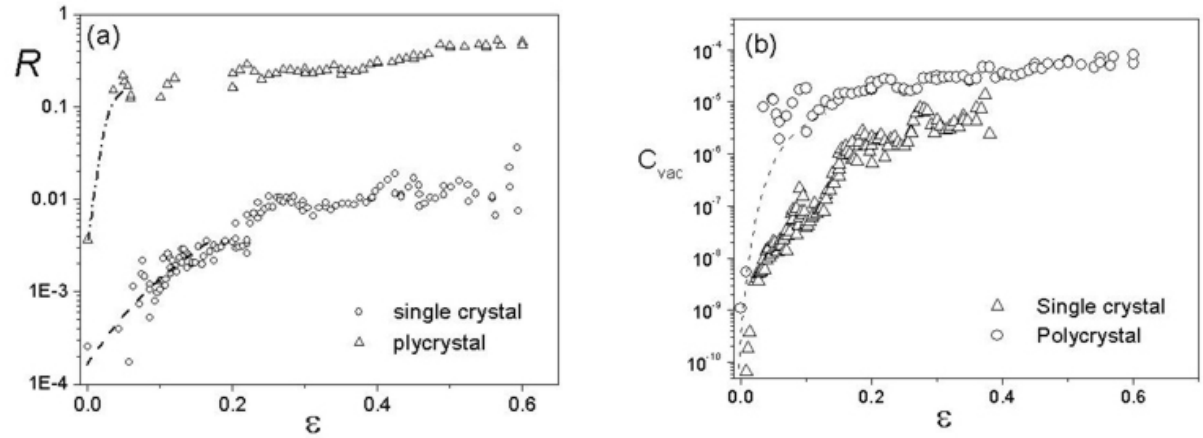

Figure 2. (a) The ratios of the background to peak areas, *R*, for the polycrystalline and single-crystal specimens as a function of compression, ε, as defined in eq. (1). (b) The evolution of the vacancy concentrations in polycrystalline and single-crystal specimens, as defined in eq. (2).

References:

[1] A. Seeger, Handbuch der Physik III. Springer-Verlag, Berlin (1955).
[2] I. Kovács, Acta Metall. **15,** 1731 (1967).
[3] M. Zehetbauer, Key Eng. Mater. 97-98, 287 (1994).
[4] E.Schafler, K.Simon, S.Bernstorff, P.Hanák , G.Tichy, T.Ungár, M.Zehetbauer, Acta Mater. **53**, 315 (2005).
[5] G. Ribárik, T. Ungár, J. Gubicza, J.Appl.Cryst. **34**, 669 (2001).
[6] T. Ungár, E. Schafler, P. Hanák, S. Bernstorff, M. Zehetbauer, Mater. Sci. Eng. A, in press (2006)
[7] M. Zehetbauer, E. Schafler, T. Ungár, Z. Metallk. **96,** 1044 (2005)

MOLECULAR ASSEMBLY OF POLYETHYLENE-*BLOCK*-POLY(ETHYLENE OXIDE) IN THERMOSETTING MATRIX STUDIED BY TIME RESOLVED SWAXS

C. Sinturel[1], M. Vayer[1], R. Erre[1] and H. Amenitsch[2]

1.) Centre de Recherche sur la Matière Divisée, 1 B rue de la Férollerie, 45071 Orléans, France
2.) Institute of Biophysics and Nanosystems Research, Austrian Academy of Sciences, Schmiedlstr. 6, 8042 Graz, Austria

We have recently performed the molecular assembly of amphiphilic block-copolymer poly(ethylene)-*block*-poly(ethylene oxide) (EEO, 1 400 g.mol-1) in unsaturated polyester (UR, thermoset polymer). At a macroscopic level, the resulting blends are homogeneous at room temperature, exhibiting LCST type behaviour upon heating, with macro phase separation occurring at 75°C in the studied range of composition. Curing at temperature < 75°C prevents from macro phase separation and permits to fix the meso-structure obtained in the initial liquid state. In these conditions, EEO platelets with high aspect ratio (6 nm thick, several μm long) are revealed by TEM in the cured state (figure 1). These structures are formed *via* the exfoliation of the pure layered EEO in the uncured liquid UR which selectively mixes the PEO segments, whereas PE is completely immiscible.

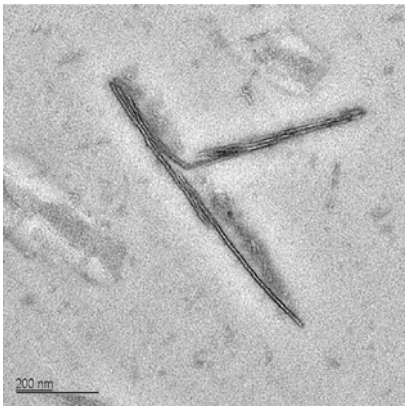

Figure 1. TEM micrograph of a poly(ethylene)-*block*-poly(ethylene oxide) platelets in a blend containing 5 % of block-copolymer. Due to preferential staining with RuO_4, PEO appears in black and therefore constitutes the border of the platelets whereas PE, in white, segregates in the centre of the platelets; the UP cured matrix constitutes the continuous grey background

Time resolved SAXS experiments were performed on the blends to get information on the molecular assembly of the block-copolymer upon temperature variations, for initiated and non initiated systems. Simultaneously, WAXS and DSC measurements were performed to study the crystallinity of the PE domains. Blends containing 2.5 to 25% of EEO were prepared.

Prior heating, initiated and non initiated systems exhibit similar behaviour with only one scattering maximum at low q values confirming that the lamellar structure of the pure EEO [1] is lost in the blends, and replaced by correlated nanometer scale domains (30-90 nm). These results are consistent with exfoliated lamellae of EEO spread homogeneously in the UR liquid via the PEO blocks. Upon heating, SAXS patterns confirm an aggregation of the platelets in the case of the non initiated systems as shown in figure 2a (shift of the initial scattering peak to higher q value) when temperature reaches the temperature of the macro phase separation. Upon cooling, we found that despite the system remains in the liquid state, aggregation of the platelets was irreversible with final state consisting in EEO rich phase domains dispersed in UR (see final scattering peak at 22°C in figure 2b). In the case of the initiated blends, we let the system at 70°C for one hour to reach the gelation in order to prevent from macro phase separation. No platelets aggregation was observed this time on the SAXS pattern that confirms the preservation of the initial state.

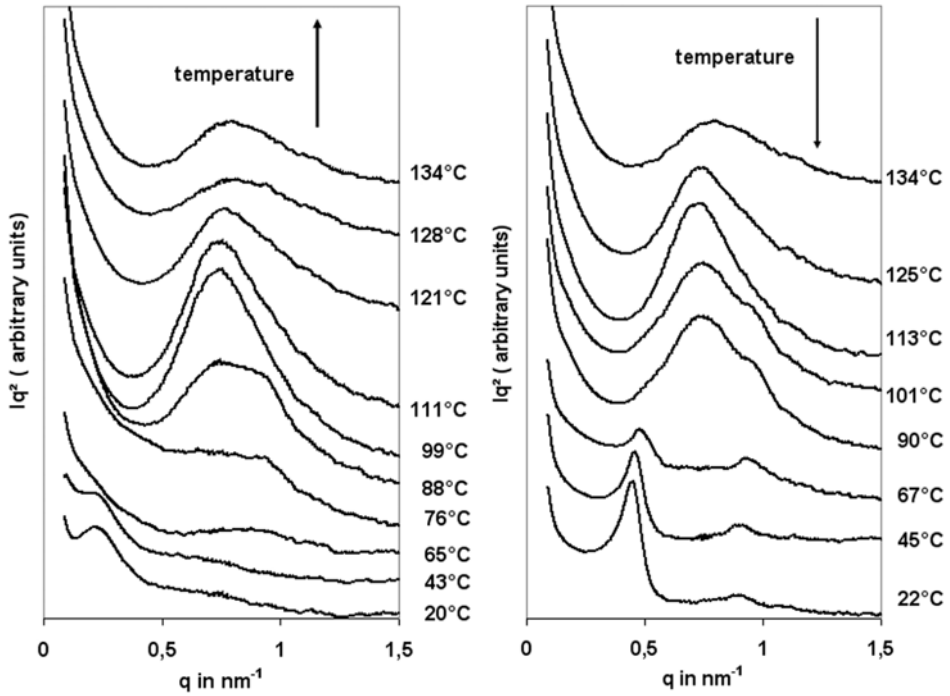

Figure 2. Temperature dependence of the SAXS profile of UR/EEO 80/20 non initiated blend uponheating from RT to 135°C at 5°C/min (left) and cooling from 135°C to RT (right)

Simultaneously, WAXS and DSC measurements were performed in order to follow the behaviour of the crystalline domains. Initial diffraction pattern clearly exhibits the intense PE(110) refection at 15.2 nm^{-1}. Upon heating, this reflection gradually decreases from 70°C and vanishes at 105°C, corresponding to the melting of the PE domains, and confirmed by the *in situ* DSC traces. The associated increase in specific volume leads to a proportional reduction of the electronic density of the PE domains, causing variation of the contrast and thus variation of the scattering intensity (see figure 3).

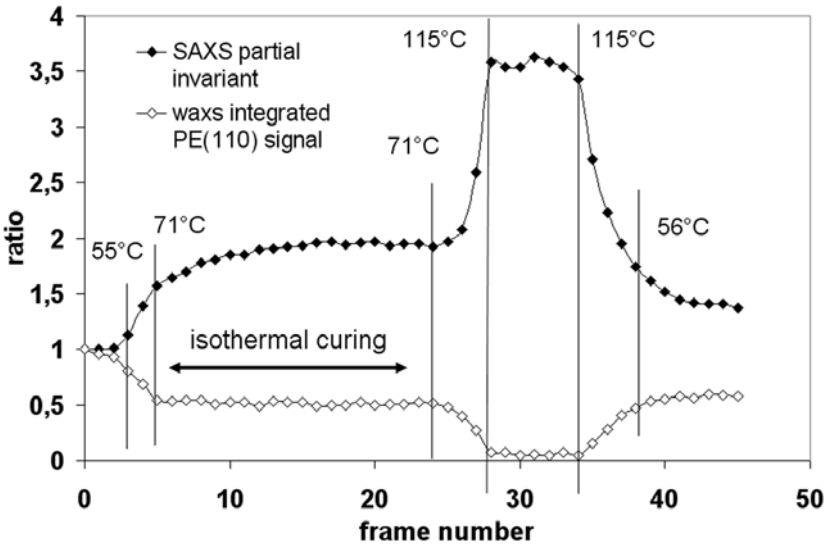

Figure 3. Evolution of the SAXS partial invariant and the PE(110) integrated intensity (ratio over the initial value) for initiated UR/EEO 80/20 blend upon heating from RT to 70°C, curing during 60 minat 70°C, heating from 70°C up to 135°C and cooling down to RT at 5°C/min.

References:

[1] Sun, L.; Liu, Y.; Zhu, L.; Hsiao, B.S.; Avila-Orta, C.A. *Polymer* **2004**, *45*, 8181.

DETERMINATION OF GRAIN SIZES AND POROSITY IN NANOPHASE VANADIUM OXIDE AND V/Ce OXIDES VIA GISAXS, GIWAXD AND GIXR TECHNIQUES

A.Turković[1], M.Lučić-Lavčević[2], P. Dubček[1], M. Pavlović[1] and S.Bernstorff[3]

1.) Institute "Ruđer Bošković", P.O. Box 180, HR-10002 Zagreb, Croatia
2.) Department of Physics, Faculty of Chemical Technology, University of Split, Teslina 10/V, 21000 Split, Croatia
3.) Sincrotrone Trieste, Strada Statale 14, km 163,5 Basovizza, 34012 Trieste, Italy

Vanadium oxide, such as V_2O_5, has been extensively studied because it tends to form a lamellar structure, which allows the intercalation/de-intercalation of different ions between its layers. The use of V_2O_5 is closely connected with a way of preparing material for its final usage. It can be used as a catalyst, in electro chromic devices, in an advanced electrochemical cell concept, especially in lithium batteries (1). V_2O_5 and V/Ce were prepared via sol-gel route from an aqueous colloidal solution of inorganic precursors (2). Atomic force microscopy (3) have revealed them be the nanophase materials. We studied grain sizes and porosity of V_2O_5 and V/Ce by GISAXS, GIXR and GIWAXD at the SAXS-beamline, as it could be also a candidate for nanophase solar cell electrode in analogy with previously used TiO_2 and CeO_2 and as intercalation electrodes with a solid polymeric electrolyte (4).
We performed an analysis of structural modifications, induced by mixing vanadium and cerium oxides and by introduction of lithium in vanadium and mixed vanadium/cerium oxide films, using the grazing incidence small angle X-ray scattering (GISAXS) technique. In analysing the GISAXS data, we consider sol-gel derived vanadium and vanadium/cerium oxide films as aggregates containing nanosized grains and pores. Assuming that the SAXS signal is caused by the difference in electron density within and around the grain, their size distribution in the film can be determined. Furthermore, two-dimensional detection of GISAXS signal gives an advantage of a more complex analysis, based on the comparison of the surface and bulk characteristics of the film.
For this presentation, we have chosen four samples as example between numerous recordings by different SAXS methods (5,6,7). Four samples were prepared: sample A, non-intercalated V oxide (V_2O_5); sample B, non-intercalated V/Ce oxide with 38 at.% of V; sample C, Li intercalated V oxide, and sample D, Li intercalated V/Ce oxide with 38 at.% of V. The details of sample preparation and intercalation of lithium ions are described in previous publication (2). Two dimensional GISAXS intensity maps, i.e. scattering patterns, for samples A, B, C and D are shown in Fig. 1.

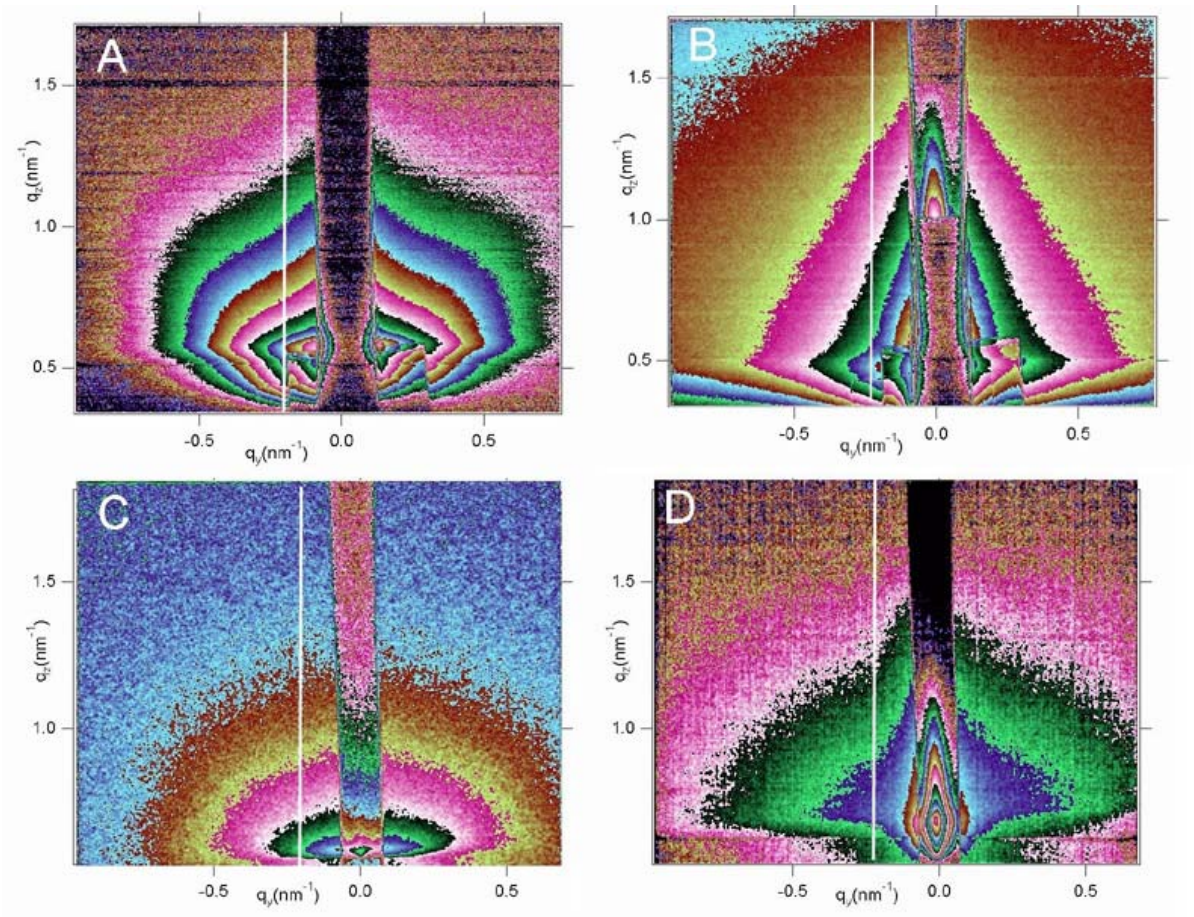

Figure 1. GISAXS patterns from V oxides (left, samples A and C) and V/Ce oxides (right, samples B and D), non-intercalated (top) and Li intercalated (bottom).

Left and right are the scattering patterns from V and V/Ce oxides, respectively, while top and bottom row are non-intercalated and Li intercalated scattering patterns, respectively. The maximum of the scattered intensity is in the direction of the specular reflection. The vertical strips in patterns are the intensities depleted by Al absorber, which was put in place to avoid detector saturation due to these high scattering intensities in the specular plane. The lower part of the scattering (below the surface plane) is missing from the pattern due to the absorption in the sample. Overview of structure parameters, for samples A and B (non-intercalated), C and D (intercalated) is shown in Table 1.

The present study shows that the application of the particle scattering model in analyzing GISAXS measurements data can be utilized for estimating the structural properties of the vanadium/cerium oxide thin films as well as for following their structural modifications in the process of lithium intercalation. However, since SAXS analysis is model-dependent and suffers from the influence of various material properties, a two dimensional detection of the scattering signal is applied and the results are compared to those of the AFM surface imaging. In conclusion, the observed aspects of the GISAXS intensity maps supported by the AFM analysis provide a contribution to the modeling of nanostructured intercalation electrodes.

Table 1. Surface roughness, χ, measured by AFM, and characteristic values of grain size distribution, R_m (mean grain size) and σ (distribution half-width), calculated from GISAXS data.

Sample 1	**χ(nm)**	**R_m(nm)**	**σ(nm)**
A	11	5.7	2.0
B	2	2.1	2.0
C	6	4.3	1.0
D	8	3.4	1.0

References:

[1] C.G. Granqvist, Handbook of Inorganic Electrochromic Materials, Elsevier, Amsterdam, 1995.
[2] Z. Crnjak-Orel, Solid State Ionics **116** 105-116 (1999).
[3] Z. Crnjak- Orel and I.Muševič, Nanostructured materials **12**, 399-404 (1999).
[4] A. Turković and Z. Crnjak-Orel, Electrical and Optical Properties of Thin Films Zn/$(PEO)_4ZnCl_2$/CeO_2, or CeO_2/SnO_2(17%),ITO Galvanic Cells, Solid State Ionics **89** (3-4), 255 (1996).
[5] A.Turković, M. Pavlović, M.Ivanda, M. Gaberšček, Z. Crnjak Orel, Journal of The Electrochemical Society (JES). **153** 1; A122-A126 (2006).
[6] Z.Crnjak Orel, M. Gaberšček, A.Turković, Solar Energy materials & Solar Cells. **86**, 19-32 (2005).
[7] M. Lučić Lavčević, P.Dubček, Z. Crnjak Orel, A.Turković, Journal of Chemical Information and Modeling. **45(6),** 1553-1557 (2005).

MORPHOLOGY AND CRYSTALLIZATION KINETICS OF SOLID POLYMER ELECTROLYTE FOR Zn RECHARGEABLE NANOSTRUCTURED GALVANIC CELLS VIA COMBINED SYNCHROTRONE SAXS-DSC TECHNIQUES

A.Turković[1*], P. Dubček[1], M.Lučić-Lavčević[2], M. Pavlović[1] and S.Bernstorff[3]

1.) Institute "Ruđer Bošković", P.O. Box 180, HR-10002 Zagreb, Croatia
2.) Department of Physics, Faculty of Chemical Technology, University of Split, Teslina 10/V, 21000 Split, Croatia
3.) Sincrotrone Trieste, ss. 14, km 163,5 Basovizza, 34012 Trieste, Italy

$(PEO)_8ZnCl_2$ polymer electrolytes and nano-composites were prepared using PEO γ-irradiated to selected doses and TiO_2 nanograins. These materials can be considered as aggregates containing nanoparticles or nanograins [1-15]. In this case, the SAXS is caused by the difference of electron density within and around the nanoparticles. Using the Guinier approximation (the scattering in the very small angle range is of Gaussian form, independent of the shape of the present particles) the sizes can be readily determined. The influence of added nanosize TiO_2 grains to polymer electrolytes and the effect of γ-radiation from a Co-60 source were studied by small-angle X-ray scattering (SAXS) simultaneously recorded with differential scanning calorimetry (DSC) at synchrotron ELETTRA. Infrared (IR) and impedance spectroscopy (IS) were also performed. Above-mentioned treatments largely enhanced the conductivity of polymer electrolyte. Room temperature conductivity increase up to two orders of magnitude was achieved. Addition of nanograins increased conductivity more than can be ascribed to crystallinity possibly because of interactions of anion with nanograins. Galvanic cells $Zn/(PEO)_8ZnCl_2/[V_2O_5\text{-}CeO_2$ (at 38 at. % of V)]; SnO_2:F have been formed [16].

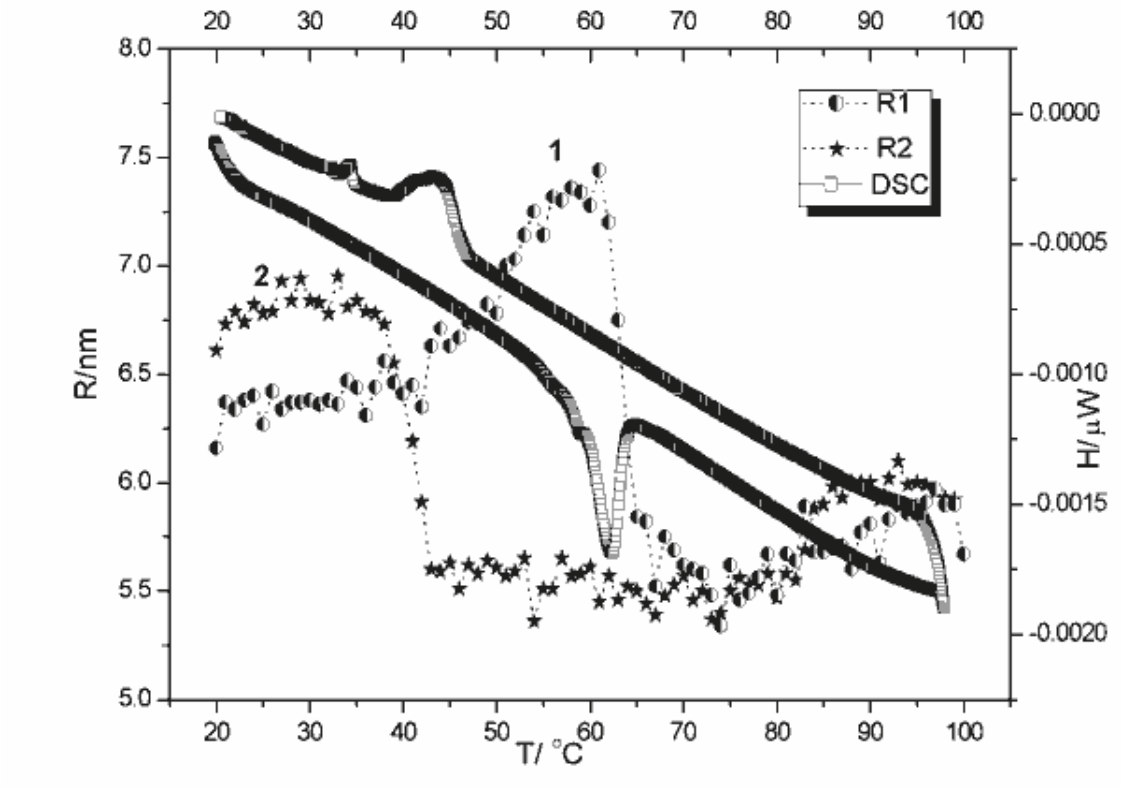

Figure 1. SAXS and DSC of $(PEO)_8ZnCl_2$ material irradiated with γ-rays of 309 kGy.

Fig 1. is showing SAXS and DSC of material irradiated with γ-rays of 309 kGy. In the heating cycle, there are two trends, first increasing of grain size, i.e. "average particle radii" to 61.03 °C and sudden drop at this phase transition temperature. It varies from 6.1 to 7.4 nm in the region below the phase transition temperature and than from 5.5 to 5.9 nm in superionic phase of polymer electrolyte. Crosslinking reduced crystalline part of the PEO matrix and temperature of phase transition is lowered to 61.03 °C comparing to 64.04 °C for non-treated sample, which can be seen in Table 1. In cooling cycle crystallization temperature dropped to 42.66 °C in regard to 48.94 °C for original sample. DSC of material irradiated with γ-rays of 309 kGy is shown on the same graph. The temperature of phase transition is lowered from non-treated samples of 68.82 °C to 62.03 °C and as well as in cooling cycle from 52.68 °C to 43.23 °C. Third temperature in cooling cycle is 34.33 °C, which shows successive crystallization and thus intermediate phase transition. The temperatures exothermic and endothermic peaks in DSC spectra (11) are in agreements with sudden drops in <R> values obtained from SAXS measurements, which is presented in Table 1.

By means of combined DSC-SAXS measurements, we have shown that nanostructure of polymer electrolyte $(PEO)_8ZnCl_2$ can be modified by two treatments applied during preparation of electrolytes: the irradiation with γ-rays and the addition of TiO_2 nanosize particles. The significant role that the dimensions of the electrolyte material play in Zn^{2+}-ion mobility, oxygen reduction in TiO_2 nano-grains and cross-linking are discussed. Both treatments largely enhanced the conductivity of polymer electrolytes. SAXS information on average grain sizes change during the phase transition gave insight to the microscopic mechanism of ionic transport in nanocomposite polymer electrolyte. By means of electrical measurements (11), we have shown that polymer electrolyte $(PEO)_8ZnCl_2$ can be combined with nanostructured V_2O_5-CeO_2 at 38 at.% of V as intercalation cathode in order to obtain all solid-state rechargeable galvanic cell. Above mentioned treatments largely enhanced the conductivity of polymer electrolytes, but did not improve the performance of the cells. The probable reason for this is in deterioration in the film cohesion and elasticity after irradiation. TiO_2 nano-particles composed with polymer electrolyte induced additional oxidation and reduction processes in galvanic cell due to free carrier absorption. Depending on the electrochemical reaction, the surface and/or bulk properties of electrode in galvanic cell may also limit ion kinetics. Therefore, understanding of the microscopic mechanism of ionic transport in nanocomposite polymer electrolyte and surface and bulk properties of electrode material is beneficial for improving performance and limitation of galvanic cells. Further optimisations of electrolyte and electrodes properties are in progress as nano-structured materials are very attractive for batteries or other types of electronic devices.

Table 1. Comparison of <R> values for three types of samples of polymer electrolyte

$(PEO)_8ZnCl_2$	Melting						
	SAXS		DSC			IS	
	t °C	R/nm	t °C	t °C[11]	ΔH J/g[11]	t °C	(1)
0 kGy	64.04	19-21	58.88, 68.82	62.6	151.3	62.5	0.37
0 kGy, TiO_2	59.03	9-10.5	58.92,68.59,	61.5	130.0	64.6	1.30
309 kGy	61.03	7,5-5.5	62.03	57.6	143.5	60.1	196.90
$(PEO)_8ZnCl_2$	Crystallization						
	SAXS		DSC			IS	
	t °C	R /nm	t °C	t °C[11]	ΔH J/g[11]	t °C	
0 kGy	48.94, 38.23, 30.23, 28.57	21-25	52.68, 48.10, 38.10, 36.49	37.0	-112.0		
0 kGy, TiO_2	52.08, 22.98	7.5-8.5	53.22, 32.28	38.4	-115.1		
309 kGy	42.66	5.5-7	43.23, 34.33	34.3	-133.5	30.0	

(1) Factor of conductivity increase at melting transition

References:

[1] X. Zhang and R. Frech, Electrochimica Acta **42,** 475-482 (1997).
[2] Z. Crnjak Orel, Solid State Ionics **116,** 105-116 (1999).
[3] Z. Crnjak Orel and I.Mušević, Nanostructured materials, **12,** 399-404 (1999).
[4] A.Turković, Z.Crnjak Orel and P.Dubček, Mater. Sc. Eng. **B79**, 11-15 (2001).
[5] D.Posedel, A.Turković, P.Dubček and Z.Crnjak Orel, Mater. Sc. Eng **B90**, 154-162 (2002).
[6] K. Zweibel, Harnessing Solar Power; The Photovoltaic Challenge, Plenum Press, New York, 1990.
[7] T.M.A. Abrantes, LJ Alcacer and C.A.C. Sequeira, Solid State Ionics **18/19**, 315 (1986).
[8] M.J.C. Plancha, C.M. Rangel and C.A.C. Sequeira, Solid State Ionics **116**, 293 (1999).
[9] L. Krawiec, L.G. Scanlon Jr., J.P. Feliner, R.A. Vaia, S. Vasudevan and E.P. Giannelis, J. Power Sources **54** (1995) 310.
[10] F. Croce, G.B. Appetecchi, L. Persi and B. Scrosati, Nature **394,** 456 (1998).
[11] I.Pucić and A.Turković , Solid State Ionics **176**, 1797 (2005).
[12] Turković and Z. Crnjak Orel, Solid State Ionics **89** (3-4), 255 (1996).
[13] M.I. Lampreia and F. Barreira, Electrochim. Acta **21**, 485 & 489 (1976).
[14] A.S. Best, A. Ferry, D.R. MacFarlaine and M. Forsyth, Solid State Ionics **126**, 269 (1999).
[15] W. Wieczorek, P. Lipka and G. Zukowska Wycislik, J. Phys. Chem. B**102,** 6968 (1998).
[16] D. Posedel, I. Pucić, M. Lučić-Lavčević, Z. Crnjak Orel, A. Turković, 3rd Croatian Symposium on Electrochemistry, Proceedings, Dubrovnik 30.05-03.06.2004, 111 (2004).

2. Life Science

SPACING AND INTENSITY OF THE M3 REFLECTION OF SKELETAL MUSCLE: PROBES OF ACTIN-MYOSIN INTERACTION?

H. Amenitsch[1], C.C. Ashley[2], M.A. Bagni[3], S. Bernstorff[4], G. Cecchi[3], B. Colombini[3] and P.J. Griffiths[2]

1.) Institute of Biophysics and Nanosystems Research, Austrian Academy of Sciences, Schmiedlstraβe 6, A-8042 Graz, Austria.
2.) University Laboratory of Physiology, Parks Road, Oxford, OX1 3PT, U.K.
3.) Dipartimento di Scienze, Università degli Studi di Firenze, Viale G.B. Morgagni 63, Firenze, I-50134, Italy.
4.) Sincrotrone Trieste, Area Science Park, Basovizza/TS, I-34012, Italy.

Myosin II, the motor protein in muscle systems, aggregates into highly ordered filaments which interdigitate with filaments of the protein actin. In skeletal muscle, these filaments overlap in a hexagonal lattice, enabling their investigation by X-ray diffraction. The subfragment 1 (S1) moiety of myosin is the protein 'engine', composed of a 'motor domain' (bearing the actin and ATP binding sites) and a 9nm long 'lever arm'. S1 projects from the surface of the myosin filament at intervals of 14.32nm. It binds to the actin filament and subsequently generates force from the free energy of ATP hydrolysis at the catalytic site. S1 produces a translational step of 4-10nm or, if isometric, 2-4pN of force.

The X-ray pattern of striated muscle has equatorial, meridional and off-meridional components, providing information on the radial, axial and helical mass distribution, respectively, within the filament lattice. The strongest meridional reflection, M3, has a spacing equal to the axial period of S1 projections from the myosin filaments (14.32nm), and its intensity (I_{M3}) originates principally from S1 X-ray scattering. It has been proposed that both I_{M3} and d_{M3} are probes of actin-myosin interaction: in the activated state, I_{M3} is claimed to arise almost entirely from X-ray scattering by actin-bound S1 [1], and therefore I_{M3} signals depend entirely on the conformation of the actin-S1 complex. d_{M3}, which increases by 15.% upon activation [2], is proposed to indicate a structural change in the myosin filament backbone which is dependent upon the number of S1 interacting with actin, so d_{M3} is a probe of the fractional actin-binding of S1 [3]. Although this proposal is widely accepted, there are puzzling anomalies in the arguments supporting it. Originally, S1 binding to actin during tetani was thought to be ca. 75%, based on the comparison of stiffnesses of myofibrillar bundles in rigor and in isometric contraction. But in recent years, this view has been challenged. At physiological ionic strength and [ATP], motility studies show less than 1% of the isometric ATPase cycle time is spent in actin-bound states [4]. So for independent S1 moieties interacting with a single actin filament, one would thus expect not more than 1% to be instantaneously actin-bound. Furthermore, optical probes bound to the lever arm report the expected amount of lever arm tilting only if the fractional binding of S1 to actin is around 10% [5]. In addition, the original stiffness data supporting high fractional attachment has since been re-evaluated in the light of the (then unknown) stiffnesses of the actin and myosin filaments, leading to a new proposed fractional attachment of 40% [6]. Despite little quantitative agreement, these studies all suggest that substantially less than half the available S1 are bound during isometric contractions. Does this large detached S1 population must contribute significantly to I_{M3} in contracting muscle? And if d_{M3} is a probe of the degree of actin-myosin interaction, in what way is this interaction communicated to the myosin filament backbone? We have re-examined these questions using filament overlap and the muscle relaxant 2,3-butanedione monoxime (BDM) to vary the fraction of S1 bound to actin.

We studied two dimensional X-ray patterns of small bundles of tibialis anterior fibres from *Rana esculenta* in the relaxed state and during isometric tetanic contractions in different [BDM] (range 0-8mM). Patterns were collected on a 2D CCD detector during a 300ms X-ray

exposure, and were corrected for background scattering and spatial aberrations in the detector response. Reflection intensities were measured by projection onto the meridian, then by fitting with gaussian intensity distributions superimposed on a polynomial background. Experiments were performed at a sarcomere length of 2.2μm (full filament overlap) and sarcomere length was measured continuously throughout the experiment using a laser diffractometer.

The dependence of the intensity ratio I_{11}/I_{10} of the equatorial reflections changed linearly with tension development in different [BDM]. This linear relation is also seen when fore is varied by changing Ca^{2+} activation in skinned fibres, and thus indicates that BDM reduces force by changing the number of actin-bound S1 moieties. I_{M3} dependence on force in BDM was quadratic in form, as would be expected if I_{M3} were composed of intensity contributions from both bound and free S1 scatterers. At the highest [BDM], where active tension was almost completely suppressed, I_{M3} was 78% of its relaxed value. Since [BDM] in this range does not affect the Ca^{2+} regulatory system, it would appear that activation *per se* does not cause the loss of an I_{M3} contribution from free S1. Similar data were obtained when S1-actin interaction was decreased by reducing myofilament overlap (i.e. increasing muscle fibre length). These findings suggest that there are no grounds for assuming zero contribution from free S1 to I_{M3} during an isometric contraction.

The variation in d_{M3} was more complex. At low BDM, d_{M3} changed little with tension, but when BDM reduced tetanic tension to less than 50%, d_{M3} began to fall rapidly towards its relaxed value. Similar data was *not* obtained, in this case, when actin-myosin interaction was decreased by reducing myofilament overlap. But we found that the departure from the active tension-I_{M3} relationship in BDM could be explained by the presence of passive tension in the overlap experiments, and that the variation of I_{M3} with passive tension in relaxed bundles precisely paralleled I_{M3} dependence on active tension in BDM over the same force range. The spacing behaviour described here refers specifically to frog muscle, parallel experiments on glycerinated rabbit psoas muscle did not lead to the same spacing dependence on passive or active tension.

These findings are of great interest. First, if detached S1 also contribute to tetanic I_{M3}, then techniques such as the investigation of the power stroke by analysis of the substructure of M3 arising from interference across the M line would need to take this into account, since not all the interfering S1 would be actin bound [2]. Secondly, d_{M3} appears to depend on muscle axial load, and the use of d_{M3} as an indicator of S1-actin interaction could cause misleading conclusions to be drawn [3].

References:

[1] Linari, M., G. Piazzesi, I. Dobbie, N. Koubassova, M. Reconditi, T. Narayanan, O. Diat, M. Irving and V. Lombardi.. Interference fine structure and sarcomere length dependence of the axial X-ray pattern from active single muscle fibres. *Proc. Nat. Acad. Sci.*, **97,** 7226-7231 (2000).

[2] Huxley, H.E. and W. Brown. 1967. The low-angle x-ray diagram of vertebrate striated muscle and its behaviour during contraction and rigor. *J.Mol.Biol.*, **30,** 383-434 (1967).

[3] Piazzesi, G., M. Reconditi, I. Dobbie, M. Linari, P. Boesecke, O. Diat, M. Irving and V. Lombardi. Changes in conformation of myosin heads during the development of isometric contraction and rapid shortening in single frog muscle fibres. *J. Physiol.*, **512,** 305-312 (1999).

[4] Molloy, J. E., J.E. Burns, J. Kendrick-Jones, R.T. Tregear and D.C.S. White. Movement and force produced by a single myosin head. *Nature*. **378,** 209-212 (1995).

[5] Corrie, J.E.T., B.D. Brandmeier, R.E. Ferguson, D.R. Trentham, J. Kendrick-Jones, S.C. Hopkins, U.A. van der Heide, Y.E. Goldman, C. Sabido-David, R.E. Dale, S. Criddle and M. Irving. Dynamic measurement of myosin light-chain-domain tilt and twist in muscle contraction. *Nature,* **400,** 425-430 (1999).

[6] Linari, M., I. Dobbie, M. Reconditi, N. Koubassova, M. Irving, G. Piazzesi and V. Lombardi. The stiffness of skeletal muscle in isometric contraction and rigor: the fraction of myosin heads bound to actin. *Biophys. J.*, **74,** 2459-2473 (1998).

MULTI-COMPONENT CATIONIC LIPID/DNA COMPLEXES: A NEW STRATEGY FOR GENE DELIVERY

G. Caracciolo[1], D. Pozzi[1], R. Caminiti[1] and H. Amenitsch[2]

1.)Department of Chemistry, Università degli Studi di Roma "La Sapienza", p.le A. Moro 5, 00185, Rome, Italy
2.) Institute of Biophysics and Nanosystems Research, Schmiedlstrasse 6, A-8042 Graz, Austria.

Cationic lipid-DNA complexes, named lipoplexes in the scientific community, are extensively used for cell transfection in vitro and are also promising candidates for in vivo gene therapy [1]. Despite the relevant contribution clarifying the structure and morphology of lipoplexes, little is known about the mechanism of formation. This lack of knowledge is essentially due to the high complexity of the self-assembly process. We give the first experimental evidence that, upon DNA-induced fusion of two distinct populations of cationic liposomes, a well-ordered four component lipoplex emerges and that, at the molecular level, a complete lipid mixing occurs. Cationic lipids DOTAP and DC-Chol, and neutral lipids DOPC and DOPE, were used. Multilamellar DOTAP-DOPC (A) and DC-Chol-DOPE (B) liposomes were prepared following routine protocols [2]. Isoelectric A-DNA and B-DNA lipoplexes were prepared by injecting DNA into lipid dispersions. SAXS patterns of isoelectric A-DNA and B-DNA lipoplexes at T =20 °C are shown in Figs. 1a and 1d. The set of sharp lamellar peaks at q_{00n} is caused by the alternating lipid bilayer-DNA monolayer structure with periodicity d =2π/q_{001}=6.45 and 6.85 nm for the A-DNA and B-DNA lipoplexes, respectively. The Bragg peaks marked by arrows arise from diffraction from the one-dimensional lattice of DNA chains sandwiched between lipid bilayers [3]. Despite of similar lamellar periodicities d, very different DNA-DNA in plane repeat distances d_{DNA}=4.32 nm (A-DNA) and 3.25 nm (B-DNA) were detected. It means that, at the isoelectric point, A-DNA lipoplexes exhibit a lower surface charge density with respect to B-DNA lipoplexes resulting in a lower DNA packing density within the complex, i.e., in a higher d_{DNA} repeat distance. Then, we mixed initially separated A and B vesicles at five relative molar ratios R=B/(A+B)=0.2, 0.4, 0.5, 0.6, 0.8. Mixed lipid dispersions were equilibrated at 30 °C for 24 h. As expected, SAXS experiments revealed that, upon mixing A and B liposomes, interparticle electrostatic repulsions dominate over short-range attractive van der Waals forces and no fusion between A and B occurs. Afterward, proper amounts of DNA solution were added to the mixed lipid dispersions paying attention to exactly neutralize the positive charge carried both by DOTAP and DC-Chol molecules. SAXS patterns of Figs. 1b and 1c show that, for each R value, only one kind of mixed A-BDNA lipoplexes exist. Indeed, if A-DNA and B-DNA lipoplexes coexisted within the sample volume, the SAXS pattern would arise from the superposition of their own patterns. Even if one could not exclude the presence of A-DNA and B-DNA-rich domains, there are several reasons that a high degree of lipid mixing at the molecular level occurs.15 First of all, both d and d_{DNA} vary monotonously as a function of R as shown in Fig. 2 (top and bottom panel). In addition, the full width at half maximum (FWHM) of all the Bragg peaks is approximately constant as a function of R (inset of Fig. 2, top panel). Furthermore, all the SAXS patterns exhibit a single DNA peak. It is well-established that the DNA-DNA distance d_{DNA} only depends on the physical properties of the lipid membrane.

Undoubtedly, mixed A-B-DNA lipoplexes can exist only if A and B liposomes break during complex formation (Fig. 3) [4]. As liposomes fusion was not observed simply by mixing A and B, it is therefore the DNA which reduces the intermembrane repulsive barrier due to electrostatic, steric, and hydration forces. Our research has also highlighted, for the first time, the possibility of forming well-ordered self-assembled lipoplexes composed of four lipid components, merely by adding DNA to dispersions containing two distinct populations of binary cationic liposomes. By varying the composition of the mixed lipid dispersion, the

physical properties of the emerging lipid carrier, such as the surface charge density and membrane thickness, can be modulated and distinct DNA packing densities may also be achieved. The development of such arrays is a very rich strand for future research in that it opens the gateway to synthesize multipart gene delivery vectors. Indeed, it is commonly accepted that there will not be a "universal vector," but each clinical indication may require a specific system.

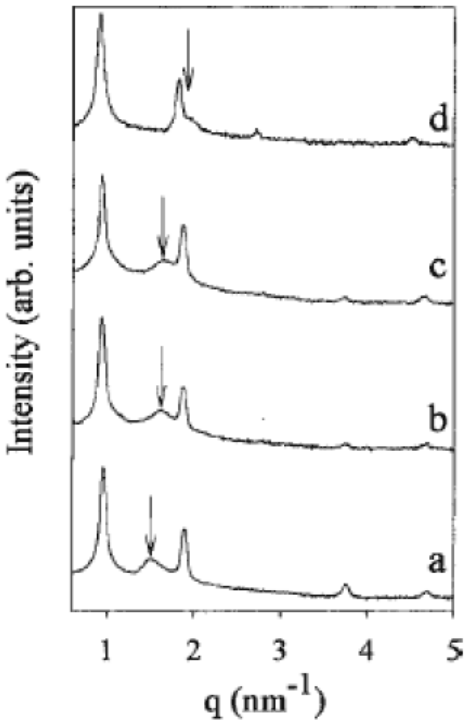

Figure 1. Representative SAXS patterns of A-B-DNA complexes as a function of increasing molar percentage of B liposomes in the lipid dispersions R=B/(A+B) from the bottom to the top: (a) R=0; (b) R=0.4; (c) R=0.6; and (d) R=1. Intermediate SAXS patterns (b) and (c) do not arise from the linear combination of (a) and (d) patterns. DNA-DNA peak is marked by an arrow.

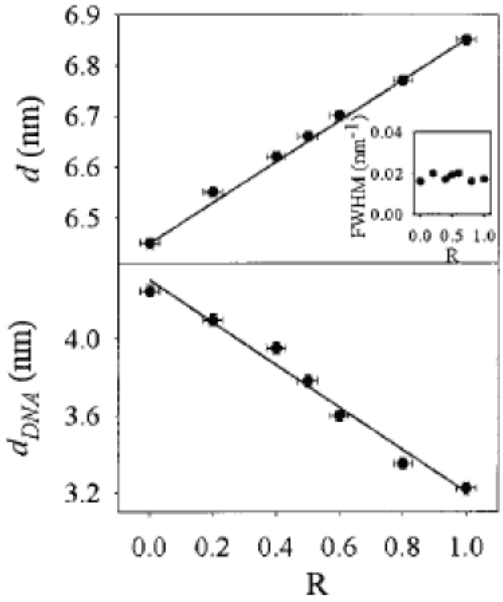

Figure 2. Interlayer distance d (top panel) and DNA-DNA interaxial distance d_{DNA} (bottom panel) as a function of R. Solid lines are the best linear fits to the data. In the inset of the top panel, the FWHM of the first-order Bragg peak is shown. Higher-order reflections exhibited similar trends.

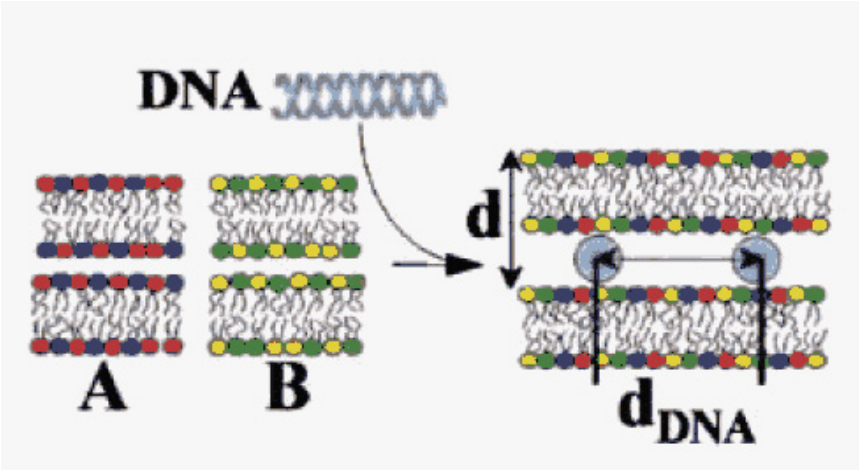

Figure 3. Schematics of the process occurring, at the molecular level, upon DNA-induced fusion of two distinct populations of cationic liposomes. A and B represent a sketch of the lipid bilayer membranes of DOTAP-DOPC (A) and DC-Chol-DOPE (B) liposomes. For clarity, each color refers to a single lipid species.

References:

[1] P. L. Felgner, G. M Ringold, Cationic liposome mediated transfection, Nature **331**, 461-462 (1989).
[2] I. Koltover, T. Salditt, J. O. Rädler, C. R. Safinya, An inverted hexagonal phase of cationic liposome-DNA complexes related to DNA release and delivery, Science **281**, 78-81 (1998).
[3] G. Caracciolo, R. Caminiti, DNA–DNA electrostatic interactions within cationic lipid/DNA lamellar complexes, Chem. Phys. Lett. **400**, 314-319 (2004).
[4] G. Caracciolo, D. Pozzi, R. Caminiti, H. Amenitsch, Lipid mixing upon deoxyribonucleic acid-induced liposomes fusion investigated by synchrotron small-angle x-ray scattering, Appl. Phys. Lett. **87**, 133901-133903 (2005).

MULTI-COMPONENT LIPOPLEXES FORMATION: $L_{\alpha}^{C} \rightarrow H_{II}^{C}$ PHASE TRANSITION

G. Caracciolo[1], D. Pozzi[1], R. Caminiti[1] and H. Amenitsch[2]

1.)Department of Chemistry, Università degli Studi di Roma "La Sapienza", p.le A. Moro 5, 00185, Rome, Italy
2.) Institute of Biophysics and Nanosystems Research, Schmiedlstrasse 6, A-8042 Graz, Austria.

With the aim of better understanding the mechanism of formation of cationic liposome/DNA complexes, we looked at the simultaneous interaction of two populations of cationic liposomes with linear DNA [1]. Multilamellar DC-Chol/DOPC (A), DOTAP/DOPE (B) and DC-Chol/DOPE (C) cationic liposomes were prepared at a molar ratio of neutral lipid in the bilayer Φ=(neutral lipid/total lipid) (mol/mol)=0.5. Then, we mixed initially separated A and B vesicles at seven relative molar ratios R_{AB}=A/(A+B)=0, 0.2, 0.4, 0.5, 0.6, 0.8, 1. The first and the latter R_{AB} values refer to pure B and A vesicles respectively. Analogously, we prepared mixed B–C dispersions at the molar ratios R_{BC}=C/(B+C)=0, 0.2, 0.4, 0.5, 0.6, 0.8, 1. SAXS pattern of Figure 1 (bottom panel) shows that A-DNA lipoplexes are assembled in the lamellar L_{α}^{C} phase. SAXS pattern of B-DNA lipoplexes (R_{AB}=0) is shown in Figure 1 (top panel). Lamellar peaks at q_{00n} arising from the lamellar L_{α}^{C} phase ($d=2\pi/q_{001}$=65.2 Å) were detected. In addition we observed Bragg peaks positioned at q_{10}=0.109 Å^{-1}, q_{20}=0.218 Å^{-1}, q_{21}=0.287 Å^{-1} (marked by red arrows in Figure 1, top panel). They were perfectly indexed on a two-dimensional hexagonal lattice with a unit cell spacing of $a=4\pi/[(3)^{0.5}q_{10}]$=66.6 Å [2].
Adding DNA to mixed A–B dispersions produces major changes in the lipid structure. SAXS patterns of Figure 2 ($0.4<R_{AB}<0.8$) show that, for each R_{AB} value, only mixed A–B lipoplexes exist. The present results have provided additional information in that high mixing of lipids between A and B liposomes occured. Thus, we have provided evidence that, upon fusion of A and B liposomes, the lipid bilayer, being a fluid mixture, allowed for lateral diffusion of lipid molecules leading to a spatial distribution of the four lipid species, on average, uniform. Significantly, we observed that the inner structure of B-DNA lipoplexes (coexisting L_{α}^{C} and the H_{II}^{C} phases) closely resemble that of pure B membranes (coexisting L_{α} and H_{II} phases) with the water space inside the inverse micelle of the H_{II} phase and the interbilayer water region of the L_{α} phase both filled by DNA (schematics in Figure 1, top panel). It means that, upon complexation, DNA lets B liposomes break up and penetrates the accessible water regions. Conversely, we observed that A–B-DNA lipoplexes are only assembled in the lamellar phase. Thus, some molecular events occurring during A–B-DNA lipoplexes formation were able to induce the $H_{II} \rightarrow L_{\alpha}$ phase transition of B membranes firstly assembled in the H_{II} phase. Although DNA-induced liposomes fusion is the first step in the lipoplex formation, it can not be the DNA to induce the observed hexagonal to lamellar phase transition. By comparing the different phase behavior of B and A–B lipid dispersions upon lipoplex formation we argue that lipid mixing is the driving force which induces the observed phase transition. In fact, lipid mixing occurring upon DNA-induced fusion of B vesicles could not produce any detectable structural change. At the molecular level, lipid mixing occurring during A and B liposomes fusion can produce major structural changes. Indeed, cationic DOTAP and DC-Chol as well as neutral DOPC have a cylindrical shape with the cross section area of headgroups approximately equal to the hydrophobic chain area. Thus they tend to self-assemble into lamellar structures with a spontaneous curvature $C_0=1/R_0=0$. DOPE, due to its cone-like molecular arrangement, gives rise to a negative natural curvature and forms inverted

hexagonal phases. Furthermore, it is well established that the shape of the molecule determines the curvature of the membrane and the structure of the self assembly. Thus, lipid mixing gradually reduces the relative molar percentage of DOPE in the emerging lipid bilayer with respect to pure B membranes and the lamellar phase becomes favored with respect to the inverted hexagonal one. Lipid mixing therefore induces the $H_{II} \rightarrow L_{\alpha}$ phase transition by controlling the spontaneous curvature of the emerging membranes. Unambiguous support to this interpretation was provided by SAXS experiments replicated on B-C ternary lipoplexes as a function of R_{BC}. As shown in Figure 3, C-DNA lipoplexes show a highly-organized lamellar structure with periodicity d=69 Å and DNA spacing d_{DNA}=29.2 Å. Ternary B–C-DNA lipoplexes formed coexisting L_{α}^{C} and the H_{II}^{C} phases up to R_{BC}=0.4. This is because, for $R_{AB}=R_{BC}$, B–C-DNA lipoplexes have higher molar percentage of DOPE in the bilayer than A–B-DNA lipoplexes (DOPC substituted by DOPE). As a result, $H_{II} \rightarrow L_{\alpha}$ phase transition can not be completed up to R=0.5. Accordingly, we identified the structural pathway leading to phase transition that is schematically described in Figure 4 [3].

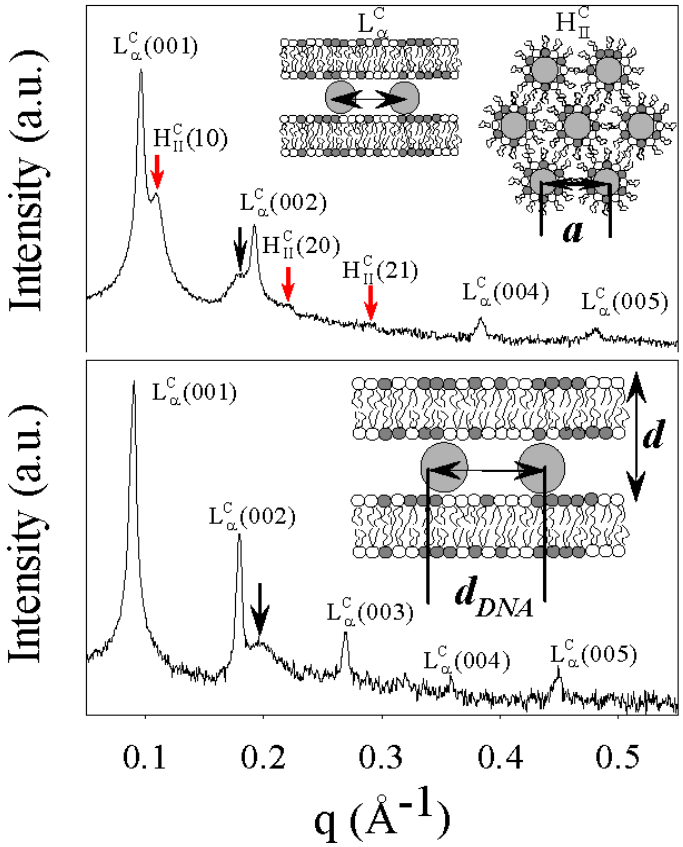

Figure 1. Bottom panel: SAXS pattern of DC-Chol/DOPC-DNA lipoplex (A-DNA in the text, R_{AB}=1). In the inset, schematics of the L_{α}^{C} lamellar phase is depicted. Top panel: SAXS pattern of DOTAP/DOPE-DNA lipoplex (B-DNA in the text, R_{AB}=0) arising from coexisting L_{α}^{C} and the H_{II}^{C} phases. Red arrows indicate the Bragg reflections of the H_{II}^{C} phase. In the inset schematics of both the phases is displayed. DNA peak of the lamellar phase is marked by a black arrow in both the panels.

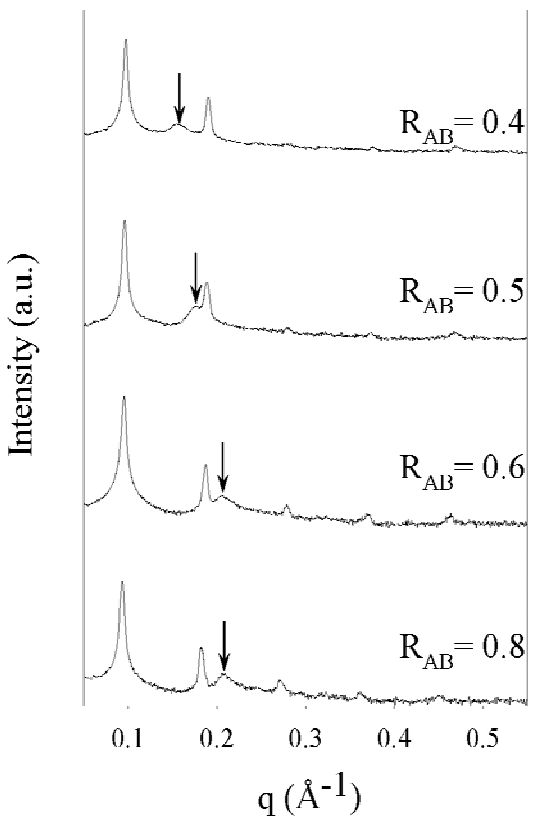

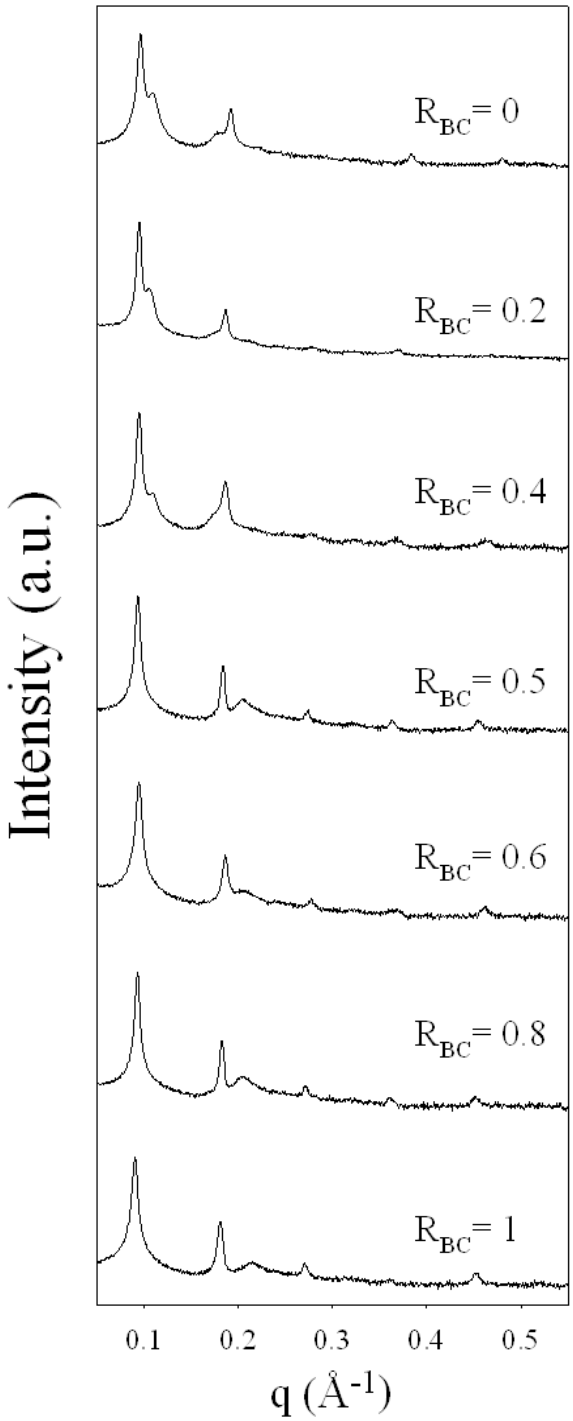

Figure 2 (left). SAXS patterns of mixed A–B-DNA lipoplexes as a function of the relative molar fraction R_{AB}=A/(A+B). As R_{AB} increases, DNA peak (marked by arrows) moves to higher *q*-values, i.e. shorter DNA spacings, as a result of higher surface charge density of the lipid membrane.

Figure 3 (right). SAXS patterns of ternary B–C-DNA lipoplexes as a function of the relative molar fraction R_{BC}=C/(B+C). As R_{BC} increases, the percentage of H_{II}^{C} phase in mixed lipoplexes decreases. At R_{BC}=0.5 only lamellar lipoplexes exist.

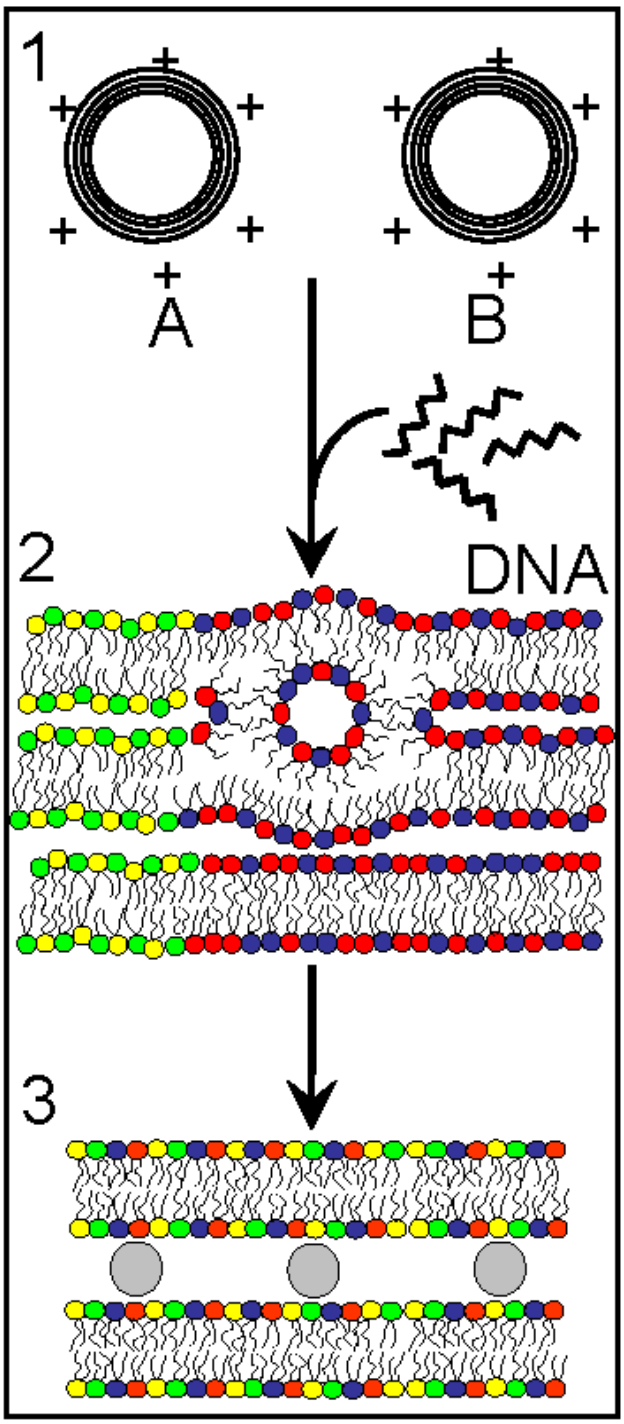

Figure 4. In the first step (1), DNA is added to a mixed dispersion containing non-interacting positively charged A and B liposomes. In the second step (2), DNA induces local aggregation and fusion of A and B. In the sketch, a rod of the hexagonal phase of B (red and blue molecules) fuse with the bilayer structure of A (green and yellow molecules). Upon fusion, large lipid mixing occurs. Lipid mixing diminishes the percentage of DOPE in the emerging bilayer with respect to that of pure B membranes and promotes the hexagonal to lamellar phase transition by controlling the curvature of membranes. As a result, only mixed A–B lipoplexes exist (3).

References:

[1] G. Caracciolo, D. Pozzi, R. Caminiti, H. Amenitsch, Lipid mixing upon deoxyribonucleic acid-induced liposomes fusion investigated by synchrotron small-angle x-ray scattering, Appl. Phys. Lett. **87**, 133901-133903 (2005).

[2] I. Koltover, T. Salditt, J. O. Rädler, C. R. Safinya, An inverted hexagonal phase of cationic liposome-DNA

[3] G. Caracciolo, D. Pozzi, R. Caminiti, H. Amenitsch, Multi-component cationic lipid-DNA complex formation: role of lipid mixing, Langmuir **21**, 11582-11587 (2005).

ONE-DIMENSIONAL THERMOTROPIC DILATATION AREA OF LIPID HEADGROPUS WITHIN CATIONIC LIPOSOME/DNA COMPLEXES

G. Caracciolo[1], D. Pozzi[1], R. Caminiti[1] and H. Amenitsch[2]

1.)Department of Chemistry, Università degli Studi di Roma "La Sapienza", p.le A. Moro 5, 00185, Rome, Italy.
2.) Institute of Biophysics and Nanosystems Research, Schmiedlstrasse 6, A-8042 Graz, Austria.

Last step in devising more efficient cationic liposome/DNA complexes (lipoplexes) will be understanding the relationship between the structural properties and function of the complexes in order to direct the self-assembly of lipoplexes towards the desired nanostructures. Very recently, many different liposomal formulations with temperature sensitivity have been reported [1]. As a result, hyperthermia and liposomal drug delivery started to be used together in attempt to exploit their mutual interactions against cancer. Although this combination therapy seems to hold great promise towards improving current TE, the molecular mechanisms by which it does remain unclear. Using simultaneous synchrotron small and wide angle X-ray scattering (SWAXS) we investigated the thermotropic behavior of cationic lipid mixture of DOTAP–DOPC liposomes complexed with linear calf thymus DNA. Figure 1 shows the SWAXS patterns of charge-neutral DOTAP–DOPC/DNA lipoplexes as a function of temperature. The series of temperature-dependent WAXS scans of Figure 1 ($1<q<1.55$ Å^{-1}) reveal that the DOTAP–DOPC lipid membranes are in the liquid-crystalline L_α phase. The equally spaced BPs in the SAXS regime ($0.05<q<0.55$ Å^{-1}) at q_{00n} are caused by alternating lipid bilayer-DNA monolayer L_α^C structure (Figure 2) with lamellar periodicity $d=2\pi/q_{001}$. The broad middle peak positioned at q_{DNA}, between the first two BPs of the L_α^C structure, is attributed to the in-plane packing of the intercalated DNA strands with spacing $d_{DNA}=2\pi/q_{DNA}$. Figure 2 shows the electron density profiles (EDPs) calculated from the lamellar BPs of Figure 1 for three different temperatures (T=5, 35 and 65 °C). According to general definitions, the bilayer thickness, d_B, is defined as the distance between headgroup peaks in the EDP whereas the thickness of the interbilayer water region is the difference between the lamellar periodicity and the bilayer thickness, $d_W=d-d_B$. Figure 3 shows the temperature dependence of the retrieved structural parameters for DOTAP–DOPC/DNA lipoplexes. At 5 °C DOTAP–DOPC/DNA lipoplexes exhibit a lamellar periodicity d=64.6 Å which is in close agreement with those previously reported [2].
Starting at 5 °C and on increasing temperature, the lamellar repeat distance d decreases from 64.6 to 60.3 Å. Figure 3 also shows that the reduction of the lamellar periodicity is due to the simultaneous thinning of both the membrane and the water region. The membrane gets thinner with increasing temperature due to the disordering of hydrocarbon chains accompanied by a decrease in the effective chain length. Temperature raising induces the continuous formation of *trans-gauche* rotamers within acyl chains. The asymptotic behavior observed above 35°C is a well known saturation effect in hydrocarbon chain melting and it is due to the finite length of the acyl chains in that only a limited number of *gauche* isomers can be generated [3]. From the temperature dependence of both the average interfacial area of lipid headgroups, A, and the DNA spacing we calculated the thermal expansion coefficients

$$\alpha_A = \frac{\Delta A}{A}\frac{1}{\Delta T} \qquad (1)$$

and

$$\alpha_{DNA} = \frac{\Delta d_{DNA}}{d_{DNA}} \frac{1}{\Delta T} \tag{2}$$

Table 1 lists both the calculated thermal expansion coefficients as a function of temperature. Interestingly, the thermal expansion coefficients are almost the same. This finding suggests that the dilatation of lipid headgroups area is not isotropic but occurs in the plane of the membrane along one direction perpendicular to the DNA axis [4]. At the molecular level, DNA acts therefore as a grid with lipid molecules constrained to follow the dilatation of the 1D DNA lattice. This finding demonstrates quantitatively that the lateral expansion of the lipid bilayer within DOTAP–DOPC/DNA lipoplexes is governed by the lateral expansion of the DNA in plane rod lattice and that the increase in DNA spacing is a direct and quantitative measure of the area dilatation of the lipid bilayer itself.

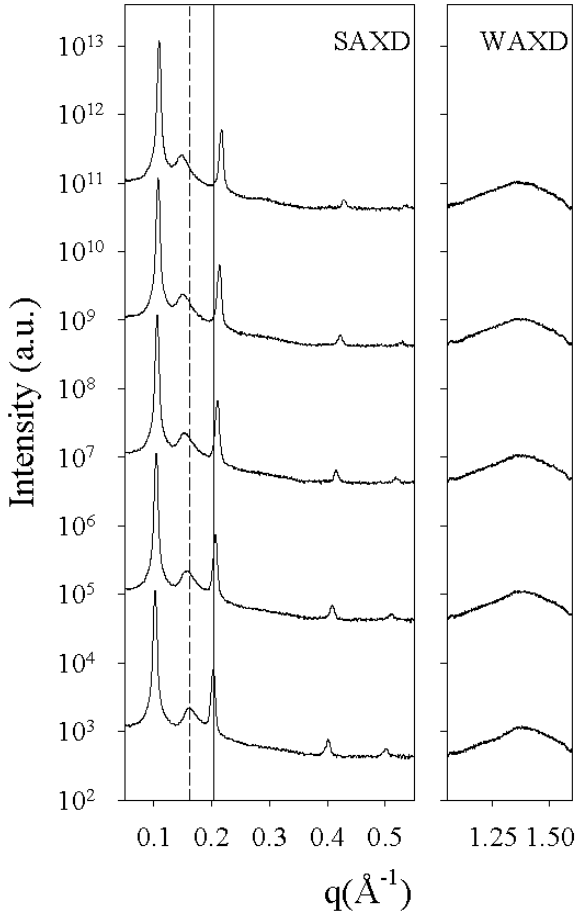

Figure 1 Synchrotron SWAXS scans for isoelectric DOTAP–DOPC/DNA lipoplexes as a function of temperature (T=5, 20, 35, 50, 65 °C from the bottom to the top). Each scan is shift by multiplicative constants for better comparison. Solid and dashed lines are guides to the eye allowing to follow the shift of the second-order BP of the lamellar lipid bilayer-DNA monolayer structure and the moving of the DNA peak respectively.

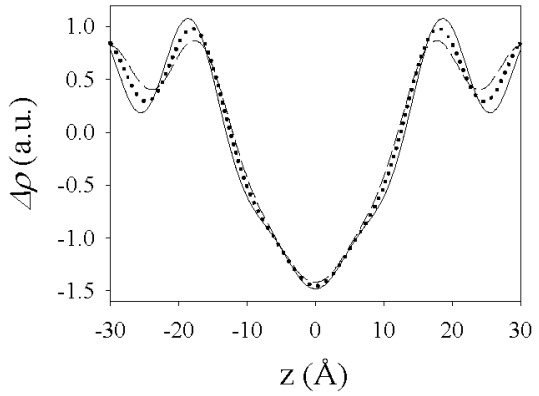

Figure 2. Electron density profiles of DOTAP–DOPC/DNA lipoplexes as a function of temperature: 5 °C (dashed line), 35°C (dotted line) and 65°C (solid line). The distance from the centre of the lipid bilayer is indicated as z.

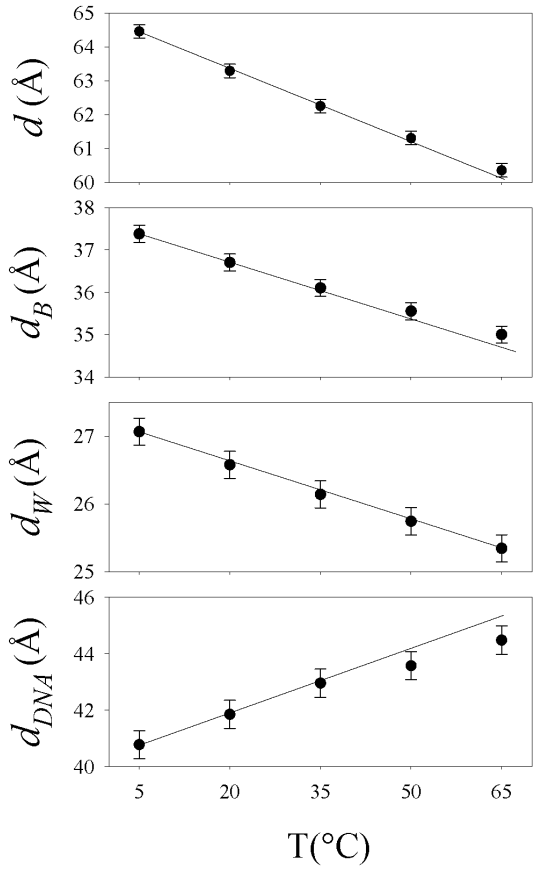

Figure 3. Temperature dependence of the lamellar spacing d, the bilayer thickness d_B, the water layer thickness d_W and the DNA rod lattice d_{DNA} of isoelectric DOTAP–DOPC/DNA lipoplexes. Solid line are linear fit to the data in the temperature range between 5°C and 35°C. As evident, the bilayer thickness and the DNA-DNA spacing show an asymptotic behavior for T>35°C.

Table 1. Structural parameters of DC-Chol–DOPE/DNA lipolexes (T=5°C) as a function of incubation time, as calculated by EDPs.

Time	α_A (10^{-3} K^{-1})	α_{DNA} (10^{-3} K^{-1})
5	1.509	1.512
20	1.470	1.472
35	1.432	1.440
50	1.412	1.417
65	1.383	1.390

References:

[1] G. Kong, G. Anyarambhatla, W. Petros, P.R.D. Braun, O.M. Colvin, D. Needham, M.W. Dewhirst, Cancer Res. **60**, 6950-6957 (2000).
[2] I. Koltover, T. Salditt, C. R. Safinya, Biophys. J. **77**, 915-924 (1999).
[3] M. Rappolt, P. Laggner, G. Pabst, Recent Res. Devel. Biophys. **3**, 363-394 (2004)
[4] G. Caracciolo, D. Pozzi, R. Caminiti, H. Amenitsch, Langmuir **22**, 4267-4273 (2006).

INSERTION OF CYTOTOXIC ANTICANCER AGENT IN SPHINGOMYELIN-CHOLESTEROL LIPOSOMES : STUDY OF LIQUID CRYSTALLINE STRUCTURES BY COUPLING DSC AND HRSAXS

C. Chemin[12], C. Bourgaux[1], JM. Péan[2], H. Amenitsch[3], P. Wüthrich[2], G. Keller[1], P. Couvreur[1] and M. Ollivon[1]

1.) Physico-Chimie des Systèmes Polyphasés, UMR 8612, Univ. Paris-Sud, 5 rue JB Clément, Chatenay, France
2.) Technologie SERVIER, 27 rue E. Vignat, 45000 Orléans, France
3.) Institute for Biophysics and Nanosystems Research, Schmiedlstr. 6, 8042 Graz, Austria

The interactions of an anticancer agent with sphingomyelin / cholesterol lipid bilayers were examined as function of temperature and medium composition by coupled SWAXS+DSC in the range 20-60C. Structural and calorimetric changes showed that the drug presence influence the organization of the membrane and it depends on the medium composition.

Introduction S12363 is an anticancer drug which has a strong activity in vitro but also a high toxicity in vivo. Intravenous administration of this drug encapsulated into long-circulating liposomes is expected to improve its therapeutic index [1]. Loading of S12363 into liposomes was achieved using two methods based on the formation of either a pH gradient [2] or an ammonium gradient [3]. These two techniques involve a ΔpH between the pH of acidic inner liposomal compartment and the final pH of outer phase, in which the drug is not soluble. High encapsulation yields (> 90 %) were obtained using both techniques for Egg sphingomyelin / cholesterol / cholesterol-PEG (ESM/Chol/Chol-PEG) vesicles. The aim of this study was to investigate the exact localization of drug substance as a function of the loading process used[4].

Experimental methods The internal pH of liposomes was determined by spectrofluorimetry measurements using an Oregon Green pH probe and compared to the external pH measured by classical electrochemistry method. The pH gradient was formed by increasing to pH 8 the external pH of vesicles formed in pH 3 citrate buffer, or by removal of external salts for vesicles formed in an ammonium sulfate buffer. To study the interactions between the encapsulated drug and the liposome membrane, ESM/Chol 90:10 lamellar phases (MLV-multilayered vesicles) were prepared by hydration of freeze-dried lipid mixtures with citrate buffer or ammonium sulfate buffer in order to reach a final concentration of lipids of 200 mg/ml. S12363 was solubilized in citrate buffer or freeze-dried with lipids before hydration with ammonium sulfate buffer . S12363 was also freeze-dried with lipids and then hydrated with water to characterize the effect of the drug incorporated into the bilayers. Interactions were studied on the SAXS beamline by Differential Scanning Calorimetry (DSC) coupled with time-resolved synchrotron X-Ray Diffraction, as a function of temperature (XRDT) in the range 20°C T 60°C using Microcalix calorimeter [5].

Results and discussion In citrate buffer and in ammonium sulfate buffer, the liposomes had an internal pH of 4. The pH gradient was stable over a period of at least 28 days. Accordingly, interactions between the drug and the lamellar phases were investigated at pH 4 in both buffers (fig 1 and 2).
The effects of the drug on thermal and structural parameters were similar for the two buffers studied. DSC showed that the encapsulated drug induced a decrease of sphingomyelin melting temperature (Tm) but not of the chain melting enthalpy. In addition, a second endotherm was observed. XRDT revealed that S12363 decreased the lamellar repeat spacing of the gel phase and increased that of the liquid crystalline phase. Therefore, the temperature-dependent changes in lamellar repeat spacing were reduced when drug is present.
In water, a single endotherm was identified; DSC showed a decrease of both sphingomyelin melting temperature and enthalpy (fig 3), consistent with incorporation of the drug within the membrane. The observed variations of the structural parameters were lower in water than those evidenced in citrate and ammonium sulfate buffers. These results show that the incorporation of the drug into the membrane does not induce important changes in lamellar d-spacing and suggest that in citrate and

ammonium buffers a part of S12363 molecule interacts with ESM polar head group.

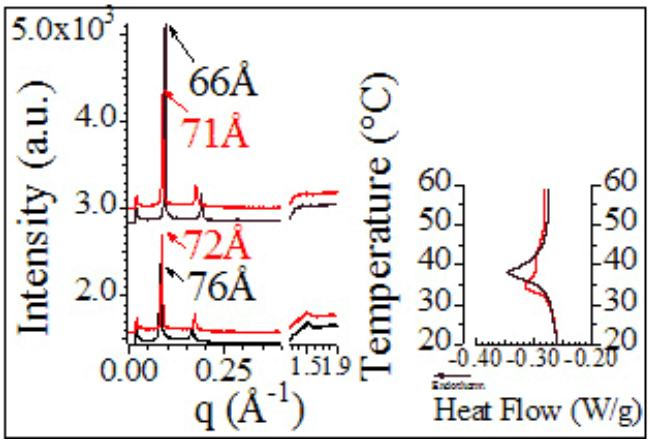

Figure 1. SWAXS diffraction patterns (left) at 20°C and 55°C of ESM/Chol bilayers hydrated with a citrate buffer pH 4 (black curves) or hydrated with a solution of S12363 in citrate buffer pH 4. The right part shows corresponding DSC curves (scanning rate 2°C/min).

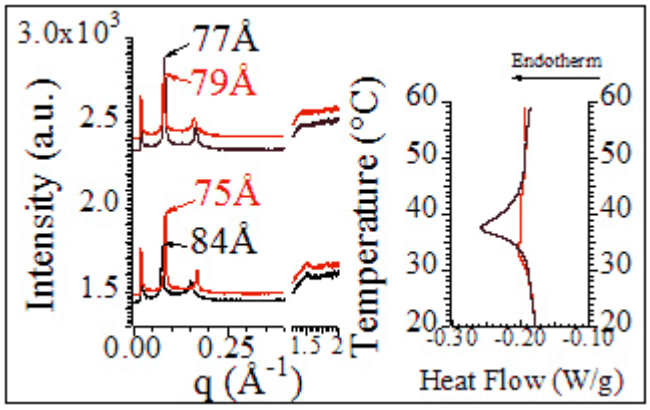

Figure 2. SWAXS diffraction patterns (left) at 20°C and 55°C of ESM/Chol bilayers (black curves) or ESM/Chol/S12363 (red curves) bilayers hydrated with an ammonium sulfate buffer pH 4 (right part as above).

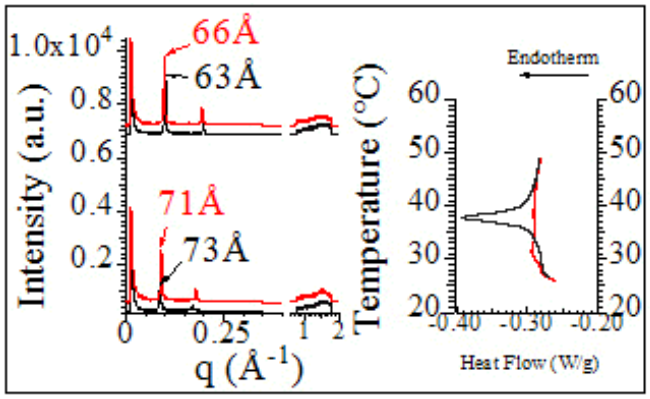

Figure 3. SWAXS diffraction patterns (left) at 20°C and 55°C of ESM/Chol bilayers (black curves) or ESM/Chol/S12363 (red curves) bilayers hydrated with water (right part as above).

Conclusion This study clearly demonstrates that the supramolecular organization of the liposomes is affected by the drug presence but not by the drug loading process. Both techniques used demonstrate that the encapsulated drug is localized in the vicinity of the ESM polar head groups and partially embedded into the sphingomyelin tails. Thank to both model system and the small size of samples used, the coupling of SWAXS and DSC allows to determine the interactions of anticancerous drug with lipidic vesicles.

References:

[1] A. Chonn, P.R. Cullis, Curr. Opin. Biotechnol. 6 (1995) 698-708.
[2] L.D. Mayer, T.D. Madden, M.B. Bally, P.R. Cullis, Liposome Technology : Entrapment of Drug and Other Materials II (1993) 27-44.
[3] E. Maurer-Spurej, K.F. Wong, N. Maurer, D.B. Fenske, P.R. Cullis, BBA 1416 (1999) 1-10.
[4] C. Chemin et al., in preparation
[5] M. Ollivon, G. Keller, C. Bourgaux, D. Kalnin, P. Villeneuve and P. Lesieur, J. Thermal Anal. and Calor., 85 (2006) 219–224.

SURFACE FUNCTIONALIZED LIPID-DNA-METAL COMPLEXES FOR GENE DELIVERY: X-RAY DIFFRACTION STUDY OF PEGYLATED LAMELLAR COMPLEXES

O. Francescangeli[1], M. Pisani[2], P.Bruni[2] and S. Bernstorff[3]

1.) Dipartimento di Fisica e Ingegneria dei Materiali e del Territorio, Via Brecce Bianche, Ancona, Italy
2.) Dipartimento di Scienze e Tecnologie Chimiche, Via Brecce Bianche, Ancona, Italy
3.) Sincrotrone Trieste S.C.p.A. Strada Statale 14, Km 163.5, I-34016 Basovizza (Trieste), Italy

Gene therapy require efficient systems for the delivery of DNA and other biological macromolecule into cells. The major constraint in this field is to devise ideal 'vehicles' to target appropiate cells and achieve physiological levels of the desired gene production. Within the general scope of providing new biological materials of potential interest for gene delivery systems we have recently undertaken a systematic study of the interactions among DNA, neutral liposomes (L) and metal cations (Me^{2+}) in triple L- DNA-Me^{2+} complexes [1-3]. The aim of the present research is the development of vectors that lead to a significant increase of the transfection efficiency. The inclusion of a biocompatible polymer shell is essential in developing a synthetic gene delivery system that can successfully evade the immune system for systemic *in-vivo* applications. The functionalization of the neutral lipids with PEG should enhance the binding of the carrier to the DNA molecules. To this purpose, we have carried out a series of x-ray diffraction experiments focused to study the nano-scale structure of ternary mixtures of polyethyleneglycol(PEG)-lipids conjugated, DNA (from calf thymus) and divalent cations (among the most common in biological cells) and their macromolecular assembly. The final goal is to gain information on the relationships between structure and physico-chemical properties of the component materials.

Even though very preliminary, the elaboration of the experimental data seems to provide quite promising results. As an example, in fig.1 we show the x-ray diffraction patterns of DOPE-PEG(350)/DOPE mixture as a function of increasing concentration of PEG(350)-lipid. The set of periodically spaced sharp peaks originates from an inverted hexagonal structure *(H_{II})*, whose structural elements are infinitely-long rigid rods, all identical and crystallographically equivalent, regularly packed in a 2D hexagonal lattice. The cylinders are filled by water and are dispersed in the continuous medium constituted by hydrocarbon chains, whereas the polar groups are located at the water-hydrocarbon chain interface. The addition of PEG(350)-lipid leads to an increase of the 2D hexagonal lattice with a unit cell spacing from a = 72 Å to a = 76 Å. At 25% of PEG(350)-lipid incorporated the hexagonal phase disappears.

Figure 2 shows the diffraction patterns related to [DOPE-PEG(350)/DOPE]-DNA-Mn^{2+} complexes at molar ratio 4:12:18. From x-ray data, at low DOPE-PEG(350) concentration, it can be observed the coexistence of two hexagonal phases one with unit cell a_1~78 Å, the other with a_2~69 Å. Increasing the DOPE-PEG(350) concentration, the scattering profiles reveal the coexistence of a cubic phase and a hexagonal phase. The Bragg peaks of the cubic lattice were spaced in the ratios √2: √3: √4: √6: √8: √9: √10, corresponding to the Q^{224} phase with the space group *Pn3m*. The lattice parameter of the *Pn3m* is a=141 Å and of the H_{II} is a = 68 Å. Increasing the PEG-lipid concentration it can be observed a transition to a cubic phase. This cubic phase *Pn3m* is observed in the DOPE-PEG(350)/DOPE]-DNA-Ca^{2+} complexes too. Based on these data, a transition from an inverted hexagonal phase to a cubic phase should occur in three-component mixtures on increasing the PEG-lipid concentration, which is a new and quite striking result. We believe that these findings can open up new exciting perspectives for the understanding of the complexes phase behaviour in the presence of PEG-lipid.

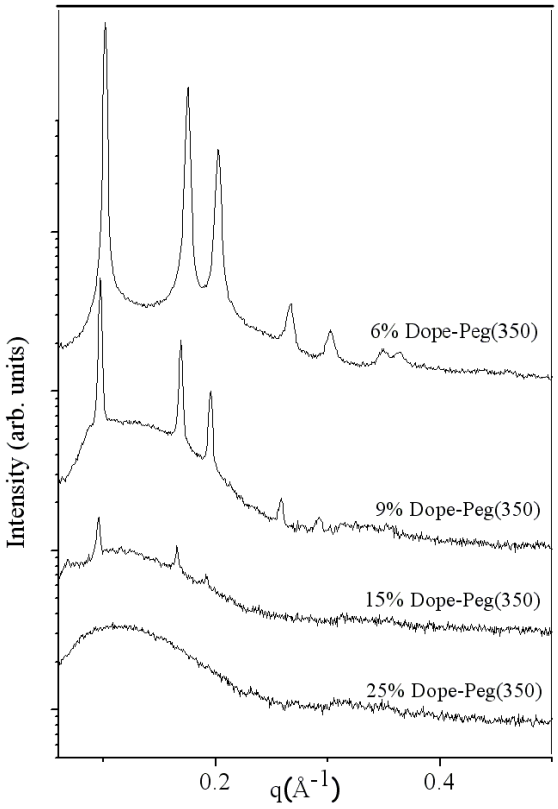

Figure 1. Synchrotron X-ray diffraction patterns of [DOPE-PEG (350)/DOPE] mixture as a function of the concentration PEG(350)-lipid.

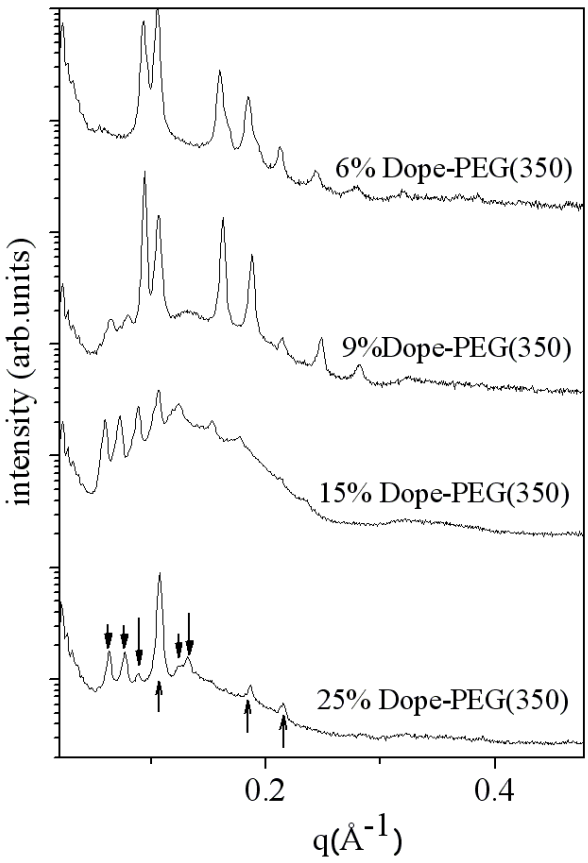

Figure 2. Synchrotron X-ray diffraction patterns of [DOPE-PEG(350)/DOPE]-DNA-Mn^{2+} mixture at molar ratio 4:12:18. The black and white arrows denote the Bragg peaks associated with the Q^{224} (*Pn3m*) cubic phase and the H_{II} hexagona$_l$ phase, respectively

References:

[1] P. Bruni, M. Pisani, A. Amici, C. Marchini, M. Montani, O. Francescangeli; "Ternary complexes formed by neutral liposomes, DNA and bivalent metal cations as promising vectors for gene transfer"; *Appl. Phys. Lett* **88**,7, 073901 (2006).

[2] M. Pisani, P. Bruni, G. Caracciolo, R. Caminiti, O. Francescangeli; "Structure and phase behavior of self-assembled DPPC-DNA-Metal cation complexes"; Journal of Physical Chemistry B, **110** (26),13203-13211 (2006).

[3] M. Pisani, P. Bruni, Conti, E. Giorgini, and O. Francescangeli; "Self-Assembled liposome-DNA-metal complexes related to DNA delivery"; Mol. Cryst. Liq. Cryst. **434**, 643 (2005).

SURFACES ENRICHED BY PLASMA-DEPOSITED PROTEINS: A GISAXS STUDY

M.G. Ortore[1], F. Spinozzi[1], R. Sinibaldi[1], S. Bernstorff[2], P. Mariani[1] and F. Rustichelli[1]

1.) Dipartimento di Scienze Applicate ai Sistemi Complessi, Via Brecce Bianche, 60131 Ancona, Italy
2.) Elettra Sincrotrone Trieste, SS 14, 34012 Basovizza, Trieste, Italy

Quite recently, thanks to the increasing use of synchrotron radiation, the conventional X-ray scattering techniques were extended to surface geometries using the phenomenon of total reflection of X-rays in the grazing incidence range. In particular, the GISAXS technique has been developed as one of the more versatile tools for characterizing size and shape of particles with nanoscale dimensions on surfaces, or in thin films [1, 2]. We used GISAXS in order to study surfaces enriched by plasma-deposited proteins: this technique results to be able to detect differences concerning layer structure, protein shape, aggregation numbers and concentrations.
We performed the experiments on two kinds of samples: on glass and on silicon substrates. For each kind of samples, a solution of protein has been mixed with the precursor (acetylene or pyrrole) and incorporated in the layer during the copolymerization in the plasma phase. The parameter that controls the layer formation is the frequency of the electric field used during the plasma formation. This new protocol used to enrich surfaces by proteins needs improvements and GISAXS experiments play a key role to refine these procedures, hence they can evaluate the amount of immobilized proteins on the surfaces.
The experimental landscape firstly suggests that the signal does change by varying the sample, the precursor, the plasma condition and the substrate. Glass/based samples give a better signal/noise ratio, compatible with a better protein adhesion or a stronger protein aggregation. In general, the morphology of the image is intermediate between an isotropic half-circular spectrum (expected for the so-called SAXS-regime) and a sequence of Bragg-stripes. We have analysed the data within the framework of the DWBA theory [3] and for this purpose an original computer program has been developed in our department.
In particular, the set of several GISAXS cross sections taken at different incidence angles for the same sample has been globally analysed, by using common fitting parameters including:

- the components of the complex refractive indexes of protein, layer and substrate;
- the thickness and the roughness of the layer, Δ and σ_l, and the substrate roughness σ_s ;
- the protein aggregate concentration N_p and the aggregation number N_{agg};
- the average protein dimensions r, w, h.

We show in Fig.1 the experimental data and the curve fitting corresponding to Alkaline phosphatase (APase, PDB entry 1ED8) samples. Changing the precursor and the frequency of the electric field, a completely different signal is detected, as it has been confirmed by fitting parameters reported in Tab.1.
Moreover, the uncertainties on the parameters confirm that GISAXS is a low-resolution technique, so that the interpretation of the protein shape with a simple geometrical model (such as an anisotropic cylinder) is justified. In particular, the thickness of the layer shows, in general, an higher relative error than the relative errors on the shape parameters; on the other hand, the layer roughness is more uncertain than the substrate roughness. Those results are a further confirmation of the capability of the DWBA theory to catch the main physical features of the plasmacoated samples.
The whole experimental landscape involves 4 different proteins immobilized on different substrates with different precursor at various frequencies of the electric field, resulting in 40

different samples. Despite of that the fitting parameters are affected by relevant errors, we would stress that the characterisation resulting from the application of the DWBA theory can be successfully correlated with biochemical activity tests, in order to elucidate the optimum plasma coating conditions.

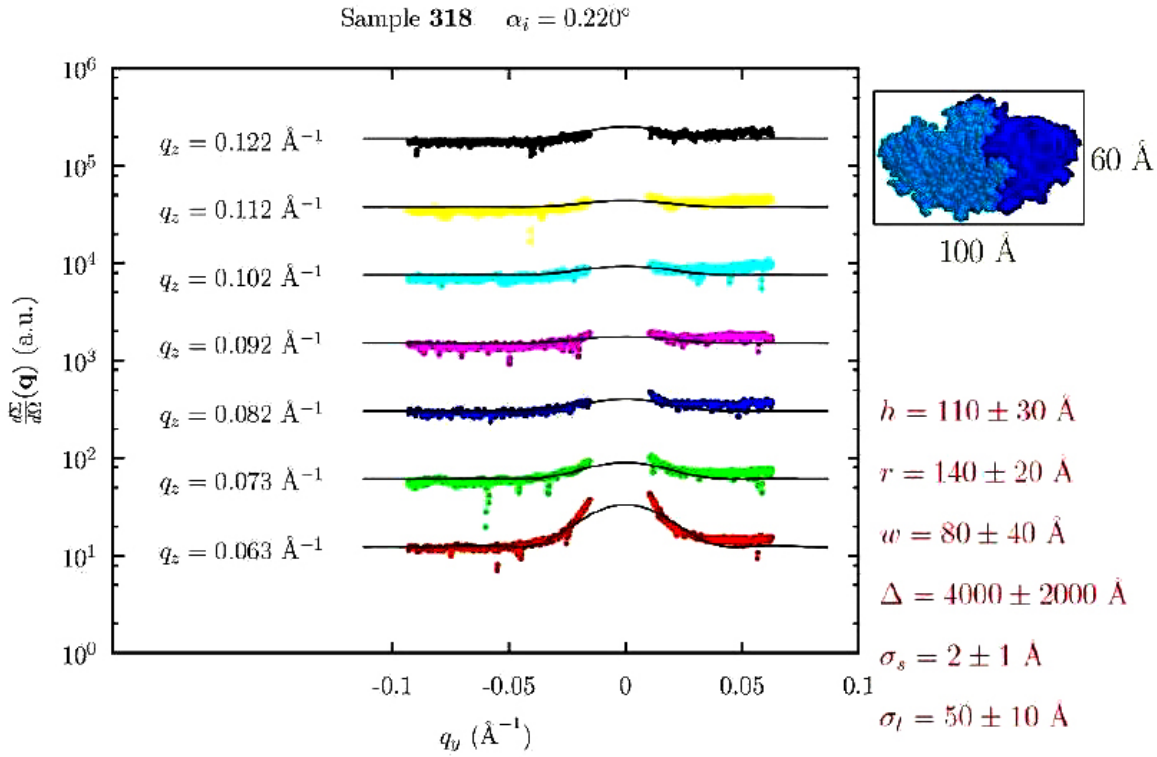

Figure 1. Fitting curves of GISAXS data for the Apase with acetylene precursor at 8 kHz. Data have been reported for different q_z values.

Table 1. Parameters obtained by ftting the GISAXS data of all the APase samples.

Precursor	Frequency (KHz)	Δ (Å)	N_{agg}	N_p (a.u.)
acetylene	4	4800±300	13±5	$(0.5\pm0.1)10^{-1}$
pyrrole	4	3000±1000	13±5	$(2.2\pm0.7)10^{-4}$
acetylene	8	4000±1000	40±10	$(0.6\pm0.1)10^{-3}$
pyrrole	8	3000±1000	10±4	$(0.4\pm0.1)10^{-4}$

References:

[1] R. Lazzari, Isgisaxs : a program for grazing incidence small-angle x-ray scattering analysis of supported islands; J. Appl. Cryst. **35**, 406-421 (2002)

[2] D. Smilgies, P. Busch, D. Posselt and C. Papadakis, Characterization of polymer thin films with SAXS under grazing incidence (GISAXS); Synchrotron Radiation News **15**, 35-41 (2002)

[3] M. Rauscher, R. Paniago, H. Metzger, Z. Kovats, J. Domke, J. Peisl, H.-D. Pfannes, J. Schulze and I. Eisele, Grazing incidence small angle x-ray scattering from free-standing nanostructures; Journal of Applied Physics **86**, 6763-6769 (1999)

FINITE SIZE EFFECTS IN THIN LIPID FILMS

G. Pabst[1], A. Hodzic[1], M. Rappolt[1], H. Amenitsch[1] and J. Katsaras[2]

1.) Institute for Biophysics and Nanosystems Research, Schmiedlstr. 6, 8042 Graz, Austria.
2.) Canadian Neutron Beam Center, National Research Council, Chalk River, ON K0J 1J0, Canada

We have measured finite-size effects on highly-aligned lipid films of dimyristoyl phosphatidylcholine (DMPC) in the gel phase at 10°C using Si-wafers as solid supports. Thin lipid films consisting of 3 to 19 layers were prepared by spin-coating a lipid/isopropanol solution, thick lipid films (> 1000 layers) were made by simply placing a drop of the lipid/isopropanol followed by evaporation of the solvent under vacuum.
For measurements, the lipid films were placed in a custom made hydration chamber [1] and hydrated with saturated salt solutions of KCl and K_2SO_4 to obtain relative humidities of 84% RH and 97% RH, respectively. 100% RH was achieved by placing a wet sponge in the vicinity of the substrate. The sample chamber also allows to control the angle of incidence of the synchrotron x-ray beam. Reflectometry scans were performed using the one-dimensional gas type detector available at the SAXS beamline. The reflectometry patterns show Kiessig fringes, typical for highly aligned thin films, from which we are able to deduce the number of bilayers on the Si substrate. The lamellar d-spacing, which includes the membrane thickness and the separation between adjacent bilayers was calculated from the position of the Bragg peaks. Figure 1 shows the d-spacing as a function of film thickness and degree of hydration. The behavior may be compared to the d-value of 59.9 Å reported for DMPC in bulk systems [2]. Reducing the number of bilayers to 10 and below leads to a continuous increase of d. This effect is enhanced at increased levels of hydration. Besides several attempts to account for the findings in terms of repulsive van der Waals interactions, surface ordering or reduced lipid surface tension, a concise theoretical understanding is presently lacking [3].

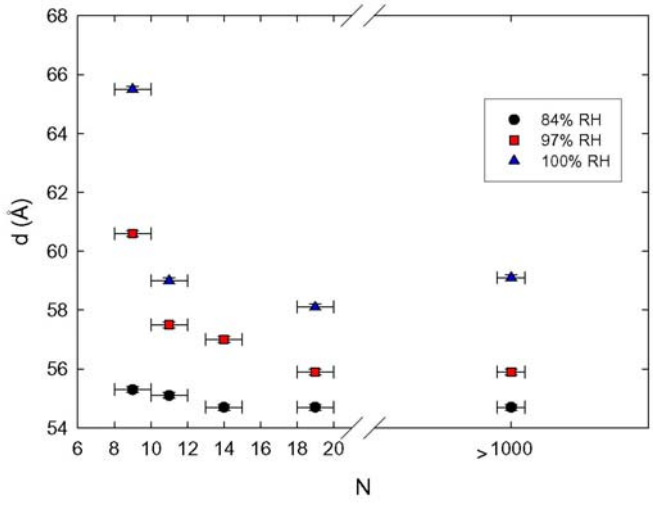

Figure 1. Lamellar repeat distance d of DMPC at 10°C as a function of N number of layers at different degrees of hydration.

Acknowledgement
The use of spin-coater from the LILIT beamline is gratefully acknowledged.

References:

[1] J. Katsaras and M. J. Watson; Sample cell capable of 100% relative humidity suitable for x-ray diffraction of aligned lipid multibilayers; Rev. Sci. Instrum. **71**, 1737-1739 (2000)
[2] J. Nagle and S. Tristram-Nagle; Structure of lipid bilayers; Biochim. Biophys. Acta **1469**, 159-195 (2000)
[3] T. A. Harroun, V. A. Raghunathan, J. Pencer, M.-P. Nieh, and J. Katsaras; Phys. Rev. E **70**, 062902 (2004)

EFFECT OF LIPID HYDRATION ON THE STRUCTURE CATIONIC LIPOSOMES/DNA COMPLEXES

D. Pozzi[1], G. Caracciolo[1], R. Caminiti[1] and H. Amenitsch[2]

1.)Department of Chemistry, Università degli Studi di Roma "La Sapienza", p.le A. Moro 5, 00185, Rome, Italy.
2.) Institute of Biophysics and Nanosystems Research, Schmiedlstrasse 6, A-8042 Graz, Austria.

The exact role of hydration, i.e. the influence of bounded DNA on the hydration of lipid bilayer, is an important question to be addressed since lipid-DNA complexes are so strongly packed that the amount of water entrapped within them should be rather limited [1]. According to standard procedures, liposomes are usually stored at 4 °C and typically used within 3 days. In the major part of works, lipoplexes are allowed to equilibrate to assure complex formation, equilibration times ranging between 20 min and a few hours. Unfortunately, a straightforward interpretation on the role of hydration on the nanometric structure of both liposomes and lipoplexes is still lacking. To shed light on this point, DC-Chol–DOPE/DNA lipoplexes, an extensively used lipid formulation, were prepared with different hydration schedules. In the first case, lipoplexes were prepared by injecting appropriate amounts of sonicated DNA solution into lipid emulsions immediately after hydration of the lipid film (assumed as initial time, t=0). Emerging structure of DC-Chol–DOPE/DNA lipoplexes was followed in time. In the second case, DC-Chol–DOPE liposomes were incubated at 30°C for 36 h and then lipoplexes were formed by adding appropriate amounts of DNA solution to liposomal dispersions. Two representative SAXS patterns are shown in Figure 1 corresponding to 24 and 36 h of incubation of the complexes. At t=0, just formed lipoplexes are not equilibrium structures. Upon hydration, the uptake of water molecules inside the lipoplex lets the volume of the interbilayer water region increase forcing the DNA molecules to separate each other. For t>36 h, no relevant structural changes could be detected in that the SAXS pattern did not vary anymore with lamellar periodicity, d, and DNA-DNA distances approaching their final value (d=6.89 nm and d_{DNA}=3.13 nm). Structure, as revealed by the SAXS pattern collected at t=36 h, was therefore assumed as the equilibrium structure of the lipoplex. Thus, a question arose if the swelling was the result of the enlargement of the water layer or of the lipid bilayer. In attempt to answer this question, electron density profiles (EDPs) along the normal to lipid bilayers were calculated [2] from the SAXS patterns of Figure 1 and are shown in Figure 2. Our results showed that the membrane thickness and the thickness of the water layer increased monotonously (Table 1) as a function of time and reached final values at t=36 h. DC-Chol–DOPE/DNA lipoplexes were also prepared following a different hydration schedule. After hydration of lipid film (t=0), DC-Chol–DOPE liposomes were incubated at 30°C for 36 h and appropriate amounts of DNA solution were added afterwards. SAXS patterns collected immediately after complex formation (t=36 h) showed a lamellar phase with repeat distance, d, of 6.90 nm and a DNA-DNA in plane distance, d_{DNA}, of 3.14 nm in excellent agreement with the above reported equilibrium values. Thus, our structural results obtained following two different hydration schedules allowed us to identify lipid hydration as the key factor regulating the equilibrium structure of lipoplexes [3] (Figure 3).

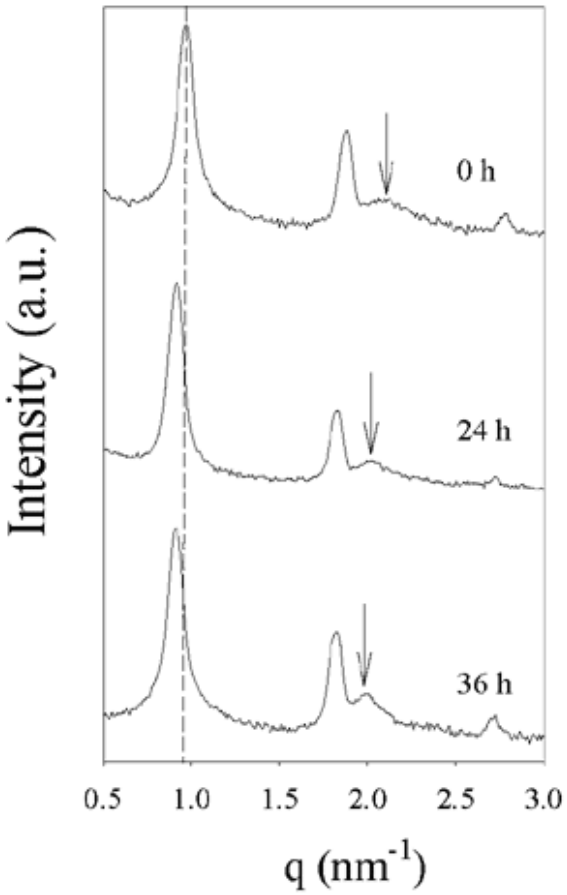

Figure 1 SAXS patterns of DC-Chol–DOPE/DNA lipoplexes collected immediately after complex formation and then after 24 and 36 h of incubation. Dashed line indicates the shift of the first order lamellar peak due to the enlargement of the lipid bilayer-DNA monolayer structure. The mobile DNA-DNA peak (indicated by arrows) moves toward smaller values of q as t increases.

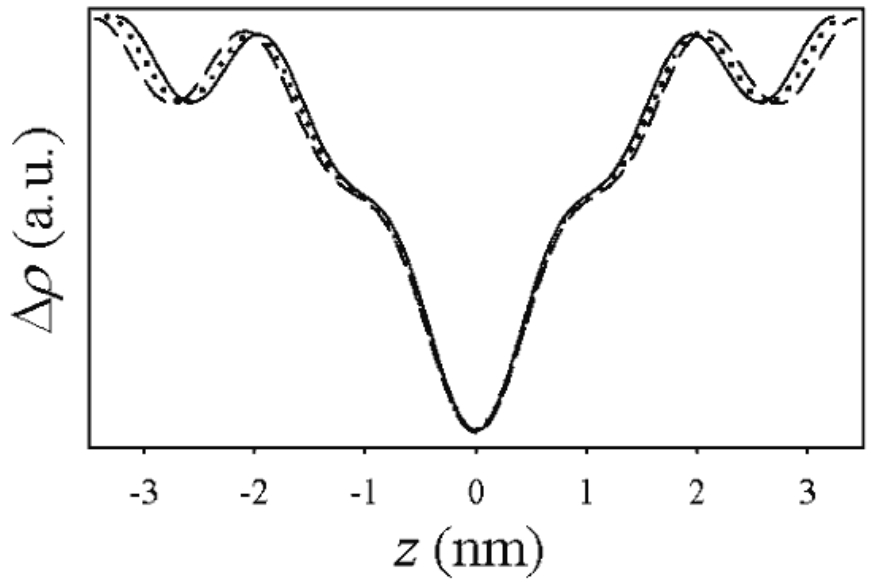

Figure 2. Electron-density profiles along the normal to the bilayers of DC-Chol–DOPE/DNA (ρ=0.6) lipoplexes at t=0 h (continuous line), t=24 h (dotted line) and t=36 h (dashed line) of incubation.

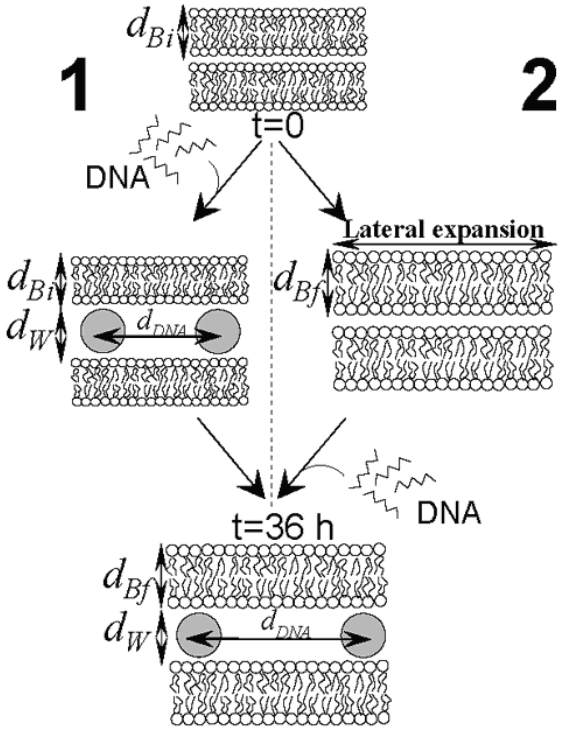

Figure 3. Schematics of the process occurring, at the molecular level, upon incubation of lipoplexes. Side 1: lipoplexes were prepared by injecting DNA into lipid emulsions immediately after hydration of the lipid film (t=0). Resulting lipoplexes were characterized as a function of time and reached equilibrium at t=36 h. Side 2: DC-Chol–DOPE liposomes were incubated at 30°C for 36 h and then lipoplexes were formed by adding DNA to liposomal dispersions. Final structures, obtained following different hydration schedules, were found to be the same.

Table 1. Structural parameters of DC-Chol–DOPE/DNA lipolexes (T=5°C) as a function of incubation time, as calculated by EDPs.

Time	d(nm)	d_B(nm)	d_W(nm)	d_{DNA}(nm)
0	6.47	3.88	2.59	3.00
24	6.86	4.12	2.74	3.11
36	6.89	4.13	2.76	3.13

References:

[1] W. Pohle, C. Selle, D. R. Gauger, R. Zantl, F. Artzner, J.O. Rädler, FTIR-Spectroscopic Characterization of a Cationic Lipid-DNA Complex and its Components, Phys. Chem. Chem. Phys. **2**, 4642-4650 (2000).

[2] G. Caracciolo, D. Pozzi, R. Caminiti, H. Amenitsch, Multi-component cationic lipid-DNA complex formation: role of lipid mixing, Langmuir **21**, 11582-11587 (2005).

[3] D. Pozzi, H. Amenitsch, R. Caminiti, G. Caracciolo, How lipid hydration and temperature affect the structure of DC-Chol-DOPE/DNA lipoplexes, Chem. Phys. Lett. 4**22**, 439-445 (2006).

RELAXATION OF HUMAN BONE AT THE NANOSCALE

S. Puchegger[1], H. Rennhofer[1], D. Loidl[2], P. Zioupos[3], S. Bernstorff[4] and H. Peterlik[1]

1.) University of Vienna, Institute of Materials Physics, Boltzmanngasse 5, A-1090 Vienna, Austria
2.) University of Natural Resources and Applied Life Sciences, Institute of Physics and Materials Science, A-1190 Vienna, Austria
3.) Cranfield University, Dept. Materials & Medical Sciences, Shrivenham, SN6 8LA, United Kingdom
4.) Sincrotrone Trieste, 34012 Basovizza / Trieste, Italy

Introduction

The importance of mineral platelets for the biomechanical properties of bone was a major theme in the 1990's [1], but in the past years the role of the collagen found increasingly interest in the scientific literature [2,3]. In particular a strong reduction of stiffness and strength is found, if the collagen is weakened by aging or damaged by the reduction of crosslinking [4]. Synchrotron radiation proved to be an extremely successful method to follow the structural development at the nanoscale *in-situ* during loading. The basic innovations in this field origin from the group of Peter Fratzl at the MPI of Colloids and Interfaces, e.g. the development of position-resolved scattering for materials with hierarchical structures [5], the splitting of the D-period in mineralized tendon during high *in-situ* loading [6] or the determination of the nanoscopic and the microscopic part in the deformation of fibrillar bone [2]. Using a similar method, in this report the relaxation of human bone is investigated by *in-situ* X-ray scattering.

Experimental

Specimens of human bone were loaded under tension by using a self-developed, transportable materials testing equipment. To prevent from drying or degradation from the X-rays, the specimens were permanently kept wet by a wick. The bone tissue was loaded and at a certain level (the start of a significant non-linearity in the stress-strain curve) the machine was stopped to investigate the relaxation behavior. Every 10 seconds scattering patterns were recorded for 5 seconds (5 seconds pause) for the SAXS-range and twice that interval was chosen for the WAXS-range. After loading and primary relaxation, the interval was increased to 5 seconds recording and 95 seconds pause.
The obtained structural parameters had to be evaluated very carefully; in particular the beam center was determined for every single scattering image to exclude effects from a possible beam shift during the measurement. Here we report the deformation behavior of the collagen (position of the third collagen reflection), of the mineral (position of the 211 peak of the mineral platelets, but due to the broadness of this peak in biological materials a contribution from the 112 reflection cannot be excluded) and the orientation of the mineral crystals (half-width at half-maximum) during relaxation. Due to the large scatter of the results, for the collagen peak and the half-width a running average (of 5 measurements) was used.

Results and Discussion

Fig. 1 shows the stress-time curve. The bone tissue is increasingly strained with a constant strain rate of approximately $2x10^{-3}$/s. Then the strain is kept constant by stopping the machine at a point, where significant non-linearity in the stress-strain curve occurs. The stress relaxation is recorded and shows an exponential decay to a final value of nearly half the initial stress value within 10^4s. The position of the collagen peak (Fig. 2, (003)-reflection) as well as the mineral peak (Fig.3, (211)-reflection) shows a very similar behavior, but the relaxation in the collagen seems to be more pronounced. The total strain at the nanoscale (the relative shift of the peak positions) is about half the macroscopic strain, which was already observed in the

literature [2]. The relative change in the mineral is also less than the relative change in the collagen, but this is probably due to the fact that the (211)-reflection is not aligned with the loading axis (which coincides with the long axis of the bone tissue). In the literature it was stated that alignment with the long axis is preferable the c-axis of the mineral crystals [7], but unfortunately the (002)-reflection was not in the accessible range. The (300)- and (310)-reflection exhibited no measurable shift within the error interval. Contrary to the behavior at the nanoscale, the orientation distribution of the mineral crystals (at a larger level, called here the microscale) decreases during loading (i.e. the orientation of the minerals with respect to the loading axis increases), but then remains constant after reaching the maximum stress.
This leads to the conclusion that during loading deformation mechanisms both at the nano- and microscale are present. Relaxation, however, takes place only at the nanoscale.

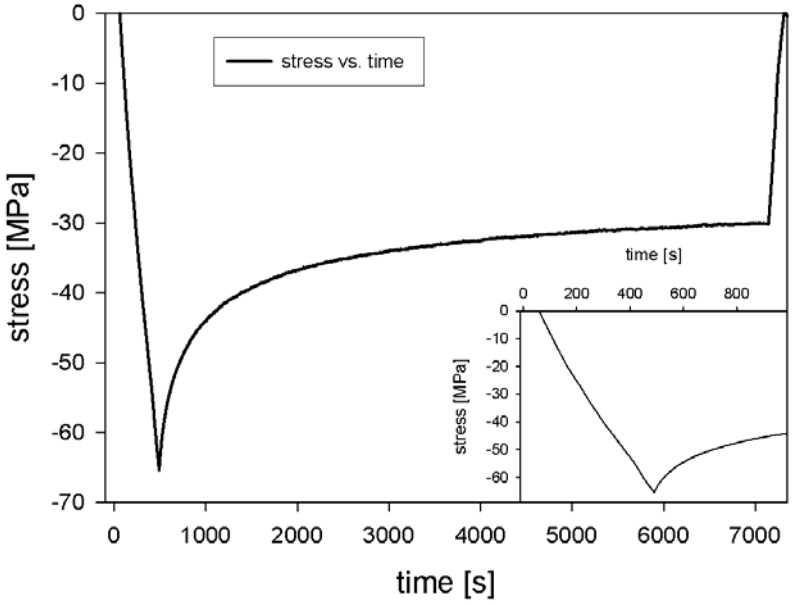

Figure 1. Macroscopic stress in the bone sample A35 in dependence on time. Notice that the sign of the tension stress is here negative for better comparison to the other figures.

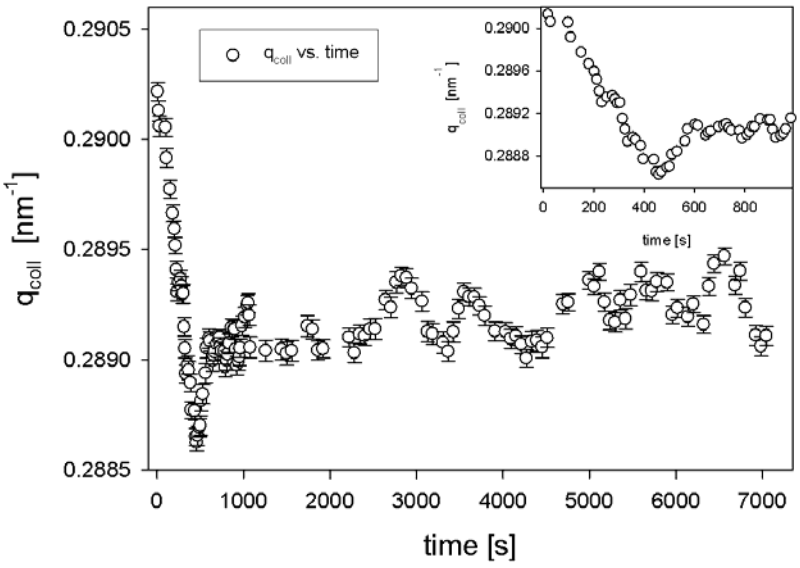

Figure 2. Position of (003)-reflection of the collagen in dependence on time. The small insert shows the loading in the regime of primary relaxation.

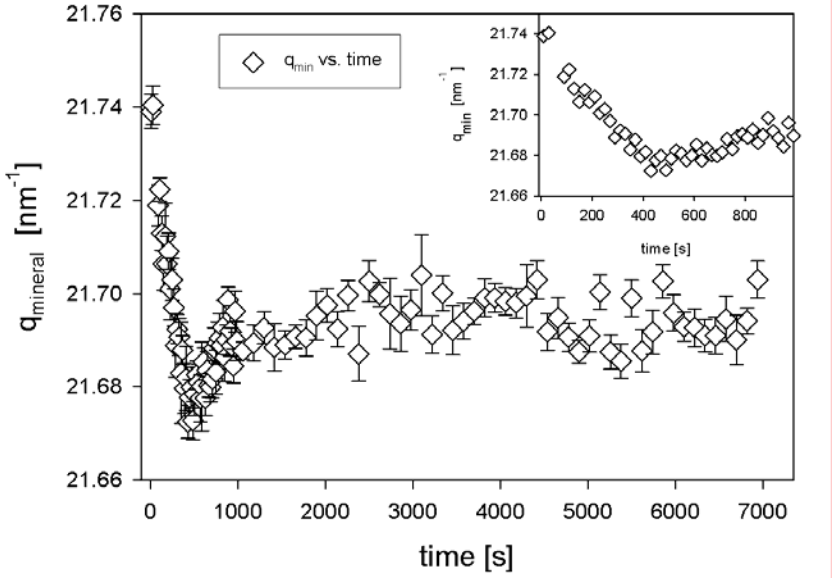

Figure 3. Position of the (211)-reflection of the mineral platelets. The small insert shows the loading in the regime of primary relaxation.

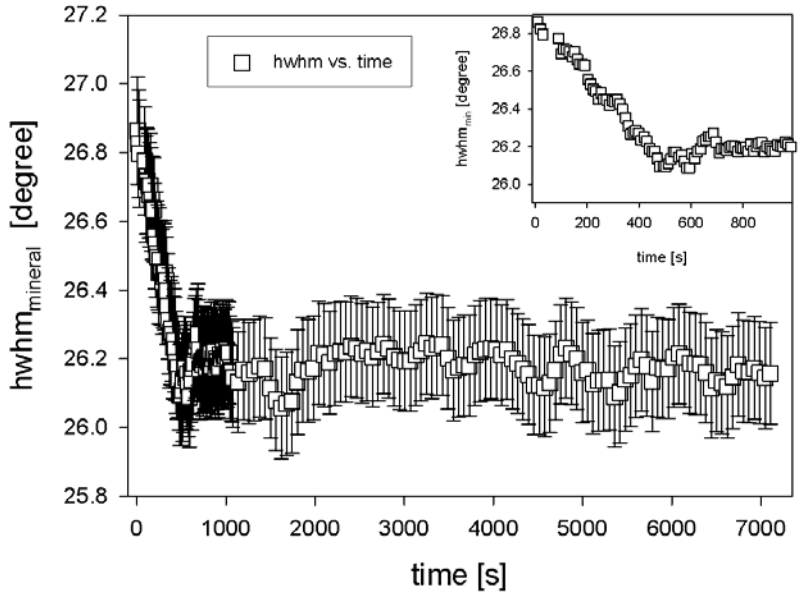

Figure 4. Orientation of mineral crystals (half-width at half-maximum). The small insert shows the loading an primary relaxation part.

References:

[1] A.C. Courtney, E.F. Wachtel, E.R. Myers and W.C. Hayes. J. Bone Joint Surgery **77A**, 387-395 (1995).
[2] H.S. Gupta, W.Wagermaier, G.A.Zickler, D.R.B. Aroush, S.S. Funari, P. Roschger, H.D.Wagner and P. Fratzl. Nano Letters **5**, 2108-2111 (2005).
[3] H. Peterlik, P. Roschger, K. Klaushofer and P. Fratzl. Nature Mater **5**, 52-55 (2006).
[4] J. D. Currey, K. Brear and P. Zioupos. J. Biomech **29**, 257-260 (1996).
[5] P. Fratzl,, H.F. Jakob, S. Rinnerthaler, P. Roschger and K. Klaushofer. J. Appl. Cryst. **30**, 765-769 (1997).
[6] H.S. Gupta, P. Messmer, P. Roschger, S. Bernstorff, K. Klaushofer and P. Fratzl. Phys Rev Lett **93**, 158101 (2004).
[7] N. Sasaki, N. Matsushima, T. Kawa, H. Yamamura and A. Fukuda. J. Biomech. **22**, 157-164 (1989).

SIMULTANEOUS DSC AND SAXS MEASUREMENTS ON SOPE

M. Rappolt

Institute of Biophysics and Nanosystems Research (IBN), Austrian Academy of Sciences, Schmiedlstr. 6, 8042 Graz, Austria.

Aqueous dispersions of 1-stearoyl-2-oleoyl-phosphatidylethanolamine (SOPE) were investtigated in a temperature range from 15 to 80 °C. A special differential scanning calorimetry cell has been used, which is designed to carry out at the same time X-ray scattering experiments [1]. In a heating scan of 1 °C/min both the transition temperatures as well as the enthalpies of the system during the L_β to L_α and the L_α to H_{II} transition have been determined (see Table 1). The changes of *d*-spacings are shown in figure 1. Additionally, X-ray diffraction experiments were carried out at a shorter camera length and exposures were taken under equilibrium conditions (figure 1, o). The later will serve for the reconstruction of the electron density maps. All the above measurements will set the basis for non-equilibrium experiments (T-jumps) and temperature gradient studies carried out on SOPE/water dispersions (compare report: Temperature Gradient Studies on the L_α to H_{II} transition in SOPE).

Acknowledgement: I would like to thank very much Michel Ollivon for his instructions given concerning the use of the DSC-cell as well for the helpful discussions concerning the DSC-data analysis. Merci Michel!

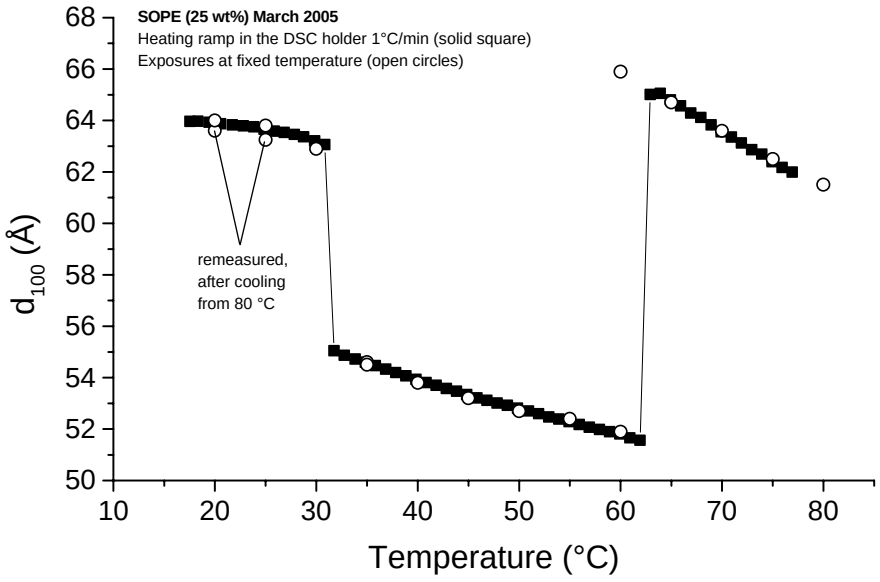

Figure 1. *d*-spacing of SOPE.

Table 1. Thermodynamic parameters of SOPE.

T_{main} (°C)	Enthalpy (kJ)	T_{hex} (°C)	Enthalpy (kJ)
30.9	6.7	61.6	0.8

Reference:

[1] G. Keller, F. Lavigne, L. Forte, K. Andrieux, M. Dahim, C. Loisel, M. Ollivon, C. Bourgaux and P. Lesieur; DSC and X-ray diffraction coupling: Specifications and applications; J. Thermal Analysis 51, 783-791 (1998).

TEMPERATURE GRADIENT STUDIES ON THE L_α TO H_{II} TRANSITION IN SOPE

M. Rappolt and A. Hodzic

Institute of Biophysics and Nanosystems Research (IBN), Austrian Academy of Sciences, Schmiedlstr. 6, 8042 Graz, Austria.

Non-bilayer structures, such as the inverted hexagonal phase, form in many phospholipid and glycolipid systems [1]. These structures and their relevance to biomembrane processes have been the object of extensive research. In particular membrane fusion is still one of the most exciting topics in biophysics [2, 3], because it is fundamental to life of eukaryotic cells. For instance, endo- and exocytose and signaling processes between different cells require carefully regulated membrane fusion. Especially the mechanism of the lamellar-to-inverted hexagonal phase transition imply useful knowledge for membrane fusion processes [1, 4]. The involved superstructures of lamellar, cubic and hexagonal phase can be determined from the X-ray diffraction pattern in the small angle regime (SAXS).

One question concerns the conservation of the long range organization across phase boundaries: does an epitaxial relationship exist or are the phases separated by disordered regions? Another interesting question is: do intermediate structures - other than bi-continuous cubic phases - form under gradient temperature conditions [5]? Siegel and Epand [4] have proposed a quite complex manner of aggregating transmonolayer contacts into a body-centered cubic or primitive tetragonal phase, which is believed to serve as a precursor for the formation of the inverted hexagonal phase. However, applying standard temperature protocols such as slow heat scans, this phase could not be found yet. Moreover, the investigation of the phase boundaries should elucidate the lifetime and stability of especially the bicontinuous cubic phases, i.e. the formation of the gyroid and primitive minimal surfaces within the lamellar-to-hexagonal phase region [6].

All the same, the carried out temperature gradient measurements on 1-stearoyl-2-oleoyl-phosphatidylethanolamine (SOPE) did not show any trace of intermediates in the phase boundary region between the fluid lamellar L_α and inverted hexagonal H_{II} phase, but interestingly the transition temperature T_{hex} depends strongly on the sample history – i.e. on the incubation temperature before the built-up of the gradient. The temperature gradient itself has only a minor influence on T_{hex}.

References:

[1] Rappolt, M., Hickel, A., Bringezu, F. and Lohner, K. (2003): *Biophys. J.* 84: 3111-3122.
[2] Rappolt, M., Amenitsch, H., Strancar, J., Teixeira, C.V., Kriechbaum, M., Pabst, G., Majerowicz, and Laggner, P. (2004). *Advances in Colloid Interface Sciences* 111: 63-77.
[3] Yang, L. and Huang, H.W. (2002): *Science* 297: 1877-1879.
[4] Siegel, D.P. and Epand, R.M. (1997): *Biophys. J.* 73: 3089-3111.
[5] Rappolt M, Di Gregorio GM, Almgren M, Amenitsch, H., Pabst, G. Laggner, P. and Mariani, P. (2006) *Europhys. Letters* 75, 267-273.
[6] Erbes, J., Czeslik, C., Hahn, W., Winter, R., Rappolt, M. , and Rapp, G. (1994): *Ber. Bunsenges. Phys. Chem.* 98, 1287-1293.

LAYER SPECIFIC TENSILE TESTING OF HUMAN ARTERIES

F. Schmid[1,2], G. Sommer[1], H. Amenitsch[2], M. Rappolt[2], P. Laggner[2], G.A. Holzapfel[1] and C.A.J. Schulze-Bauer[1]

1.)Institute of Structural Analysis, Computational Biomechanics, Graz University of Technology, Austria
2.)Institute of Biophysics and Nanosystems Research, Austrian Academy of Sciences, Graz, Austria

The understanding of the static and dynamic mechanical behaviour of the different layers of an artery is an essential prerequisite for the design of constitutive computer models. Collagen fibres are an arterial constituent of major mechanical importance. Hence, the coupling between the nano–structural orientation of the collagen fibres and macroscopic changes in stress and strain due to an applied load yields important information for simulation. This study is using SAXS (Small Angle X–ray scattering) to determine the orientation and stretch of collagen fibres in human arteries during 1-dimensional tensile testing.

The arteries are collected and frozen right after autopsy until further use. Before the experiment they are thawed, separated into their layers (intima (inner), media and adventitia) and cut into stripes of different orientation (along and perpendicular to the arterial axis). A fully computer controlled custom made 1-dimensional tensile testing apparatus is used for uniaxial stretching of the samples. Simultaneously 2D diffraction patterns are taken. The use of a video-extensometer recording geometrical changes of the sample allows the reconstruction of true stress and strain at given points in time during the experiment.

Figure 1 shows the connection of mechanical load and the behaviour of the collagen fibres in the tissue during a load – unload cycle.

The curve of mechanical stress over strain (top curve in the graph) of collagenous tissues is commonly divided into three sections (Phase I-III): the “toe” region, where stress does not increase significantly, followed by the “heel” where stress starts to increase and finally the “lock” region, which is characterized by a nearly linear increase of stress.

The middle curve – named “sigma of fibre orientation” – can be regarded as a measure for the angular fibre distribution. The higher it is, the more randomly the fibres are distributed. Smaller angles accordingly mean an orientation towards the tensile axis. For reasons of simplicity it shall be referred to as “fibre angle”.

Finally, the bottom graph is the strain of the d-spacing of the collagen fibres in percent.

As can be seen, in the toe region of the mechanical stress/strain curve, the fibre angle slowly starts to decrease and also the d-spacing increases only slightly. This is attributed to a straightening of the collagen fibres. In the heel region, when macroscopic mechanical stress starts to increase significantly, a heavy decrease of the fibre angle is observed and also the d-spacing increases stronger than before. Fibres are turning towards the tensile axis while they start to get stretched as well. In the lock region finally, when mechanical stress increases rather linearly, the rotation of the fibres seems to have come to a stop, the fibre angle does not change any more. Only the d-spacing increases – the fibres have reached their final angular position and get stretched, taking up more and more load.

To overcome certain limitations of 1-dimensional tensile tests, the development of a 2-dimensional stretching device is planned for 2006.

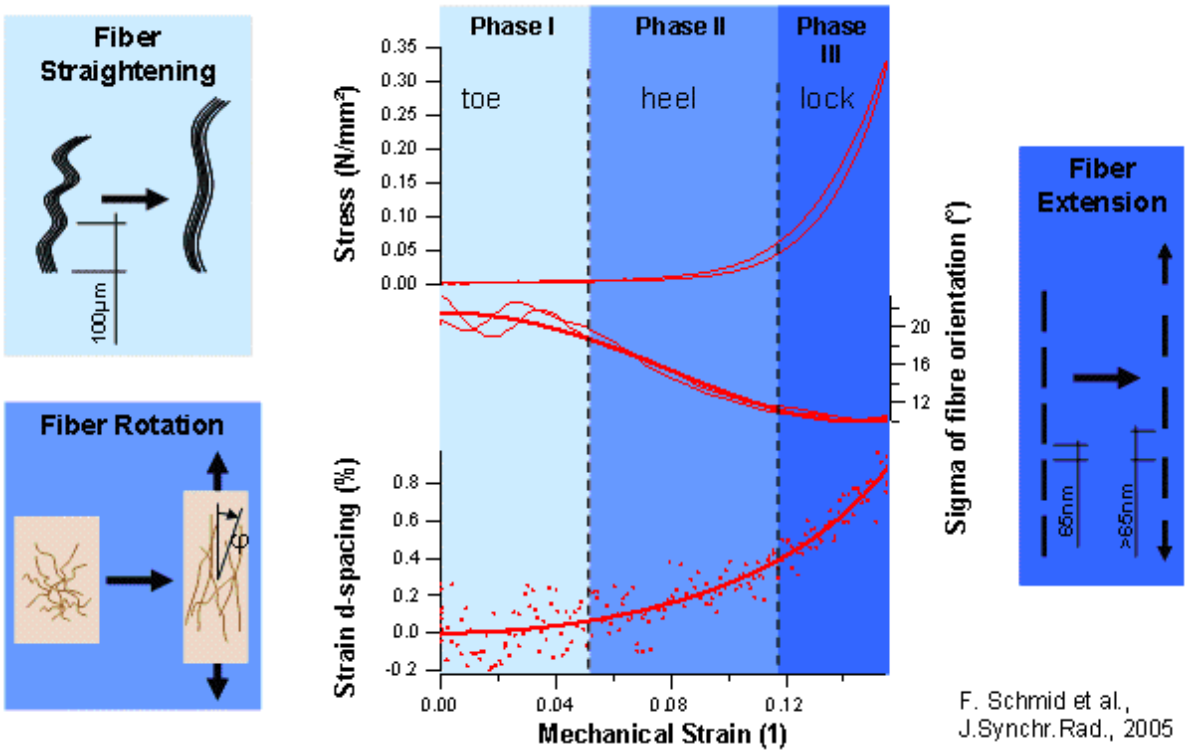

Figure 1. Comparison of mechanical stress, fibre angle and change in d-spacing over mechanical strain during a quasi-static load-unload experiment

References:

[1] Schmid,F., G.Sommer, M.Rappolt, P.Regitnig, G.Holzapfel, P.Laggner, and H.Amenitsch. 2005. Bidirectional Tensile Testing Cell for In Situ Small Angle X-ray Scattering Investigations of Soft Tissue. *NIMB*.

[2] Schmid,F., G.Sommer, M.Rappolt, C.A.J.Schulze-Bauer, P.Regitnig, G.A.Holzapfel, P.Laggner, and H.Amenitsch. 2005. In situ tensile testing of human aortas by time-resolved small-angle X-ray scattering. *Journal of Synchrotron Radiation* 12:727-733.

3. Chemistry

TIME-RESOLVED IN-SITU STUDY OF CUBIC Pm3n MESOSTRUCTURED SILICA

N. Baccile[1], C.V. Teixeira[2], H. Amenitsch[4], S. Tolbert[3], M. Lindén[2] and F. Babonneau[1]

1.) Chimie de la Matière Condensée, Université Pierre et Marie Curie, 4 place Jussieu, 75252 Paris, France
2.) Department of Physical Chemistry, Åbo Akademi University, Porthaninkatu 3-5, FIN-20500 Turku, Finland
3.) Department of Chemistry and Biochemistry, University of California, Los Angeles, California 90095, USA
4.) Institute of Biophysics and Nanosystems Research, 8042 Graz, , Schmiedlstr. 6, Austria

Highly organised mesostructured silica based materials are, at present, a widespread research topic. Ever since 1992, date of the first paper on MCM-41 [1] and 1994, date of the acidic route based catalysis breakthrough [2], a number of groups devoted their time and skills to the progress of these nano-controlled materials. Several good quality reviews are available on this topic, starting from the proposed formation mechanism up to their potential applications [3, 4].

Our personal interest in the subject is mainly addressed towards the acidic synthesis route and more precisely in highly curved micellar surfaces like the cubic *Pm3n* SBA-1 material firstly introduced by Huo *et al.* [5] in 1996. They showed how cubic mesostructured silica powders could be obtained by a room temperature synthesis from Tetraethoxysilane (TEOS) in a highly acidic medium in presence of Cetyltriethylammonium bromide (CTEAB). One of the main issue of this work was the proof, for these systems, of the validity of the well known "g" parameter, which was introduced by Israelachvili [6] to model the surfactant behaviour in aqueous solution. We focused our research at Elettra on the formation of the cubic Pm3n silica mesophase by time-resolved *in-situ* Small Angle X-ray Scattering technique performed on the SAXS beamline.

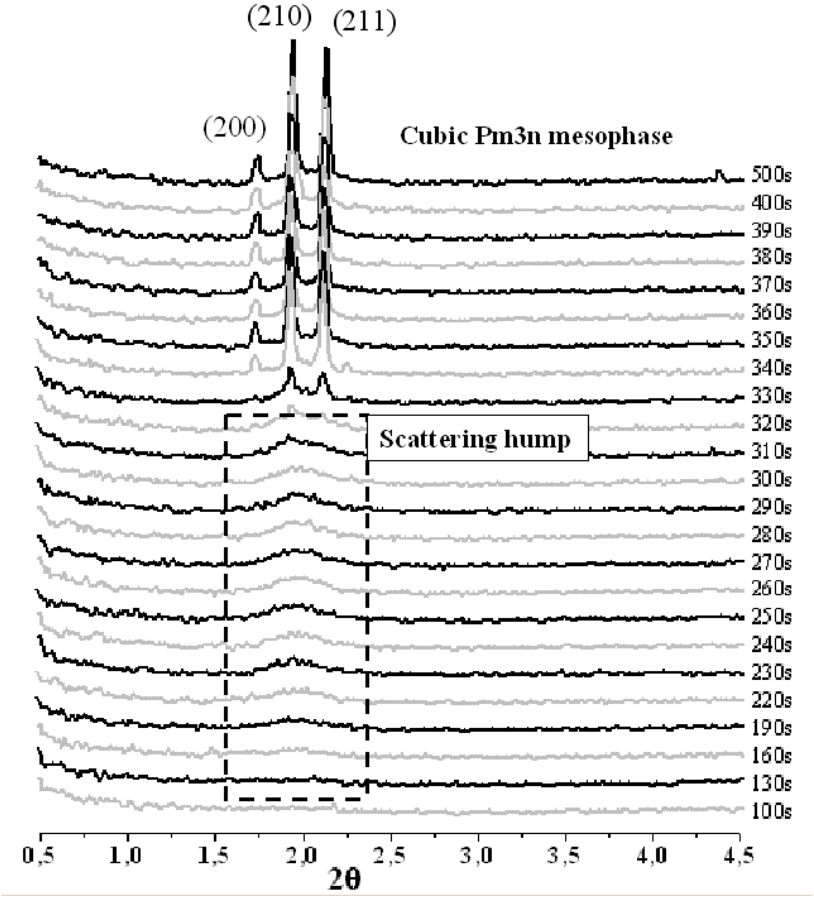

Figure 1. Small Angle X-ray Scattering (SAXS) patterns of CTEAB-templated silica with time.

Figure 1 shows the evolution of time-resolved in-situ SAXS spectra for the CTEAB-templated system. We firstly observe the direct formation of the cubic Pm3n mesophase characterized by the three typical reflections (200), (210) and (211) after about 300 s from TEOS addition to solution. Then, a scattering hump, footprint of the cubic Pm3n phase formation, is observed at low angle.

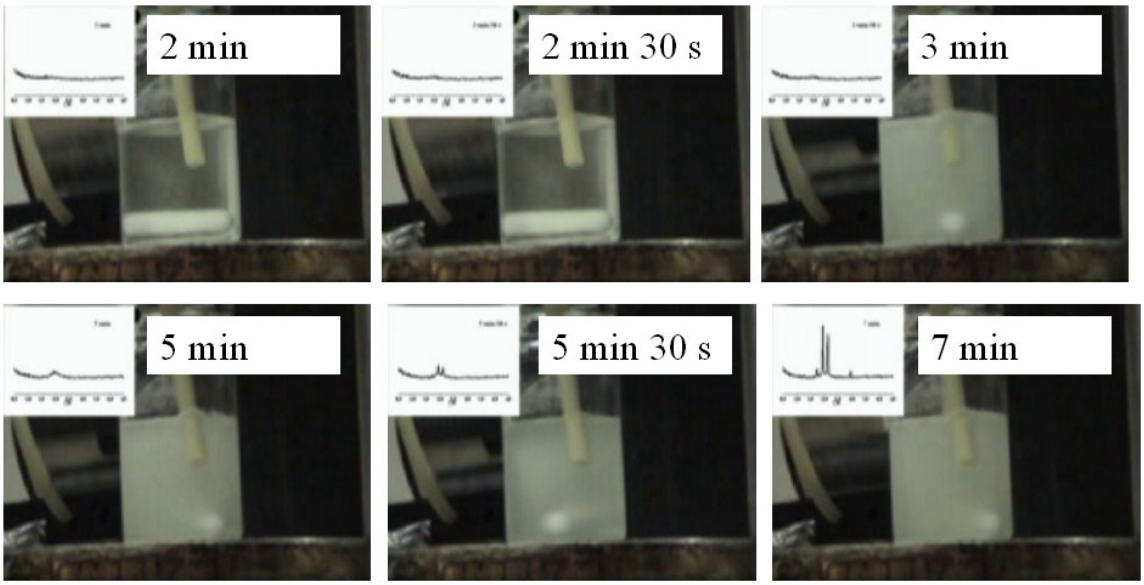

Figure 2. Series of images taken during the self-assembly process of CTEAB-templated silica. The corresponding diffraction patterns are shown in the upper left-hand corner of each image.

Figure 2 presents a sequence of time-resolved images of the corresponding beaker during the self-assembly process: they show that the scattering hump appears simultaneously with the formation of the precipitate. These data leads to the conclusion that when the precipitate forms, silica surrounded micelles are close enough and their average distance causes the scattering hump to appear. Then, micelles locally organise within a few minutes time span to pack in a cubic Pm3n space group.

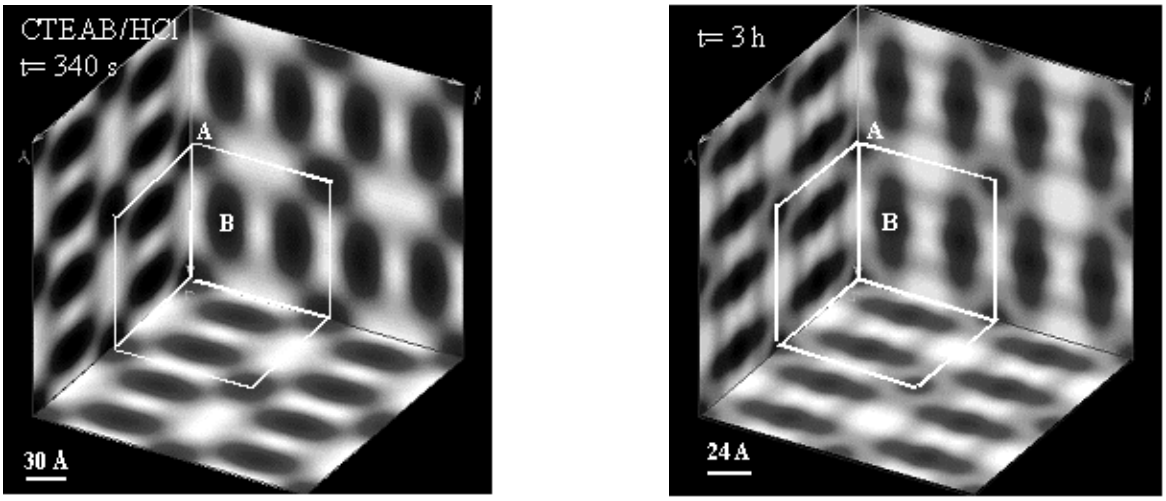

Figure 3. Evolution of electron density maps, calculated from corresponding SAXS patterns, of the cubic Pm3n mesophase. Clear regions refer to high electron density contrast (silica) and dark regions refer to CTEAB micelles.

From the representation of the cubic Pm3n mesophase, we expected two type of micelles of different size and shape, since the necessary condition to pack micelles in a cubic Pm3n structure is to deform them. Thus, we explore the possibility to visualize the distribution of the micelles within the structure during the material formation. We have then reconstructed electron density maps by performing inverse Fourier Transform calculation of diffracted SAXS intensities as a function of time [7]. Figure 3 shows the evolution of electron density maps of cubic CTEAB templated silica at two different times of material formation, t = 340 s and t = 3 h. Such an approach let us visualize the evolution of the micellar shapes (dark regions) and of the silica parts (clear regions) from the onset of ordering till the end of the powder aging process and to verify the prolate form of B-type micelles.

References:

[1] J.S. Beck, J.C. Vartuli, W.J. Roth, M.E. Leonowicz, C.T. Kresge, K.D. Schmitt, C.T.W. Chu, D.H. Olson, E.W. Sheppard; J. Am. Chem. Soc., **114**, 10834-43 (1992)

[2] Q. Huo, D.I. Margolese, U. Ciesla, P. Feng, T.E. Gier, P. Sieger, R. Leon, P.M. Petroff, F. Schueth, G.D. Stucky; Nature, **368**, 317 (1994)

[3] G. J. de A. A. Soler-Illia, C. Sanchez, B. Lebeau.and J. Patarin ; Chem. Rev. **102**, 4093 (2002)

[4] J. Patarin, B. Lebeau, and R. Zana; Curr. Op. Coll. Interf. Sci., **7**, 107-15 (2002)

[5] Q. Huo, D. Margolese, D.Stucky; Chem. Mater. **8**, 1147 (1996)

[6] J. N. Israelachvili, D. J. Mitchell, B. W. Ninham; J. Chem. Soc. Faraday Trans, I **72**, 1528 (1976)

[7] K. Flodstroem, H. Wennerstroem, C.V. Teixeira, H. Amenitsch, M. Linden and V. Alfredsson; Langmuir, **20**, 10311 (2004)

PHASE TRANSFORMATIONS PHENOMENA IN BLOCK COPOLYMER BLENDS

J. Baldrian[1], M. Steinhart[1], H. Amenitsch[2] and S. Bernstorff[3]

1.) Institute of Macromolecular Chemistry, A.S. CR, Heyrovsky Sq.2, 162 06 Prague, Czech Republic
2.) Institute of Biophysics and Nanosystems Research, A.A.S., Schmiedlstrasse 6, 8010 Graz, Austria
3.) Sincrotrone Trieste, Area Science Park, 34012 Trieste, Italy

Introduction

Higher-order structure formation in crystallization of semicrystalline BCPs and their blends has been extensively studied [1] using mainly time-resolved X-ray techniques. Since these systems have microphase-separated disordered (D) and ordered structure (O) in the melt. Structure in the crystalline state (Cr) may be formed by competition or combination of crystallization and microphase separation. In crystallization it is of main interest whether BCPs crystallize within microdomains or not, that is, whether microphase-separation structure in the melt is destroyed by crystallization. The aim of this work was to study described structural phenomena D-O-Cr-O-D occurring in the two-component symmetrical tri-*block*-copolymers and their blends with the neat polymer during crystallization and melting using time-resolved simultaneous measurements of SAXS/WAXS/DSC.

Experimental

The series of block-copolymers PEO-*b*-PPO-*b*-PEO (BCP) (Pluronics P105, F108 and F127) and the blends with pure PEO (P2) of $M_w \sim 2000$ were selected for the study. The structure development was studied by SAXS in high temperature region (180 °C – 70 °C) and by simultaneous WAXS/SAXS/DSC measurements on synchrotron during cooling from the melt and during subsequent heating (70 °C → 30 °C → 70 °C, rate 1°C/min.).

Results and Discussion

At high temperatures the phase separated systems in melt are in the disordered states approximately described by mean-field theory [2]. Periodicity is proportional to Rg of BCP systems. This structure changes at lower temperatures (T_{MF}), where the fluctuation effect become increasingly important changes to the disordered state which can be described by the concentration fluctuation theory. For the phase transition temperature T_{MF} was obtained in the case of the F108 and F127 copolymers value around T_{MF} = 90 °C and for copolymer P105 value around T_{MF} = 68 °C.

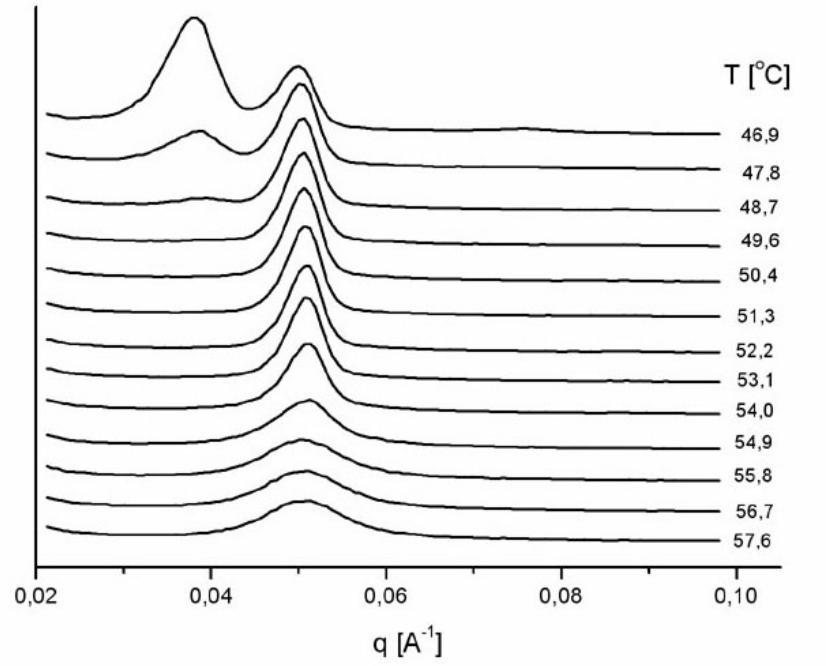

Figure 1. SAXS peak of the blend F127/P2 8/2 during cooling

Figure 1 displays changes of SAXS peak of the blend F127/P2 8/2 during cooling from 54.9 °C to 46.9 °C. The abrupt change of intensity of SAXS reflection, which indicates disorder-order transition [2] was observed in the case of copolymer F127 and in its blend with P2 only. Results of simultaneous real-time measurements SAXS/WAXS/DSC for the mentioned blend are summarized on Fig.2. From the steep changes of SAXS peak parameters (I,σ) follows that disordered melt structure starts to transform to ordered melt structure at T_{ODT} = 53 °C and at 50 °C is this transformation completed. At T_C = 46 °C starts to decrease intensity of SAXS reflection characteristic for ordered melt structure and disappears at 41 °C. At temperature T_C appears new SAXS reflection (Fig.2) shifted to lower angles, WAXS crystalline reflections appear, and DSC crystallization peak begins to develop. The crystallization starts at this temperature. The periodicity corresponding to the new SAXS peak is LP = 161 Å and is much higher than the periodicity in molten state LP = 124 Å. The crystallization from the melt destroys microphase segregated structure forming a new structure consisting of a crystalline lamellae and amorphous layers. The systems are weakly segregated [3]. Smaller breadths of SAXS peak in the ordered melt σ_{melt} than in the crystalline state σ_{110} points out to the better organized nanostructure in ordered melt (Fig.2).

Crystallinity of copolymer (I_{110}) (Fig.2), gradually increases in the temperature interval from 45 °C to 40 °C and intensity of SAXS reflection of the ordered melt I_m^{SAXS} simultaneously decreases to zero in temperature interval 46 °C to 41 °C. In this temperature interval coexists both structures i.e. structure of the ordered melt and the crystalline structure. The structure parameters change during further heat treatment up to 42 °C only little. At temperature approaching T_m, decrease crystallinity (intensity I_{110} and I_m^{SAXS}) and quality of crystalline structure (decrease of σ_{110}). Very steeply increases lamellar periodicity LP from 161 Å to 214 Å. Steep changes of structure parameters in the narrow temperature interval (58 °C – 62 °C) determine melting temperature of blend to T_m = 59 °C. At this temperature interval appears again the same melt periodicity as during cooling. But the melt separated structure does not reveal markedly OD transition and the melt structure transforms directly to disordered state.

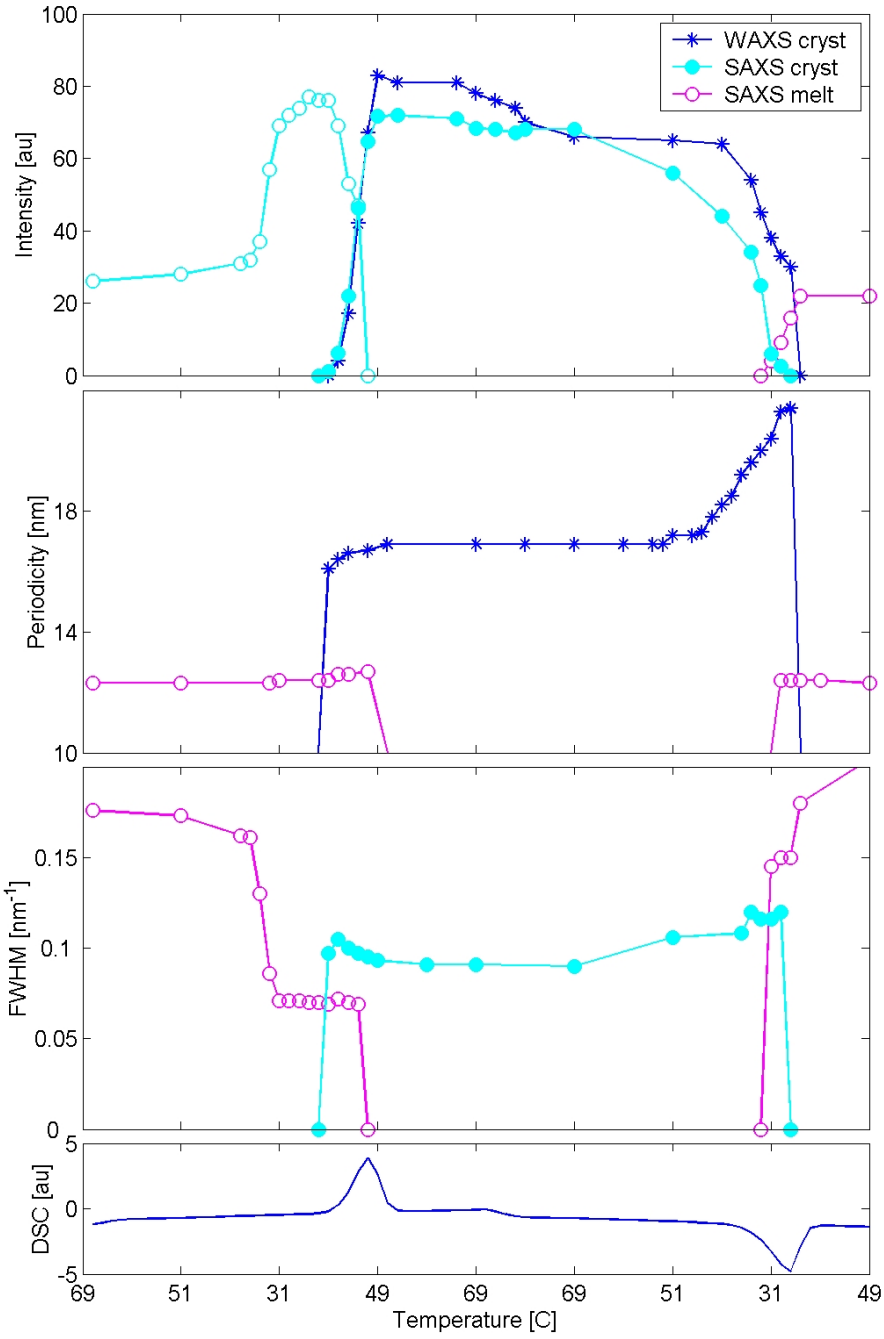

Figure 2. Structure parameters of the blend F127/P2 8/2 during cooling and heating.

References:

[1] A. Rohadi, R. Endo, S. Tanimoto, S. Sasaki and S. Nojima; Effect of Molecular Weight and Crystallization Temperature on the Morphology Formation in Asymmetric Diblock Copolymers with a Highly Crystalline Blocks, *Polym. J.* 32, 602-609 (2000)**,**

[2] I.W. Hamley, *The Physics of Block Copolymers*; Oxford: New York, Chapter 5 (1998)

[3] A.J. Ryan, I.W. Hamley, W Bras and F.S. Bates; Structure Development in Semicrystalline Diblock Copolymers Crystallizing from the Ordered Melt, *Macromolecules* 28, 3860-3868 (1995)

TEMPERATURE DEPENDENT SAXS MEASUREMENTS ON SUPRAMOELCULAR POLYMERS

W.H. Binder[1], D. Farnik[1], C. Kluger[1], L. Petraru[1] and S. Bernstorff [2]

1.) Institute of Applied Synthetic Chemistry, Division of Macromolecular Chemistry, Vienna Univesity of Technology, Getreidemarkt 9 / 163 / MC, A-1060 Wien, Austria
2.) Sincrotrone Trieste ScpA, Strada Statale 14, km 163.5, in Area, Science Park, I-34012 Basovizza / Trieste, Italy

Introduction

The concept of supramolecular polymer chemistry offers an interesting approach to combine strongly different polymers by use of intermolecular bonds instead of covalent linkages [1]. Especially, the combination of polymeric materials with strongly differing properties is an important tool to engineer tailored polymers for a wide range of applications. Thus the combination between extremely soft polymers (i.e.: low T_g polymers exhibiting high chain flexibility) and stiff polymers (i.e.: those characterized by inflexible, rod-type chains with a usually high glass transition temperature) is a technically important task offering the possibility to generate processable materials with high mechanical flexibility. The generation of tunable supramolecular materials made from two strongly phase separating polymeric fragments has become possible by affixing hydrogen bonding elements (showing an A-B type structure) with a variable association strength (i.e.: displaying an association constant of either 800 M^{-1} or ~3.10^4 M^{-1}) onto strongly phase separating poly(isobutylene) (PIB)- and poly(etherketone) (PEK)-polymers respectively in order to combine these two strongly different polymers by use of a directed supramolecular interaction. As depicted in Figure 1, an unusual temperature behaviour changing between micro- and macrophase separated states can be expected, due to the competing micro/macrophase separation and the attractive hydrogen bonding interactions between the telechelic PIB- and PEK fragments. The complex interplay between microphase- and macrophase separation of the resulting materials (featuring *pseudo-block copolymers,* BCPs) is demonstrated by use of temperature dependent SAXS-measurements.

Results and Discussion

In order to check for the distribution and size of the domains, additional information on the microphase separation was collected from SAXS-measurements (see Figure 2) [2]. The presence of separated PIB- and PEK-microphases with sizes of approx. 14 nm for the block copolymers is demonstrated. As expected from the molecular design sheet-like structures consisting of alternating layers of PEK and PIB are observed.

The polymers were investigated by temperature-dependent SAXS-measurements in order to reveal their phase behaviour as a function of temperature. As expected, there is a strong interplay between micro/macrophase separation and the strength of the hydrogen bonding systems between the PIB and PEK-telechelics. Temperature-dependent SAXS-measurements clearly show the dynamic feature of the hydrogen bonds within the supramolecular polymer. As seen in the scattering curves (Figure 2a – 2c), there is an increase of the repeating distance with increasing temperature, starting on from about ~100°C. However, materials with different hydrogen bonding systems display very different behaviour when plotting the repeating distance as a function of temperature.

Conclusion

Temperature dependent SAXS-measurements are an excellent tool to follow the microphase separation of block copolymers, being able to monitor the weakening of a designed supramoelcular interaction. Clearly, due to the fastness of this method at Elettra, a significant insight into the relaxation behaviour of such complex polymeric systems can be achieved.

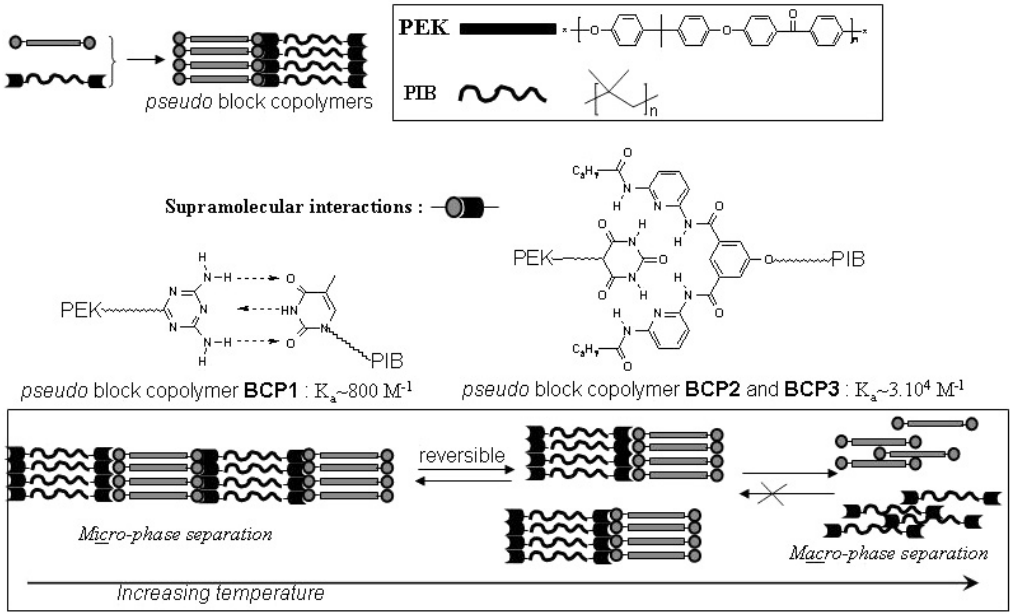

Figure 1. Thermoreversibility of supramolecular polymers held together by medium- to strong hydrogen bonding systems.

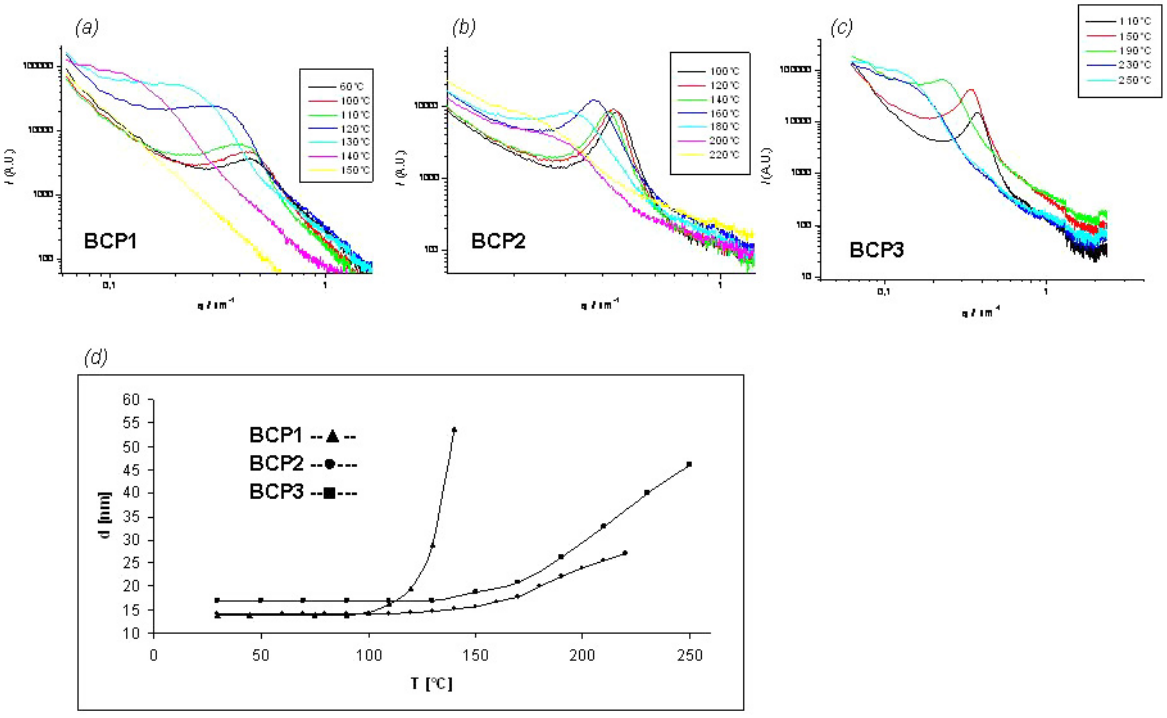

Figure 2. (a-c) Temperature dependent SAXS-spectra of three types of block copolymers. (d) Distance variation of the repeating unit as a function of temperature.

References:

[1] (a) W.H. Binder, M. J. Kunz, C. Kluger, R. Saf, G. Hayn, Macromolecules 37, 1749 – 1759 (2004). (b) M.J. Kunz, G. Hayn, R. Saf, W. H. Binder, J. Polym. Sci. 42, 661 – 674 (2004). (c) W. H. Binder, Monatshefte f. Chemie 1 – 19 (2005). (d) W. H. Binder, M. J. Kunz, E. Ingolic, J. Polym. Sci. 42, 162 – 172 (2004). (d) W. H. Binder, C. Kluger, Macromolecules 9321 – 9330 (2004). (e) W. H. Binder, C. Kluger, L.- Petraru, C. Kunz, D. Machl, V. Torma, H. Peterlik, S. Bernstorff, Elettra-Reports (2004). (f) W. H. Binder, S. Bernstorff, C. Kluger, L. Petraru, M. J. Kunz, V. Torma, Polym. Prepr, 620 - 621 (2004).

[2] W. H. Binder, S. Bernstorff, C. Kluger, L. Petraru, M. J. Kunz, Adv. Mater. 17, 2824 – 2828 (2005)

ENTROPY-DRIVEN SELF-ASSEMBLY IN MESOSTRUCTURED HAFNIA FILMS

S. Costacurta[1], L. Malfatti[1], T. Kidchob[1], P. Falcaro[2], P. Schiavuta[2], H. Amenitsch[3] and P. Innocenzi[1]

1.) Laboratorio di Scienza dei Materiali e Nanotecnologie, Dipartimento di Architettura e Pianificazione, University of Sassari and Nanoworld Institute, Palazzo Pou Salid, Piazza Duomo 6, 07041 Alghero (SS), Italy.
2.) Associazione CIVEN - Nano Fabrication Facility, Via delle Industrie 9, 30175 Marghera, Venezia, Italy.
3.) Institute of Biophysics and Nanosystems Research, Austrian Academy of Sciences, Schmiedlstrasse 6, A-8042 Graz, Austria.

In the last years, extensive work of research on mesoporous silica and transition-metal oxide films has allowed to unravel the formation mechanisms of the ordered mesophases and the main parameters which influence the final mesostructure. At present it is possible to synthesize mesoporous films with an accurate control on the physical (pore dimension, symmetry of mesophase, crystallization of inorganic walls) and chemical (composition, presence of chemical functional groups) properties. A typical synthesis procedure involves the preparation of a precursor solution containing an alkoxyde or a salt as the inorganic precursor and a block copolymer as the structure-directing agent. The films are obtained by dip-coating a suitable substrate (typically Si or soda-lime glass) with the precursor solution. The evaporation of the solvent from the film triggers the self-assembly of the block copolymer into a supramolecular structure (micelles) and the organization of these into a periodic mesophase, hence the name of this strategy of synthesis: *evaporation-induced self-assembly* (EISA). The organic ordered mesophase is then removed by thermal decomposition and leaves an ordered array of well-defined pores.[1]

A very interesting phenomenon occurs after the solvent evaporation, when changes in the symmetry of the mesophase and disorder-to-order transitions can be induced by the external environment, as long as the viscosity of the film doesn't inhibit structural rearrangments. This particular state is generally referred to as modulable steady state (MSS). A phenomenon that is typically observed in as-deposited mesostructured thin films is the possibility to induce phase transitions by changes in the external relative humidity (RH). Water diffuses from the environment into the film and is adsorbed preferentially on the hydrophilic headgroups of the block copolymers, swelling the interface of the micelle and thus increasing its curvature. The increase in water content also lowers the viscosity of the gel, allowing for structural rearrangments. Mesophase symmetries associated to spherical micelles can therefore be obtained from cilindrical or lamellar structures, and different types of ordered mesostructures can be obtained simply by varying the RH during the dip-coating or even at a later time during the MSS.[2]

We have made an interesting discovery that extends the implications of the MSS and gives new insight on the mechanism of formation of the mesostructure. This is based on two SAXS experiments performed in situ on a mesostructured hafnia film.[3]

Firstly, we noted that the dip-coating of a mesostrucutred hafnia film in low RH conditions results in the formation of micelles which are not organized in a periodic mesophase (disordered state). These pre-formed micelles self-assemble in an ordered mesostructure only when the film is exposed to water vapours, even a few minutes after deposition: this causes a notable swelling of the micelles, which soon afterwards rearrange into the formation of a highly ordered mesostructure (see Figure 1). Since well-defined spots are visible both in grazing incidence and in transmission mode, we conclude that the mesophase has a

periodicity both in-plane and out-of-plane, at least in the region probed by the incident radiation.

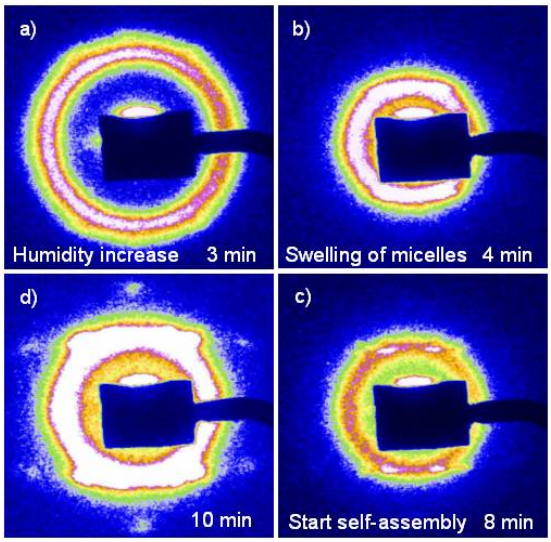

Figure 1. Self-assembly induced by water absorption and micelle swelling. The SAXS patterns are recorded at different times after dip-coating. The increase in humidity (a) causes a micelle swelling (b) that after 8 min (c) produces self-assembly of the HfO2 films (d).

Secondly, as the incident radiation (we used 8 keV) impinges on the film for a prolonged time (on the order of minutes) the mesophase progressively corrupts and, after about 30 minutes of irradiation, the order is lost (Figure 2). This disordering effect is not induced by other external sources, since RH is kept constant during the whole experiment. Moreover, it is a local phenomenon which extends in the area of the sample affected by the radiation, since an ordered mesostructure is always detected just outside this region. Surprisingly, if the radiation is turned off for a certain period of time, an ordered mesostructure is again detected in the region where it previously disappeared (Figure 2d).

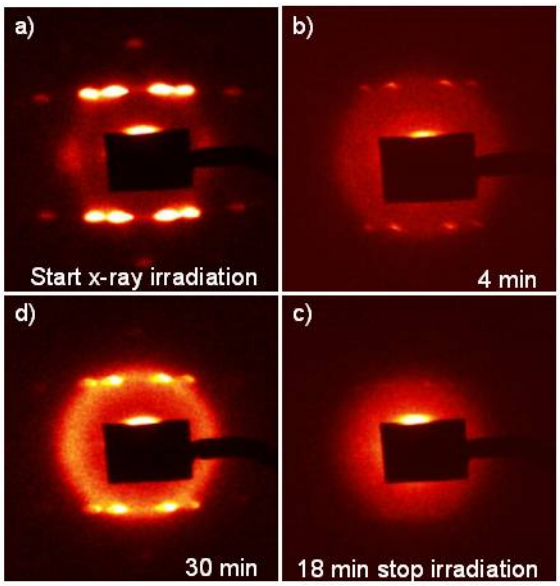

Figure 2. Organization disarray induced by intense X-ray radiation and disorder-to-order transition. In situ SAXS patterns recorded at different irradiation times. A high flux radiation causes on a highly organized film (a) the disarray of the rhombohedral mesophase (b). After 18 min of irradiation the organization is completely disrupted. Self-assembly is again observed after switching off the X-ray flux and maintaining the film in stationary conditions of humidity and temperature.

These two experiments led us to postulate the existence of a different principle leading towards self-assembly, which is based on entropic effects rather than solvent evaporation. The counterintuitive idea that entropy is the source of order is based on the fact that the loss in entropy associated with ordering is more than compensated for by the gain in entropy due to the increase in free volume of the ordered films. In the first case, no ordering is observed during and after solvent evaporation, and only after the swelling of the micelles caused by the high RH an ordered pattern appears. The swelling of the micelles increases the volumetric

fraction of the organic mesophase within the film, so that the micelles have lower translational entropy. In these conditions, the only way to maximize the entropy of the whole system is to increase the free volume by packing the micelles in an ordered structure.[4,5] Organization is allowed with the only external condition that the oxide framework is compliant enough to allow micelle reorganization. The organization achieved in the second part of the experiment when the micelles self-order after their disruption is also an entropy-driven process. This example is of particular importance because the self-ordering process is never pushed by solvent evaporation but only driven by the maximization of the entropy of the system.

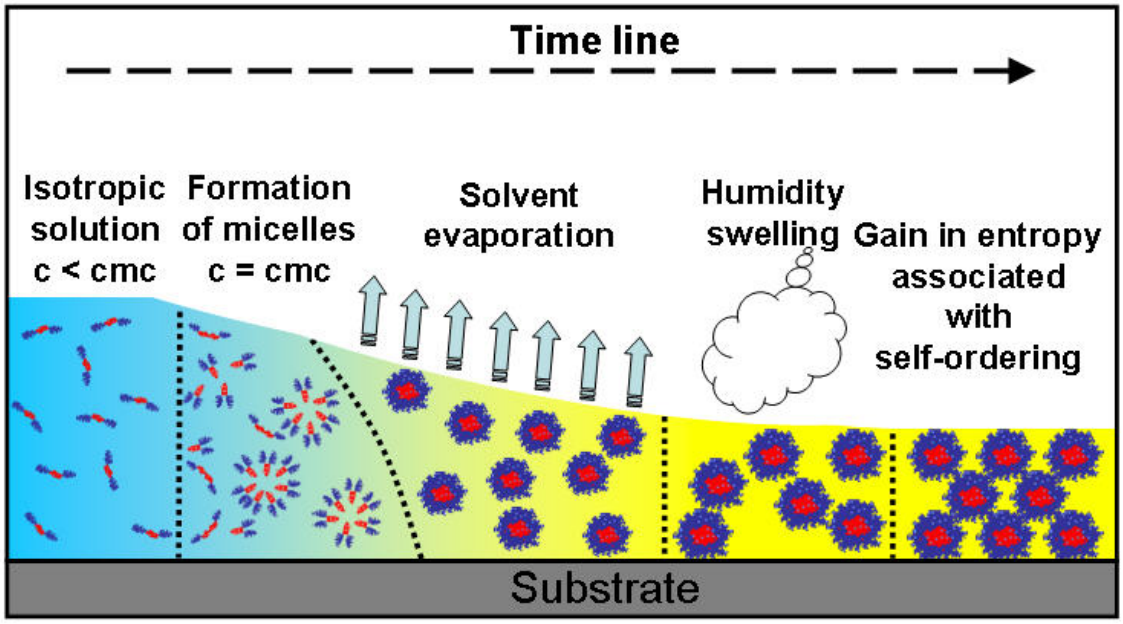

Figure 3. Schematic drawing of the self-assembly taking place during the experiments on a mesostructured hafnia film, which is caused by humidity swelling of the micelles.

These findings open a new scenario for the interpretation of self-assembly in mesostructured films, in that entropic effects might have be to be taken into account in order to formulate a mechanistic model for the creation of an ordered mesostructure. These entropic effects can also be exploited in technological applications: we could, for example, create a disordered region in an orderer sample (or vice versa) using a lithographic mask, or directly "write" in the mesostructure. We are currently planning new experiments in order to elucidate the phenomena described in this report.

References:

[1] C. J. Brinker and D. R. Dunphy; Morphological control of surfactant-templated metal oxide films; *Curr. Opinion Colloid Interf. Sci.* **11**, 126-132 (2006).
[2] F. Cagnol, D. Grosso, G. J. de A A Soler-Illia, E. L. Crepaldi, F. Babonneau, H. Amenitsch and C. Sanchez; Humidity-controlled mesostructuration in CTAB-templated silica thin film processing. The existence of a modulable steady state; *J. Mater. Chem.* **13**, 61-66 (2003).
[3] L. Malfatti, T. Kidchob, S. Costacurta, P. Falcaro, P. Schiavuta, H. Amenitsch and P. Innocenzi; Highly ordered self-assembled mesostructured hafnia thin films: An example of rewritable mesostructure; *Chem. Mater.* **18**, 4553-4560 (2006).
[4] H. N. W. Lekkerkerker and A. Stroobants; Ordering entropy; *Nature* **393**, 305-306 (1998).
[5] A. G. Yodh, K.-H. Lin, J. C. Crocker, A. D. Dinsmore, R. Verma and P. D. Kaplan, Entropically driven self-assembly and interaction in suspension. *Phil. Trans. R. Soc. Lond. A* **359**, 921-937 (2001).

IN-SITU TR-SWAXS EXPERIMENTS OF ZINC NANOPARTICLES UNDERGOING AN OXIDATION PROCESS

S. Di Stasio[1], P. Forte[1] and H. Amenitsch[2]

1.) Istituto Motori C.N.R., Aerosol and Nanostructures Lab, Via Marconi 8 – 80125 Napoli – Italy
e-mail: s.distasio@im.cnr.it
2.) Institute of Biophysics and Nanosystems Research, Austrian Academy of Science, Schmiedlstr. 6, Graz, Austria

This work has been performed at SAXS beamline at Elettra under the experiment #2004729. The experimental set-up is the same previously reported [1]. It is constituted by two quartz reactors connected in cascade. The first reactor flowing nitrogen carrier gas is the generator of zinc aerosol particles. In it metal vapors, which are obtained by evaporation of Zinc bulk grains at temperatures T_{evap}=460 to 580 °C, undergo expansion/cooling and Zn nanoparticles are formed by homogeneous nucleation. The second reactor flowing nitrogen plus oxygen is the oxidation stage to zinc oxide nanoparticles. In a previous experiment #2002319, we studied the gas-phase born nanoparticles of Zinc with larger dimensions (~50-100 nm). A series of very interesting results were found out such as, for instance, some variation of the size distribution of Zn particles output from generator while they approach the high temperature zone in the oxidation furnace. This effect was previously observed by our group by measurements performed with Diffusion Batteries Aerosol Size Spectrometer and XRD [2-4].

In the current experiment #2004729 we try to follow the same process of generation and oxidation for the Zinc aerosol particles in the size range below 50 nm. The available q-range in the present experiment was 0.115 to 3 nm^{-1}, corresponding to an observation size window between 2 and 50 nm, $q=4\pi/\lambda \sin\theta$, 2θ scattering angle, E=8 keV, λ=0.154 nm. The dimension of the spot at sample is 2×0.3 mm (H×V). The distance sample-detector is 1.75 m. At the exit section (X=0 mm) of first reactor and before the hot zone (starting at Z=20 mm) of second reactor, two mica windows allow to probing the aerosol particles at different locations indicated with X1-X8 and Z1-Z5, respectively.

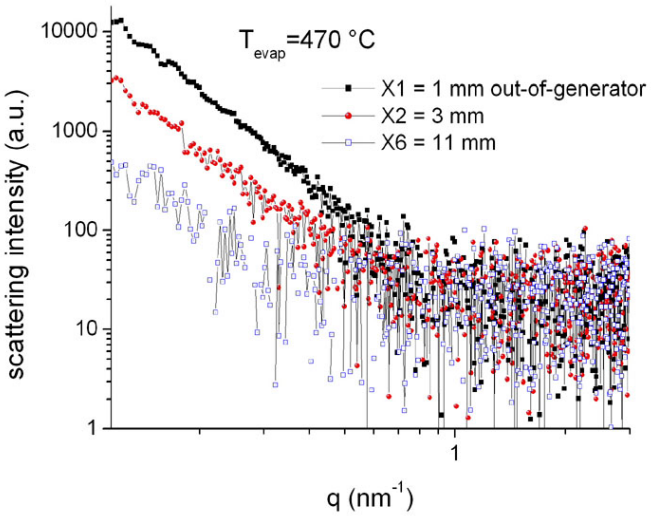

Figure 1. SAXS intensities from Zn aerosol particles measured at different axial locations X's out of Zn particle generator with T_{evap}=470 °C.

Fig. 1 shows the scattering intensities from Zn aerosol particles in correspondence of axial abscissas X1=1 mm to X6=15 mm, step 2 mm (T_{evap}=470 °C). Radius of gyration evaluated from Guinier fit in the reciprocal space returns values about 17 to 21 nm at different axial

positions. Unfortunately, Guinier fit does not yield information about the evolution of the size distribution of particles.

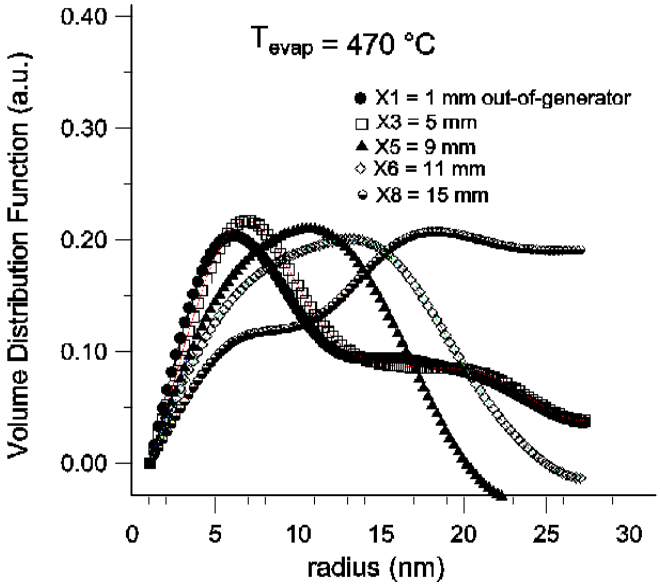

Figure 2. Volume Distribution Functions of Zn nanoparticles at different X's out of the generator oven

The Volume Distribution Functions (VDFs) of Zn nanoparticles out of generator with T_{evap}=470 °C are plotted in Fig.2. SAXS measurements return time resolved information about the agglomeration and partial sintering processes of Zn nanoparticle occurring at the exit of the first reactor. At the outlet section of the generation oven the measured temperature is about 350 K corresponding to carrier gas velocity about 9.7 cm/s. Thus a step 2 mm in axial position X signifies a time step about 20 ms.

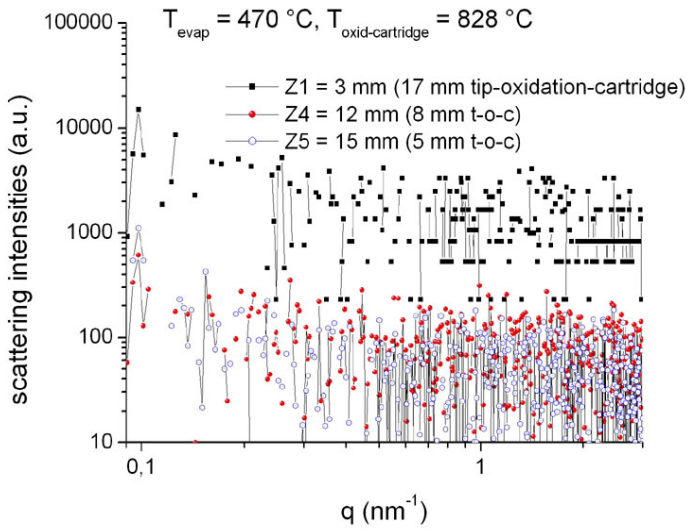

Figure 3. SAXS intensities from Zn particles undergoing oxidation at different positions along the axis of second reactor. Hot zone corresponds to abscissa Z=20 mm.

Fig. 3 are the scattering intensities from the aerosol nanoparticles measured within the oxidation reactor in correspondence of axial abscissas Z1 to Z5 starting at 0 mm up to 15 mm with a step 3 mm. The hot cartridge is positioned along the reactor axis at right of the abscissa 20 mm. Thus, the hottest zone is at Z5, that is at 5 mm from the tip of the oxidation cartridge, which is at temperature 828 °C. The Z1, Z2, Z3, Z4 correspond to increasing temperatures.

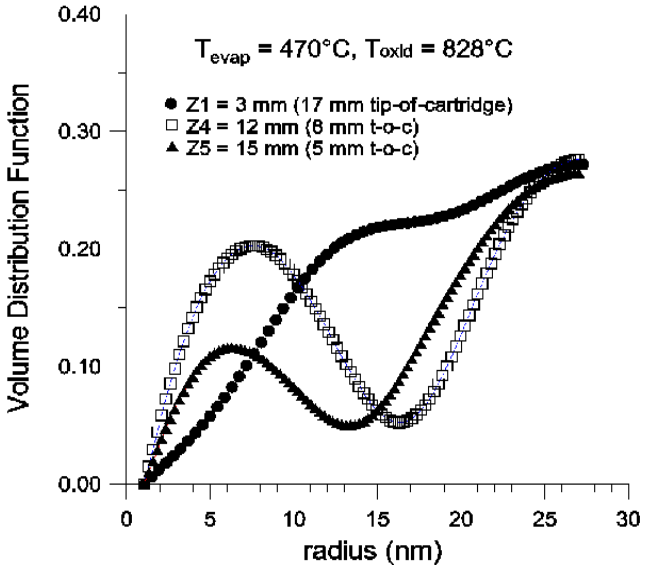

Figure 4. Volume Distribution Functions of Zn nanoparticles subjected to oxidation in the second reactor at different positions Z's with respect to the tip of oxidation cartridge (hot zone at 828 °C).

Fig. 4 are the VDFs of Zn nanoparticles undergoing oxidation in the second reactor where nitrogen (1 L/min) and oxygen (0.4 L/min) co-flow. Relatively far from the hot zone (axial abscissa Z1) we retrieve the same distribution observed at the exit of the generation stage after that coagulation and partial sintering occurred (abscissa X8=15 mm). In particular, the residual of a size mode at about 15 nm radius is visible and only particles with radius above 20 nm are present. The hot zone starts at Z=20 mm (tip of the oxidation cartridge) and extends at larger Z's. We observe that approaching the hotter zone (abscissa Z4) a second mode corresponding to smaller particles grows up at about 9 nm radius. At location (abscissa Z5) still closer to the proximity of the hot oxidation cartridge tip the secondary mode shifts to the left at about 7 nm. The phenomenon is coherent with the results of previous expriment #2002319 and strongly supports the possibility that the smaller Zinc particles with radii about 15 nm can actually re-evaporate partially contemporarily with the formation of a ZnO surface layer. After that the oxide shell has been formed, the evaporation is hindered and the VDF remains the same while oxidation mechanism proceeds from the external shell towards the interior of the particles.

References:

[1] S. di Stasio, G. Verrengia, A. Onischuk, H. Amenitsch (2003). In-situ SAXS study of size and morphology variations of zinc aerosol nanoparticles undergoing oxidation process. Annual Report of the SAXS-beamline, pp. 96-98.

[2] S. di Stasio, A. Onischuk, A. Baklanov (2005). Size and microstructure changes of aerosol zinc nanoparticles and cluster undergoing oxidation process. Unpublished paper.

[3] S. di Stasio(2003). Experiments of static light scattering to investigate in-situ carbon and metal agglomerates of nanoparticles synthesized in gas-phase processes. In: Recent Research developments in Applied Physics, Vol. 6 Part II pp.867-911 (Transworld International Inc, Trivandrum, Kerala, India) ISBN 81-7895-085-5

[4] S. di Stasio, H. Amenitsch (2006). Chem. Phys. Lett. In preparation.

IN-SITU SAXS INVESTIGATION OF MESOSTRUCTURE EVOLUTION IN A NANOCOMPOSITE DERIVED BY SOL-GEL CHEMISTRY

C. Fritscher[1], N. Hüsing[2], S. Bernstorff[3], D. Brandhuber[4], T. Koch[1], S. Geist[2], S. Seidler[1] and H.C. Lichtenegger[1]

1.) Institute of Materials Science and Technology, Vienna University of Technology, Favoritenstrasse 9-11/308, A-1040 Vienna, Austria
2.) Institute of Inorganic Chemistry I, Ulm University, Albert-Einstein-Allee 11, 89069 Ulm, Germany
3.) Sincrotrone Trieste, Strada Statale 14, Km. 163.5, in AREA Science Park 34012 Basovizza/Trieste, Italy
4.) Institute of Materials Chemistry, Vienna University of Technology, Getreidemarkt 9/165, A-1060 Vienna, Austria

The combination of soft and hard matter to form nanocomposites is commonly thought to be a sophisticated attempt to tune the mechanical properties of a material. Different attempts have been made to interweave organic and inorganic components on a small length scale. One promising material from the inorganic point of view is based on mesostructured silica prepared by sol-gel-chemistry, e.g., truly lamellar inorganic-organic nanocomposite materials were obtained for mesostructured silica films by Sellinger et al. [1].
In this project we focused on the formation of nanocomposite materials prepared by a true liquid crystal templating approach combined with sol−gel processing of a siliceous precursor with and without the addition of organic monomers (e.g., acrylic acid 2-(butylcarbamoxy) ethyl ester or lauryl acrylate) to the sol. Subsequent polymerization of the additional organic phase was induced by either thermal initiation (AIBN) or photo-initiation. To obtain an inorganic network we used an ethylene glycol−modified silane and Pluronic P123 in 1 M HCl as amphiphilic structure directing agent. In a typical procedure the components are mixed rapidly. Gelation and aging take place at 313 K and after one week a hierarchically organized monolithic material with a hexagonally oriented mesostructure of a periodicity of 10 to 12 nm in a macroscopically phase separated network is obtained [2, 3].

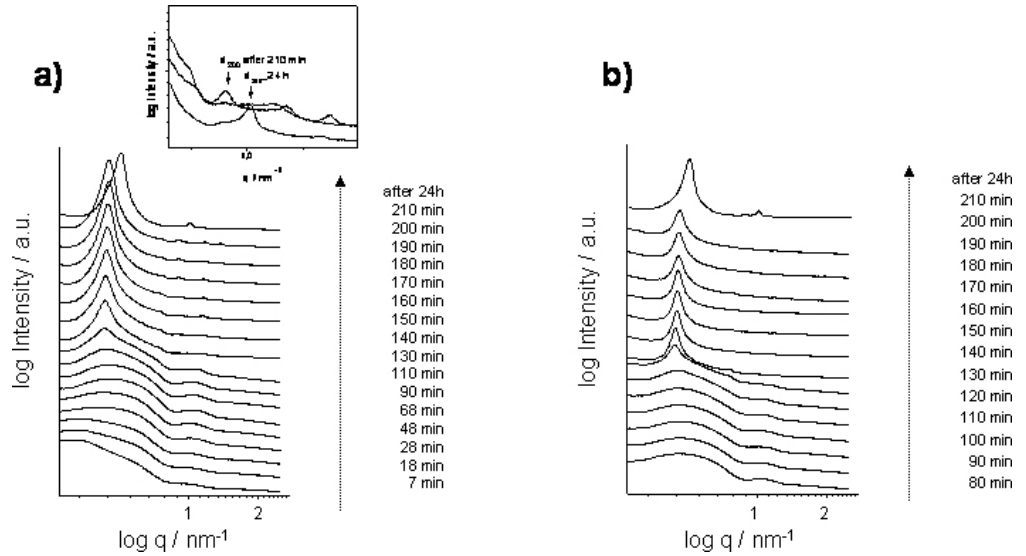

Figure 1. a) Gelation and evolution of the hexagonal mesostructure in the reference system. b) Gelation and evolution of the hexagonal mesostructure in the presence of acrylic acid 2-(butylcarbamoxy) ethyl ester and trimethylolpropantriacrylate.

In a first step we followed the gelation and the formation of the hexagonal mesostructure *in-situ* without organic species immediately after mixing and transferring the sample into the

SAXS chamber. The sample was kept at 313 K all along. The results are depicted in Figure 1a).
Interestingly, the evolution of the mesostructure started only after 130 min. After 210 min a hexagonal structure has evolved with d_{100} = 14 nm. 24 hours later the structure has shrunk further to a value for d_{100}=12.4 nm. To obtain a nanocomposite material, acrylic acid 2-(butylcarbamoxy) ethyl ester and trimethylolpropantriacrylate as polymerizable species were added to the primary formulation in a ratio of 5 wt.-% to Pluronic P123. Furthermore AIBN as thermal initiator was added to the sol. Gelation and mesostructure formation was followed *in-situ* after 80 min of external aging at 313 K. As shown in Figure 1b) a very similar behavior as in the reference system was observed.
This leads to the conclusion that the gelation process and the mesostructure formation in the system were not influenced at the addition of small amounts of organic monomers. The influence of increasing addition of organic species on the mesoscopic organization is shown in Figure 2. The depicted curves correspond to systems with a concentration of 0, 5, 10 and 15 % of polymerizable species to the templating agent added to the sol. It can clearly be seen that the degree of mesoscopic ordering decreases with increasing amount of monomers. Formation of the organic polymer was induced after 14 hours (after formation of the mesophase) by heating the sample to 343 K. After heating the sample for 20 min, the *d*-spacing had decreased by 2 % (0.6 % smaller than the reference system after 24 hours), indicating an additional shrinkage, partly due to syneresis and polymerization of the organic phase. Further experiments were carried out with lauryl acrylate and 1,4-butanediol dimethacrylate as monomers leading to similar results.

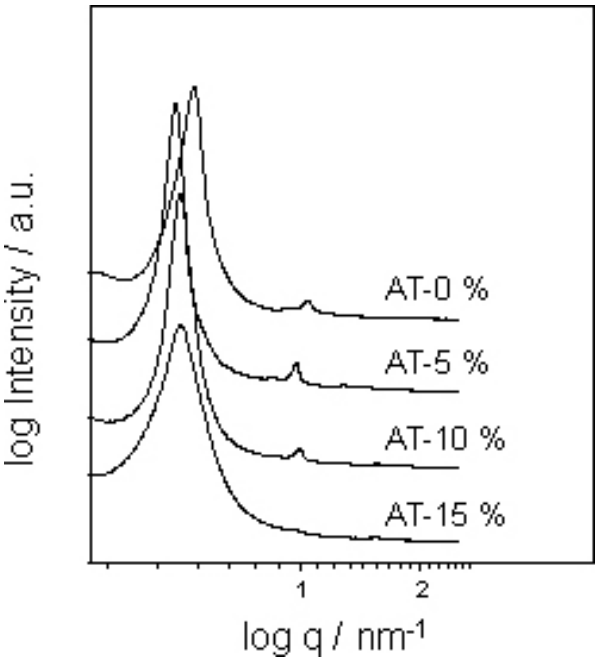

Figure 2. X-ray scattering pattern of mesostructured silica gels with increasing amount of organic monomer (in a mixture of acrylic acid 2-(butylcarbamoxy) ethyl ester and trimethylolpropantriacrylate) added to the sol.

References:

[1] A. Sellinger, P. M. Weiss, Anh Nguyen; Y. Lu, R. A. Assink, W. Gong, and J. C Brinker; Continuous self-assembly of organic-inorganic nanocomposite coatings that mimic nacre; Nature **394**, 256-260 (1998)
[2] N. Huesing, C. Raab, V. Torma, A. Roig, H. Peterlik; Periodically Mesostructured Silica Aerogel Monoliths from Diol-Modified Silanes; Chem. Mater. **15**(14), 2690-2692 (2003)
[3] D. Brandhuber, V. Torma, C. Raab, H. Peterlik, A. Kulak, N. Huesing; Glycol-Modified Silanes in the Synthesis of Mesoscopically Organized Silica Monoliths with Hierarchical Porosity; Chemistry of Materials **17**, 4262 (2005)

GISAXS ANALYSIS OF CERAMIC NANO-PATTERNINGS

M. Kuemmel[1], C. Boissière[1], H. Amenitsch[2], D. Grosso[1] and C. Sanchez[1]

1) Chimie de la Matière Condensée de Paris, UMR UPMC-CNRS 7574, Université Pierre et Marie Curie (paris 6), 4 place Jussieu, Tour 54-5E, 75252 Paris 05, France.
2) Institute of Biophysics and Nanosystems Research, Austrian Academy of Sciences, Schmiedlstr. 6, 8042 Graz, Austria.

Patterning of surfaces and the resulting creation of heterogeneities of surface tension, reactivity, or topography, have always been an important issue for the design of complex components used in high technological devices, especially in electronic. Control over the dispersion, the organisation and the dimension of the domains spread over the surface becomes a real challenge when these fall below 50 nm in size. But it is also the characterisation of the synthesized patterns which becomes more difficult.

The recent progresses made in the field of thin ceramic film nanostructuration through Evaporation Induced Self-Assembly[1,2,3] was utilised to successfully extend this latter approach to the formation of nanopatterns. The EISA method involves the chemical liquid deposition technique, the polycondensation of inorganic precursors and the nanotexturation in presence of surfactant micelles as template. Such method is simple, gives high reproducibility, can easily be scaled up, is cheap and does not require any expensive and specific equipment. On the other hand, a higher control on the chemical and processing conditions is necessary to achieve high ordered during patterning. It is also important to use specific block copolymers that are large enough (MW > 15000g.mol^{-1}) and contain at least two blocks with great hydrophilicity contrast.

As reported previously[4], we have deposited ultra-thin layers of TiO_2 bearing nano-perforations on SiO_2 substrates using Poly(ethylene-*co*-butylene)-*block*-poly(ethylene oxide)[5] with the formula BH_{320}-b-EO_{568}. The perforations or craters were controlled between 10 and 30nm in diameter and were homogeneously distributed within the titania layer making well-ordered nano-patterns as confirmed by AFM and SEM-FEG.

The thickness of the array was difficult to assess by AFM since analyses were performed in non contact mode. Ellipsometry analyses confirmed that layers were less than 10 nm in thickness. An accurate value of the thickness cannot be determined by this latter technique because it is model dependant and the layer is not plain but has to be seen as an approximation of an effective medium composed of oxide and void. One of the main challenges associated to the formation of these patterns is the verification that a single layer has effectively been deposited, which has been done by GI-SAXS analyses conducted at the Austrian SAXS beam line of Elettra's synchrotron (Italy). Samples were placed under the incident beam at an angle of 0.2°. Scattered patterns were collected on an X-Ray-sensitive CCD camera (Energy: 8 KeV, beam size: 400μm, sample-detector distance: 130cm, acquisition time: 2min).

The GI-SAXS bidimensional diagram of the highly ordered nano-crater sample (Figure 1 and 2) is displayed in Figure 3. Much morphological information can be extracted from the scattered radiations. First, intense Bragg diffractions, and their corresponding second order, are collected off-plane at q_{x1} = 0.22 nm^{-1} and q_{x2} = 0.44 nm^{-1} respectively. These diffractions correspond to highly ordered features distributed on the surface of the substrate with a characteristic separating distance of 28nm, which is in agreement with previous topological studies. The presence of the second order is associated to a high degree of ordering. The X-ray incident beam was 400 μm wide, which suggests that a wide surface of the sample was irradiated. Since only one narrow diffraction signal (see signal intensity profile in the x direction) was recorded in the x direction, one supposes that the carters are homogeneously

distributed on the whole surface. The second information of great importance is extracted from the extension of the diffracted signal in the y direction. These are addressed as diffraction rods and are characteristic of a monolayer of features spread over a surface. At increasing values of q_y, the diffraction rods decrease in intensity before regaining intensity. This is related to interference construction and destruction associated to the propagation of the diffracted signal in the layer (Kiessig fringes from diffracted radiation).
The second rods observed at higher q_y values are thus the harmonics of rods collected at low q_y values. Their presence confirms the high homogeneity of the monolayer thickness. Modelisation of the signal profile revealed that layer thicknesses are around 10 nm. A precise determination of the feature morphology and of the thickness is possible through the determination of the form factor associated to the scattered signals. Such an investigation could not be performed with the diagram of Figure 3, but will be done with future GI-SAXS patterns that will be recorded with higher resolution during an incoming synchrotron beam time.

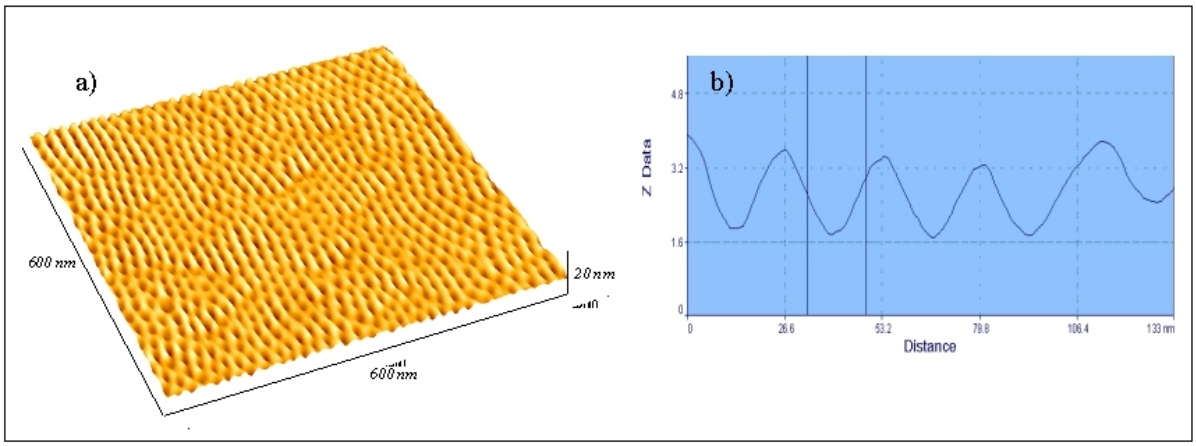

Figure 1. AFM image (a) and line profile (b) of the ultra-thin nano-array of TiO_2 on a SiO_2 surface. (recorded in non contact mode)

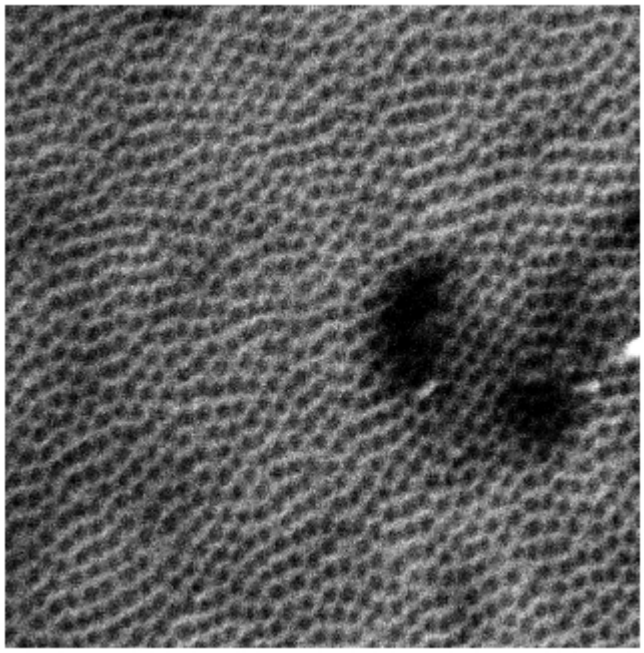

Figure 2. SEMFEG image of the pattern shown in Fig. 1

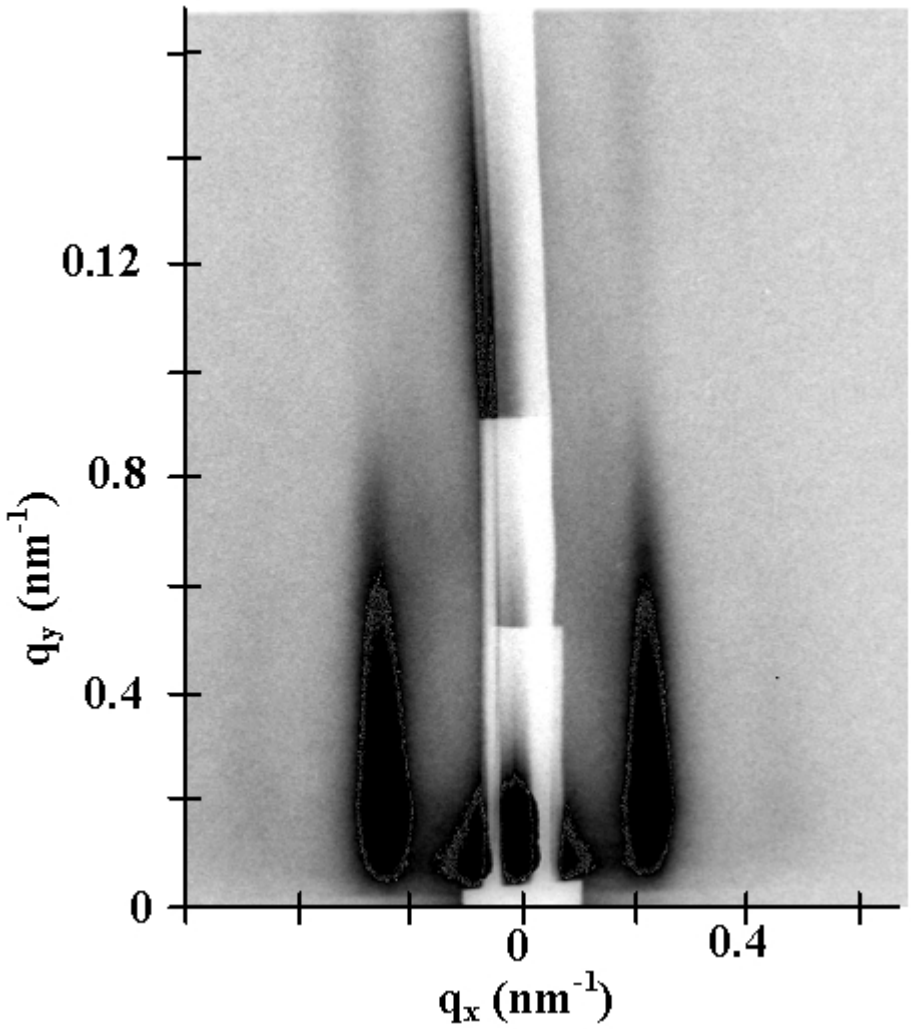

Figure 3. GISAXS pattern of an ultra-thin layer of TiO_2

References:

[1] a) H. Yang, N. Coombs, I. Sokolov, G.A. Ozin, Nature **381**,589 (1996); b) H. Yang, A. Kuperman, N. Cooms, S. Mamiche-Afara, G.A. Ozin, Nature **379**, 703 (1996)
[2] a) C.J. Brinker, Y. Lu, A Sellinger, H. Fan, Adv. Mater, 1999, **11**, 579; b) Y. Lu, H. Fan, A. Stump, T.L. Ward, T. Rieker, C.J. Brinker, Nature 1999, **398**, 223.
[3] D. Grosso, F. Cagnol, G.J. A.A. Soler-Illia, E.L. Crepaldi, H. Amenitsch, A. Brunet-Bruneau, A. Bourgeois, C. Sanchez, Adv. Funct. Mater. **14**, 309. (2004)
[4] A.Fisher, M.Kuemmel, M.Järn, M.Linden, C.Boissière, L.Nicole, C.Sanchez, D.Grosso, Small, **2**, No.4, 569, (2006)
[5] A. Thomas, H. Schlaad, B. Smarsly, M. Antonietti, Langmuir **19**, 4455, (2003)

TIME-RESOLVED GI-SAXS STUDY OF VACUUM INDUCED MESO-STRUCTURING OF SILICA-BASED LAYERS.

N. Petkov[1], M.P. Copley[1], J.M. O'Callaghan[1], M.A. Morris[1], T.R. Spalding[1], J.D. Holmes[1] and H. Amenitsch[2]

1) Department of Chemistry, Materials Section and Supercritical Fluid Centre, University College Cork, Cork, Ireland.
2) Institute for Biophysic and Nanosystems Research, Austrian Academy of Sciences, Schmiedlstr. 6, 8402, Graz, Austria.

Surfactant templated mesoporous materials showing ordered mesoporosity, extremely high surface areas and a variety of mesophase structures have applications as catalyst supports, nano-reactors and as hosts for nanostructured materials with appealing optoelectronic properties [1, 2]. Undoubtedly the latter applications will benefit from the preparation of preferentially aligned and ordered arrays of mesostructured channels analogous to those of the pores of the AAMs. Exploiting the shape and strength of the solid/liquid/air interfaces mesoporous films have been prepared by so-called evaporation induced self-assembly method (EISA) showing mono-oriented mesostructured domains [3,4]. The dynamic conditions during the preparation of mesoporous films (spin or dip coating) by EISA provide difficulties with respect to mechanistic studies because the film deposition proceeds for no more than about one minute. Nevertheless, by applying time-resolved GI-SAXS measurements using a two-dimensional CCD camera, high-flux synchrotron radiation, it was possible to follow the formation mechanism of the thin mesoporous films deposited by dip coating. In many of the studied cases, time-resolved measurements reveal the existence of a very complex mixture of co-existing or subsequently disappearing and newly formed mesophases even before the film is fully dry.

Here we utilize vacuum induced solvent evaporation to promote meso-structuring in the silica layers on Si wafers combined with high-flux synchrotron radiation to observe this process. The fast solvent evaporation drives the mesophase formation to ordered and oriented structures for less than a second after evacuating the deposition chamber. Nevertheless the final mesophase structure was followed for a number of minutes and showed interesting trends with coexisting mesophases. Since the structuring of the mesophase layers is performed in evacuated chamber, the influence of external parameters such as relative humidity can be excluded.

Figure 1 shows time evolution of the GI-SAXS patterns for a P123 surfactant templates thing film deposited on the surface of the Si wafer and evacuated at 2 mbar. The GI-SAXS patterns were recorded for about 22s prior to evacuation of the deposition chamber and the meso-structuring process was followed for additional 5 min. In the course of the first 22s (before evacuation of the chamber) diffuse scattering from disordered micellar objects was observed. After evacuation (usually it took about a second to reach vacuum of about 2 mbar) the rapid disorder to order transition occurred leading to formation of oriented, hexagonally ordered mesophase structure, indexed in the hexagonal *(p6m)* mesophase structure with tubular channels running parallel to the sample surface. The vague intensity of the diffraction ring comes from the scattering from micellar structures with the same characteristic dimensions as those forming the hexagonally ordered structure. The chamber was kept evacuated for 5 additional minutes and the collected GI_SAXS data showed preservation of the hexagonal structure with increasing intensity of the reflections (including appearance of the third order reflections after 1 min) suggesting enhanced meso-structural order.

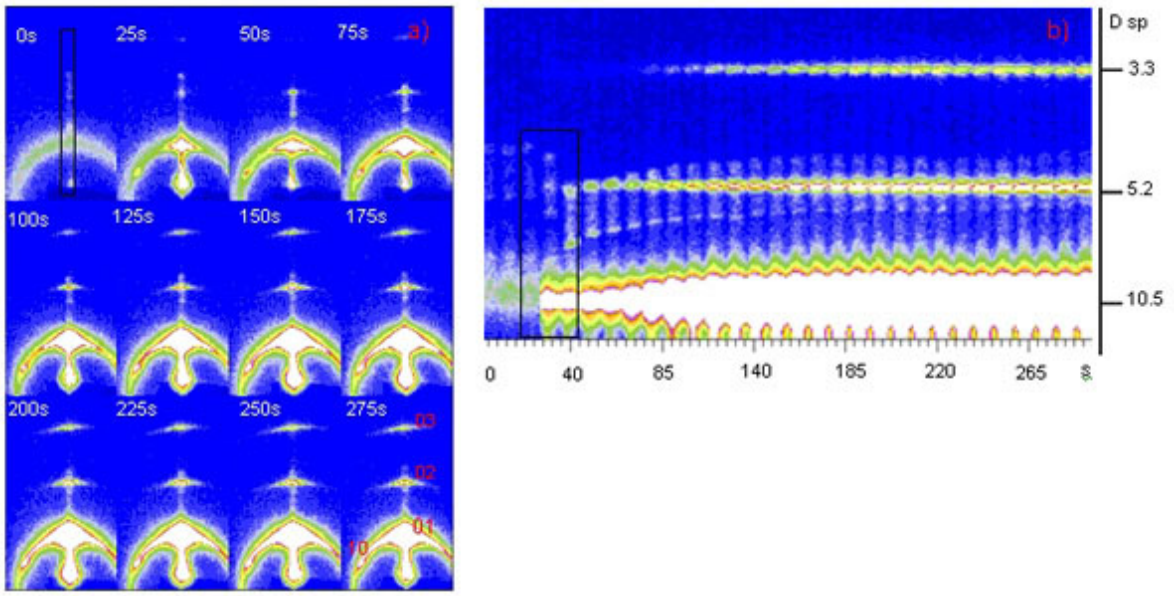

Figure 1 Time resolved GI-SAXS patterns following the structural evolution of thin film sample subjected to vacuum at 22s, a) 2D patterns and B) 1D profiles of the region shown on Figure 1a.

Closer examination of the early stages of the formation process (number of seconds before and after evacuation) showed coexistence of other oriented mesophase structures (Figure 2). Before evacuation attenuated reflection spots were observed that may be attributed to oriented mesophase structures that are present in the system besides the disordered micellar objects. The correct identification of these phases is still debatable but it seems that they are parallel to the substrate which may suggest lamellar ordering. Interestingly the time evolution of these phases after evacuation is completely different than that of the major hexagonally ordered mesophase.

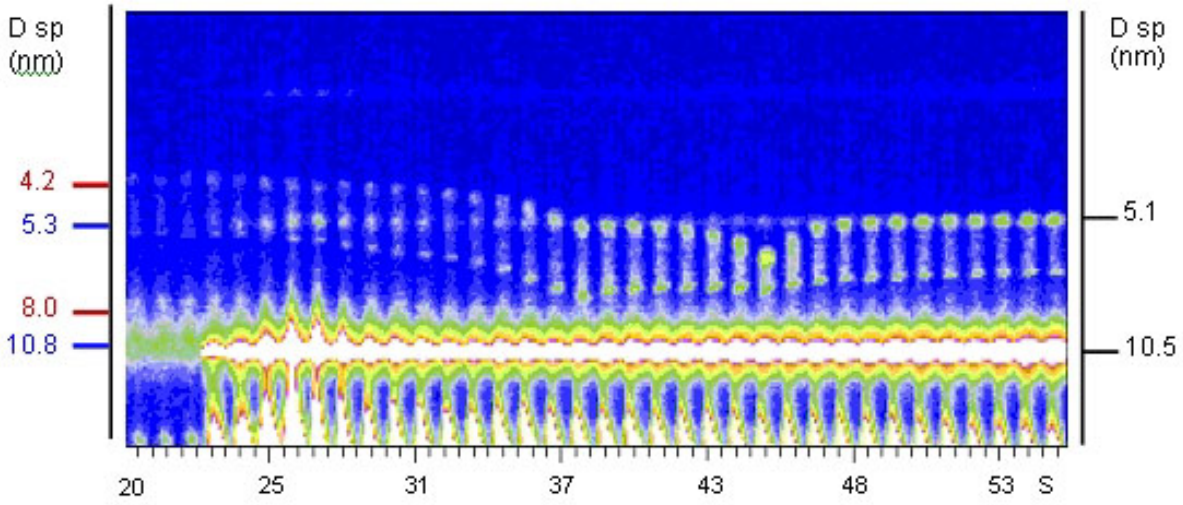

Figure 2 1D profiles of the time resolved GI-SAXS patterns following the structural evolution of a thin film sample subjected to vacuum shown on Figure 1b.

For example, after evacuation at 22s, the newly formed hexagonal mesophase does not alter its d-spacing until the end of the experiment, unlike the already existing lamellar phases which follow a very complex evolution scheme involving increasing and decreasing d-spacings, tangentially approaching the reflections of the major hexagonal phase (Figure 2). The intensity profile shows that after evacuation the intensity of the lamellar phases is lower

than that of the major hexagonal phase, and also shows that the lamellar phase eventually vanishes (Figure 1b). The dynamic evolution of the lamellar phases with time and their lower intensity with respect to the major hexagonal phase suggests that they are meta-stable and probably formed at the interfaces (solid/liquid or liquid/gas) where the concentration of the regents is quite different than that of the bulk. Despite the existence of such a large number of phases, the desired hexagonally ordered phase is achieved immediately after the evacuation of the chamber and was sustained without mesophase distortion. Since the structuring of the mesophase layers is performed in evacuated chamber, the influence of external parameters such as relative humidity can be excluded that may improve the repeatability of the deposition of the mesoporous layers and thin films.

References:

[1] A. P. Wight and M. E. Davis, *Chem. Rev.,* 2002, 102, 3589.
[2] S. J. Brian, G. Wirnsberger and G. D. Stucky, *Chem. Mater.,* 2001, 13, 3140.
[3] C. J. Brinker, Y. Lu, A. Sellinger, H. Fan, *Adv. Mater.,* **1999**, 11, 579.
[4] D. Grosso, F. Babonneau, P.-A. Albouy, H. Amentisch, A. R. Balkenende, A. Brunet-Bruneau, J. Rivory, *Chem. Mater.,* **2002,** 14, 931

IN-SITU X-RAY DIFFRACTION STUDY ON THE FORMATION OF A PERIODIC MESOPOROUS ORGANOSILICA MATERIAL

M. Tiemann[1], C.V. Teixera[2], M. Cornelius[1], J. Morell[1], H. Amenitsch[3], M. Lindén[2] and M. Fröba[1]

1.) Institute of Inorganic and Analytical Chemistry, Justus Liebig University, Heinrich-Buff-Ring 58, D-35392 Giessen, Germany
2.) Department of Physical Chemistry, Åbo Akademi University, Porthansgatan 3-5, FIN-20500 Turku, Finland
3.) Institute of Biophysics and Nanosystems Research, Austrian Academy of Sciences, Schmiedlstraße 6, A-8042 Graz, Austria

Recently the synthesis of a new periodic mesoporous organosilica (PMO) material, including the preparation of the respective organosilane precursor, 1,4-bis-((E)-2-(triethoxysilyl)vinyl)benzene (BTEVB), was reported simultaneously and independently by Cornelius et al. [1] and by Wang and Sayari [2]. The organic unit consists of an aromatic and an unsaturated component conjugated to each other. The PMO material exhibits cylindrical mesopores periodically arranged in a two-dimensional hexagonal p6mm symmetry as evidenced by powder X-ray diffraction (see below) and TEM. Nitrogen physisorption reveals typical mean pore diameters (BJH) and specific surface areas (BET) of 2.6 nm and 730 m2 g-1, respectively. Within the pore walls the organic units are aligned in a crystal-like fashion, similar to those in some phenylene- [3, 4], biphenylene [5], and ethylene-bridged PMOs [6]. For further details on the synthesis and structural properties of the products see reference 1. Characterization of the PMO material by X-ray diffraction yields two pieces of information. First, the low-angle region of the diffraction pattern shows peaks which correspond to the periodic two-dimensional hexagonal order of the mesopores. Second, the wide-angle region exhibits a series of equidistant reflections which are created by the periodic, crystal-like arrangement of the organic groups within the pore walls. These two sets of information obtained from a single X-ray diffraction experiment over the entire scattering region, i.e. low angle and wide angle, make it possible to tackle the question whether or not the formation of crystal-like ordering in the pore walls occurs simultaneously with the generation of the periodically arranged mesopores [7]. In-situ X-ray diffraction experiments were carried out at the Austrian SAXS beamline at the ELETTRA synchrotron source in Trieste, Italy, using a 2D CCD-detector. Prior to each measurement BTEVB was dispersed in an aqueous solution of octadecyltrimethyammonium chloride (OTACl) and NaOH (BTEVB/OTACl/NaOH/H2O = 1/1.4/11.9/660) and allowed to hydrolyze at room temperature for 24 hours under vigorous stirring. A fraction of the homogeneous mixture was then transferred to an X-ray capillary. The sealed capillary was mounted in the sample holder where it was heated to 95 ¡C under constant rotation during the measurement. These experimental conditions correspond to those of the synthesis reported in reference 1. The diffraction patterns were corrected for variations in the primary intensity as well as for a background of pure water. Positions and intensities of the reflections were obtained by fitting Lorentzian profiles to the experimental data.

Figure 1 shows the temporal evolution of the diffraction patterns during the PMO synthesis. The generally high intensity in the low-angle region is mainly due to contributions from the primary beam. At the beginning of the measurement a poorly-resolved contribution by diffuse scattering from micelles is also observed in the low-angle region. After ca. 50 minutes a low-angle Bragg reflection (s = 0.21 nm-1) is visible, corresponding to the formation of the periodic surfactant-organosilane mesophase. About simultaneously (see below) two additional Bragg reflections in the wide-angle region (s = 0.85 nm-1 and 1.70 nm-1) are detected which correspond to the periodic, crystal-like arrangement of the organic groups within the pore walls. The low-angle peak's integral intensity is plotted as a function of the reaction time in Figure 1. During the first 50 minutes the peak is not unambiguously distinguishable from noise. The large scattering of the data, especially after longer reaction times, is presumably caused by inhomogenities of the sample in the rotating capillary. However, extrapolation of the mean peak intensity towards zero suggests that the formation of the mesophase starts approximately at the onset of the measurement, i.e. at t = 0. Figure 1b shows the temporal evolution of the second wide-angle peak's intensity. (The second wide-angle peak was

chosen instead of the first one because it has a higher signal-to-noise ratio.) Again, the peak cannot be distinguished from noise at short reaction times, but extrapolation indicates that it has its origin at approximately t = 0. These findings indicate that both the formation of the mesophase and the local ordering in the walls occur simultaneously, i.e. in a cooperative fashion. Similar results have been reported for the synthesis of a PMO material with a different organic unit [7].

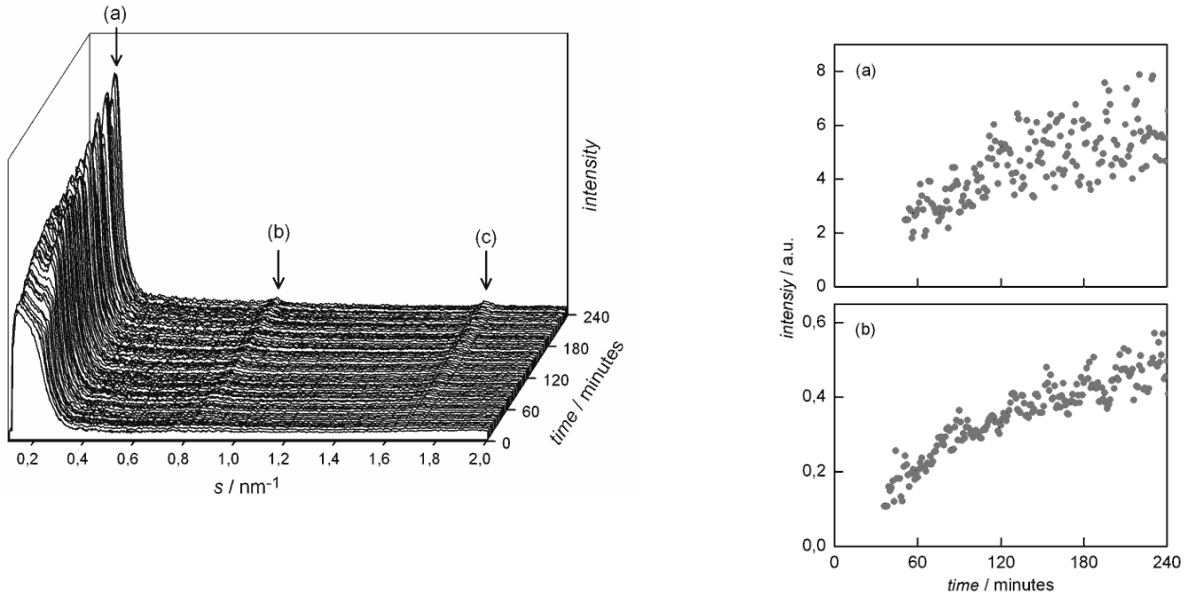

Figure 1: Left: Temporal evolution of the X-ray diffraction pattern for the formation of a periodic mesoporous organosilica material. The peak at low-angle (a) corresponds to the periodic surfactant-organosilane mesophase; the peaks in the wide-angle region (b) characterize the periodic arrangement of the organic groups within the pore walls. Right: Temporal evolution of the intensities of (a) the low-angle reflection and (b) the second wide-angle reflection. Extrapolation of both plots to zero suggests that both peaks start to evolve simultaneously at t = 0.

The d values of all three reflections remain approximately constant during the in-situ measurement. This is in contrast to the slight subsequent decrease which is frequently observed during the formation of mesostructured silica materials from precursors which are not organically modified [8-9,10]. However, in the in-situ measurements the low-angle reflection is located at a slightly larger d value (4.89 nm) than in the powder diffraction pattern of the final porous material after removal of the surfactant (4.72 nm [1]). This shift in the repeat distance by ca. 4 % is attributable to a shinkage of the mesostructure due to additional condensation of the building units in the pore walls upon removal of the surfactant. For the wide-angle reflections no such difference between the in-situ measurements and the powder diffraction pattern is observed; in both cases the d values are 1.19 nm for the first peak and 0.60 nm for the second peak, respectively, indicating that the repeat distance in the regular arrangement of the organic units is widely inflexible.

References:

[1] Cornelius, M.; Hoffmann, F.; Fröba, M. Chem. Mater. 2005, 17, 6674.
[2] Sayari, A.; Wang, W. J. Am. Chem. Soc. 2005, 127, 12194.
[3] Inagaki, S.; Guan, S.; Fukushima, Y.; Ohsuna, T.; Terasaki, O. Nature 2002, 416, 304.
[4] Kapoor, M. P.; Yang, Q.; Inagaki, S. Chem. Mater. 2004, 16, 1209.
[5] Kapoor, M. P.; Yang, Q.; Inagaki, S. J. Am. Chem. Soc. 2002, 124, 15176.
[6] Xia, J.; Wang, W.; Mokaya, R. J. Am. Chem. Soc. 2005, 127, 790.
[7] Morell, J.; Teixeira, C. V.; Cornelius, M.; Rebbin, V.; Tiemann, M.; Amenitsch, H.; Fröba, M.; Linden, M. Chem. Mater. 2004, 16, 5564.
[8] Agren, P.; Linden, M.; Rosenholm, J. B.; Schwarzenbacher, R.; Kriechbaum, M.; Amenitsch, H.; Laggner, P.; Blanchard, J.; Schüth, F. J. Phys. Chem. B 1999, 103, 5943.
[9] Tiemann, M.; Goletto, V.; Blum, R.; Babonneau, F.; Amenitsch, H.; Linden, M. Langmuir 2002, 18, 10053.
[10] Flodstršm, K.; Teixeira, C. V.; Amenitsch, H.; Alfredsson, V.; Linden, M. Langmuir 2004, 20, 4885.

STUDY OF THE GROWTH OF SEMICONDUCTING CdS AND ZnS NANOCRYSTALS USING SAXS TECHNIQUE.

R. Viswanatha[1], P.K. Santra[1], H. Amenitsch[2] and D.D. Sarma[1]

1.) Solid State and Structural Chemistry Unit, Indian Institute of Science, Bangalore-560012, India
2.) Institute of Biophysics and Nanosystems Research, Austrian Academy of Sciences, Schmiedlstr. 6, 8042 Graz, Austria

Molecular self-assembly, the spontaneous formation of molecules into covalently bonded, well-defined, stable structures is a very important concept in biological systems and has increasingly become a focus of non-biological research. Self-assembly is a sophisticated chemical reaction, mostly carried out by nature; understanding the strong interplay in these systems plays a crucial role in designing molecules to form ordered structures for various devices. One-dimensional inorganic nanostructures (rods, wires and tubes) are of relevance for both theoretical and technological aspects, as they exhibit a wide range of electrical and optical properties that depend on both size and shape. It is well known that semiconducting nanoparticles provide us the unprecedented opportunity to tailor-make electronic and optical properties by varying the size and shape of the nanoparticles via the quantum confinement effect. The solution route synthesis of such nanocrystals, owing to its simplicity, flexibility and tunability, provide an interesting route to produce such monodisperse particles of different shapes and sizes; [1,2] this method depends basically on controlling the reaction process leading to the formation of the semiconductor in a solution by controlling various factors like temperature, concentration and by the addition of a capping agent that binds to the preferential sites on the surface of the growing nanoparticle, thus allowing a preferential direction of growth. However, the primary difficulty of this method is the strong interplay between various factors in a way that is very little understood. Thus, the ability to grow nanocrystals of required size and shape are presently only in the realm of trial and error methods. Besides the fact that an understanding of the growth of these nanocrystals of various shapes will be useful to improve the quality and the control of such nanocrystals, at a fundamental level there is little known about the mechanisms leading to anisotropic shapes of these nanocrystals. Obviously there is a need to understand the mechanisms leading to anisotropy in these nanocrystals obtained from such chemical routes. It is indeed, an intriguing question- how do the nearly spherical nanocrystal seeds in the smallest size regime evolve into strongly anisotropic rod-like objects in systems with nearly isotropic (cubic or near-cubic) crystal structures.

In this work, we have used *in-situ* Small Angle X-ray scattering (SAXS) technique to study the asymmetric growth of TiO_2 nanorods [3] by varying the base as well as the reactant concentrations. Using the results obtained from these experiments, we try to model and understand the growth mechanism in these nanocrystals, thus being able to predict the growth mechanism leading to the formation of nanorods.

Oleic acid (OLEA) was first dried at 140˚C for several hours. Titanium tetra iso-propoxide (TTIP) was added to the dried OLEA at ~ 85˚C–90˚C forming the TTIP complex. After 5mins from the addition of TTIP to the solvent, 0.5ml-2.5ml 2M base solution (EDIA) was added to the OLEA-TTIP mixture, sealed in a capilliary and the SAXS patterns were monitored at 110˚C for about 4 hours. The evolution of the patterns were monitored with a time resolution of 2 minutes. The time resolved scattering patterns for TiO_2 nanorods were normalized and background subtracted and the resulting patterns are shown in Figure 1 for different concentrations of the base as well as water.

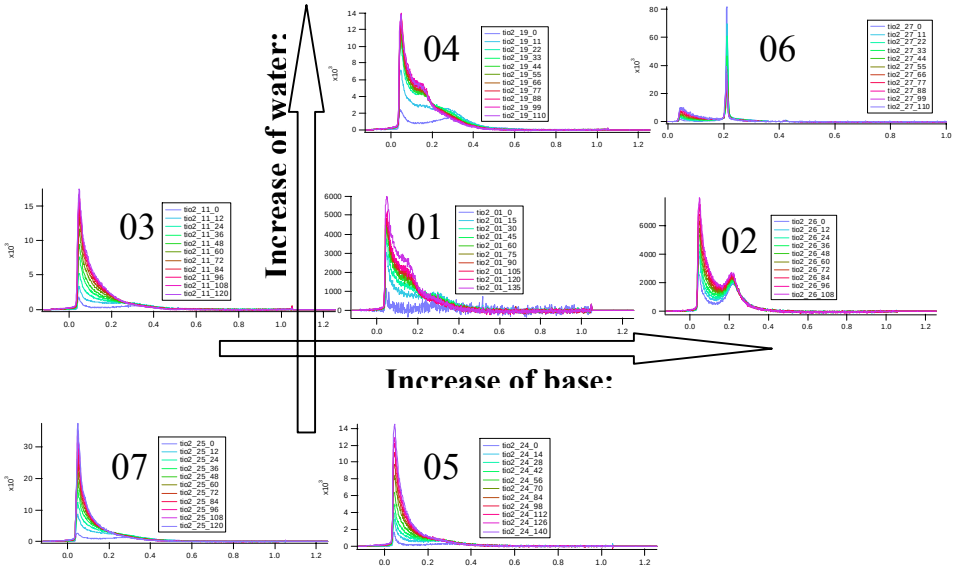

Figure 1. Time resolved scattering patterns of TiO_2 at different water and base concentrations.

It is interesting to note that point 06 in Fig. 1 shows a lamellar phase which is also known to produce crystalline phase of TiO_2. Hence in order to understand the effect of water and EDIA, the base, we have plotted the phase diagram in Fig. 2. The figure clearly shows that there exists a specific region where we observe a lamellar phase. More detailed investigations about the exact mechanism of formation of TiO_2 nanorods are being carried out.

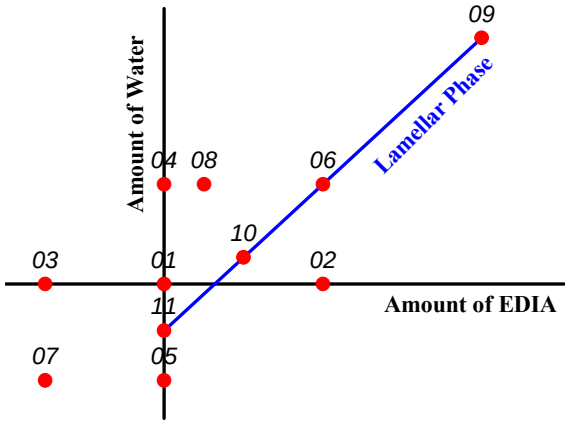

Figure 2. Phase diagram of TiO_2 nanorods with different concentrations of water and base.

References:

[1] Z.A. Peng and X. Peng, J. Am. Chem. Soc., 123, 1389 (2003)
[2] C.B. Murray, D. B. Norris, M. G. Bawendi, J. Am. Chem. Soc. 115, 8706 (1993)
[3] P.D. Cazzoli, A. Kornowski and H. Weller, J. Am. Chem. Soc., 125, 14539 (2003).

Publications

Publications in 2005

V. Alfredsson, H. Amenitsch, K. Flodström, M. Lindén, C.V. Teixeira and H. Wennerström
In-situ studies of the formation mechanism of SBA-15
Studies in Surface Science and Catalysis 156, 69-74 (2005)

V. Alfredsson, H. Amenitsch, F. Kleitz, M. Lindén, P. Linton and C.V. Teixeira
Formation mechanism of mesoporous silica formed with triblock copolymers; effect of salt addition
Studies in Surface Science and Catalysis 158 A, 97-104 (2005)

J. Baldrian, M. Steinhart, A. Sikora, H. Amenitsch and S. Bernstorff
Phase structure of symmetric tri-block-copolymers and their blends
Fibres and Textiles in Eastern Europe 13(5), 35-40 (2005)

W.H. Binder
Polymeric Ordering by H-Bonds: Mimicking Nature by Smart Building Blocks Monatshefte f. Chemie 138, 1–19 (2005)

W.H. Binder, S. Bernstorff, C. Kluger, L. Petraru and M.J. Kunz
Tunable Materials from Hydrogen-Bonded Pseudo Block Copolymers
Adv. Mater. 17, 2824-2828 (2005)

W.H. Binder, C. Kluger, C.J. Straif and G. Friedbacher
Directed Nanoparticle Binding onto Microphase Separated Block Copolymer Thin Films
Macromolecules 38, 9405–9410 (2005)

W.H. Binder and D. Machl
Poly(etherketone)-Poly(isobutylene) Block Copolymers : Synthesis and Phase Behavior
J. Polym. Sci. Polym. Chem Part A, 188 – 202 (2005)

Brezesinski,T., B.Smarsly, K.Iimura, D.Grosso, C.Boissiere, H.Amenitsch, M.Antonietti and C.Sanchez
Self-assembly and crystallization Behavior of mesoporous, crystalline HfO2 thin films: A model system for the generation of mesostructured transition-metal oxides
Small 1, 889-898 (2005)

Z. Budrovic, S. Van Petegem, P. M. Derlet, B. Schmitt, H. Van Swygenhoven, E. Schafler, and M. Zehetbauer
Footprints of deformation mechanisms during in situ x-ray diffraction: Nanocrystalline and ultrafine grained Ni
Appl. Phys. Lett. 86, 231910 (2005)

D. Buso, P. Falcaro, S. Costacurta, M. Guglielmi, A. Martucci, P. Innocenzi, L. Malfatti, V. Bello, G. Mattei, C. Sada, H. Amenitsch, I. Gerdova and A. Haché
PbS-doped mesostructured silica films with high optical nonlinearity
Chem. Mater. 17, 4965-4970 (2005)

G. Caracciolo, H. Amenitsch, C. Sadun and R. Caminiti
In situ formation of solid-supported lipid/DNA complexes
Chem. Phys. Lett. 405, 252-257 (2005)

G. Caracciolo, D. Pozzi, H. Amenitsch and R. Caminiti
Multicomponent cationic lipid-DNA complex formation: Role of lipid mixing
Langmuir 21,11582-11587 (2005)

G. Caracciolo, D. Pozzi, R. Caminiti and H. Amenitsch
Lipid mixing upon deoxyribonucleic acid-induced liposomes fusion investigated by synchrotron small-angle x-ray scattering
Appl. Phys. Lett. 87,133901–133903 (2005)

S. Chattopadhyay, D. Erdemir, J.M.B. Evans, J. Ilavsky, H. Amenitsch, C.U.Segre and A.S. Myerson
SAXS study of the nucleation of glycine crystals from a supersaturated solution
Crystal Growth and Design 5, 523-527 (2005)

D. Chaudhuri, S. Datar, R. Viswanatha, D. D. Sarma and H. Amenitsch
Self-organization of polyaniline nanorods: Towards achieving a higher conductivity
Appl. Phys. Lett. 87, 093117-093119 (2005)

Z. Crnjak Orel, M. Gaberscek and A. Turkovicc
Electrical and spectroscopical characterization of nanocrystalline V/Ce oxides
Solar Energy Materials & Solar Cells. 86, 19-32 (2005)

U.V. Desnica, P. Dubcek, K. Salamon, I.D. Desnica-Frankovic, M. Buljan, S. Bernstorff, U. Serincan andR. Turan
The evolution of the morphology of Ge nanocrystals formed by ion implantation in SiO_2
Nucl. Instr. Methods Phys. Res. B 238, 272-275, (2005)

I.D. Desnica-Frankovic, P. Dubcek, M. Buljan, K. Furic, U.V. Desnica, S. Bernstorff, H. Karl, I. Großhans and B. Stritzker
Influence of stoichiometry deviations on properties of ion-beam synthesized CdSe QDs
Nucl. Instr. Methods Phys. Res. B 238, 302-305 (2005)

D.O. de Zarate, C. Boissiere, D. Grosso, P.A. Albouy, H. Amenitsch, P. Amoros and C.Sanchez
Preparation of multi-nanocrystalline transition metal oxide (TiO2-NiTiO3) mesoporous thin films
New Journal of Chemistry 29,141-144 (2005)

P. Dubcek
Nanostructure as seen by the SAXS
Vacuum 80, 92-97 (2005)

P. Dubcek, U. Desnica, D. Desnica-Frankovic and S. Bernstorff
Structure of ion beam synthesized II-VI nanocrystals
Semiconductor Nanocrystals. B. Podor, Zs. J. Horvath and P. Basa (eds.), Magyar Todomanyos Akademia, Budapest, Hungary, pp.147-150 (2005).

V. Erokhin, S. Carrara, C. Paternolli, L. Valkova, S. Bernstorff and C. Nicolini
X-ray stduy of structural reorganization in phthalocyanine containing Langmuir-Blodgett heterostructures
Applied Surface Science 245, 369-375 (2005)

P. Falcaro, S. Costacurta, G. Mattei, H. Amenitsch, A. Marcelli, M. Cestelli Guidi, M. Piccinini, A. Nucara, L. Malfatti, T. Kidchob and P. Innocenzi
Highly ordered "defect-free"self-assembled hybrid films with a tetragonal mesostructure
J. Am. Chem. Soc. 127, 3838-3846 (2005)

D. Farnik, W.H. Binder and N. Hüsing
Novel Carbohydrate Based Surfactants for the Preparation of Imprinted Silica
Polym. Preprints 46(2), 1140-1141 (2005)

J.I. Flege, T. Schmidt, G. Alexe, T. Clausen, S. Bernstorff, I. Randjelovic, V. Aleksandrovic, A. Kornowski, H. Weller and J. Falta
*$CoPt_3$ nanoparticles adsorbed on SiO_2: a GISAXS and SEM study**
Materials Research Society Symposium Proceedings 840, 143-148 (2005)
*paper has won the "Ribbon Award" at MRS Boston conference in Nov. 2004

C. Fritscher, N. Husing, S. Bernstorff, D. Brandhuber, T. Koch, S. Seidler and H. C. Lichtenegger
In situ SAXS study on cationic and non-ionic surfactant liquid crystals using synchrotron radiation
J. Synchrotron Rad. 12, 717-720 (2005)

P. Garidel, M. Rappolt, A.B. Schromm, J. Howe, K. Lohner, J. Andrae, M.H.J. Koch and K. Brandenburg
Divalent cations affect chain mobility and aggregate structure of lipopolysaccharide from Salmonella minnesota reflected in a decrease of its biological activity
Biochim. Biophys. Acta 1715, 122-131 (2005)

D. Gracin, K. Juraic, P. Dubcek, A. Gajovic and S. Bernstorff
Analysis of the nano-structural properties of thin film silicon–carbon alloys
Vacuum 80, Issue 1-3, pp. 98-101 (October 14, 2005)

P. J. Griffiths, M. A. Bagni, B. Colombini, H. Amenitsch, S. Bernstorff, C.C. Ashley and G. Cecchi
Myosin lever disposition during length oscillations when power stroke tilting is reduced
Am. J. Physiol. Cell. Physiol. 289, C177-C186 (2005)

A. Gupta, P. Rajput, A. Saraiya, V.R. Reddy, M. Gupta, S. Bernstorff and H. Amenitsch
Depth profiling of marker layers using x-ray waveguide structures
Phys. Rev. B 72, 075436-1 until 075436-8 (2005)

P. Innocenzi, L. Malfatti, T. Kidchob, P. Falcaro, S. Costacurta, M. Guglielmi, G. Mattei, V. Bello and H. Amenitsch
Thermal-induced phase transitions in self-assembled mesostructured films studied by small-angle X-ray scattering
J. Synchrotron Rad. 12, 734-738 (2005)

P. Innocenzi, L. Malfatti, T. Kidchob, P. Falcaro, MC. Guidi, M. Piccinini andA. Marcelli
Kinetics of polycondensation reactions during self-assembly of mesostructured films studied by in situ infrared spectroscopy
Chem Commun (Camb). 18, 2384-2386 (2005)

P. Innocenzi, P. Falcaro, J. Mio Bertolo, A. Bearzotti and H. Amenitsch
Electrical responses of silica mesostructured films to changes in environmental humidity and processing conditions
Journal of Non-Crystalline Solids 351, 1980-1986 (2005)

D. Kalnin, P. Lesieur, F. Artzner, G. Keller and M. Ollivon
Systematic investigation of lard polymorphism using combined DSC and time-resolved synchrotron X-ray diffraction
European Journal of Lipid Science and Technology 107, 594-606 (2005)

A. Kancler, A. Zidansek, G. Lahajnar, S. Kralj, H. Amenitsch and S. Bernstorff
Smectic ordering of 8CB Liquid Crystal Confined to a Controlled-Pore Glass
Molecular Crystals Liquid Crystals 439, 1899-1908 (2005)

M. Kerber, E. Schafler and M. Zehetbauer
Processing and evaluation of X-ray line profiles measured from nanostructured materials produced by severe plastic deformation
Rev. Adv. Mater. Sci. 10(5), 427-433 (2005)

I. Kovacevic, P. Dubcek, H. Zorc, N. Radic, B. Pivac and S. Bernstorff
GISAXS characterization of Ge islands on Si(100) substrates
Vacuum 80, 69-73 (2005)

M. Kuemmel, D. Grosso, C. Boissière, B. Smarsly, T. Brezesinski, P.A. Albouy, H. Amenitsch and C. Sanchez
Thermally stable nanocrystalline gamma-alumina layers with highly ordered 3D mesoporosity
Angewandte Chemie 44, 4589-4592 (2005)

M. Lindén, C.V. Teixeira, H. Amenitsch, V. Alfredsson, F. Kleitz
In situ SAXS/XRD on mesoscopically ordered surfactant-silica mesophases; What can we learn?
Materials Research Society Symposium Proceedings 847, 495-505 (2005)

M. Lucic Lavcevic, P. Dubcek, Z. Crnjak Orel and A. Turkovic
GISAXS View of Vanadium Cerium Oxide Thin Films and Influence of Lithium Intercalation
Journal of Chemical Information and Modeling 45, 1553-1557 (2005)

D. Ortiz de Zarate,C. Boissière,D. Grosso,P.A. Albouy,H. Amenitsch,P. Amoros and C. Sanchez
Preparation of multi nano-crystalline transition metal oxide (TiO2-NiTiO3) mesoporous thin films
New Journal of Chemistry 29, 141-144 (2005)

B. Pivac, I. Kovacevic, P. Dubcek, N. Radic, S. Bernstorff, B. Vlahovic and I. Zulim
Study of Ge Islands on Si(100) Substrates
Proceedings of the 20th European Photovoltaic Solar Energy Conference.W. Palz, H. Ossenbrink and P. Helm (eds.), pp. 421-423 (2005)

T. Roth, P.W. Groh, V. Palfi, B. Ivan and W.H. Binder
Supramolecular Three-Arm Star Polyisobutylenes by Sharpless-Type "Click" Reactions
Polym. Preprints 46, 1166-1167 (2005)

E. Schafler, G. Steiner, E. Korznikova, M. Kerber and M. Zehetbauer
Lattice defect investigation of SPD Cu by means of X-Ray Line Profile Analysis, Calorimetry and Electrical Residual Resistivity
Mater. Sci. Eng. A 410-411, 169-173 (2005)

E. Schafler, K. Simon, S. Bernstorff, P. Hanak, G. Tichy, T. Ungar and M. Zehetbauer
A second-order phase-transformation of the dislocation structure during plastic deformation determined by in situ synchrotron X-ray diffraction
Acta Mater. 53, 315-322 (2005)

E. Schafler and M. Zehetbauer
Characterization of nanostructured materials by X-ray Line Profile Analysis
Rev. Adv. Mater. Sci. 10, 28-33 (2005)

F. Schmid, G. Sommer, M. Rappolt, C. A. J. Schulze-Bauer, P. Regitnig, G. A. Holzapfel, P. Laggner and H. Amenitsch
In situ tensile testing of human aortas by time-resolved small-angle X-ray scattering
J. Synchrotron Rad. 12, 727-733 (2005)

T. Schmidt, E. Roventa, T. Clausen, J. I. Flege, G. Alexe, S. Bernstorff, C. Kübel, A. Rosenauer, D. Hommel, and J. Falta
Ordering mechanism of stacked CdSe/ZnS_xSe_{1-x} quantum dots: A combined reciprocal-space and real-space approach
Phys. Rev. B 72, 195334-195343 (2005)

T. Schmidt, E. Roventa, T. Clausen, J. I. Flege, G. Alexe, S. Bernstorff, C. Kübel, A. Rosenauer, D. Hommel, and J. Falta
Ordering mechanism of stacked CdSe/ZnS_xSe_{1-x} quantum dots: A combined reciprocal-space and real-space approach
Virtual Journal of Nanoscale Science & Technology 12, (2005)

R. Supplit, N. Hüsing, C. Fritscher, P. Jakubiak, V. G. Kessler, G. A. Seisenbaeva and S. Bernstorff
Iron Oxide – Doped Mesostructured Silica Films
Mater. Res. Soc. Symp. Proc. 847, EE9.13 (2005)

V. Torma, H. Peterlik, U. Bauer, W. Rupp, N. Hüsing, S. Bernstorff, M. Steinhart, G. Görigk and U. Schubert
Mixed Silica Titania Materials Prepared from a Single-Source Sol-Gel Precursor: A Time-Resolved SAXS Study of the Gelation, Aging, Supercritical Drying, and Calcination Processes
Chem. Mater. 17, 3146-3153 (2005)

B. Toury, R. Blum, V. Goletto and F. Babonneau
Thermal Stability of Periodic Mesoporous SiCO Glasses
J. Sol-Gel Sci. Techn. 33, 99-102 (2005)

R. Triolo, F. Lo Celso, V. Benfante, A. Triolo, A. Wiedenmann and S. Bernstorff
Small angle scattering study of poly(methylmethacrylate)-blockpoly(ethylene oxide) block co-polymer in aqueous solution
Progress in Colloid and Polymer Science 130, 79 –84 (2005)

A. Turkovic, P. Dubcek and N.D. Fox
Self-organization of nanoparticles in a TiO_2 thin film on a glass substrate
Vacuum 80, 108-112 (2005)

T. Ungár, E. Schafler, P. Hanák, S. Bernstorff and M. Zehetbauer
Vacancy concentrations determined from the diffuse background scattering of X-rays in plastically deformed copper
Zeitschrift f. Metallkunde 96(9), 578-583 (2005)

M. Zehetbauer, E. Schafler and T. Ungar
Vacancies in plastically deformed copper
Z. Metallkunde 96(9), 1044-1048 (2005)

M. Zehetbauer, E. Schafler and T. Ungar
Quantification of Nanocrystallization by Means of X-Ray Line Profile Analysis
Arch. Metall.Mater. 50, 515-533 (2005)

Publications from January to September 2006

I. Beurroies, P. Agren, G. Buchel, J.B. Rosenholm, H. Amenitsch, R. Denoyel and M. Linden
Detailed in Situ XRD and Calorimetric Study of the Formation of Silicate/Mixed Surfactant Mesophases under Alkaline Conditions. Influence of Surfactant Chain Length and Synthesis Temperature
J. Phys. Chem. B. 110, 16254-16260 (2006)

T. Brezesinski, M. Groenewolt, N. Pinna, H. Amenitsch, M. Antonietti and B. Smarsly
Surfactant-mediated Generation of Iso-oriented Dense and Mesoporous Crystalline Metal Oxide Layers
Adv. Mater. 18, 1827 (2006)

G. Caracciolo, D. Pozzi, H. Amenitsch and R. Caminiti
One-Dimensional Thermotropic Dilatation Area of Lipid Headgroups within Lamellar Lipid/DNA Complexes
Langmuir 22(9), 4267-73 (April 25, 2006)

G. Caracciolo, D. Pozzi, R. Caminiti and H. Amenitsch
Formation of overcharged cationic lipid/DNA complexes
Chem. Phys. Lett. 429, 250-254 (2006)

I.D. Desnica-Frankovica, P. Dubcek, U.V. Desnica, S. Bernstorff, M.C. Ridgway and C.J. Glover
GISAXS studies of structural modifications in ion-beam amorphized Ge
Nucl. Inst. Meth. Phys. Res. B 249, 114-117 (2006)

U.V. Desnica, M. Buljan, P. Dubcek, Z. Siketic, I. Bogdanovic Radovic, S. Bernstorff, U. Serincan and R. Turan
Ion beam synthesis and characterization of Ge nanocrystals in SiO_2
Nucl. Inst. Meth. Phys. Res. B 249, 843-846 (2006)

A.B. Dros, D. Grosso, C. Boissiere, G.J.d.A.A. Soler-Illia, P.A. Albouy, H. Amenitsch and C. Sanchez
Niobia-stabilised anatase TiO2 highly porous mesostructured thin films
Microporous and Mesoporous Materials 94, 208-213 (2006)

J. I. Flege, Th. Schmidt, V. Aleksandrovic, G. Alexe, T. Clausen, B. Gehl, A. Kornowski, H. Weller, S. Bernstorff and J. Falta
Grazing-incidence small-angle X-ray scattering investigation of spin-coated CoPt3 nanoparticle films
Nucl. Inst. Meth. Phys. Res. B 246, 25-29 (2006)

D. Gracin, K. Juraic, P. Dubcek, A. Gajovic and S. Bernstorff
The nano-structural properties of hydrogenated a-Si and Si-C thin films alloys by GISAXS and vibrational spectroscopy
Applied Surface Science 252, 5598-5601 (2006)

P.J. Griffiths, M.A. Bagni, B. Colombini, H. Amenitsch, S. Bernstorff, S. Funari, C.C. Ashley and G. Cecchi
Effects of the number of actin-bound S1 and axial force on X-ray patterns of intact skeletal muscle
Biophys. J. 90, 975-984 (2006)

P. Kenesei, G. Horváth, S. Bernstorff, T. Ungár and J. Lendvai
Early stages of nucleation and growth of Guinier–Preston zones in Al–Zn–Mg and Al–Zn–Mg–Cu alloys
Zeitschrift f. Metallkunde 97, 315-320 (2006)

M. Kerber, E. Schafler, P. Hanak, G. Ribàrik, S. Bernstorff, T. Ungàr and M. Zehetbauer
Spatial fluctuations of the microstructure during deformation in Cu Single Crystals
Z. Krist. Suppl. 23, 105 (2006)

I. Kovacevic, B. Pivac, P. Dubcek, N. Radic, S. Bernstorff and A. Slaoui
A GISAXS study of SiO/SiO2 superlattice
Thin Solid Films 511-512, 463-467 (2006)

L. Malfatti, P. Falcaro, H. Amenitsch, S. Caramori, R. Argazzi, C.A. Bignozzi, S. Enzo, M. Maggini, and P. Innocenzi
Mesostructured self-assembled titania films for photovoltaic applications
Microporous and Mesoporous Materials 88, 304-311 (2006)

L. Malfatti, T. Kidchob, S. Costacurta, P. Falcaro, P. Schiavuta, H. Amenitsch and P. Innocenzi
Highly ordered self-assembled mesostructured hafnia thin films: a rewritable mesostructure driven by entropy
Chem. Mater. 18, 4553-4560 (2006)

G. Pabst
Global properties of biomimetic membranes: perspectives on molecular features
Biophysical Reviews and Letters 1, 57–84 (2006)

B. Pivac, P. Dubcek, I. Kovacevic, S. Bernstorff, R. Mu, M. Wu, A. Ueda and B. Vlahovic
GISAXS study of gold implanted fused silica
Scripta Materialia 55, 135-138 (2006)

B. Pivac, I. Kovacevic, P. Dubcek, N. Radic, S. Bernstorff and A. Slaoui
Self-organized growth of Ge islands on Si(100) substrates
Thin Solid Film 511, 153-156 (2006)

B. Pivac, I. Kovacevic, P. Dubcek, N. Radic and S. Bernstorff
GISAXS study of Si nanocrystals formation in SiO_2 thin films
Thin Solid Films 515, 756-758 (2006)

D. Pozzi, H. Amenitsch, R. Caminiti and G. Caracciolo
How lipid hydration and temperature affect the structure of DC-Chol-DOPE/DNA lipoplexes
Chem. Phys. Lett. 422, 439-445 (2006)

N. Radic, B. Pivac, P. Dubcek, I. Kovacevic and S. Bernstorff
Growth of Ge islands on Si substrates
Thin Solid Films 515, 752-755 (2006)

M. Rappolt, G.M. Di Gregorio, M. Almgren, H. Amenitsch, G. Pabst, P. Laggner and P. Mariani
Non-equilibrium formation of the cubic Pn3m phase in a monoolein/water system
Europhys. Letters 75, 267-273 (2006)

E. Schafler, K. Nyilas, S. Bernstorff, L. Zeipper, M. Zehetbauer and T. Ungàr
Microstructure of post deformed ECAP-Ti investigated by Multiple X-Ray Line Profile Analysis
Z. Krist. Suppl. 23, 129 (2006)

F. Schmid, G. Sommer, M. Rappolt, P. Regitnig, G.A. Holzapfel, P. Laggner and H. Amenitsch
Bidirectional tensile testing cell for in situ small angle X-ray scattering investigations of soft tissue
Nuclear Inst. Meth. B 246, 262-268 (2006)

F. Spinozzi, P. Mariani, F. Rustichelli, H. Amenitsch, F. Bennardini, G.M. Mura, A. Coi and M.L. Ganadu
Temperature dependence of chaperone-like activity and oligomeric state of alphaB-crystallin
Biochim. Biophys. Acta 1764(4), 677-687 (2006)

A. Turkovic, M. Pavlovic, M. Ivanda, M. Gaberscek and Z. Crnjak Orel
Influence of Intercalated Lithium on Structural and Electrical Properties of V2O5, Mixed V/Ce Oxide and Fe2O3
Journal of the Electrochemical Society 153, A122-A126 (2006)

M. J. Zehetbauer, G. Steiner, E. Schafler, A. Korznikov, E. Korznikova
Deformation induced vacancies with Severe Plastic Deformation: Measurements and Modelling
Mater.Sci.Forum 503-504, 57-64 (2006)

International Conferences and Workshops in 2005

V. Aleksandrovic, I. Randjelovic, A. Kornowski, A. Meyer, H. Weller, J. I. Flege, Th. Schmidt, G. Alexe, T. Clausen, J. Falta, B. Gehl, S.Bernstorff
Ligand exchange on CoPt3 nanoparticles and its influence on film formation
Bunsentagung 2005, Frankfurt, Germany (poster)

Vesna Aleksandrovic, J. I. Flege, Th. Schmidt, A. Kornowski, I. Randjelovic, G. Alexe, T. Clausen, J. Falta, S. Bernstorff, M. Stolzenburg, S. Förster, H. Weller
Polymers as surface modifiers for preparation of CoPt3 nanoparticle monolayer films
Nanomeeting 2005, Minsk (poster)

H. Amenitsch
Time-resolved scattering and GISAXS
4th European Winter School (Research with Neutron And Synchrotron Radiation: NESY 2005), Planneralm, Styria, Austria, 9.3.2006 (invited lecture)

H. Amenitsch, B. Sartori, M. Rappolt, G. Pabst, P. Laggner and D.Grosso
Evaporation induced self-assembly of phospholipids studied with surface diffraction
E-MRS 2005 Spring Meeting, Strasbourg, France, May 31 – June 3, 2005 (poster)

Niki Baccile
Study of organic/inorganic interactions at nanostructured silica interface. A solid state NMR contribution
EuroChem conference, Nancy, France, August 28th – September 1st 2005
(the presentation received the prize for the best symposium talk)

Baldrian J., Steinhart M., Amenitsch H., Bernstorff S., Staneva M.
Disorder – order – crystalllization phenomena in block-copolymer blends
Workshop on Advanced Materials (WAM III) focusing on Nanostructured Advanced Materials, Stellenbosch 2005, Book of Abstracts, poster No 2

S. Bernstorff
Synchrotron sources and instrumentation
4th European Winter School (Research with Neutron And Synchrotron Radiation: NESY 2005), Planneralm, Styria, Austria, 7.3.2005 (invited lecture)

S. Bernstorff
Scattering a basso angolo a incidenza radente da film sottili
1. Schuola "Applicazioni della radiazione di sincrotrone allo studio dei materiali nanostrutturati e dei film sottili" (ARS1), Trento, 14-17 June 2005 (invited lecture)

S. Bernstorff, P. Dubcek, B. Pivac, I. Kovacevic, A. Sassella and A. Borghesi
GIXR and GISAXS Study of Silicon Oxinitride Films
E-MRS 2005 Spring Meeting, Strasbourg, France, May 31 – June 3, 2005

S. Bernstorff, K. Salamon, P. Dubcek, M. Buljan, N. Radic and U.V. Desnica
GISAXS studies of the formation of Ge nanocrystals in SiO_2 in (Ge+SiO_2)/SiO_2 multilayers deposited by magnetron sputtering
E-MRS 2005 Spring Meeting, Strasbourg, France, May 31 – June 3, 2005 (poster)

W.H. Binder
Nanostrukturierte Membranen, Oberflächen und Materialien aus massgeschneiderten Polymeren : im Grenzbereich zwischen organische Chemie und Polymerchemie.
Universität Osnabrück, Germany, 14.4.2005 (invited lecture)

W.H. Binder
Nanostrukturierte Membranen, Oberflächen und Materialien aus massgeschneiderten Makromolekülen : Im Grenzbereich zwischen organischer Chemie und Polymerchemie.
Universität Regensburg, 27.1.2005 (invited lecture)

W.H. Binder, M. J. Kunz, C. Kluger, L. Petraru, S. Bernstorff, V. Torma
Poly(etherketone)-poly(isobutylene) pseudo block-copolymers : Phase behavior via SAXS.
2005 Spring National ACS Meeting, San Diego, March 13-17, 2005 (talk)

W.H. Binder
Supramolekulare Chemie mit Polymeren : Neue Zugänge zu funktionalen Oberlächen und Materialien
Universität Leipzig / Institut f. Oberflächenmodifizierung (IOM), 27. Oktober 2005 (invited lecture)

W.H. Binder
Supramolekulare (Material-)Chemie mit Polymeren
Technische Universität-München, 17. November 2005 (invited lecture)

W.H. Binder
Modulative Materials Based upon Hydrogen Bonding Systems via Self Assembly
STIPOMAT-workshop, Obernai, 29. Oktober 2005 (invited lecture)

W.H. Binder
Von nanostrukturierten Polymeren zu neuen Hybridmaterialien und Oberflächen
Universität Halle / Saale, 10. Oktober 2005 (invited lecture)

W.H. Binder
Selective Binding of Nanoparticles via Directed Hydrogen Bonding Interactions
Polymers for Advanced Technology (PAT), Budapest 2005 (lecture)

W.H. Binder
New Nanostructured Supramolecular Polymeric Materials with Modulative Properties
Chemietage Leoben, September 2005 (lecture)

W.H. Binder
Selective Binding of Au-Nanoparticles onto Surfaces Mediated by Direct Hydrogen Bonding Interactions
Scanning Probe Microscopy, Sensors and Nanostructures, Cancun, June 5-8, 2005 (lecture)

W.H. Binder
Assembly of Polymeric Building Blocks into Nanoscaled Structures
7th Austrian Polymer Meeting, Graz, 2005 (lecture)

W.H. Binder
Combining 1,3-cycloaddition-"click"-reactions with living polymerization-chemistry
11th BDSCH, Brünn 2005 (invited lecture)

W.H. Binder
Lipid Rafts and their Biological Significance: Engineering Lipid Order and Density
Joint Meeting on Medicinal Chemistry 2005, Wien (invited lecture)

W.H. Binder
Von nanostrukturierten Polymeren zu neuen Hybridmaterialien und Oberflächen
Universität Leoben, Austria, 21. Februar 2005 (invited lecture)

T. Brezesinski, D. Grosso, B. Smarsly, M. Antonietti, C. Boissière, C. Sanchez , H. Amenitsch and P. A. Albouy
The Preparation and Characterization of Mesostructured Thin Films of Perovskites and Ternary Oxides
Nanoporous Materials – IV, Niagara Falls, Ontario, Canada, June 7 – 10, 2005 (Abstract)

G. Caracciolo, D. Pozzi, H. Amenitsch, R. Caminiti
First European Conference on Chemistry for Life Sciences, Rimini, Italy, 3-7 October, 2005

S. Chattopadhyay, D. Erdemir, J.M.B. Evans, J. Ilavsky, H. Amenitsch, C.U. Segre and A.S. Myerson
SAXS Studies of Nucleation of Glycine from its Supersaturated Solution
XX Congress of the International Union of Crystallography (IUCr2005), Florence, Italy, 23.-31.8.2005

G. Croce, M. Milanesio, D. Viterbo and H. Amenitsch
A Mesoporous Pattern Created by Nature in Siliceous Spicules from Marine Sponges
XX Congress of the International Union of Crystallography (IUCr2005), Florence, Italy, 23.-31.8.2005

I.D. Desnica-Francovic, P. Dubcek, U.V. Desnica, S. Bernstorff, M.C. Ridgway and C.J. Glover
GISAXS studies of structural modifications in ion-beam amorphized Ge
17th International Conference on Ion Beam Analysis (IBA 2005), Sevilla, Spain, June 26 - July 1, 2005

U.V. Desnica, M. Buljan, P. Dubcek, Z. Siketic, I. Bogdanovic Radovic, S. Bernstorff, U. Serincan and R. Turan
Ion beam synthesis and characterization of Ge nanocrystals in SiO_2
17th International Conference on Ion Beam Analysis (IBA 2005), Sevilla, Spain, June 26 - July 1, 2005

P. Dubcek, B. Pivac, S. Bernstorff, F. Corni, R. Tonini, G. Ottaviani
Grazing-incidence X-RAY reflectivity study of hydrogen implanted Silicon
E-MRS 2005 Spring Meeting, Strasbourg, France, May 31 – June 3, 2005

P. Dubcek, A. Turkovic, M. Lucic-Lavcevic, Z. Crnjak-Orel and S. Bernstorff
Nanostructure of Vanadium Oxide and V/Ce Oxide Films and the Influence of Li+ Intercalation
207th Meeting of The Electrochemical Society, Quebec City, Canada, May 15 - 20, 2005 (lecture)

Paolo Falcaro
Thermally stable highly ordered self-assembled hybrid films
International Workshop on Sol-Gel Science 2005, Los-Angeles, 21-26 august 2005 (poster)

J. Falta, Th. Schmidt, T. Clausen, J.I. Flege, G. Alexe, D. Hommel, S. Bernstorff
Small angle X-ray scattering investigation of self-organized CdSe/ZnSeS quantum dot alignment
E-MRS 2005 Spring Meeting, Strasbourg, France, May 31 – June 3, 2005 (poster)

J.I. Flege, Th. Schmidt, G. Alexe, T. Clausen, J. Falta, I. Randjelovic, V. Aleksandrovic, A. Kornowski, H. Weller, S. Bernstorff
Highly-ordered ultra-thin colloidal nanoparticle films
European Materials Research Society Spring Meeting 2005, Strasbourg, France, May 31 – June 3, 2005 (talk)

J.I. Flege
Modified silicon substrates - from atomic adsorbates to highly-ordered self-assembled nanoparticle arrays
Joint Chemistry/Center for Functional Nanomaterials Seminar, Brookhaven National Laboratory, USA, 2005 (talk)

J.I. Flege
Highly ordered self-assembled colloidal nanoparticle films studied by grazing-incidence small-angle x-ray scattering
XIII Elettra Users' Meeting 2005, Trieste, Italy, December 14-16 2005 (invited talk as receiver of the "Luciano Fonda and Paolo Maria Fasella Award" which is assigned each year to a young scientist for outstanding experiments using Elettra synchrotron light)

O. Francescangeli, M. Pisani, P. Bruni
Supramolecular ordering of self-assembled lipid-DNA-Metal complexes related to gene therapy
8th European Conference on Liquid Crystals ECLC-05, Sesto (BZ), Italy, February 27-04March, 2005 (poster)

D. Gracin, K. Juraic, A. Gajovic, P. Dubcek, W.J. Soppe, C. Devilee and H.J.Muffler, *The structural ordering of amorphous-nanocrystalline silicon thin films by SAXS, vibrational and optical spectroscopy*
ICANS 21 (International Conference of Amorphous and Nanocrystalline Solids) Lisabon, 4-9 Sept. 2005

D.Gracin, K.Juraic, P.Dubcek, A.Gajovic and S.Bernstorff
Analysis of the nano-structural properties of thin film silicon-carbon alloys
ICT 13 (International Congress on Thin Films) Stockholm, Sweden, 19-23 June 2005

D. Grosso, C. Boissière, and C. Sanchez
Nanocrystalline Mesoporous Oxides films.
ACS 2005, Section F: Nucleation and growth of nanostructured materials, San Diego, March 2005, USA (invited talk)

D. Grosso, B. Smarsly, T. Brezesinski, M. Groenewolt, M. Antonietti, C. Boissière and C. Sanchez
Generation of functional mesoporous thin films of binary and ternary metal oxides with crystalline pore walls using novel block copolymer templates and characterization by suitable analytical techniques
ACS 2005, Section A: Surfactants for new materials, San Diego, March 2005, USA

D. Grosso, C. Boissiere, P.A. Albouy, H. Amenitsch, and C. Sanchez
In situ SAXS WAXS investigations of crystallisation in metal oxide mesoporous ordered thin layers
E-MRS 2005 Spring Meeting, Strasbourg, France, May 31 – June 3, 2005 (talk)

A. Hahn, Z. Bayram-Hahn, H. Amenitsch, S. Kallus, J. Ramsay, K.K. Unger,
Online-studies on the formation of silicate-I monitored via small angle scattering techniques
E-MRS 2005 Spring Meeting, Strasbourg, France, May 31 – June 3, 2005 (poster)

A. Hahn, D. Kumar, G. Büchel, H. Amenitsch, T. Narayanan and K.K. Unger
Nucleation and growth of mesoporous spherical silica nanoparticles studied by time-resolved small angle X-ray scattering
E-MRS 2005 Spring Meeting, Strasbourg, France, May 31 – June 3, 2005 (talk)

A. Hodzic, H. Amenitsch, M. Rappolt, P. Laggner and G. Pabst
Effects of plant sterols on structure and fluctuations of lipid membranes
55. Annual Meeting of the Austrian Physical Society, Vienna, Austria, 27.-29.9.2005 (poster)

P. Innocenzi, L. Malfatti, T. Kidchob, P. Falcaro, S. Costacurta, G. Mattei, H. Amenitsch, A. Marcelli, M. Cestelli Guidi, M. Piccinini, A. Nucara
"Defect-free" self-assemled hybrid films with a tetragonal mesostructure
E-MRS 2005 Spring Meeting, Strasbourg, France, May 31 – June 3, 2005 (talk)

M. Kerber, E. Schafler, M. Zehetbauer
Processing and evaluation of X-ray line profiles measured from nanostructured materials produced by severe plastic deformation
2. Int. Conf. Nanomaterials and Nanotechnologies (NN2005),Crete, Greece, June 2005 (poster)

I. Kovacevic, B. Pivac, P. Dubcek, N. Radic and S. Bernstorff
A GISAXS study of SiO/SiO_2 superlattice
E-MRS 2005 Spring Meeting, Strasbourg, France, May 31 – June 3, 2005

H.C. Lichtenegger
Synchrotron micro-SAXS and micro-diffraction scanning techniques for the study of complex (bio-)materials
E-MRS 2005 Spring Meeting, Strasbourg, France, May 31 – June 3, 2005 (talk)

M. Lindèn, Cilaine V. Teixeira, H. Amenitsch, V. Alfredsson, F. Kleitz
In situ SAXS/XRD studies of the formation of mesoscopically ordered surfactant-silica mesophases
E-MRS 2005 Spring Meeting, Strasbourg, France, May 31 – June 3, 2005 (talk)

M. Linden, H. Amenitsch, C.V. Teixeira, V. Alfredsson and F. Kleitz
In situ SAXS/XRD studies of the formation of mesoscopically ordered surfactant-silica mesophases
229th ACS National Meeting, San Diego, CA, United States, March 13-17, 2005

M. Ollivon., G. Keller, C. Bourgaux, D. Kalnin and P. Lesieur
Microcalix : a Coupling of DSC and High Resolution X-Ray Diffraction for Biomaterials Studies
NATAS 2005, Anaheim, California, Septembre 2005 (invited lecture)

M. Ollivon, S. Ueno, K. Sato and P. Lesieur
Mechanism of Chain Ordering Observed during Cristallization of Triacylglycerols by Time-Resolved Synchrotron X-Ray Diffraction
26thWorld Congress of the ISF, Prague (CZ), 25-28 September 2005 (invited, Keynote lecture)

M. Ollivon
Cristallization in milk fat emulsion
Campina Science Day, Milk Fat Technology, Wageningen (NL), 12-13 octobre 2005 (invited lecture)

G. Pabst, H. Amenitsch, M. Rappolt, P. Laggner, J. Katsaras, K. Lohner, and A. Hickel
Effect of chain length on the lateral organization of charged lipid membranes
E-MRS 2005 Spring Meeting, Strasbourg, France, May 31 – June 3, 2005 (poster)

G. Pabst, M. Rappolt, A. Hodzic, J. Katsaras, P. Laggner and H. Amenitsch
Finite - Size Effects in Solid Supported Lipid Films
55. Annual Meeting of the Austrian Physical Society, Vienna, Austria, 27.-29.9.2005 (talk)

M. Pisani, O. Francescangeli and P. Bruni
Studi Strutturali di complessi ternari Lipidi-DNA- ioni metallici
XXIV Congresso TUMA - Firenze, Italy, 30 Settembre-1 Ottobre 2005 (talk)

B. Pivac, I. Kovacevic, P. Dubcek, N. Radic and S. Bernstorff
Self-organized growth of Ge islands on Si(100) substrates
E-MRS 2005 Spring Meeting, Strasbourg, France, May 31 – June 3, 2005

B. Pivac, I. Kovacevic, P. Dubcek, N. Radic, S. Bernstorff, B. Vlahovic and I. Zulim
Study of Ge Islands on Si(100) Substrates
20th European Photovoltaic Solar Energy Conference, Barcelona, Spain, 6-10 June 2005 (poster)

M. Rappolt
Physics of Membranes: Structure and Elasticity.
23. International Physics Congress, University Mugla, Turkey, 12.09.-16.09.2005 (invited talk)

M. Rappolt
The power of SAXS: Exploration of the magic world of biomaterials
Workshop on "Research with Synchrotron Radiation" organized by Kevin Prince (Sincrotrone Trieste) and Vladimir Matolin (Charles University Prague), Synchrotron Light Laboratory ELETTRA, Basovizza, Italy: 30.05.-31.05.2005 (Invited lecture:))

M. Rappolt, J. Strancar, A. Hodzic, P. Laggner & G. Pabst
Influence of Sodium and Calcium Chloride on the Fluidity of Phosphatidylcholine Membranes.
International Biophysics Congress, Montpellier, France, 26.08.-30.08.2005 (Poster)

M. Rappolt & G. Pabst
To be lamellar or to be non-lamellar: a Shakespeare's view on lipid model membranes.
Department of Physics, Theoretical Biophysics Group of Prof R. Podgornic, University of Ljubljana. 23.5.2005 (invited lecture)

M. Rappolt
Lipid/water mesophases as „seen“ by X-rays.
Faculty of Engineering, Laboratory of Physics, University of Ljubljana. Prof. V. Kralj-Iglic and Prof. A. Iglic. 31.03.2005 (invited lecture).

M. Rappolt
Saxs: Powerful Tool For Nanostructured Materials.
T.C. Hacettepe University, Faculty of Engineering Department of Physics Engineering Ankara, Turkey, 22-23.11.2005. Tutorial in SAXS Data Treatment: Liquid Crystal Membranes.

M. Rappolt, J. Strancar, A. Hodzic, P. Laggner & G. Pabst
Influence of sodium and calcium chloride on the global and local properties of phosphatidylcholine bilayers: Small angle X-ray scattering and electron paramagnetic resonance studies
Regional Biophysics Meeting, Hotel Dobrava, Terme Zreče, Slovenia, 16.-20.03.2005 (Poster)

E. Schafler, K. Simon, S. Bernstorff, G. Tichy, T. Ungar, M. J. Zehetbauer
A Second-Order Phase-Transformation of the Dislocation Structure during Plastic Deformation Determined by In-Situ Synchrotron X-Ray Diffraction
55. Annual Meeting of the Austrian Physical Society, Vienna, Austria, 27.-29.9.2005 (poster)

E. Schafler, G. Steiner, E. Korznikova, M. Kerber, M. J. Zehetbauer
Lattice defect investigation of ECAP-Cu by means of X-Ray Line Profile Analysis, Calorimetry and Electrical Resistometry
TMS Annual Meeting, The Langdon Symposium: “Flow and Forming of Crystalline Materials”, San Francisco, USA, February 2005 (lecture)

E. Schafler, M. Zehetbauer
Characterization of nanostructured materials by X-ray Line Profile Analysis
2. Int. Conf. Nanomaterials and Nanotechnologies (NN2005),Crete, Greece, June 2005 (lecture)

F. Schmid, H. Amenitsch, G. Sommer, M. Rappolt, P. Regitnig, P. Laggner, G.A. Holzapfel
Biomechanics of human arteries studied with small angle X-ray scattering
E-MRS 2005 Spring Meeting, Strasbourg, France, May 31 – June 3, 2005 (poster)

F. Schmid, G. Sommer, M. Rappolt, P. Regitnig, C. A. Schulze-Bauer, G. A. Holzapfel, H. Amenitsch and P. Laggner
Layer Specific Tensile Testing of Human Arteries at the Austrian SAXS Beamline at ELETTRA
55. Annual Meeting of the Austrian Physical Society, Vienna, Austria, 27.-29.9.2005 (talk)

M. Smolle, A.E. Prior, A.E. Brown, O. Byron and J.G. Lindsay
Protein-protein interactions within the human pyruvate dehydrogenase complex
The Protein Society 19th Symposium, Boston, US, 30th July-3rd August 2005

R. Supplit and N. Hüsing,
Synthesis and characterization of transition metal oxide doped mesostructured silica films
E-MRS 2005 Spring Meeting, Strasbourg, France, May 31 – June 3, 2005 (talk)

Turkovic, Aleksandra; Pavlovic, Mladen; Ivanda, Mile; Gaberscek, Miran; Crnjak Orel, Zorica
Influence of Intercalated Lithium on Structural and Electrical Properties of V2O5, Mixed V/Ce Oxide and Fe2O3
Meeting Abstracts of the Electrochemical Society, Ma 2005-01, Quebec City, May 15-20, 2005. 1356-1356 (lecture)

T. Ungár, E. Schafler, P. Hanák, S. Bernstorff, M. Zehetbauer
Vacancy Production During Plastic Deformation in Copper Determined by In-situ X-ray Diffraction
10. International Symposium on Physics of Materials ISPMA 10, Prague, Sept. 2005 (lecture)

R. Vishwanatha, Heinz Amenitsch and D.D. Sarma
Study of growth mechanism in cadmium sulfide nanocrystals
E-MRS 2005 Spring Meeting, Strasbourg, France, May 31 – June 3, 2005 (poster)

M. J. Zehetbauer, G. Steiner, E. Schafler, A. Korznikov, E. Korznikova
Deformation induced vacancies with Severe Plastic Deformation: Measurements and Modelling
3. Int. Conf. on Nanomaterials by Severe Plastic Deformation – NanoSPD3, Fukuoka, Japan, Sept. 2005 (lecture)

ELETTRA Highlights 2004-2005

S. Costacurta, P. Falcaro, G. Mattei, H. Amenitsch, L. Malfatti, T. Kidchob and P. Innocenci
Self-assembled highly-ordered mesostructured hybrid films
Elettra Research Highlight, pp. 60-63 (2005)

D. Grosso, C. Boissiere, C. Sanchez, B. Smarsly, T. Brezesinski, N. Pinna, M. Antonietti, P.A. Albouy, H. Amenitsch
Periodically ordered mesoporous filmscomposed of nanocrystalline multimetallic oxides
Elettra Research Highlight, pp. 64-67 (2005)

H.S. Gupta, P. Fratzl, P. Messmer, P. Roschger, K. Klaushofer and S. Bernstorff
Fibrillar Deformation in Mineralized Tendon
Elettra Research Highlight, pp. 56-59 (2005)

SAXS training courses

In March 2005, H. Amenitsch, S. Bernstorff, M. Kriechbaum, M. Rappolt and Barbara Sartori participated at the international school "HERCULES", organized by the university "Joseph Fourier" (Grenoble, France) and the National Polytechniche Institute of Grenoble with the help of ERSF, ILL, ELETTRA, LLB, CEA and CNRS. They gave 8 tutorials a' 4 hours, including hands-on experience for the students during the measurements performed in the

SAXS-lab and at the Austrian SAXS-beamline.

Luciano Fonda and Paolo Maria Fasella Award

During the XIII ELETTRA Users' Meeting (Trieste, December 14-16 2005) our user Jan Ingo Flege (University of Bremen, Germany), received the ELETTRA Award in Memory of Luciano Fonda and Paolo Maria Fasella, which is assigned each year to a young scientist for outstanding experiments using Elettra synchrotron light. His studies were concerning the precise structural investigation of nanoparticle self-assemblies of high technological interest with respect to the development of more efficient catalysts and future opto-electronic as well as magnetic storage devices.

PhD Thesis 2005

Paolo Falcaro
Sintesi di film mesostrutturati attraverso tecniche di autoassemblaggio sopramolecolare e relative applicazioni
Università di Bologna, sede di attività: Università di Padova, Italia, December 2005

F.R. Kogler:
Synthesis and Characterization of Transition Metal Oxo Clusters and their Use as Co-Monomers in the Preparation of Hybrid Polymers
TU Wien, Austria, 2005

Guenther Maier
Strukturuntersuchungen an polymeren Materialien und Knochen mit Hilfe der Röntgenkleinwinkelstreuung
University of Leoben, Austria, Nov. 2005

Lydia Paccamiccio
Proprietà energetiche e strutturali di sistemi lipidici non lamellari: implicazioni biologiche del polimorfismo
Università di Ancona, Italy, 2005

Christel Raffournier
Caractérisation d'objets bi-compartimentaux lipidiques
Univ. Paris-Sud, defended 11.7.2005

Raffaele Sinibaldi
Proprietà strutturali, stabilità ed aggregazione di proteine solubili
Università di Ancona, Italy, 2005

Master Theses (Tesi di Laurea) 2005

R. Zirbs
Selektive Anbindung von Nanopartikeln an Oberflächen mittels supramolekularer Wechselwirkungen
TU Wien, Institut für Angewandte Synthesechemie, Austria, 2005

Author Index